Stress Analysis of Rotating Annular Uniform-Thickness and Thickness-Tapered Discs made of Orthotropic and Laminated Composite Materials

Parteek Arora

A thesis

in

the Department

of

Mechanical and Industrial Engineering

Presented in Partial Fulfillment of the Requirements

For the Degree of

Master of Applied Science (Mechanical Engineering) at

Concordia University

Montreal, Quebec, Canada

April 2021

CONCORDIA UNIVERSITY
School of Graduate Studies

This is to certify that the thesis prepared

By: Parteek Arora

Entitled: Stress Analysis of Rotating Annular Uniform-Thickness and Thickness-Tapered Discs made of Orthotropic and Laminated Composite Materials

and submitted in partial fulfillment of the requirements for the degree of

Master of Applied Science (Mechanical Engineering)

complies with the regulations of the University and meets the accepted standards with respect to originality and quality.

Signed by the final examining committee:

Dr. Mehdi Hojjati — Chair

Dr. Mehdi Hojjati — Examiner

Dr. Sang Hyeok Han — Examiner

Dr. Rajamohan Ganesan — Supervisor

Approved By

Dr. Sivakumar Narayanswamy, Graduate Program Director

Dr. Mourad Debbabi, Dean of Faculty

Date April 27, 2021

ABSTRACT

Stress analysis of rotating annular uniform-thickness and thickness-tapered discs made of orthotropic and laminated composite materials

Parteek Arora

Favorable mechanical properties such as high strength-to-weight ratio, high stiffness-to-weight ratio, low specific weight and high fatigue strength, and stiffness tailoring capabilities have enabled the use of composite materials in turbomachinery, automotive and aviation industries. Recent developments on the applications to rotating tapered structures such as thickness-tapered flywheels and rotors in gas turbines and airplane engines have shown increasing use of continuous fiber-reinforced composite materials. Rotating annular thickness-tapered discs made of orthotropic and fiber-reinforced composite materials have preferential stress state as compared to the uniform-thickness discs made of isotropic materials rotating at the same speed. Therefore, due to their distinct characteristics from uniform-thickness discs and wide range of applications, the design of thickness-tapered rotating discs requires comprehensive research to understand their elastic behavior under different loading and boundary conditions.

In the present work, the in-plane stress and displacement analyses of rotating annular uniform-thickness and thickness-tapered discs made of orthotropic and fiber-reinforced composite materials are conducted considering different boundary conditions. A computational solution based on the Rayleigh-Ritz method with finite-element-like modification is developed to evaluate the elastic response of rotating annular thickness-tapered discs made of orthotropic materials. Linear taper and Stodola taper profiles are considered in the elastic analysis of thickness-tapered orthotropic discs with the free-free and the clamped-free boundary conditions. The accuracy of the developed formulation for the elastic response of thickness-tapered orthotropic discs is established based on the convergence of the results obtained for the elastic response using the sub-domain-wise application of Rayleigh-Ritz method in terms of the number of divisions of the thickness-tapered disc, to the results obtained using closed-form analytical solutions available in the literature. For rotating annular uniform-thickness and thickness-tapered fiber-reinforced composite discs with the clamped-free boundary condition, the Rayleigh-Ritz method in

conjunction with the Classical Laminate Theory in cylindrical coordinate system is used to evaluate the elastic response. The finite element analysis tool ANSYS® is used to model the various three-dimensional internal taper configurations of rotating annular thickness-tapered fiber-reinforced composite discs. The results obtained for the elastic response of uniform-thickness and thickness-tapered fiber-reinforced composite discs using the SOLID185 and SHELL181 elements in ANSYS® are used to verify the results obtained for the same using the Rayleigh-Ritz method based on the Classical Laminate Theory in cylindrical coordinate system. Numerical and symbolic calculations to solve the boundary value problem using the Rayleigh-Ritz method are performed using the technical computing language MATLAB®. The effects of degree of orthotropy, taper profile and taper parameter values on the in-plane stress distributions and radial displacement distribution in the rotating annular thickness-tapered discs made of orthotropic materials are observed for the free-free and clamped-free boundary conditions through extensive parametric studies. The influences of fiber orientation, radius ratio, rotational velocity, laminate configuration, ply reduction and internal taper configuration on the elastic response of rotating annular thickness-tapered fiber-reinforced composite discs are thoroughly examined considering the clamped-free boundary condition. For the parametric studies, a wide range of orthotropic materials are chosen and also, the NCT-301 graphite-epoxy prepreg is chosen as a fiber-reinforced composite material. Important design aspects are systematically brought out.

ACKNOWLEDGEMENT

First of all, I would like to express my invaluable gratitude to the almighty creator who gave me the ability to complete this thesis and contribute my research to the emerging technology in the world.

Then, I offer my sincere gratitude to my supervisor Dr. Rajamohan Ganesan, who has supported me throughout my research with his patience, enthusiasm and immense knowledge. His valuable guidance during the research and thesis writing period helped me a lot to successfully complete the thesis.

I am thankful to my parents Mr. Anil Arora and Mrs. Sunita Arora and all my family members for their love, encouragement and support to pursue my master's degree.

I wish to thank my friends Puneet K. Jagpaul, Pramod Kumar and Ajeesh S. Nair at graduate research office EV 13.167 who supported me by sharing ideas and discussions during my research at the university. Also, I wish to thank my friends Jaspreet S. Kamboj, Harpreet Singh and Gurveer Singh for all the support they provided during my tenure in Montreal and at the university.

I gratefully acknowledge the funding sources for my master's thesis provided by the NSERC and Concordia University.

Thank You.

Dedicated to

SHRI KRISHNA

कर्मण्येवाधिकारस्ते मा फलेषु कदाचन ।
मा कर्मफलहेतुर्भूर्मा ते सङ्गोऽस्त्वकर्मणि ॥४७॥

karmaṇy-evādhikāraste mā phaleṣu kadācana
mā karma-phala-hetur bhūr mā te saṅgo'stv-akarmaṇi

Bhagavad Geeta

Chapter -2, *Verse* -47

Meaning in English: Do your duty and be detached from its outcome. Do not be driven by the end product, instead, enjoy the process of getting there.

Meaning in French: Faites votre devoir et soyez détaché de son issue. Ne soyez pas motivé par le produit final, profitez plutôt du processus pour y arriver.

Table of Contents

List of Figures

List of Tables

Nomenclature

N	Number of divisions of the thickness-tapered disc
r_i, r_o	Inner and outer radii of the disc
R_i^N, R_o^N	Inner and outer radii of the N^{th} division
h_i, h_o	Thickness of the disc at the hub and at the free end
H_i^N, H_o^N	Thicknesses at the inner and the outer surface of the N^{th} division
h_{midN}	Thickness at the mid-plane of the N^{th} division
L_r	Length of each division given along the radial direction of the disc
n, s	Taper parameters for the linearly-tapered disc and Stodola disc
ω	Angular velocity of rotation
ρ	Density
r	Radial coordinate
U	Strain energy of the uniform-thickness disc
U_{ortho}^{uni}	Strain energy of the uniform-thickness orthotropic disc
$U_{ortho}^{tapered}$	Strain energy of the thickness-tapered orthotropic disc
V_{ortho}^{uni}	Potential energy originated from the centrifugal loading of uniform-thickness orthotropic disc
$V_{ortho}^{tapered}$	Potential energy originated from the centrifugal loading of thickness-tapered orthotropic disc
$\Pi_{tapered}$	Total potential energy of the rotating annular thickness-tapered disc
λ	Degree of orthotropy
$\bar{h}$	Thickness reduction ratio of the annular thickness-tapered orthotropic disc
T	Number of sampling points taken along the radial direction of the disc
$u_1(r), u_2(r)$	Displacements of the rotating annular disc in principal material directions 1 and 2
z	Position of a point in the k-th ply of the laminated disc
u_r^o, u_θ^o, w_o	Radial, circumferential and transverse displacements of a point in the mid-plane of the laminated disc

u_r, u_θ, w	Radial, circumferential and transverse displacements of a point in the k-th ply of the laminated disc
$[Q]$	Reduced stiffness matrix of the material of the disc
θ	Fiber orientation angle
$\overline{[Q]}_k$	Transformed reduced stiffness matrix of the k-th ply in the laminated disc
t_k	Thickness of the k-th ply in the laminated disc
h	Total thickness of the uniform-thickness laminated disc
$z_k,\ z_{k-1}$	Distances from the top and bottom surfaces of the k-th ply to the mid-plane of the laminated disc
β	Radius ratio of the laminated disc
U_k	Strain energy of the k-th ply in the laminated disc
U	Strain energy of the annular uniform-thickness laminated disc
A_{ij}	Elements of the stretching stiffness matrix of the uniform-thickness laminate
B_{ij}	Elements of the coupling stiffness matrix of the uniform-thickness laminate
D_{ij}	Elements of the bending stiffness matrix of the uniform-thickness laminate
V	Potential energy originated from the centrifugal loading of annular uniform-thickness laminated disc
Π	Total potential energy of rotating annular uniform-thickness laminated disc
φ	Taper angle of the annular thickness-tapered laminated disc
$[T_{\sigma\theta}]_k$	Stress transformation matrix of the k-th ply which is a function of the fiber orientation angle θ
$\left[T_{\sigma\varphi}\right]_k$	Stress transformation matrix of the k-th ply which is a function of the taper angle φ
δ	Number of dropped plies in the annular thickness-tapered laminated disc
N_C	Number of plies at the clamped end of the thickness-tapered laminated disc
N_F	Number of plies at the free end of the thickness-tapered laminated disc
$A_{ij}(r)$	Elements of the stretching stiffness matrix of the thickness-tapered laminate
$B_{ij}(r)$	Elements of the coupling stiffness matrix of the thickness-tapered laminate

$D_{ij}(r)$	Elements of the bending stiffness matrix of the thickness-tapered laminate
U_{plies}	Strain energy of the fiber-reinforced plies
Nr	Total number of resin pockets in the thickness-tapered laminated disc
L_b	Length of an individual resin pocket along the radius of the disc
$[Q_{resin}]$	Stiffness matrix of the resin material
$U_{resin\,pkt}$	Total strain energy of the resin pockets
$U_{tapered}$	Strain energy of the thickness-tapered laminated disc
V_{plies}	Potential energy originated from the centrifugal loading of the fiber-reinforced plies in the thickness-tapered laminated disc
$V_{resin\,pkt}$	Total potential energy originated from the centrifugal loading of the resin pockets in the thickness-tapered laminated disc
$V_{tapered}$	Total potential energy originated from the centrifugal loading of the thickness-tapered laminated disc
Π_T	Total potential energy of the thickness-tapered laminated disc

Chapter 1

Introduction

1.1 Stress analysis in mechanical design

In layman's terms, stress is the force per unit area in a body under the application of an external load. The atoms of a material are bonded together by a system of cohesive forces that keeps the atoms in place while still allowing them to vibrate about their fixed position, resulting in fluctuating motion from a state of equilibrium. Under the application of an external force, the object deforms and due to this deformation, the atoms tend to dislocate from their original bonded position which in turn leads to the development of internal forces, which when divided by the unit cross-sectional area gives the amount of stress experienced by the object.

Stress analysis is one of the most important steps in any structural design practice. A suitable stress analysis technique should provide reasonably accurate and reliable results in terms of the magnitude and the direction of the stress induced at any material point in a structure or component under any arbitrary loading and boundary condition. Stress analysis is an important aspect of engineering, since the failure of most of the engineering components occurs due to the accumulation of stress to a level that exceeds the strength of the material.

1.2 Fiber-reinforced composite materials in rotating structures

In a broad sense, the word *composite* means – made of two or more different parts. A composite material consists of an assemblage of two materials with different engineering properties, allowing us to obtain a material of which the set of performance characteristics is greater than that of the component materials taken separately. A composite material consists of one or more discontinuous phases, called as the reinforcement or the reinforcing material, which can be in the form of long and short fibers, particles or flakes, and are distributed in one continuous phase called as the matrix. The matrix helps to bind the reinforcement together and to transfer the load to and in between the reinforcement. In the case of composite materials in which the reinforcement is made of long continuous fibers, the orientation of fibers plays a vital role in determining the anisotropy of the composite material. This aspect forms one of the fundamental

characteristics of the composite materials, namely the possibility of controlling the anisotropy of the finished laminated product.

Due to favorable engineering properties of the fiber-reinforced composite materials, such as high stiffness-to-weight ratio, high strength-to-weight ratio, and high damage tolerance, they are widely used in aerospace, automotive and construction industries. The arrangement of the fibers and their orientation allow the designers to tailor the mechanical properties of the laminated structure. The thickness reduction of the laminated structure is achieved by terminating plies within the structure at discrete locations which reduces the overall weight of the structure and allows it to maintain sufficient strength and stiffness.

There are numerous examples of using fiber-reinforced composite materials in rotating structures. One such example is the application of carbon-fiber reinforced polymer in flywheels. Flywheel is a disc that rotates, sometimes at very high speeds, and using conservation of energy it can store surges from a power system and then release the power back as and when needed. In the late 1960s, URENCO in Buckinghamshire, U.K., developed a flywheel that used carbon-fiber reinforced polymer to manufacture the rotor, which significantly increased the tensile strength of the rotor and boosted the energy storage efficiency up to 97 percent.

In 1988, Piramoon [1] at Beckman Instruments Inc. in California, U.S.A., patented a centrifuge rotor made of high strength carbon fibers reinforced with resin. The rotor included a top and bottom disc separated by a spacer belt to form the rotor assembly. The top and the bottom discs were manufactured by overlapping multiple layers of composite tape, the tape being made of longitudinally extending and parallel fibers held together by the resin. Successive layers of the tape were oriented at $0°$, $+45°$, $-45°$ and finally $90°$ with respect to a pre-selected radius vector from the spin axis of the rotor. The pattern of orienting the tape was repeated until the tape was compiled in multiple layers to the preferred thickness of the top and bottom discs. The objective was to create a lightweight rotor in order to reduce the amount of kinetic energy stored in the high-speed rotor spinning at centrifuging speed. Consequently, owing to the light weight of the discs in the rotor assembly, the wear on the bearings and drive train was drastically reduced compared to the wear observed in the rotor made of heavy weight metallic discs.

Recently in 2018, Tremelling et al. [2] at ABB Research Ltd. in Zurich, patented rotors and hollow shafts made of fiber-reinforced composite materials for their use in various rotating machines. The suitable fibers for the fabrication of rotors and shafts included carbon, aramid (such

as Kevlar^{TM}), glass, polyester, polyethylene (such as Spectra^{TM}), quartz, boron and aluminum. In some applications, the shaft was fabricated using ultra-high modulus carbon fibers, i.e., carbon fibers having a modulus greater than 450 *GPa* or even 500 *GPa*. The suitable matrix materials for the fiber-reinforced composite rotors and shafts included inorganic and organic polymers, including thermoplastic and thermosetting resins (such as epoxides and other cross-linking polymer resins). In some applications, one or more filler materials (such as boron nitride or aluminum oxide) would be added in the matrix material to provide desired thermal, mechanical and electrical properties.

1.3 Stress analysis of rotating structures

Rotating discs are an integral part of all machinery, in automobile and aviation industries. High-performance light weight designs of rotating discs are required in several applications to achieve higher operating speeds. Depending on the application, rotating discs can have uniform thickness and/or linearly and non-linearly decreasing thickness along the radius of the disc. In some applications, the rotating discs with non-linear thickness variations have proven to be advantageous over linearly-tapered discs in terms of induced stresses and displacements in the disc. For instance, in the aerospace applications of rotating discs, the disc is simultaneously subjected to severe mechanical and thermal loads. A disc may be under internal pressure due to the shrink fit onto the mounting shaft. Also, an external load may be applied onto its outer edge via blades installed on the outer periphery of the disc.

When a disc rotates, it is subjected to radial and circumferential stresses, and the localization of these stresses degrades the stiffness and the strength of the disc thereby making the disc prone to various kinds of failure such as cracks and delamination in discs made of fiber-reinforced composite materials.

With the increasing use of orthotropic and composite materials in rotating discs, the stress analysis of the rotating discs has acquired the attention of many researchers. Detailed experimental and theoretical studies based on the linear elastic analysis of the rotating discs have been conducted globally. In any application, the stress and displacement analyses of the disc have to be conducted at the early stages of its design so as to determine the amounts of stresses experienced by the disc under various loading and boundary conditions, to locate the critically stressed points and to

prevent the accumulation of stress, which can cause severe damages resulting in the failure of the system. Therefore, studying the elastic behavior of rotating discs is one of the major interests of the researchers.

In the present thesis, stress and displacement analyses of thin annular uniform-thickness and thickness-tapered discs subjected to centrifugal loading and made of orthotropic and continuous fiber-reinforced composite materials are carried out for various boundary conditions of engineering interest. The influences of key parameters such as taper profiles, fiber orientation, radius ratio, laminate configuration, number of dropped plies and the arrangement of dropped plies on the in-plane stress distributions and on the radial displacement distribution in rotating annular discs are comprehensively studied and important design aspects are systematically brought out.

1.4 Rayleigh-Ritz method in stress analysis

The Rayleigh-Ritz method was introduced by Walter Ritz in 1911 and is an extension of the Rayleigh's method. It is an approximate method that can be used for the static and dynamic analyses of mechanical structures such as plates, shells, beams and discs etc. The method offers a convenient procedure for obtaining solutions to a boundary value problem based on the principle of minimum total potential energy. The basic idea behind the use of the Rayleigh-Ritz method is to approximate the displacement field of a structure by assuming a series of shape functions that are multiplied by constant coefficients. It is known that by assuming a definite number of terms in the displacement functions, a certain limitation on the deformed shape of the structure is imposed and hence, the results obtained for the stress distributions and natural frequencies in the static and dynamic analyses using the Rayleigh-Ritz method are often relatively higher than the results obtained for the same using the exact solutions.

Let $\psi_1(r)$, $\psi_2(r)$, … be a series of the function $\psi_N(r)$ that suitably represents *Y*, the deformed shape of the rotating disc. Therefore, we have

$$Y = q_1\psi_1(r) + q_2\psi_2(r) + \cdots + q_N\psi_N(r) \tag{1.1}$$

where, q_1, q_2, …, q_N are the constant coefficients that together with the assumed shape functions satisfy the geometric boundary conditions of the rotating disc and *N* is the total number

of terms in the assumed displacement function. For a rotating disc, approximate functions for the displacements in radial, circumferential and transverse directions are expressed in terms of algebraic polynomial series in cylindrical coordinate system.

Next, the total potential energy of the rotating disc, denoted by Π, is derived as the addition of the strain energy and the potential energy originated due to the centrifugal loading of the disc in terms of the assumed displacement functions. In order to have the approximation of the results for the elastic response obtained using the Rayleigh-Ritz method as close as possible to the exact solution, the obtained potential energy is minimized with respect to each set of assumed coefficients in displacement functions. i.e.,

$$\frac{\partial \Pi}{\partial q_N} = 0 \tag{1.2}$$

The above Equation (1.2) represents *N* number of algebraic equations that are solved to yield the values of the coefficients q_N, which are then used to obtain the required deformations and the stress distributions in the rotating disc.

The Rayleigh-Ritz method proves advantageous for the static and dynamic analyses of rotating structures over the finite element analysis using commercial FEA software such as ANSYS®, wherein the latter, the analysis is based on formal displacement formulation, and the differential stress-equilibrium equations and the compatibility equations are not always satisfied in the entire domain.

1.5 Literature Review

The analysis of the in-plane stress distributions and the radial displacement distribution in rotating annular uniform-thickness and thickness-tapered discs made of homogenous isotropic materials has been carried out in many textbooks [3, 4]. In this section, a detailed literature survey is presented to explore the contributions of researchers for analyzing the elastic response of rotating solid and annular uniform-thickness and thickness-tapered discs made of orthotropic and fiber-reinforced composite materials.

1.5.1 Rotating solid and annular orthotropic discs

At the early stage of research on orthotropic discs, Tang [5] presented closed-form analytical solutions to evaluate the radial and circumferential stresses in rotating uniform-thickness discs made of orthotropic materials for the cases of an unpierced disc, a disc with traction-free surfaces and a disc mounted on a rigid circular shaft having traction-free outer surface. He observed that there will be an infinite amount of radial stress induced at the center of a rotating solid disc, if the degree of orthotropy of the material of the disc is less than unity.

In the late 20th century, Reddy and Srinath [6] developed closed-form analytical solutions to study the effects of density, thickness parameter values and the degree of orthotropy on the in-plane stress distributions and radial displacement distribution in rotating annular discs having variable thickness and variable density along the radius of the disc. They obtained the variations of the radial and circumferential stresses and the radial displacement with the above-mentioned parameters for the case of rotating orthotropic discs with the free-free and the clamped-free boundary conditions. Chang [7] evaluated the elastic response of rotating uniform-thickness solid discs and solid cylinders made of general orthotropic materials based on the closed-form solutions. He proved that the induced radial and circumferential stresses in the rotating disc and cylinder are the functions of the radial coordinate only and also, the induced shear stress is equal to zero.

Kirkhope and Wilson [8] performed the static and the dynamic analyses of rotating annular parabolically-tapered and hyperbolically-tapered discs using the finite element method for the free-free boundary condition. They used annular finite elements, with each element having four degrees of freedom, to correctly estimate the stress state and the natural frequencies of the rotating annular thickness-tapered discs. They showed that by increasing the number of finite elements, the results obtained for the in-plane stresses and the non-dimensional frequency parameter match well with the results obtained for the same using the exact solutions.

Genta et al. [9] evaluated the elastic response of rotating annular uniform-thickness orthotropic discs with the free-free boundary condition using the principle of virtual work. They proved that a 7th degree polynomial in radial coordinates provides satisfactory results for the elastic response of rotating discs using the displacement methods. In another study, Genta and Gola [10] proposed closed-form analytical solutions to evaluate the elastic response of rotating solid and annular discs with the free-free boundary condition and made of a special kind of orthotropic

material, the elements of the compliance matrix of which satisfies the equation which was first proposed by De St. Venant [11] and Wolf [12].

Nigh and Olson [13] presented a finite element formulation for the stress and vibration analyses of thin rotating annular uniform-thickness discs made of structural steel material and with the traction-free boundary condition using triangular finite elements. For the static and dynamic analyses, they preferred the use of triangular finite elements over annular finite elements because of the ability of the former to be used in the case of non-axisymmetric geometry, for example - a split saw blade. Also, the centrifugal loading of the disc is considered as a pre-stress environment to calculate the natural frequencies of the rotating disc. Cookson and Sathianathan [14] developed closed-form analytical solutions based on the Filonenko-Borodich small displacement technique to study the effects of degree of orthotropy, Poisson's ratio and radius ratio values on the in-plane stress and displacement distributions in rotating annular uniform-thickness discs made of orthotropic materials with the traction-free boundary condition. Amada [15] studied the influence of acceleration on the induced in-plane shear stress and circumferential displacement in a rotating annular uniform-thickness disc made of an isotropic material with the clamped-free boundary condition. He obtained the solution to the boundary value problem using Laplace transformation in conjunction with the Cauchy's integral theorem and he concluded that for a disc accelerating exponentially with time, the induced in-plane shear stress varies cyclically as a sine function of time.

Guven [16] extended the work done by Reddy and Srinath [4] to observe the influences of the density and the thickness parameter values on the elastic-plastic stress distributions in rotating annular non-linearly-tapered discs having variable density along the radius of the disc for the free-free boundary condition. Ray and Sinha [17] proposed an analytical solution to evaluate the induced radial and circumferential stresses in a disc having variable thickness along its radius and subjected to centrifugal loading with various boundary conditions. They also developed a numerical procedure to optimize the taper profile of the disc by replacing the variable-thickness disc with a system of rings that are joined together at their respective faces, in order to lower the amount of induced stresses in the disc. Megahed and Kader [18] conducted the elastic-plastic stress analysis of a thin rotating annular uniform-thickness disc made of a non-linear strain hardening material which is shrink-fitted onto an elastic shaft. They developed a quasi-analytical solution to study the influence of hardening parameter values on the plastic hoop strain and on the induced

in-plane stresses in the rotating disc. They observed that the applicability of the developed quasi-analytical solution was limited to some specific values of the strain hardening parameter, whereas, an approximate solution, if employed for the same study, would have proved advantageous in studying the effect of the hardening parameter on the induced stresses in the disc.

Jain et al. [19] proposed a numerical procedure based on closed-form solutions to design a rotating annular uniform-thickness disc of uniform strength by radially tailoring the orthotropic elastic constants. They showed that a specific radial variation of the orthotropy parameter (which they defined as the ratio of the Young's modulus in the material principal direction 2 to the Young's modulus in the principal direction 1) leads to an equal amount of induced radial and circumferential stresses in the rotating orthotropic disc. They also verified the results obtained for the stress distributions using the proposed solution, with the results obtained for the same using finite element method. In another study, Jain et al. [20] examined stress singularities in thin rotating solid discs, shallow shells and conical shells made of polar orthotropic materials. They expressed the order of singularity by means of an analytical solution in terms of modified Bessel function with complex argument and compared the results obtained using the developed solution for the in-plane stress and displacement distributions with the results obtained for the same using finite element method. They observed that the order of singularity depends only on the degree of orthotropy of the material of the disc and/or the shells and that there is no stress singularity when the degree of orthotropy of the material is greater than or equal to unity.

Tutuncu [21] addressed the problem of instability in rotating solid and annular uniform-thickness discs made of orthotropic materials by including the radial displacement in the calculation of centrifugal force, which is not done in the classical approach to calculate the in-plane stresses in the rotating disc. He studied the influences of degree of orthotropy, Poisson's ratio and the radius ratio values on the critical rotational parameter of the rotating solid and annular discs and observed that the solid discs have a relatively lower value of the critical rotational parameter as compared to the annular discs with the clamped-free boundary condition. He also observed that the Poisson's ratio has a minimal effect on the stability of the rotating solid discs and that the increase in the radius ratio and the relative increase in the circumferential stiffness with respect to the radial stiffness, increases the stability of the rotating annular discs.

In the early 2000s, Zhou and Ogawa [22] evaluated the elastic response of rotating solid discs made of cubic anisotropic materials based on the direct displacement method by assuming

radial and circumferential displacements in terms of algebraic polynomial series in cylindrical coordinate system. Eraslan [23] obtained closed-form analytical solutions to investigate the elastic-plastic stress state of rotating annular non-linearly-tapered discs subjected to various boundary conditions of engineering interest. He observed that depending upon the boundary condition of the rotating annular thickness-tapered disc, the plastic core can contain one, two or three different plastic regions which are governed by different mathematical forms of the Tresca's yield criterion. Analytical and numerical methods to evaluate the elastic and residual stresses, and to observe the effects of degree of orthotropy and temperature distribution on the elastic-plastic stress state of rotating annular non-linearly-tapered discs were developed in the late 2000s by Kaya [24]. He showed that the degree of orthotropy of the material of the disc has a significant effect on the amounts of residual stresses in the rotating annular disc with a rigid inclusion.

Zenkour and Mashat [25] presented an exact solution and a modified Runge-Kutta numerical method to evaluate the elastic response of rotating annular exponentially-tapered discs made of orthotropic materials and with the free-free boundary condition. For the parametric studies, they considered convex and concave exponentially-tapered profiles of the thickness-tapered disc and they proved that the results obtained for the elastic response of exponentially-tapered discs using the modified Runge-Kutta method are in good agreement with the results obtained for the same using the analytical methods. Peng and Li [26] proposed a numerical solution to investigate the influence of degree of orthotropy on the in-plane stress distributions and on the radial displacement distribution in rotating annular functionally-graded polar orthotropic discs with various boundary conditions. They also studied the influences of the grading parameter of the principal elastic moduli and the density variation of the material according to the Voigt rule, on the elastic response of rotating annular functionally-graded orthotropic discs. Lately, Sondhi et al. [27] used the Galerkin's principle in conjunction with the Gram-Schmidt orthogonalization scheme to study the influence of grading parameters on the elastic response of rotating annular uniform-thickness discs made of functionally-graded orthotropic materials and with the free-free boundary condition.

Recently, Eraslan et al. [28] developed an analytical solution in terms of hypergeometric functions to estimate the elastic stress distributions and radial displacement distribution in rotating annular parabolically-tapered discs made of orthotropic materials and with a variety of boundary conditions, some of which include a disc with traction-free boundary condition and discs subjected

to internal and external pressure. The developed method could also be used to determine the limit angular speed of the rotating thickness-tapered orthotropic disc under a variety of boundary conditions.

Yildirim [29] proposed closed-form analytical solutions to determine the elastic response of rotating annular hyperbolically-tapered discs made of either a single homogenous isotropic material, or a single homogenous polar orthotropic material, or a heterogenous material formed by the combination of two functionally power-law graded orthotropic materials. He conducted an extensive research to observe the influences of elastic moduli grading parameters, values of the hyperbolic taper parameter and different orthotropic material properties on the in-plane stress distributions and on the radial displacement distribution in rotating annular thickness-tapered discs under a variety of boundary conditions. More recently, in another study, Yildirim [30] introduced a Complementary Functions Method (CFM) for the solution of the boundary value problem for the linear elastic analysis of rotating annular uniform-thickness discs made of orthotropic materials subjected to different boundary conditions. He showed that the results obtained for the elastic response using the CFM were in good agreement with the results obtained for the same using the closed-form solutions that have been proposed by him earlier.

1.5.2 Rotating solid and annular fiber-reinforced composite discs

In the past, an adequate amount of work has been done on the elastic analysis of rotating solid and annular uniform-thickness and thickness-tapered discs made of homogenous isotropic and orthotropic materials. Recently, researchers have put their attention into analyzing the elastic response of rotating solid and annular uniform-thickness and thickness-tapered discs made of fiber-reinforced composite materials.

At first, Bert [31] developed closed-form analytical solutions based on the Kirchhoff hypothesis for the elastic analysis of rotating uniform-thickness solid discs made of glass-fiber and graphite-fiber epoxy materials and having uni-directional, cross-ply and quasi-isotropic laminate configurations. He conducted an extensive parametric study to observe the effects of various laminate configurations and total number of 0° plies on the elastic response of quasi-isotropic and cross-ply laminated rotating solid discs respectively.

Tsuda et al. [32] performed the stress analysis of rotating annular uniform-thickness discs made of glass-fiber reinforced plastic material for the cases of radially-reinforced discs, discs reinforced in the direction tangent to the inner radius and circumferentially-reinforced discs. They obtained the stress variations and the allowable speeds of the discs with the above-mentioned types of reinforcement for the traction-free boundary condition. They also performed experimental spin tests to calculate the burst speed of the rotating annular uniform-thickness laminated disc with various kinds of reinforcement. Shiratori et al. [33] proposed two fiber reinforcing methods to increase the radial strength of a circumferentially-reinforced rotating annular uniform-thickness disc. One of the methods is to laminate filament wound discs on both sides of the circumferentially-reinforced disc and the other is to wind fibers of high specific elasticity around the fundamental (CR) disc. They also conducted the stress analysis of the proposed discs using the finite element method and compared the results obtained for the elastic response with the results obtained for the same using the lamination theory.

Gur and Stavsky [34] presented closed-form solutions to study the in-plane stress distributions in a rotating annular uniform-thickness symmetric laminated disc made of polar orthotropic materials for the traction-free, clamped-free and clamped-clamped boundary conditions. They also studied the effect of angular acceleration on the induced shear stress in the rotating laminated disc for the above-mentioned boundary conditions. Genta et al. [35] computed the stress distributions in rotating solid and annular conical discs made of graphite-epoxy composite material and with uni-directional laminate configurations.

Sitzer [36] studied the in-plane stress distributions in rotating annular uniform-thickness laminated discs made of heterogenous orthotropic materials under the action of a time-dependent loading and for the free-free boundary condition. He presented closed-form analytical solutions in terms of modified Bessel and Lommel functions to evaluate the radial and circumferential stress resultants acting on a rotating annular uniform-thickness laminated disc with various symmetrical laminate configurations. Lakshminarayana [37] performed the finite element analysis of rotating annular uniform-thickness fiber-reinforced composite discs for the free-free boundary condition using the TRIPLT finite element which is an acronym for a shear-flexible triangular laminated composite plate finite element. The element is defined by three nodes and 15 degrees of freedom at each node. He studied the influences of the fiber-reinforced composite material's properties and various laminate configurations, some of which include the uni-directional and cross-ply laminated

configurations, on the elastic response of rotating annular uniform-thickness laminated discs with the free-free boundary condition.

Carpino [38] developed a theoretical model to study the induced in-plane force resultants and moments, which in turn causes the ripple effect in an annular uniform-thickness laminated disc clamped at the inner radius and made of different orthotropic materials and is rotating at a high speed near a flat plate. He observed that the ripple at the outer edge of the rotating disc is a result of the variation of the density and material properties along the thickness of the laminated disc. Tutuncu [39] presented closed-form analytical solutions based on the Classical Laminate Theory in cylindrical coordinate system to determine the elastic response of rotating annular uniform-thickness symmetric cross-ply laminated discs for the clamped-free and the clamped-guided boundary conditions.

Hild and Leckie [40] analyzed the distribution of radial and circumferential stresses in rotating solid uniform-thickness discs made of fiber-reinforced ceramic matrix composite materials using finite element method. Using a one-dimensional study of fiber breaking modelled by a single damage variable, they derived a one-dimensional approach to the boundary value problem, which they then generalized into a 2-dimensional plane stress analysis with the alignment of fibers in 2 mutually perpendicular directions, based on a law of mixture in terms of the specific Helmholtz free energy. The model is then applied to determine the strength of rotating solid discs. Tutuncu and Durdu [41] determined the critical speeds as a function of the fiber orientation angle, of rotating solid and annular uniform-thickness discs made of graphite-epoxy (T300/5208) composite material and with constrained outer boundary. They obtained the expressions for the radial compressive stresses generated due to the centrifugal loading of the disc using standard cubic Hermite polynomials in one-dimensional finite element analysis. They observed that for the solid disc with constrained outer boundary, increasing the fiber orientation angle of the disc beyond a certain point decreases the stability of the disc, i.e., beyond a certain fiber orientation angle, the critical speed of the solid disc decreases with the increasing fiber orientation angle, and for the annular disc with clamped-guided boundary condition, the critical speed increases with the increasing value of the radius ratio of the disc.

Durodola and Attia [42] studied the relative influences of elastic moduli grading parameters, centrifugal and thermal loading on the in-plane stress and displacement distributions in rotating annular uniform-thickness discs made of Ti – 6Al – 4V metal matrix reinforced with

SiC long fibers along the circumferential direction. The major aim of their research work was to demonstrate the effect of non-uniform distribution of fibers on the induced thermal and mechanical stresses and the displacement in the rotating metal-matrix disc with the clamped-free boundary condition.

Arnold et al. [43] emphasized on the deformation and stress analysis of rotating solid and annular uniform-thickness discs made of fiber-reinforced composite materials and subjected to combined loading, i.e., discs simultaneously subjected to rotation, internal and external pressures, interfacial misfits and thermal loads. They presented analytical and numerical methods to study the influence of material anisotropy on the induced stresses and displacement in the rotating discs for the cases of a single disc and discs made by shrink-fitting *n* number of concentric rings. They also conducted an extensive parametric study to examine the influences of key design variables such as mean radius, thickness, composite material's properties, load gradation and rotational speed on the elastic response of rotating annular composite discs. Also, they determined the allowable limit speed of rotating annular uniform-thickness composite discs under monotonic and cyclic loading conditions. Tahani et al. [44] developed a semi-analytical method based on the layer wise theory in conjunction with Hamilton's principle for the deformation and three-dimensional stress analyses of rotating annular uniform-thickness discs made of cylindrically orthotropic nested rings for the free-free and the clamped-free boundary conditions. The disc considered for the static analysis is made of a Kevlar-epoxy ring which is shrink-fitted onto a S-2 glass-epoxy ring and that both rings are circumferentially wound. They concluded that due to discontinuity of the material properties, the stress field is three-dimensional at the interface of two rings.

Koo [45] performed the stress analysis of rotating annular uniform-thickness discs made of fiber-reinforced composite materials with the clamped-free boundary condition. He obtained the distribution of in-plane stress resultants for the composite discs with either radially or circumferentially aligned fibers and also calculated the maximum allowable speeds for the discs made of E-glass-epoxy, carbon-fiber reinforced polymer and polycarbonate material. Zenkour and Allam [46] developed analytical solutions for the in-plane stress and deformation analyses of rotating solid and annular exponentially-tapered discs made of viscoelastic fiber-reinforced composite materials subjected to various boundary conditions. The influences of the radial reinforcement and the circumferential reinforcement of the fibers, along with the values of the exponential taper parameter on the radial and circumferential stress distributions and on the radial

displacement distribution in rotating solid and annular exponentially-tapered fiber-reinforced composite disc are studied.

Callioglu et al. [47] investigated the elastic-plastic stress state of rotating annular uniform-thickness fiber-reinforced composite discs using analytical solutions based on the Airy's stress function approach for the free-free boundary condition. They used aluminum metal as a matrix and steel fibers as a reinforcement to study the elastic and plastic stress distributions in the fiber-reinforced composite disc. They also investigated the presence of residual stresses in the disc and observed that for the free-free boundary condition, the plastic yielding of the disc occurs at the inner boundary and hence, the residual stresses are found to be higher at the inner surface of the composite disc. Fabien [48] used the closed-form analytical solutions in conjunction with the Classical Laminate Theory to calculate the induced radial and circumferential stresses in a laminated flywheel operating under the traction-free boundary condition. In addition to determining the stresses in the flywheel, he used various failure theories to predict the burst speed of the flywheel and he concluded that to increase the failure speed of such fiber-reinforced composite structures, the radial plies should be laid out with a continuously varying fiber orientation angle along the radius of the disc.

In the late 2000s, Koo [49] performed an extensive research to observe the relative effects of 0° plies and the fiber-reinforced composite material's properties on the induced loads in the radial and circumferential directions of a rotating annular uniform-thickness cross-ply laminated disc with the clamped-free boundary condition. He developed closed-form solutions to determine the in-plane stress resultants and as an application of the developed solution, the maximum allowable rotating speeds of the cross-ply discs were obtained using the Tsai-Wu failure criterion. In another study, Koo and Lesieutre [50] proposed a bi-material disc, called as the fiber-reinforced composite-isotropic ring that proved advantageous in increasing the critical speed of the rotating discs. They constructed the bi-material disc using an isotropic material at the inner radius of the disc and a fiber-reinforced composite material at its outer circumference. Finite element method with Hermite interpolation functions was used to evaluate the in-plane stress distributions and to calculate the natural frequencies of the rotating bi-material disc.

Almasi [51] presented explicit analytical solutions based on the Taylor series expansion of the assumed 3D displacement functions in a rotating solid fiber-reinforced composite disc to determine the out-of-plane stresses, interlaminar stresses, transverse displacements and the stress

concentrations near the inner edge of the rotating laminated disc. He observed that the out-of-plane stresses in a rotating solid laminated disc becomes more and more localized with the increase in the diameter-to-thickness ratio of the solid disc. Zhou et al. [52] evaluated the stress and strain distributions in a rotating annular composite disc made of Carbon-fiber reinforced carbon-matrix composite material based on the Ritz method in conjunction with the Classical Laminate Theory in cylindrical coordinate system. They also performed the experimental spin tests of the C/C laminated discs for the cross-ply and the quasi-isotropic laminate configurations of the disc and calculated the burst speeds of the rotating laminated discs corresponding to the maximum shear stress failure theory.

More recently, Yildirim [53] introduced a Complementary Functions Method for the solution of the boundary value problem for the linear static analysis of rotating annular hyperbolically-tapered discs made of composite materials with both radially and circumferentially aligned fibers. He investigated the variation of various elastic fields such as the in-plane radial and circumferential stresses and the radial displacement with the values of the hyperbolic taper parameter and the fiber orientation angle of the composite disc. He concluded that regardless of the boundary condition and the rotating speed, the alignment of fibers along the radius of the disc, helps to minimize the amounts of in-plane stresses in the disc. He also disclosed the fact that for the rotating annular hyperbolically-tapered laminated discs with the clamped-free boundary condition, the fiber orientation angle has a significant effect on the location of Von-Mises equivalent stress in the disc.

1.6 Motivation and Objectives of the thesis

The presented literature survey mostly provides the insight on the elastic response of rotating solid and annular uniform-thickness and thickness-tapered discs made of isotropic, orthotropic and functionally-graded materials based on the closed-form analytical solutions for various boundary conditions. Apparently, there is little to no research work available that provides the up-to-date information on the elastic response of rotating annular thickness-tapered discs made of continuous fiber-reinforced composite materials.

The present work is highly motivated by the lack of adequate research works on the in-plane stress and displacement analyses of uniform-thickness and thickness-tapered discs made of fiber-reinforced laminated composite materials under various loading and boundary conditions.

The main objectives of the present thesis are as follows:

1. To evaluate the elastic response of rotating annular linearly-tapered and Stodola discs made of orthotropic materials using the sub-domain-wise application of the Rayleigh-Ritz method for the free-free and the clamped-free boundary conditions. Established is the accuracy of the developed formulation for the elastic response in terms of the number of divisions of the thickness-tapered disc.
2. To study the influences of the degree of orthotropy of the material of the disc, taper profiles and the values of the linear and Stodola taper parameters on the in-plane stress distributions and on the radial displacement distribution in rotating annular thickness-tapered discs made of orthotropic materials with the free-free and the clamped-free boundary conditions.
3. To evaluate the elastic response of rotating annular uniform-thickness and thickness-tapered discs made of fiber-reinforced composite laminated material using the Rayleigh-Ritz method in conjunction with the Classical Laminate Theory in cylindrical coordinate system for the clamped-free boundary condition. Verified are the results obtained for the elastic response using the Rayleigh-Ritz method with the results obtained using the FEA tool ANSYS®.
4. To conduct a comprehensive parametric study to examine the influences of fiber orientation, radius ratio values, rotational velocity, laminate configuration, number of dropped plies and the arrangement of dropped plies on the in-plane stress distributions and on the radial displacement distribution in rotating annular thickness-tapered fiber-reinforced composite discs considering the clamped-free boundary condition.

1.7 Scope of the thesis

The present thesis aims at developing a generalized formulation based on the Rayleigh-Ritz method to study the elastic response of annular uniform-thickness and thickness-tapered discs subjected to centrifugal loading and made of orthotropic and fiber-reinforced composite materials.

For the orthotropic discs, the distribution of in-plane stresses and displacements are obtained using the sub-domain-wise application of the Rayleigh-Ritz method in cylindrical coordinate system. The results obtained for the elastic response using the developed formulation are verified with the results obtained for the same using the existing closed-form analytical solutions and also with the solutions obtained using the FEA tool ANSYS®. Various orthotropic materials are chosen for the parametric study on the elastic response of rotating orthotropic discs with the traction-free and clamped-free boundary conditions. The influences of degree of orthotropy, taper profiles (linear and Stodola profiles in the present case) and the values of the taper parameters on the in-plane stress distributions and on the radial displacement distribution are thoroughly studied.

For the uniform-thickness and thickness-tapered fiber-reinforced composite discs, the distribution of in-plane stresses and displacements are obtained using the Rayleigh-Ritz method in conjunction with the Classical Laminae Theory (CLT) in cylindrical coordinate system. Three different kinds of three-dimensional internal taper configurations of the thickness-tapered fiber-reinforced composite discs are considered, namely, the taper configuration B (staircase arrangement of dropped plies), taper configuration C (overlapping continuous plies) and taper configuration D (continuous plies interspersed), and are modelled in ANSYS® ACP-Pre module. The results obtained for the elastic response of fiber-reinforced composite discs using the FEA tool ANSYS® are used to verify the results obtained for the same using the developed formulation based on the Rayleigh-Ritz method in conjunction with the Classical Laminate Theory in cylindrical coordinate system. The NCT-301 graphite-epoxy prepreg is chosen as a fiber-reinforced composite material and the influences of key parameters such as fiber orientation, radius ratio, rotational velocity, laminate configuration, ply reduction and internal taper configuration on the elastic response of rotating annular uniform-thickness and thickness-tapered fiber-reinforced composite discs are thoroughly examined considering the clamped-free boundary condition.

For the annular uniform-thickness and thickness-tapered discs made of orthotropic and fiber-reinforced composite materials, all numerical and symbolic calculations to determine the total potential energy of the rotating disc and subsequently to solve the boundary value problem using the Rayleigh-Ritz method are performed using the technical computing language MATLAB®.

1.8 Layout of the thesis

The present chapter provides brief introduction and literature survey on the elastic response of rotating solid and annular uniform-thickness and thickness-tapered discs made of orthotropic, functionally-graded and fiber-reinforced composite materials under various loading and boundary conditions.

In Chapter 2, the elastic response of rotating annular linearly-tapered and Stodola discs made of orthotropic materials is obtained using a computational solution based on the Rayleigh-Ritz method with finite-element-like modification for various boundary conditions. A numerical procedure is developed to model the linear taper and Stodola taper profiles of the thickness-tapered disc. The accuracy of the developed formulation for the elastic response of thickness-tapered orthotropic discs is established based on the convergence of the results obtained for the elastic response using the sub-domain-wise application of Rayleigh-Ritz method in terms of the number of divisions of the thickness-tapered disc, to the results obtained using closed-form analytical solutions available in the literature. The results obtained for the elastic response using the developed formulation are also compared with the results obtained using the SHELL181 and SOLID185 elements in ANSYS®. A parametric study is conducted to investigate the effects of the degree of orthotropy, taper profile and taper parameter values on the in-plane stress distributions and radial displacement distribution in the rotating annular thickness-tapered orthotropic discs for the free-free and clamped-free boundary conditions.

Chapter 3 presents the generalized formulation to determine the elastic response of rotating annular uniform-thickness discs made of fiber-reinforced composite materials by using the Rayleigh-Ritz method in conjunction with the Classical Laminate Theory (CLT) in cylindrical coordinate system. The total potential energy of the rotating disc is derived in terms of the laminate stiffness matrix of the fiber-reinforced composite material. The results obtained for the elastic response of rotating annular uniform-thickness fiber-reinforced composite discs considering the clamped-free boundary condition using the developed formulation are compared with the results obtained for the same using the SHELL181 and SOLID185 elements in ANSYS®. A comprehensive parametric study is conducted to investigate the effects of fiber orientation, radius ratio values, rotational velocity and laminate configuration on the in-plane stress distributions and

the radial displacement distribution in rotating annular uniform-thickness fiber-reinforced composite discs considering the clamped-free boundary condition.

In Chapter 4, the formulation developed in Chapter 3 is re-employed to determine the elastic response of rotating annular thickness-tapered fiber-reinforced composite discs with the clamped-free boundary condition. The total potential energy of the rotating thickness-tapered disc is derived by the addition of the potential energy of the fiber-reinforced plies and the potential energy of the resin pockets. The finite element modeling of the rotating annular thickness-tapered fiber-reinforced composite disc with the clamped-free boundary condition for various internal taper configurations is carried out in ANSYS® R19.2. Considering the clamped-free boundary condition, a comprehensive parametric study is conducted to investigate the effects of fiber orientation, radius ratio values, number of dropped plies, arrangement of dropped plies and the laminate configuration on the in-plane stress distributions and the radial displacement distribution in rotating annular thickness-tapered fiber-reinforced composite discs.

Chapter 5 brings the thesis to its end by providing the prime conclusions of the present research work and by providing some recommendations for the future work.

Chapter 2

Elastic response of rotating annular thickness-tapered discs made of isotropic and orthotropic materials

2.1 Introduction

Rotating discs are an integral part of all machines. High-performance light weight designs of rotating discs are required in several applications to achieve higher operating speeds. Thus, the increasing demand for the realistic stress analysis of such structural components in turbomachinery and automotive applications necessitates the development of robust models and their solution techniques.

This chapter presents the generalized formulation to determine the elastic response of rotating annular thickness-tapered discs by using the Rayleigh-Ritz method with finite-element-like modification. The radial deformations and the radial and circumferential stresses in rotating tapered disc made up of isotropic or orthotropic materials with the free-free and the clamped-free boundary conditions are computed. In the present chapter, two kinds of tapered disc are considered: linearly-tapered disc and Stodola disc. In all of the parametric studies for the rotating disc, four different materials are considered, the material properties of which are given in the Table 2.3. Effects of different taper profiles on the stress distributions in the rotating disc with the free-free and the clamped-free boundary conditions are studied. The obtained Rayleigh-Ritz solutions for the elastic response are compared with the results obtained for the same using closed-form analytical solutions that are available in the literature and also with the solutions obtained using the finite element analysis software ANSYS®.

2.2 Modelling

The basic approach in FEM (Finite Element Method) is to solve a complicated problem by replacing it with a corresponding simpler one. Specifically, the entire domain of the problem is represented as an assemblage of smaller units called as the finite elements that are joined together. These elements are inter-connected at the boundaries with the neighboring elements. These joints are referred to as nodes.

For the structural analysis of any mechanical component, each of the field variables of interest, the radial and circumferential displacements in the present case, is assumed inside a finite element using simple approximation functions. These functions can be represented as a linear combination of constant coefficients with the algebraic displacement terms in the polar coordinate system. The functions are such that they satisfy at least the geometric boundary conditions of the structure under consideration.

To derive the necessary equations, the Lagrange functional (total potential energy of the rotating tapered disc in the present case) is minimized with respect to each nodal unknown coefficient. This way, the finite element method can be summarized as an element-wise application of the Rayleigh-Ritz method.

In the present numerical procedure, the entire domain of the tapered disc is divided into sub-domains, as in the case of finite element method. Further, an approximate solution is developed over the entire domain of the tapered disc, not just over each element as in the case of Finite Element Method. Hence this approach leads to the use of lesser number of terms in the assumed displacement functions that are required to determine the elastic response of rotating annular tapered discs.

Consider an annular linearly-tapered disc as shown in the Figure 2.1(a). r_i and r_o represent the inner and the outer radii of the linearly-tapered disc respectively and, h_i and h_o represent the thicknesses of the disc at the hub and at the free end respectively.

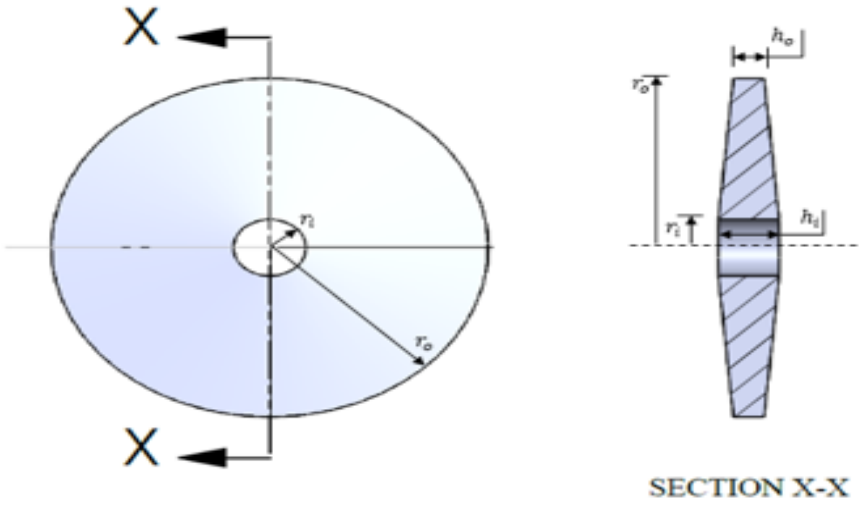

Figure 2.1(a) Annular linearly-tapered disc

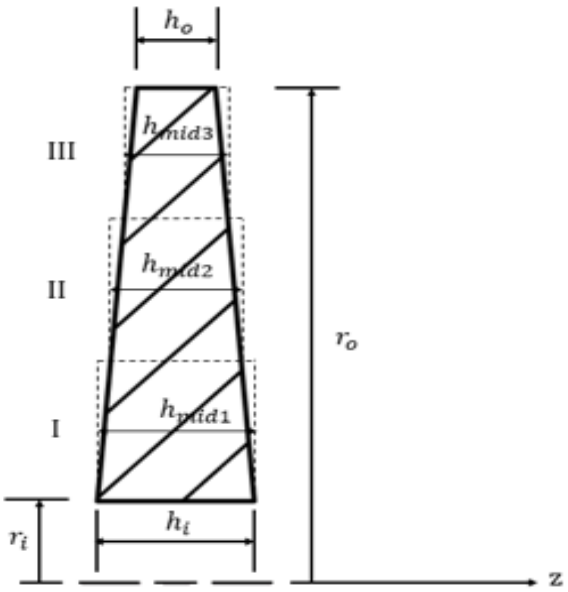

Figure 2.1(b) Upper half view of the diametral cross section X-X of the linearly-tapered disc

The tapered disc can be divided into a number of divisions, say '*N*', where *N* is a positive integer. For illustrative purpose, in the above Figure 2.1(b), the linearly-tapered disc is divided into 3 divisions represented by the numbers I, II and III respectively, each having an equal size along the radial direction. Further, h_{mid1}, h_{mid2} and h_{mid3} are the thicknesses at the mid-plane of each division respectively.

In order to use the Rayleigh-Ritz method, the total potential energy of the rotating annular tapered disc, which is the sum of the strain energy and the work potential of the centrifugal force, must be formulated. In the present approach, the strain energy and the work potential are calculated for each division, keeping the assumed displacement functions global over the entire domain of the disc. Later, the energies are added in order to derive the total potential energy of the rotating tapered disc.

2.2.1 Modelling the taper profile of the disc

As discussed previously in the section 2.2, the rotating annular tapered disc can be divided into a number of divisions, each having an equal size along the radius of the disc. Therefore, each division has its own geometric properties. The strain energy and the work potential are determined for each division by integrating the energies of the infinitesimal volume element of each division

considering the geometric properties of the respective division [54]. For calculating the geometric properties of each division, the following procedure has been implemented:

The inner and the outer radii of each division are calculated using:

$$R_i^N = r_i + (N-1)L_r \tag{2.1}$$

$$R_o^N = r_i + (N)L_r \tag{2.2}$$

where, N is the number of divisions, $N \in Z^+$ (positive integer), R_i^N and R_o^N are the inner and the outer radial distance of the N^{th} division from the center of the disc and L_r is the length of each division given along the radial direction of the disc.

$$L_r = \frac{(r_o - r_i)}{N} \tag{2.3}$$

The thickness at the middle plane of the N^{th} division can be calculated as:

$$h_{midN} = \frac{H_i^N + H_o^N}{2} \tag{2.4}$$

where, H_i^N and H_o^N are the thicknesses at the inner and the outer surfaces of the respective division i.e., the thicknesses at the inner and the outer radii (R_i^N and R_o^N respectively) of the respective division. Owing to different taper profiles, the thickness at the outer radial distance of each division is modelled differently for each profile, as represented in the following Table 2.1.

Type of disc	Thickness Profile	Thickness at the outer radial distance of N^{th} division
Linearly-tapered disc	$h(r) = h_i\left[1 - n\frac{(r - r_i)}{r_o}\right]$	$H_o^N = h_i\left[1 - n\left(\frac{R_o^N - r_i}{r_o}\right)\right]$
Stodola disc	$h(r) = h_i\left[\frac{r_i}{r}\right]^s$	$H_o^N = h_i\left[\frac{r_i}{R_o^N}\right]^s$

Table 2.1 Thickness profiles for linearly-tapered disc and Stodola disc

In the above Table 2.1, n and s are the taper parameters for the linearly-tapered disc and Stodola disc respectively. The domain of the taper parameters n and s is [0,1], where 0 represents

the uniform-thickness disc. Thus, the thickness at the inner radius for each division is equal to the thickness at the outer radius of the previous division. i.e.,

$$H_i^N = H_o^{(N-1)} \tag{2.5}$$

2.2.2 Formulation for strain energy

Strain energy is the energy stored inside the body due to deformation. If the form for the strain energy of any material is known, then the stress-strain relationship for that material may be deduced. Conversely, if the stress-strain relationship of the material is known, then so is the form of strain energy. There is a non-zero contribution to the strain energy stored in a deformable body only if the body bends, stretches or otherwise deforms. If it rotates or translates like a rigid body without deforming, then these displacements will not contribute to the strain energy of the body. In measuring the displacements of particles in the body, it is imperative to measure them with respect to the translated and/or rotated rigid body motion. This is accomplished by fixing a coordinate frame to the body. The translation and rotation of this body-fixed frame describes the rigid body motions of the body. Displacements with respect to this frame then contribute to the strain energy stored in the body [55].

Figure 2.2 shows an annular uniform-thickness disc with the cylindrical coordinate system and rotating at a constant angular velocity ω. r_i and r_o are the inner and the outer radii of the circular disc respectively and h is the thickness of the rotating disc.

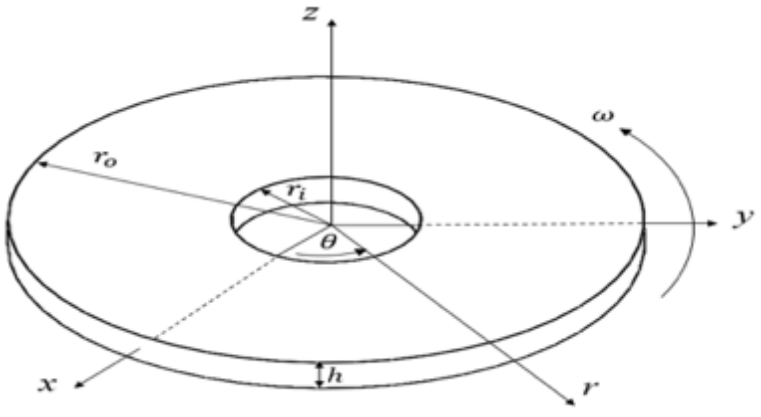

Figure 2.2 Rotating annular uniform-thickness disc and the cylindrical coordinate system

The strain energy per unit volume (i.e., the strain energy density) of the disc is denoted by U_o and is given as:

$$U_o = \frac{1}{2}[\sigma][\varepsilon] \tag{2.6}$$

where, $[\sigma]$ represents the stress matrix that contains radial stress, circumferential stress and in-plane shear stress and $[\varepsilon]$ represents the strain matrix containing the corresponding strains. Small strains are assumed so that the stress-strain relationship is linear. Note that this indicates only that the strains are small and not the displacements. For a thin rotating disc, plane stress condition is assumed. i.e., $\sigma_{rz} = \sigma_{zz} = \sigma_{\theta z} = 0$. Integrating Equation (2.6) over the entire volume of the disc, the total strain energy of the disc can be calculated. This way, the total strain energy of the uniform-thickness disc can be given as:

$$U = \frac{1}{2}\int_{\frac{-h}{2}}^{\frac{h}{2}}\int_{0}^{2\pi}\int_{r_i}^{r_o}[\sigma_{rr} \quad \sigma_{\theta\theta} \quad \tau_{r\theta}]\begin{Bmatrix}\varepsilon_{rr}\\ \varepsilon_{\theta\theta}\\ \gamma_{r\theta}\end{Bmatrix} r.dr.d\theta.dz \tag{2.7}$$

where, U is the strain energy of the uniform-thickness disc, σ_{rr}, $\sigma_{\theta\theta}$ and $\tau_{r\theta}$ are the radial stress, circumferential stress and the in-plane shear stress respectively, and ε_{rr}, $\varepsilon_{\theta\theta}$ and $\gamma_{r\theta}$ are the corresponding strains.

Nowadays, engineers are focused on orthotropic materials, the material properties of which vary along its principal material directions. These materials have high strength-to-weight ratio and outstanding mechanical properties. This section deals with the formulation for the total strain energy for the cases of rotating annular linearly-tapered disc and Stodola disc made up of orthotropic material.

In the present formulation, the principal material coordinate system has been used. The axis 1 is aligned along the radial direction of the disc and the axis 2 is in the plane of the uniform-thickness disc and is also perpendicular to the radial direction. The axis 3 coincides with the z-axis of the rotating disc.

Recalling the strain energy obtained for the case of rotating uniform-thickness disc from Equation (2.7), it can be rewritten as:

$$U_{ortho}^{uni} = \frac{1}{2}\int_{\frac{-h}{2}}^{\frac{h}{2}}\int_{0}^{2\pi}\int_{r_i}^{r_o}[\sigma_1 \quad \sigma_2 \quad \tau_{12}]\begin{Bmatrix}\varepsilon_1\\ \varepsilon_2\\ \gamma_{12}\end{Bmatrix} r.dr.d\theta.dz \tag{2.8}$$

where, U_{ortho}^{uni} is the total strain energy of the uniform-thickness orthotropic disc, σ_1, σ_2 and τ_{12} are the stresses in the principal material directions 1 and 2, and ε_1, ε_2 and γ_{12} are the corresponding strains.

For the orthotropic materials, the stress-strain relations for the case of plane stress are given as:

$$\begin{Bmatrix}\sigma_1\\ \sigma_2\\ \tau_{12}\end{Bmatrix} = \begin{bmatrix}Q_{11} & Q_{12} & 0\\ Q_{12} & Q_{22} & 0\\ 0 & 0 & Q_{66}\end{bmatrix}\begin{Bmatrix}\varepsilon_1\\ \varepsilon_2\\ \gamma_{12}\end{Bmatrix} \tag{2.9}$$

where, Q_{ij} $i, j = 1, 2$ and 6 are the elements of the reduced stiffness matrix of the orthotropic material given as:

$$Q_{11} = \frac{E_1}{1-\nu_{12}\nu_{21}} \qquad Q_{22} = \frac{E_2}{1-\nu_{12}\nu_{21}}$$
$$Q_{12} = \frac{\nu_{12}E_2}{1-\nu_{12}\nu_{21}} \qquad Q_{66} = G_{12} \tag{2.10}$$

In the Equation (2.10), E_1 and E_2 are the Young's modulus of the orthotropic material in the principal material directions 1 and 2 respectively, ν_{12} and ν_{21} are the major and minor Poisson's ratios of the orthotropic material respectively and G_{12} is the in-plane shear modulus. The strain-displacement relations in cylindrical coordinate system are written as:

$$\varepsilon_1 = \frac{du_1(r)}{dr} \tag{2.11}$$

$$\varepsilon_2 = \frac{u_1(r)}{r} \tag{2.12}$$

$$\gamma_{12} = \left(\frac{du_2(r)}{dr} - \frac{u_2(r)}{r}\right) \tag{2.13}$$

where, $u_1(r)$ and $u_2(r)$ are the displacements of the rotating disc in the principal material directions 1 and 2 respectively. Substituting Equations (2.9) - (2.13) into the Equation (2.8), the total strain energy of a rotating annular uniform-thickness disc made up of orthotropic material can be given as:

$$U_{ortho}^{uni} = \frac{1}{2}\int_{\frac{-h}{2}}^{\frac{h}{2}}\int_{0}^{2\pi}\int_{r_i}^{r_o}\left\{\left[Q_{11}\left(\frac{du_1(r)}{dr}\right)^2\right]+\left[2Q_{12}\left(\frac{u_1(r)}{r}\right)\left(\frac{du_1(r)}{dr}\right)\right]+\left[Q_{66}\left(\frac{du_2(r)}{dr}-\frac{u_2(r)}{r}\right)^2\right]+\left[Q_{22}\left(\frac{u_1(r)}{r}\right)^2\right]\right\}r.dr.d\theta.dz \tag{2.14}$$

In order to obtain the strain energy of a rotating annular tapered disc, the above Equation (2.14) is modified i.e., unlike in the case of a rotating annular uniform-thickness disc, where the strain energy density given in the Equation (2.6) is integrated over the entire volume of the disc given in the Equation (2.8), the strain energy density is now integrated considering the geometric properties of each division and then the strain energies of all the division are added together in order to get the total strain energy of the tapered disc. i.e.,

$$\begin{aligned} U_{ortho}^{tapered} = {} & \frac{1}{2}\int_{\frac{-h_{mid1}}{2}}^{\frac{h_{mid1}}{2}}\int_{0}^{2\pi}\int_{R_i^1}^{R_o^1}\left\{\left[Q_{11}\left(\frac{du_1(r)}{dr}\right)^2\right]+\left[2Q_{12}\left(\frac{u_1(r)}{r}\right)\left(\frac{du_1(r)}{dr}\right)\right]+\left[Q_{66}\left(\frac{du_2(r)}{dr}-\frac{u_2(r)}{r}\right)^2\right]+\left[Q_{22}\left(\frac{u_1(r)}{r}\right)^2\right]\right\}r.dr.d\theta.dz \\ & + \\ & \frac{1}{2}\int_{\frac{-h_{mid2}}{2}}^{\frac{h_{mid2}}{2}}\int_{0}^{2\pi}\int_{R_i^2}^{R_o^2}\left\{\left[Q_{11}\left(\frac{du_1(r)}{dr}\right)^2\right]+\left[2Q_{12}\left(\frac{u_1(r)}{r}\right)\left(\frac{du_1(r)}{dr}\right)\right]+\left[Q_{66}\left(\frac{du_2(r)}{dr}-\frac{u_2(r)}{r}\right)^2\right]+\left[Q_{22}\left(\frac{u_1(r)}{r}\right)^2\right]\right\}r.dr.d\theta.dz \\ & + \ldots\ldots\ldots\ldots\ldots\ldots\ldots + \end{aligned} \tag{2.15}$$

$$\frac{1}{2}\int_{\frac{-h_{midN}}{2}}^{\frac{h_{midN}}{2}}\int_{0}^{2\pi}\int_{R_i^N}^{R_o^N}\left\{\left[Q_{11}\left(\frac{du_1(r)}{dr}\right)^2\right]+\left[2Q_{12}\left(\frac{u_1(r)}{r}\right)\left(\frac{du_1(r)}{dr}\right)\right]\right.$$
$$\left.+\left[Q_{66}\left(\frac{du_2(r)}{dr}-\frac{u_2(r)}{r}\right)^2\right]+\left[Q_{22}\left(\frac{u_1(r)}{r}\right)^2\right]\right\}r.dr.d\theta.dz$$

The above Equation (2.15) represents the strain energy of a rotating annular tapered disc made up of orthotropic material. The above formulation for the strain energy can also be used for rotating annular uniform-thickness disc, as a special case (by putting the values of the taper parameters *n* and/or *s* equal to zero resulting in $H_i^N = H_o^N = h_i$ and therefore, $h_{mid1} = h_{mid2} = h_{midN} = h_i$), and also for the disc made up of isotropic material, as another special case (by putting $E_1 = E_2$ which results in $\nu_{12} = \nu_{21}$ and hence, $Q_{11} = Q_{22}$).

2.2.3 Formulation for work potential of applied forces

It is confirmed from the formulation developed in sub-section 2.2.2 that, the strain energies of a rotating disc and a stationery disc are the same, as the strain energy is independent of the angular velocity of rotation ω. Upon rotation at a constant angular velocity, the disc experiences a work potential due to the body forces caused by centrifugal action.

For an infinitesimal element of the rotating disc, the work potential can be given as [52]:

$$V_{element} = -\rho r\omega^2 u_1(r) \tag{2.16}$$

where, ρ is the density of the material of the disc. Integrating Equation (2.16) over the entire volume of the disc, the total work potential (i.e., the potential energy originated from the centrifugal loading), V_{ortho}^{uni} of the rotating annular uniform-thickness disc is given as:

$$V_{ortho}^{uni} = -h\int_{\frac{-1}{2}}^{\frac{1}{2}}\int_{0}^{2\pi}\int_{r_i}^{r_o}\rho r\omega^2 u_1(r)r.dr.d\theta.dz \tag{2.17}$$

Similar to the formulation developed for the strain energy in sub-section (2.2.2), the work potential of the applied centrifugal force is calculated for each division and then added in order to get the total work potential of the rotating tapered disc. i.e.,

$$V_{ortho}^{tapered} = -h_{mid1}\int_{\frac{-1}{2}}^{\frac{1}{2}}\int_{0}^{2\pi}\int_{R_i^1}^{R_o^1}\rho r\omega^2 u_1(r) r.dr.d\theta.dz$$

$$-h_{mid2}\int_{\frac{-1}{2}}^{\frac{1}{2}}\int_{0}^{2\pi}\int_{R_i^2}^{R_o^2}\rho r\omega^2 u_1(r) r.dr.d\theta.dz \qquad (2.18)$$

$$\ldots\ldots\ldots\ldots$$

$$-h_{midN}\int_{\frac{-1}{2}}^{\frac{1}{2}}\int_{0}^{2\pi}\int_{R_i^N}^{R_o^N}\rho r\omega^2 u_1(r) r.dr.d\theta.dz$$

The above Equation (2.18) represents the work potential of a rotating annular tapered disc. The above formulation for the potential energy originated from the centrifugal loading can also be used for rotating annular uniform-thickness disc, as a special case (by putting the values of the taper parameters *n* and/or *s* equal to zero resulting in $H_i^N = H_o^N = h_i$ and therefore, $h_{mid1} = h_{mid2} = h_{midN} = h_i$).

2.2.4 Solution by Rayleigh-Ritz method

As an alternate to the methods based on differential equations, the analysis of stress and deformation can be accomplished through the use of energy methods. The Rayleigh-Ritz method offers a convenient procedure for obtaining solutions by the principle of minimum potential energy [4]. To use this method, it is necessary to represent the deformed shape of the structure by assuming a series of shape functions that are multiplied by constant coefficients. The assumed functions should be such that they satisfy at least the geometric boundary conditions of the structure to be analyzed, and also these functions describe any end constraints pertaining to deflection and slopes. Another kind of condition, a static boundary condition, which equates the internal forces (and moments) at the edges of the member to prescribed external forces (and moments), need not to be

fulfilled. Next, the potential energy of the structure is determined in the terms of constant coefficients that are multiplied with the shape functions. This indicates that the constant coefficients govern the variation of the total potential energy.

Let the displacements in the principal material directions be expressed in terms of algebraic polynomial series in polar coordinates given as:

$$u_1(r) = n_r \sum_{j=0}^{m_1} a_j r^j \tag{2.19}$$

$$u_2(r) = n_\theta \sum_{j=0}^{m_2} b_j r^j \tag{2.20}$$

where, n_r and n_θ are the constraint functions that together with the assumed shape functions satisfy the geometric boundary conditions. a_j and b_j are the constant coefficients and r is the radial coordinate. m_1 and m_2 are the total number of terms required in the assumed displacement functions in the principal material directions 1 and 2 respectively to correctly estimate the elastic response of the rotating disc with $m_1, m_2 \in Z^+$ (positive integer).

The following Table 2.2 shows the constraint functions used for the free-free and the clamped-free boundary conditions.

Constraint Function	Free-Free	Clamped-Free
$n_r = n_\theta$	1	$(r - r_i)$

Table 2.2 Constraint functions for the free-free and clamped-free boundary conditions

The total potential energy of the rotating annular tapered disc denoted by $\Pi_{tapered}$ is the sum of the strain energy and the work potential of the centrifugal force derived in Equations (2.15) and (2.18) respectively. i.e.,

$$\Pi_{tapered} = U_{ortho}^{tapered} + V_{ortho}^{tapered} \tag{2.21}$$

The obtained potential energy is then minimized with respect to each set of assumed coefficients in the radial and circumferential displacement functions so as to obtain the closest approximation of the elastic response of the rotating annular tapered disc made up of orthotropic or isotropic materials. i.e.,

$$\frac{\partial \Pi_{tapered}}{\partial a_j} = 0 \tag{2.22}$$

$$\frac{\partial \Pi_{tapered}}{\partial b_j} = 0 \tag{2.23}$$

The above Equations (2.22) and (2.23) represent a set of algebraic equations that are solved to yield the coefficients a_j and b_j. A MATLAB® code is developed to determine the values of these coefficients, which are then used to obtain the required deformations and the stress distributions in the rotating annular tapered discs made up of isotropic or orthotropic material with the free-free and clamped-free boundary conditions.

2.3 Verification

In this section, the elastic response obtained using the Rayleigh-Ritz method based on the potential energy of the rotating annular tapered disc made up of isotropic or orthotropic material with the free-free and the clamped-free boundary conditions is verified with the response obtained for the same using closed-form analytical solutions that are available in the literature as well as with the solution obtained using the finite element analysis software ANSYS®. Four different materials are considered for the elastic analysis of rotating annular tapered discs, the material properties of which are given below in the following Table 2.3.

Mechanical Property	MAT-1	MAT-2	MAT-3	MAT-4
	Polycarbonate [29]	Glass-Fiber Reinforced Plastic [29]	Graphite-Fiber Reinforced Plastic (NCT-301) [29]	Nylon6 composite* [30]
E_1 *(GPa)*	2.20	28.6	113.9	12.0
E_2 *(GPa)*	2.20	8.27	7.98	20.0
ν_{12}	0.30	0.26	0.288	0.21
$\rho(Kg/m^3)$	1220	1800	1480	1600
λ	1.0	0.289	0.07	1.67

Table 2.3 Mechanical properties of different materials considered

* E_2 of an injection molded Nylon6 composite material containing 40wt% short glass fibers is greater than E_1 [30]. In the above Table 2.3, λ is the degree of orthotropy of the material, given as $\lambda = \frac{E_2}{E_1}$.

The rotating disc has an inner radius of r_i = 24 *mm*, an outer radius of r_o = 120 *mm*, and thickness at the hub of the disc h_i = 2.4 *mm* and it is rotating at a constant angular velocity of ω = 1000 *rad/s* i.e., 9554.14 *rpm*. The following results for the elastic response of the rotating annular tapered discs are compared:

a) The elastic response of a rotating annular linearly-tapered-disc made up of Graphite-fiber reinforced plastic material NCT-301 [29] and with the free-free boundary condition obtained using the Rayleigh-Ritz method is verified with the response obtained for the same using the closed-form analytical solution available in the literature.

b) The elastic response of a rotating annular Stodola disc made up of Graphite-fiber reinforced plastic material NCT-301 with the clamped-free boundary condition obtained using the Rayleigh-Ritz method is verified with the response obtained for the same using the closed-form analytical solution available in the literature.

c) The elastic response of a rotating annular uniform-thickness disc made up of Polycarbonate material [29] and with the clamped-free boundary condition obtained using the Rayleigh-Ritz method is verified with the response obtained for the same

using the closed-form analytical solutions available in the literature as well as with the solutions obtained using the finite element analysis software ANSYS® (using SOLID185 and SHELL181 elements).

The following Table 2.4 shows the values of the thickness reduction ratios $\bar{h}$ (which is the ratio of the thickness of the disc at its outer circumference, h_o, to the thickness of the disc at the hub, h_i, i.e., $\bar{h} = \frac{h_o}{h_i}$) for the linearly-tapered disc and Stodola disc considered corresponding to their taper parameters *n* and *s* respectively.

Linearly-tapered disc		Stodola disc	
Taper parameter (n)	Thickness reduction ratio ($\bar{h}$)	Taper parameter (s)	Thickness reduction ratio ($\bar{h}$)
0	1.0	0	1.0
0.2	0.8333	0.2	0.7083
0.4	0.6667	0.4	0.5417
0.6	0.50	0.6	0.3807
0.8	0.36	0.8	0.2759
1.0	0.20	1.0	0.20

Table 2.4 Thickness reduction ratios corresponding to taper parameters for the linearly-tapered and Stodola discs

In the above Table 2.4. the taper parameters *n* and *s* equal to zero, corresponds to the uniform-thickness disc. Note that corresponding to the taper parameters value of 1, the value of the thickness reduction ratio ($\bar{h}$) is the same for both of the linearly-tapered and Stodola discs. The dissimilarity in the values of the thickness reduction ratio for the same taper parameter value of both the discs in the interval [0.2, 0.8] is due to their taper profile.

The following Table 2.5 shows the comparison of the results obtained using the Rayleigh-Ritz method for the radial and circumferential stress distributions and the radial displacement distributions for a rotating annular linearly-tapered disc with the free-free boundary condition, with the results obtained for the same using the closed-form analytical solutions that are available in

the literature. The comparison is done for a linearly-tapered disc with a taper parameter value of n = 0.4 and made up of Graphite-Fiber Reinforced Plastic material (NCT-301).

Rotating annular linearly-tapered orthotropic disc made up of Graphite-Fiber Reinforced Plastic material (NCT-301) and with the free-free boundary condition						
n = 0.4			$\bar{h}$ = 0.6667			
Radial distance in *mm* from the center of the disc	σ_r (in MPa)		σ_θ (in MPa)		u_r (in mm)	
	R-R Solution	Closed-form Solution [28]	R-R Solution	Closed-form Solution [28]	R-R Solution	Closed-form Solution [28]
24.0	4.47e-08	0.00	19.0198	18.7528	0.057176	0.05715
33.6	4.1698	4.2380	13.6216	13.4396	0.057	0.0567
43.2	5.7254	5.6101	10.6700	10.5253	0.057137	0.05713
52.8	6.0217	5.9043	8.7972	8.6772	0.057403	0.05739
62.4	5.7138	5.6825	7.4947	7.3940	0.057704	0.057701
72.0	5.1530	5.1612	6.5315	6.4452	0.057993	0.057999
81.6	4.4540	4.4335	5.7863	5.7098	0.05825	0.058194
91.2	3.5947	3.5414	5.1875	5.1182	0.058457	0.058457
100.8	2.5253	2.5029	4.6898	4.6275	0.058597	0.05859
110.4	1.2815	1.3233	4.2652	4.2097	0.05865	0.05865
120.0	1.05e-11	0.00	3.8994	3.8456	0.058607	0.058606
Average % difference	1.127		1.344		0.067	

Table 2.5 Comparison of the distribution of the radial and circumferential stresses and the radial displacement distributions in a rotating annular linearly-tapered disc made up of Graphite-Fiber Reinforced Plastic material (NCT-301) and with the free-free boundary condition for n = 0.4

The following Table 2.6 shows the comparison of the results obtained using the Rayleigh-Ritz method for the radial and circumferential stress distributions and the radial displacement distributions in a rotating annular Stodola disc with the clamped-free boundary condition, with the results obtained for the same using the closed-form analytical solutions that are available in the literature. The comparison is done for a Stodola disc with a taper parameter value of s = 0.4 and made up of Graphite-Fiber Reinforced Plastic material (NCT-301).

Rotating annular Stodola disc made up of Graphite-Fiber Reinforced Plastic material (NCT-301) and with the clamped-free boundary condition						
s = 0.4			$\bar{h}$ = 0.5417			
Radial distance in *mm* from the center of the disc	σ_r (in *MPa*)		σ_θ (in *MPa*)		u_r (in *mm*)	
	R-R Solution	Closed-form Solution [29]	R-R Solution	Closed-form Solution [29]	R-R Solution	Closed-form Solution [29]
24.0	19.5834	19.4024	0.3951	0.3911	0	0
33.6	15.6134	15.6472	0.6607	0.6600	0.001455	0.001452
43.2	13.0799	13.1139	0.7517	0.7521	0.002641	0.002639
52.8	11.1404	11.1262	0.7750	0.7745	0.003641	0.00364
62.4	9.4247	9.4068	0.7640	0.7633	0.004488	0.004486
72.0	7.8130	7.8188	0.7334	0.7332	0.005195	0.005195
81.6	6.2737	6.2862	0.6909	0.6910	0.005771	0.005771
91.2	4.7700	4.7631	0.6405	0.6402	0.00622	0.00618
100.8	3.2362	3.2198	0.5833	0.5827	0.006543	0.00654
110.4	1.6272	1.6363	0.5196	0.5196	0.006735	0.006731
120.0	3.87e-13	0.00	0.4524	0.4514	0.006793	0.00679
Average % difference	0.207		0.158		0.104	

Table 2.6 Comparison of the distribution of the radial and circumferential stresses and the radial displacement distributions in a rotating annular Stodola disc made up of Graphite-Fiber Reinforced Plastic material (NCT-301) and with the clamped-free boundary condition for s = 0.4

It should be noted that for the results shown in the above Tables 2.5 and 2.6, 20 divisions of the tapered disc have been made. Also, the average percentage difference has been calculated using the following formula:

$$\text{Average percentage difference} = \frac{\sum_{i=1}^{T}\left[\frac{(\text{R} - \text{R Solution}) - (\text{Closed} - \text{form Solution})}{\text{R} - \text{R Solution}}\right]}{\text{T}} \text{x } 100 \tag{2.24}$$

where, R-R stands for the Rayleigh-Ritz solution and T is the total number of sampling points taken along the radial direction of the rotating disc. For the present case, T = 11.

It can be seen from the above Tables 2.5 and 2.6 that the results obtained for the elastic response of a rotating annular linearly-tapered disc with the free-free boundary condition and that of a rotating annular Stodola disc with the clamped-free boundary condition respectively, using the Rayleigh-Ritz method are in good agreement with the results obtained for the same using the closed-form analytical solutions that are available in the literature.

Furthermore, it can also be noted that the average percentage differences in the results for the radial displacement distributions are low as compared with the results for the radial and circumferential stress distributions.

The following Tables 2.7 - 2.9 shows the comparison of the results obtained for the radial and circumferential stress distributions and the radial displacement distributions using the Rayleigh-Ritz method, in a rotating annular uniform-thickness disc made up of Polycarbonate material and with the clamped-free boundary condition, with the results obtained for the same using the finite element analysis software ANSYS® (using SOLID185 and SHELL181 elements), and also with the results obtained using the closed-form analytical solution that are available in the literature. The geometry, node locations and the element coordinate system for the SOLID185 and SHELL181 elements has been shown in Appendix A.

Rotating annular uniform-thickness disc made up of Polycarbonate material and with the clamped-free boundary condition				
$n = 0$			$\bar{h} = 1$	
Radial distance in *mm* from the center of the disc	Radial stress, σ_r (in *MPa*)			
	R-R Solution	ANSYS® Solution (SOLID185)	ANSYS® Solution (SHELL181)	Closed-form Solution [30]
24.0	10.4577	12.356	10.291	10.5643
33.6	8.4638	8.4580	8.4528	8.4445
43.2	7.2995	7.3232	7.3186	7.3157
52.8	6.4712	6.4736	6.4700	6.4683
62.4	5.7042	5.6952	5.6923	5.6911
72.0	4.9051	4.9069	4.9045	4.9034
81.6	4.0623	4.0716	4.0697	4.0688
91.2	3.1708	3.1716	3.1701	3.1691
100.8	2.2036	2.1966	2.1953	2.1943
110.4	1.1353	1.1405	1.1395	1.1385
120.0	1.93e-006	-3.7479e-005	-1.05e-004	0

Table 2.7 Comparison of the distribution of the radial stresses in a rotating annular uniform-thickness disc made up of Polycarbonate material and with the clamped-free boundary condition

Rotating annular uniform-thickness disc made up of Polycarbonate material and with the clamped-free boundary condition				
$n = 0$			$\bar{h} = 1$	
Radial distance in *mm* from the center of the disc	Circumferential stress, σ_θ (in *MPa*)			
	R-R Solution	ANSYS® Solution (SOLID185)	ANSYS® Solution (SHELL181)	Closed-form Solution [30]
24.0	3.1373	4.7530	3.0959	3.1679
33.6	4.8585	4.8376	4.8505	4.8492
43.2	5.3901	5.3877	5.3950	5.3934
52.8	5.5107	5.5064	5.5112	5.5099
62.4	5.4154	5.4078	5.4110	5.4101
72.0	5.1773	5.1736	5.1759	5.1747
81.6	4.8394	4.8391	4.8407	4.8399
91.2	4.4255	4.4239	4.4250	4.4241
100.8	3.9415	3.9374	3.9381	3.9373
110.4	3.3859	3.3856	3.3860	3.3853
120.0	2.7794	2.7722	2.8043	2.7717

Table 2.8 Comparison of the distribution of the circumferential stresses in a rotating annular uniform-thickness disc made up of Polycarbonate material and with the clamped-free boundary condition

Rotating annular uniform-thickness disc made up of Polycarbonate material and with the clamped-free boundary condition				
$n = 0$			$\bar{h} = 1$	
Radial distance in *mm* from the center of the disc	Radial displacement, u_r (in *mm*)			
	R-R Solution	ANSYS® Solution (SOLID185)	ANSYS® Solution (SHELL181)	Closed-form Solution [30]
24.0	0	0	0	0
33.6	0.0354	0.0352	0.0353	0.0355
43.2	0.0628	0.0626	0.0628	0.0625
52.8	0.0857	0.0855	0.0856	0.0856
62.4	0.1051	0.1049	0.1050	0.1048
72.0	0.1213	0.1211	0.1212	0.1211
81.6	0.1343	0.1341	0.1342	0.1341
91.2	0.1440	0.1439	0.1440	0.1439
100.8	0.1503	0.1502	0.1502	0.1502
110.4	0.1528	0.1527	0.1527	0.1526
120.0	0.1513	0.1511	0.1512	0.1511

Table 2.9 Comparison of the distribution of the radial displacements in a rotating annular uniform-thickness disc made up of Polycarbonate material and with the clamped-free boundary condition

It can be seen from the above Tables 2.7 – 2.9 that the results obtained for the radial and circumferential stress distributions and the radial displacement distributions in a rotating annular uniform-thickness disc made up of a Polycarbonate material and with the clamped-free boundary condition using the Rayleigh-Ritz method are in good agreement with the results obtained for the same using the finite element analysis software ANSYS® and also with the closed-form analytical solutions that are available in the literature. It can also be noted from the Table 2.7 and 2.8 that the values of the radial and circumferential stresses at the hub of the disc obtained using ANSYS® (using SOLID185 elements) are a bit higher than the values obtained for the same using other solution techniques considered in the present case.

2.3.1 Convergence Study

It has been proved earlier [9] that a 7th degree polynomial in radial coordinate provides satisfactory results for the elastic response of rotating discs using the principle of virtual work. Therefore, in the present study, a total of 8 terms in assumed displacement functions have been

used. For the elastic response of rotating annular tapered disc using the Rayleigh-Ritz method, it is the number of divisions of the tapered disc that accounts more for the accuracy of the results.

For the convergence study, the dependence of the elastic response of a Stodola disc made up of Graphite-Fiber Reinforced Plastic material (NCT-301) having a taper parameter value of s = 0.4 and with the clamped-free boundary condition, on the number of divisions N is shown in the following Tables 2.10 – 2.12.

Rotating annular Stodola disc made up of Graphite-Fiber Reinforced Plastic material (NCT-301) and with the clamped-free boundary condition						
s = 0.4						
Radial distance in *mm* from the center of the disc	Radial stress, σ_r (in MPa)					
	Rayleigh-Ritz Solution					Closed-Form Solution [29]
	N = 5	N = 10	N = 15	N = 18	N = 20	
24.0	22.1047	20.2191	19.7531	19.6349	19.5834	19.4024
33.6	15.3578	15.5034	15.5820	15.6038	15.6134	15.6472
43.2	12.7043	12.9970	13.0584	13.0735	13.0799	13.1139
52.8	11.1013	11.1615	11.1475	11.1427	11.1404	11.1262
62.4	9.4952	9.4512	9.4321	9.4270	9.4247	9.4068
72.0	7.8081	7.7976	7.8081	7.8115	7.8130	7.8188
81.6	6.2226	6.2498	6.2669	6.2717	6.2737	6.2862
91.2	4.7811	4.7807	4.7733	4.7711	4.7700	4.7631
100.8	3.3029	3.2624	3.2437	3.2385	3.2362	3.2198
110.4	1.6214	1.6110	1.6222	1.6257	1.6272	1.6363
120.0	1.4e-05	1.02e-05	5.76e-06	4.46e-09	3.87e-013	0.00

Table 2.10 Dependence of the radial stress distribution on the number of divisions for a rotating annular Stodola disc with the clamped-free boundary condition for a taper parameter value of s = 0.4

Rotating annular Stodola disc made up of Graphite-Fiber Reinforced Plastic material (NCT-301) with the clamped-free boundary condition						
$s = 0.4$						
Radial distance in *mm* from the center of the disc	Circumferential stress, σ_θ (in *MPa*)					
	Rayleigh-Ritz Solution					Closed-Form Solution [29]
	$N = 5$	$N = 10$	$N = 15$	$N = 18$	$N = 20$	
24.0	0.4460	0.4080	0.3986	0.3962	0.3951	0.3911
33.6	0.6706	0.6614	0.6608	0.6607	0.6607	0.6600
43.2	0.7494	0.7505	0.7514	0.7516	0.7517	0.7521
52.8	0.7760	0.7755	0.7751	0.7750	0.7750	0.7745
62.4	0.7674	0.7649	0.7643	0.7641	0.7640	0.7633
72.0	0.7353	0.7335	0.7334	0.7334	0.7334	0.7332
81.6	0.6914	0.6906	0.6908	0.6909	0.6909	0.6910
91.2	0.6418	0.6408	0.6406	0.6405	0.6405	0.6402
100.8	0.5860	0.5840	0.5835	0.5834	0.5833	0.5827
110.4	0.5210	0.5196	0.5196	0.5197	0.5196	0.5196
120.0	0.4558	0.4539	0.4529	0.4526	0.4524	0.4514

Table 2.11 Dependence of the circumferential stress distribution on the number of divisions for a rotating annular Stodola disc with the clamped-free boundary condition for a taper parameter value of $s = 0.4$

Rotating annular Stodola disc made up of Graphite-Fiber Reinforced Plastic material (NCT-301) with the clamped-free boundary condition						
$s = 0.4$						
Radial distance in *mm* from the center of the disc	Radial Displacement, u_r (in *mm*)					
	Rayleigh-Ritz Solution					Closed-Form Solution [29]
	$N = 5$	$N = 10$	$N = 15$	$N = 18$	$N = 20$	
24.0	0	0	0	0	0	0
33.6	0.001461	0.001457	0.001456	0.001455	0.001455	0.001452
43.2	0.002653	0.002647	0.002644	0.002642	0.002641	0.002639
52.8	0.003655	0.003649	0.003645	0.003643	0.003641	0.00364
62.4	0.004509	0.004501	0.004494	0.004490	0.004488	0.004486
72.0	0.00521	0.005202	0.005198	0.005196	0.005195	0.005195
81.6	0.005786	0.005780	0.005776	0.005772	0.005771	0.005771
91.2	0.006235	0.006228	0.006224	0.006221	0.00622	0.00618
100.8	0.006557	0.006552	0.006548	0.006545	0.006543	0.00654
110.4	0.006751	0.006746	0.006741	0.006737	0.006735	0.006731
120.0	0.006813	0.006808	0.006802	0.006797	0.006793	0.00679

Table 2.12 Dependence of the distribution of the radial displacements on the number of divisions for a rotating annular Stodola disc with the clamped-free boundary condition for a taper parameter value of $s = 0.4$

It can be seen from the above Tables 2.10 – 2.12 that as the number of divisions of the rotating annular Stodola disc is increased from $N = 5$ to $N = 20$, the results obtained for the radial stress and the circumferential stress distributions and the radial displacement distributions using the Rayleigh-Ritz method with finite-element-like modification tend to converge with the results obtained for the same using the closed-form analytical solutions that are available in the literature.

The following Table 2.13 shows the variation with the number of divisions *N* of the average percentage differences in the results obtained for the elastic response of a rotating annular Stodola disc with the clamped-free boundary condition and made up of Graphite-Fiber Reinforced Plastic material NCT-301, for a taper parameter value of s = 0.4, using the Rayleigh-Ritz method and the closed-form solutions.

Rotating annular Stodola disc made up of Graphite-Fiber Reinforced Plastic material (NCT-301) with the clamped-free boundary condition and with a taper parameter value of *s* = 0.4			
Number of divisions of the tapered disc (*N*)	Variation of average percentage difference in the results obtained for the elastic response of the tapered disc using Rayleigh-Ritz method and closed-form solutions		
	Radial stress distribution	Circumferential stress distribution	Radial displacement distribution
5	2.13	1.58	0.4
10	0.977	0.534	0.269
15	0.486	0.263	0.189
18	0.350	0.193	0.132
20	0.291	0.158	0.104

Table 2.13 Variation of average percentage difference in the results obtained for the elastic response of rotating annular Stodola disc made up of Graphite-Fiber Reinforced Plastic material (NCT-301) with the clamped-free boundary condition for a taper parameter value of *s* = 0.4

It can be concluded from the above Table 2.13 that the average percentage difference in the values of the radial stress and the circumferential stress distributions and the radial displacement distributions obtained using the Rayleigh-Ritz Method and the closed-form analytical solutions decreases, as the number of divisions of the tapered disc is increased from *N* = 5 to *N* = 20. Also, in the above Table 2.13, the average percentage difference is calculated according to the following relation:

$$\text{Average percentage difference} = \frac{\sum_{i=1}^{T} \frac{(\text{R} - \text{R solution})^{N} - (\text{Closed} - \text{form solution})}{(\text{R} - \text{R solution})^{N}}}{\text{T}} * 100 \quad (2.25)$$

In the above formula, R-R solution stands for the Rayleigh-Ritz solution, N is the number of divisions of the tapered disc for which the Rayleigh-Ritz solution is obtained, and T is the number of sampling points taken along the radial direction of the disc (which is 11 in the present case).

2.4 Parametric Study

A comprehensive parametric study on the radial displacements and the radial and the circumferential stress distributions in rotating annular tapered discs for the free-free and the clamped-free boundary conditions has been conducted and the results are presented in this section. Linearly-tapered disc and Stodola disc made up of different isotropic or orthotropic materials, the material properties of which have been mentioned earlier in the Table 2.3 are taken into consideration. The rotating disc has the same geometric properties as mentioned in the verification section i.e., it has an inner radius of r_i = 24 *mm*, an outer radius of r_o = 120 *mm*, and thickness at the hub of the disc h_i = 2.4 *mm* and it is rotating at a constant angular velocity of ω = 1000 *rad/s* i.e., 9554.14 *rpm*. The effects of the taper parameters (n) and (s), and the degree of orthotropy (λ) of the material of the disc are studied on the distribution of radial stresses and circumferential stresses, and on the radial displacements in the tapered discs.

2.4.1 Rotating annular linearly-tapered disc with the free-free boundary condition

This sub-section deals with the parametric study on the elastic response of rotating annular linearly-tapered disc with the free-free boundary condition. The effect of the linear taper parameter (n) and the effect of the degree of orthotropy (λ) of the material of the disc on the radial stress and circumferential stress distributions and on the radial displacement distributions are studied. Graphical results for the stress and displacement distributions are presented and the percentage change in the maximum stresses and displacement values are calculated for rotating annular linearly-tapered disc made up of an isotropic material (MAT-1) and various orthotropic materials.

2.4.1.1 Effect of the linear taper parameter (n) on the elastic response

The following Figures 2.3(a), (b), (c) and (d) show the radial stress distributions in rotating annular linearly-tapered discs with the free-free boundary condition for different values of the

linear taper parameter n for an isotropic material and various orthotropic materials. The taper parameter value $n = 0$ represents the uniform-thickness disc.

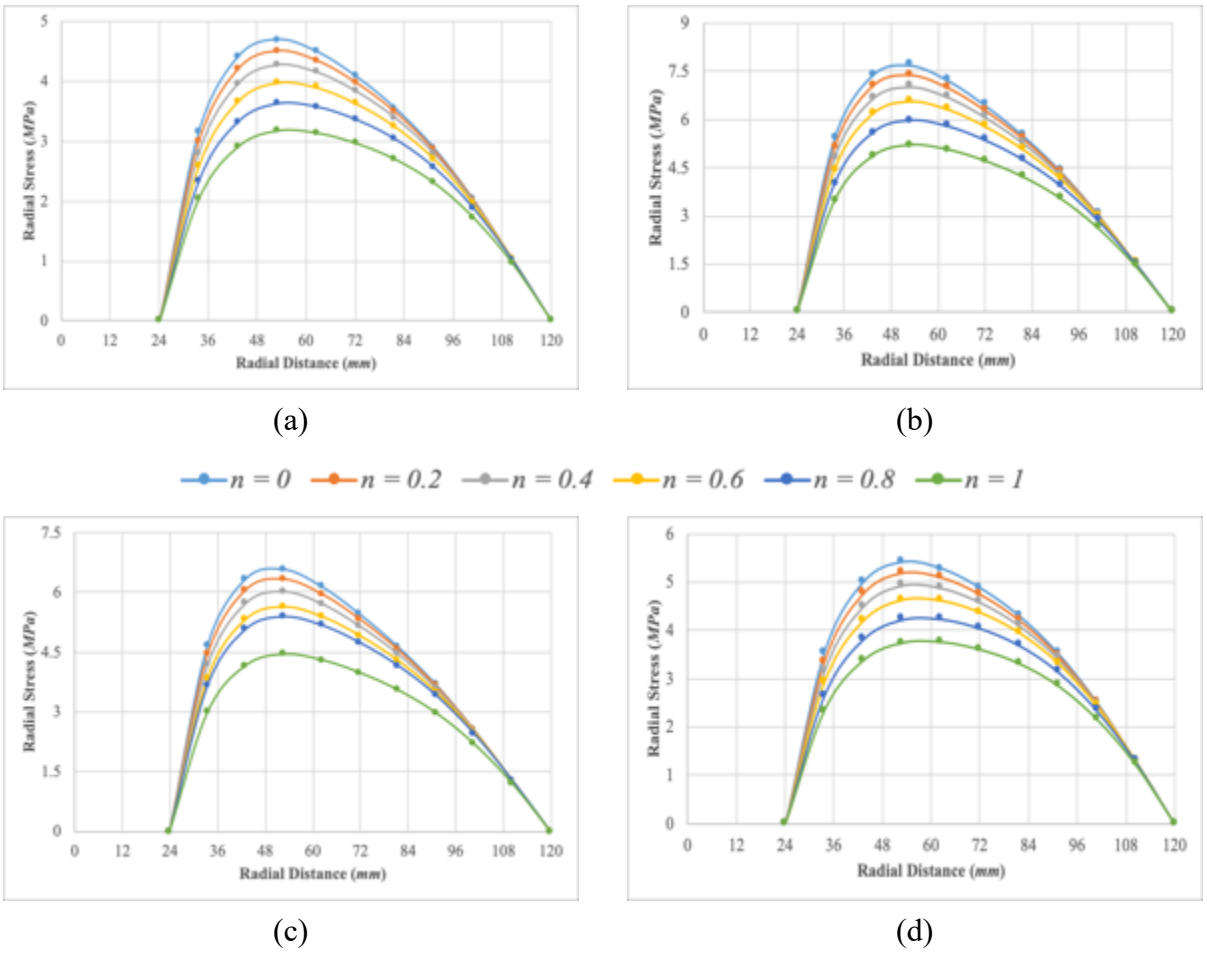

Figure 2.3 Radial stress distributions in a rotating annular linearly-tapered disc with the free-free boundary condition for **(a)** MAT-1 **(b)** MAT-2 **(c)** MAT-3 **(d)** MAT-4

It can be observed from the above plots that the uniform-thickness disc with $n = 0$, experiences the maximum radial stress and as the taper parameter (which in turn is the representation of the taper angle of the disc) is increased, the radial stress decreases accordingly and is the least for a taper parameter value of $n = 1$.

It is known that for an annular disc rotating at a constant speed under the free-free boundary condition, the radial stress is always zero at both the inner and the outer radii of the disc. Further for the uniform-thickness disc, the locus of the point experiencing the maximum amount of radial stress is equal to the geometric mean radius of the disc. For the disc of given geometric properties

as mentioned earlier in the verification section, the geometric mean radius is equal to 53.67 *mm*. Also, the locus of the point experiencing the maximum radial stress does not change with the increasing value of the taper parameter *n*. i.e., for the free-free boundary condition, the radial stress in a rotating annular linearly-tapered disc is always maximum at the geometric mean radius of the disc. This observation holds true irrespective of the material of the disc.

The following Tables 2.14 - 2.17 show the maximum radial stress and the percentage decrease in the maximum radial stress with the linear taper parameter *n* for rotating annular linearly-tapered discs with the free-free boundary condition and made up of different materials. Since the uniform-thickness disc is subjected to the maximum amount of radial stress, the value of the maximum radial stress in the uniform-thickness disc is considered as a benchmark while calculating the percentage difference in the following tables. Also, in the below Tables 2.14 - 2.17, the percentage decrease in the maximum radial stress is calculated according to the following formula:

$$\text{Percentage decrease in stress} = \frac{(\text{Maximum stress value for } n = 0) - (\text{Maximum stress value for } n = i)}{\text{Maximum stress value for } n = 0} * 100 \quad (2.26)$$

where, $i = 0.2, 0.4, \ldots, 1.0$.

Rotating annular linearly-tapered disc made of Polycarbonate material (MAT-1) and with the free-free boundary condition					
Maximum radial stress corresponding to $n = 0$ is equal to 4.69 *MPa*					
Linear taper parameter value	$n = 0.2$	$n = 0.4$	$n = 0.6$	$n = 0.8$	$n = 1.0$
Maximum radial stress (in *MPa*)	4.499	4.266	3.979	3.622	3.170
% decrease in the stress	4.06	9.022	15.140	22.766	32.402

Table 2.14 Percentage decrease in the maximum radial stress with the linear taper parameter *n* in a rotating annular linearly-tapered disc made of Polycarbonate material (MAT-1) and with the free-free boundary condition

Rotating annular linearly-tapered disc made of Glass-Fiber Reinforced Plastic material (MAT-2) and with the free-free boundary condition					
Maximum radial stress corresponding to $n = 0$ is equal to 7.677 *MPa*					
Linear taper parameter value	$n = 0.2$	$n = 0.4$	$n = 0.6$	$n = 0.8$	$n = 1.0$
Maximum radial stress (in *MPa*)	7.384	7.017	6.552	5.958	5.190
% decrease in the stress	3.809	8.595	14.654	22.393	32.390

Table 2.15 Percentage decrease in the maximum radial stress with the linear taper parameter n in a rotating annular linearly-tapered disc made of Glass-Fiber Reinforced Plastic material (MAT-2) and with the free-free boundary condition

Rotating annular linearly-tapered disc made of Graphite-Fiber Reinforced Plastic material (MAT-3) and with the free-free boundary condition					
Maximum radial stress corresponding to $n = 0$ is equal to 6.582 *MPa*					
Linear taper parameter value	$n = 0.2$	$n = 0.4$	$n = 0.6$	$n = 0.8$	$n = 1.0$
Maximum radial stress (in *MPa*)	6.335	6.021	5.621	5.381	4.439
% decrease in the stress	3.755	8.517	14.591	18.248	32.550

Table 2.16 Percentage decrease in the maximum radial stress with the linear taper parameter n in a rotating annular linearly-tapered disc made of Graphite-Fiber Reinforced Plastic material (MAT-3) and with the free-free boundary condition

Rotating annular linearly-tapered disc made of Nylon-6 composite material (MAT-4) and with the free-free boundary condition					
Maximum radial stress corresponding to $n = 0$ is equal to 5.4 *MPa*					
Linear taper parameter value	$n = 0.2$	$n = 0.4$	$n = 0.6$	$n = 0.8$	$n = 1.0$
Maximum radial stress (in *MPa*)	5.189	4.933	4.617	4.225	3.727
% decrease in the stress	3.901	8.650	14.491	21.766	30.978

Table 2.17 Percentage decrease in the maximum radial stress with the linear taper parameter n in a rotating annular linearly-tapered disc made up of Nylon-6 composite material (MAT-4) and with the free-free boundary condition

It can be seen from the above Tables 2.14 - 2.17 that irrespective of the material of the disc, the percentage decrease in the maximum value of the radial stress, increases with the increase in the value of the linear taper parameter and is highest for the taper parameter value of $n = 1$. Furthermore, the percentage decrease in the maximum radial stress in the rotating disc made up of Graphite-Fiber Reinforced Plastic material is maximum for a linear taper parameter value of $n = 1$ and is equal to 32.55 %.

The following Figures 2.4 (a), (b), (c) and (d) show the circumferential stress distributions in rotating annular linearly-tapered discs with the free-free boundary condition for different values of the linear taper parameter n for an isotropic material and various orthotropic materials.

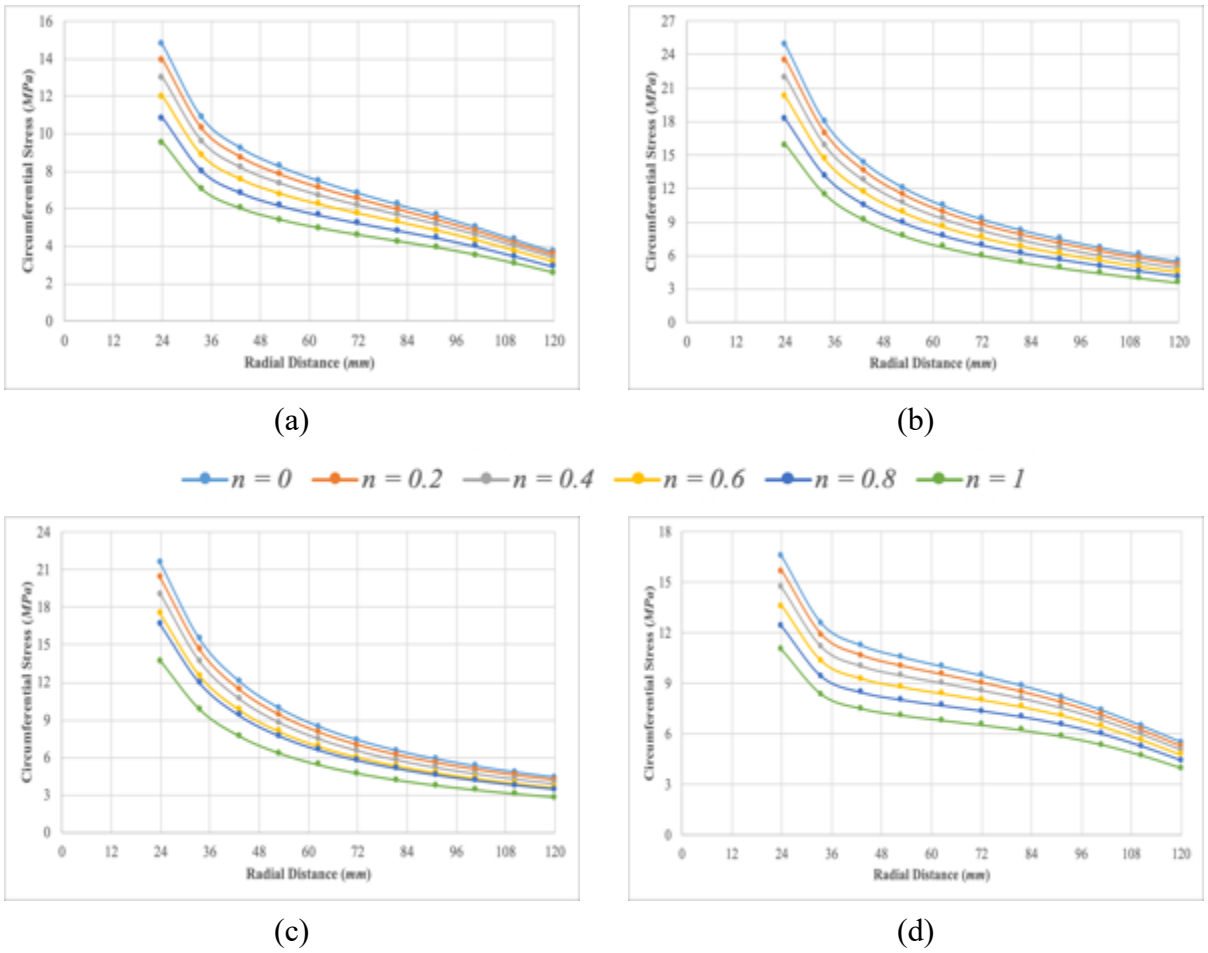

Figure 2.4 Circumferential stress distribution in a rotating annular linearly-tapered disc with the free-free boundary condition for **(a)** MAT-1 **(b)** MAT-2 **(c)** MAT-3 **(d)** MAT-4

It can be observed from the above Figure 2.4 that similar to the radial stress distributions, the uniform-thickness disc with $n = 0$ experiences the maximum circumferential stress and as the taper parameter is increased, the circumferential stress in the disc decreases accordingly and is the least for a taper parameter value of $n = 1$.

It is known that for a uniform-thickness annular disc rotating at a constant speed with the free-free boundary condition, the circumferential stress is always maximum at the inner radius of the disc (which is 24 *mm* in the present case) and decreases to a minimum value at its outer radius. It is also clear from the above plots that, the locus of the point experiencing the maximum circumferential stress does not change with the increasing value of taper parameter.

The following Tables 2.18 - 2.21 show the maximum circumferential stress and the percentage decrease in the maximum circumferential stress with the linear taper parameter n for rotating annular linearly-tapered discs with the free-free boundary condition and made up of different materials. Also, in the below Tables 2.18 - 2.21, the percentage decrease in the stress is calculated using the formula given in the Equation (2.26).

Rotating annular linearly-tapered disc made of Polycarbonate material (MAT-1) and with the free-free boundary condition					
Maximum circumferential stress corresponding to $n = 0$ is equal to 14.748 *MPa*					
Linear taper parameter value	$n = 0.2$	$n = 0.4$	$n = 0.6$	$n = 0.8$	$n = 1.0$
Maximum circumferential stress (in *MPa*)	13.914	12.993	11.97	10.822	9.519
% decrease in the stress	5.659	11.902	18.840	26.623	35.456

Table 2.18 Percentage decrease in the maximum circumferential stress with the linear taper parameter n in a rotating annular linearly-tapered disc made of Polycarbonate material (MAT-1) and with the free-free boundary condition

Rotating annular linearly-tapered disc made of Glass-Fiber Reinforced Plastic material (MAT-2) and with the free-free boundary condition					
Maximum circumferential stress corresponding to $n = 0$ is equal to 24.871 *MPa*					
Linear taper parameter value	$n = 0.2$	$n = 0.4$	$n = 0.6$	$n = 0.8$	$n = 1.0$
Maximum circumferential stress (in *MPa*)	23.502	21.960	20.212	18.207	15.882
% decrease in the stress	5.506	11.701	18.732	26.791	36.140

Table 2.19 Percentage decrease in the maximum circumferential stress with the linear taper parameter n in a rotating annular linearly-tapered disc made of Glass-Fiber Reinforced Plastic material (MAT-2) and with the free-free boundary condition

Rotating annular linearly-tapered disc made of Graphite-Fiber Reinforced Plastic material (MAT-3) and with the free-free boundary condition					
Maximum circumferential stress corresponding to $n = 0$ is equal to 21.538 *MPa*					
Linear taper parameter value	$n = 0.2$	$n = 0.4$	$n = 0.6$	$n = 0.8$	$n = 1.0$
Maximum circumferential stress (in *MPa*)	20.35	19.019	17.49	16.64	13.67
% decrease in the stress	5.48	11.69	18.78	22.71	36.49

Table 2.20 Percentage decrease in the maximum circumferential stress with the linear taper parameter n in a rotating annular linearly-tapered disc made of Graphite-Fiber Reinforced Plastic material (MAT-3) and with the free-free boundary condition

Rotating annular linearly-tapered disc made of Nylon-6 composite material (MAT-4) and with the free-free boundary condition					
Maximum circumferential stress corresponding to $n = 0$ is equal to 16.54 *MPa*					
Linear taper parameter value	$n = 0.2$	$n = 0.4$	$n = 0.6$	$n = 0.8$	$n = 1.0$
Maximum circumferential stress (in *MPa*)	15.654	14.67	13.592	12.381	11.0
% decrease in the stress	5.383	11.295	17.841	25.162	33.46

Table 2.21 Percentage decrease in the maximum circumferential stress with the linear taper parameter n in a rotating annular linearly-tapered disc made up of Nylon-6 composite material (MAT-4) and with the free-free boundary condition

It can be seen from the above Tables 2.18 - 2.21 that irrespective of the material of the disc, the percentage decrease in the maximum value of the circumferential stress, increases with the increase in the value of the linear taper parameter and is highest for the taper parameter value of n = 1. Furthermore, the percentage decrease in the maximum circumferential stress in the rotating disc made up of Graphite-Fiber Reinforced Plastic material is maximum for a linear taper parameter value of n = 1 and is equal to 36.49 %.

The following Figures 2.5 (a), (b), (c) and (d) show the radial displacement distributions in rotating annular linearly-tapered discs with the free-free boundary condition for different values of the linear taper parameter n for an isotropic material and various orthotropic materials.

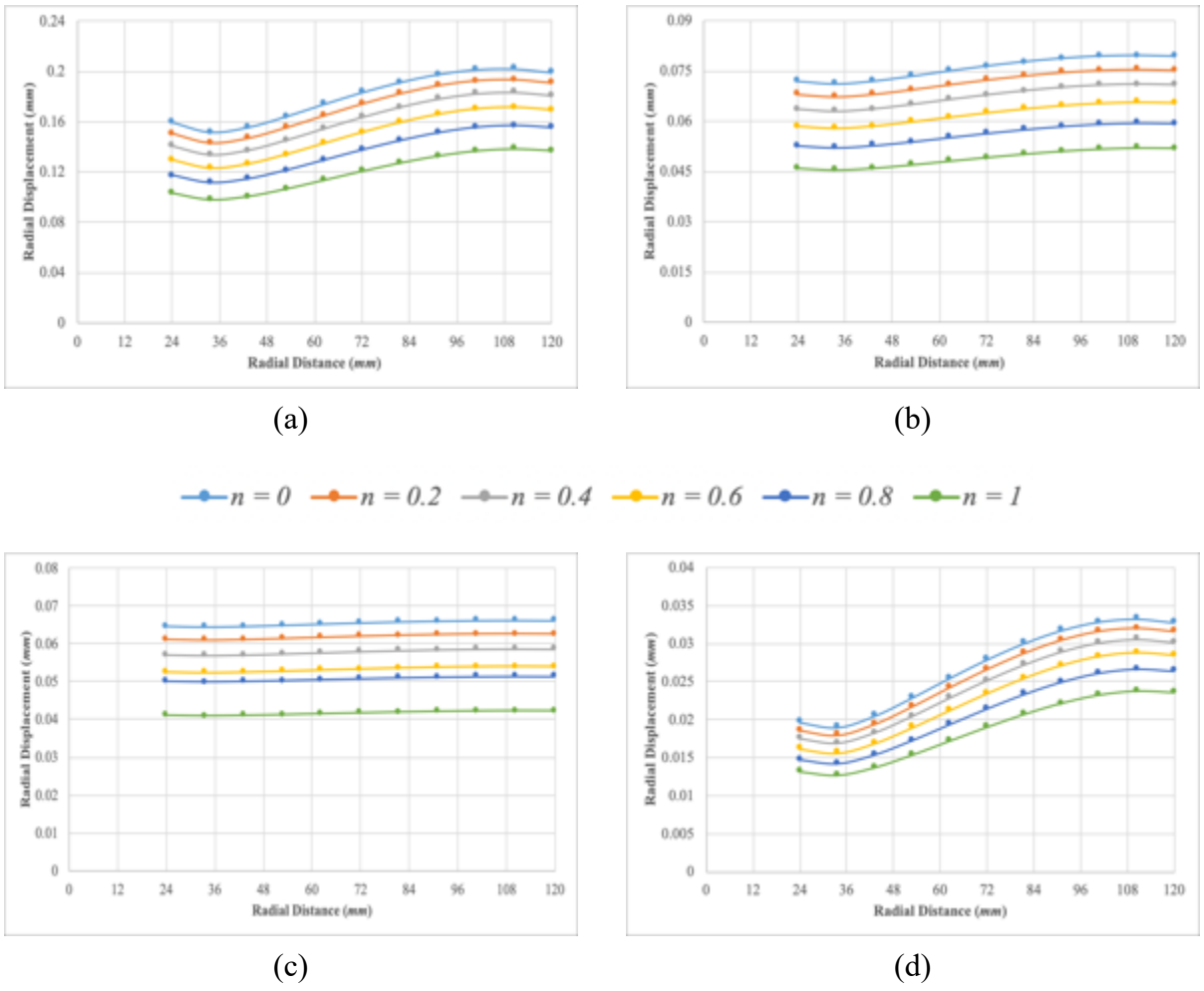

Figure 2.5 Radial displacements in a rotating annular linearly-tapered disc with the free-free boundary condition for **(a)** MAT-1 **(b)** MAT-2 **(c)** MAT-3 **(d)** MAT-4

It can be observed from the above plots that the radial displacement is maximum in the uniform-thickness disc with $n = 0$, and as the taper parameter is increased, the radial displacement decreases accordingly and is the least for a taper parameter value of $n = 1$. Also, in the case of rotating disc with the free-free boundary condition, there exists a radial displacement at both the inner and the outer radii of the disc and the displacement is maximum at the outer radius of the disc.

Furthermore, it can be seen from the above Figure 2.5 that the distributions of the radial displacements are significant in the case of rotating discs made up of Polycarbonate material (MAT-1) and Nylon-6 composite material (MAT-4) i.e., the distributions are significant for the material whose degree of orthotropy is greater than or equal to 1. For the rotating discs made up of materials whose degree of orthotropy is less than 1 i.e., for the discs made up of MAT-2 and MAT-3, the distributions are not that significant.

The following Tables 2.22 - 2.25 show the maximum radial displacement and the percentage decrease in the maximum radial displacement with the linear taper parameter n for rotating annular linearly-tapered discs with the free-free boundary condition and made up of different materials. Also, in the below Tables 2.22 - 2.25, the percentage decrease in the value of the maximum radial displacement is calculated according to the following formula.

$$\text{Percentage decrease in the displacement} = \frac{(\text{Maximum displacement for } n = 0) - (\text{Maximum displacement for } n = i)}{\text{Maximum displacement for } n = 0} * 100 \quad (2.27)$$

where, $i = 0.2, 0.4, \ldots, 1.0$.

Rotating annular linearly-tapered disc made of Polycarbonate material (MAT-1) and with the free-free boundary condition					
Maximum radial displacement corresponding to $n = 0$ is equal to 0.202 *mm*					
Linear taper parameter value	$n = 0.2$	$n = 0.4$	$n = 0.6$	$n = 0.8$	$n = 1.0$
Maximum radial displacement (in *mm*)	0.19351	0.18340	0.17143	0.15690	0.13855
% decrease in the displacement	4.303	9.305	15.224	22.411	31.483

Table 2.22 Percentage decrease in the maximum radial displacement with the linear taper parameter n in a rotating annular linearly-tapered disc made of Polycarbonate material (MAT-1) and with the free-free boundary condition

Rotating annular linearly-tapered disc made of Glass-Fiber Reinforced Plastic material (MAT-2) and with the free-free boundary condition					
Maximum radial displacement corresponding to $n = 0$ is equal to 0.07956 *mm*					
Linear taper parameter value	$n = 0.2$	$n = 0.4$	$n = 0.6$	$n = 0.8$	$n = 1.0$
Maximum radial displacement (in *mm*)	0.075586	0.07103	0.065748	0.05953	0.052047
% decrease in the displacement	5.00	10.728	17.365	25.181	34.585

Table 2.23 Percentage decrease in the maximum radial displacement with the linear taper parameter *n* in a rotating annular linearly-tapered disc made of Glass-Fiber Reinforced Plastic material (MAT-2) and with the free-free boundary condition

Rotating annular linearly-tapered disc made of Graphite-Fiber Reinforced Plastic material (MAT-3) and with the free-free boundary condition					
Maximum radial displacement corresponding to $n = 0$ is equal to 0.0622 *mm*					
Linear taper parameter value	$n = 0.2$	$n = 0.4$	$n = 0.6$	$n = 0.8$	$n = 1.0$
Maximum radial displacement (in *mm*)	0.062677	0.05865	0.054025	0.051445	0.042329
% decrease in the displacement	5.347	11.429	18.413	22.310	36.075

Table 2.24 Percentage decrease in the maximum radial displacement with the linear taper parameter *n* in a rotating annular linearly-tapered disc made of Graphite-Fiber Reinforced Plastic material (MAT-3) and with the free-free boundary condition

Rotating annular linearly-tapered disc made of Nylon-6 composite material (MAT-4) and with the free-free boundary condition					
Maximum radial displacement corresponding to $n = 0$ is equal to 0.03321 *mm*					
Linear taper parameter value	$n = 0.2$	$n = 0.4$	$n = 0.6$	$n = 0.8$	$n = 1.0$
Maximum radial displacement (in *mm*)	0.031991	0.030543	0.02879	0.026594	0.023706
% decrease in the displacement	3.678	8.035	13.316	19.926	28.624

Table 2.25 Percentage decrease in the maximum radial displacement with the linear taper parameter *n* in a rotating annular linearly-tapered disc made up of Nylon-6 composite material (MAT-4) and with the free-free boundary condition

It can be seen from the above Tables 2.22 - 2.25 that the percentage decrease in the maximum radial displacement in the rotating disc made up of Graphite-Fiber Reinforced Plastic material (MAT-3) is maximum for a linear taper parameter value of n = 1 and is equal to 36.075 %.

2.4.1.2 Effect of the degree of orthotropy (λ) on the elastic response

The following Figures 2.6 and 2.7 show the variation of the maximum radial stress and maximum circumferential stress in a rotating annular linearly-tapered disc for the free-free boundary condition with the degree of orthotropy of the material of the disc for different values of the linear taper parameter n.

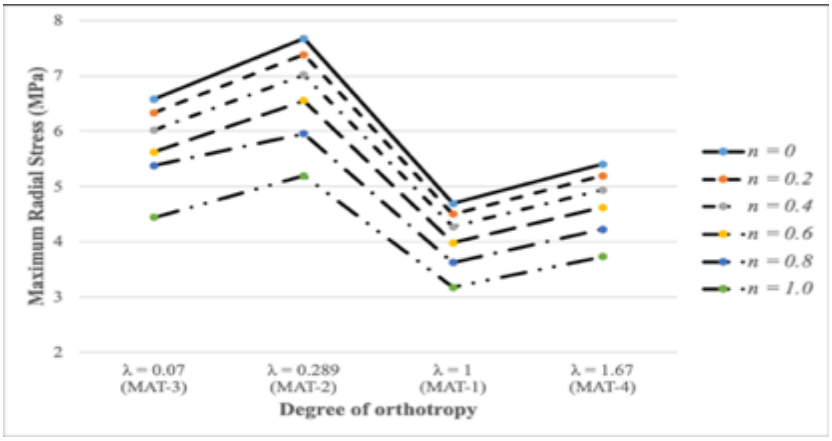

Figure 2.6 Effect of degree of orthotropy on the maximum radial stress in a rotating annular linearly-tapered disc for different values of the linear taper parameter n and for the free-free boundary condition

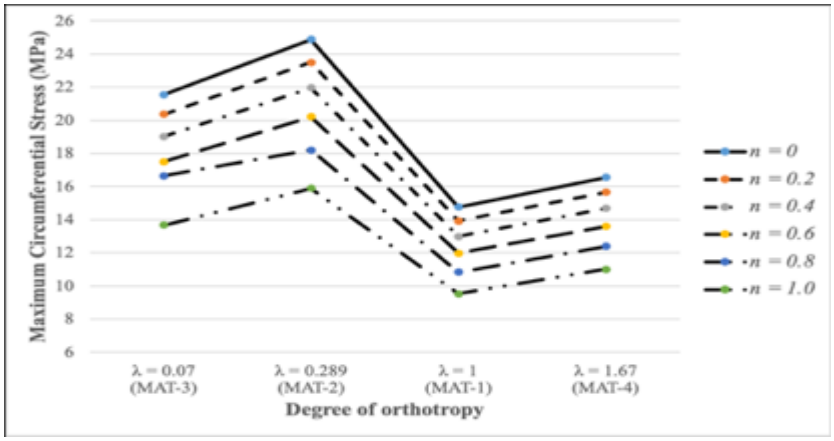

Figure 2.7 Effect of degree of orthotropy on the maximum circumferential stress in a rotating annular linearly-tapered disc for different values of the linear taper parameter n and for the free-free boundary condition

It can be seen from the above Figures 2.6 and 2.7 that irrespective of the linear taper parameter n, the rotating disc made of MAT-2 with $\lambda = 0.289$ experiences the maximum radial and circumferential stresses while the disc made up of MAT-1 with $\lambda = 1.0$, experiences the minimum amount of radial and circumferential stresses.

The following Figure 2.8 shows the variation of the maximum radial displacement in a rotating annular linearly-tapered disc for the free-free boundary condition with the degree of orthotropy of the material of the disc for different values of the linear taper parameter n.

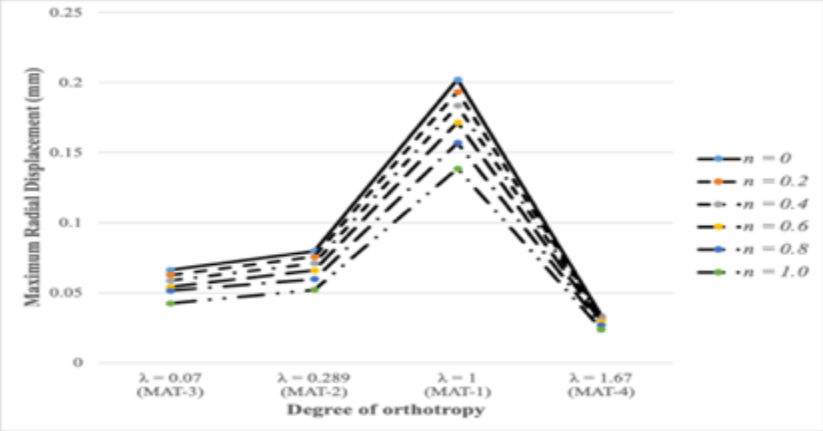

Figure 2.8 Effect of degree of orthotropy on the maximum radial displacement in a rotating annular linearly-tapered disc for different values of the linear taper parameter n and for the free-free boundary condition

It can be seen from the above Figure 2.8 that irrespective of the value of the taper parameter of the rotating disc, the radial displacement increases with the increasing value of the degree of orthotropy λ of the material of the disc till it reaches unity. Also, the radial displacement is maximum in a rotating annular linearly-tapered disc made of isotropic material (MAT-1, $\lambda = 1.0$) for the free-free boundary condition as compared with the rotating discs made of other materials.

Furthermore, the value of maximum radial displacement decreases when the degree of orthotropy of the material of the disc is greater than unity and is the least for a disc made of MAT-4 with $\lambda = 1.67$. The cause for such a variation can be explained by the fact that for MAT-4, the Young's modulus in the principal material direction 2 is greater than that in the principal material direction 1 making the disc stiffer in the circumferential direction.

2.4.2 Rotating annular Stodola disc with the free-free boundary condition

This sub-section deals with the parametric study on the elastic response of rotating annular Stodola disc with the free-free boundary condition. The effect of Stodola taper parameter (s) and the effect of the degree of orthotropy (λ) of the material of the disc on the radial stress and circumferential stress distributions and the radial displacement distributions are studied. Graphical results for the stress and displacement distributions are presented and the percentage change in the maximum stress and displacement values are calculated for rotating annular Stodola discs made up of an isotropic material (MAT-1) and various orthotropic materials.

2.4.2.1 Effect of Stodola taper parameter (s) on the elastic response

The following Figures 2.9(a), (b), (c) and (d) show the radial stress distributions in rotating annular Stodola discs with the free-free boundary condition for different values of the Stodola taper parameter s for an isotropic material and various orthotropic materials. The taper parameter value $s = 0$ represents the uniform-thickness disc.

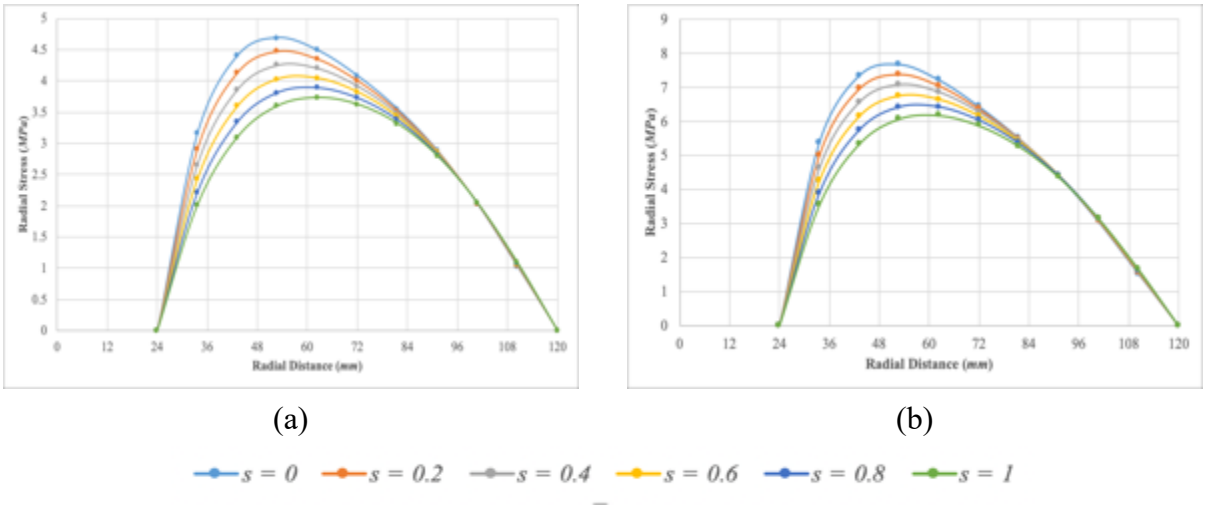

(a) (b)

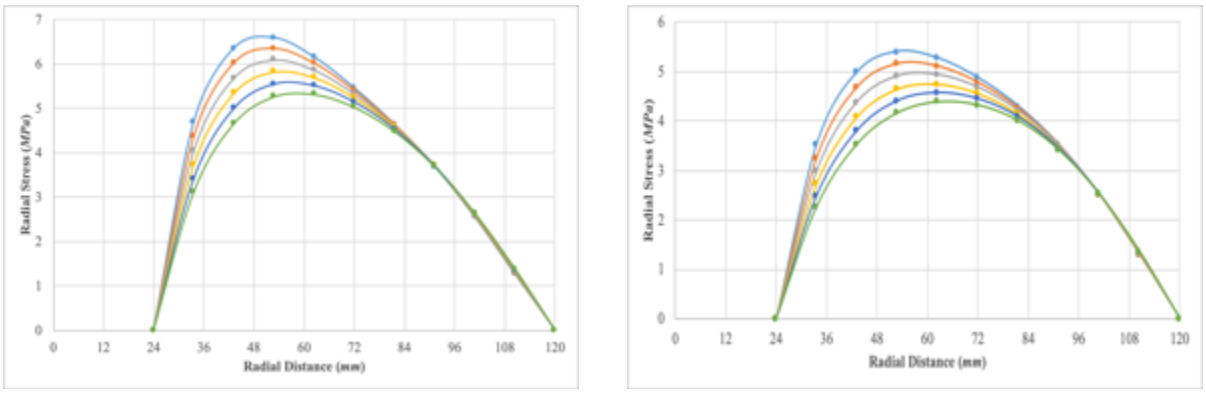

(c) (d)

Figure 2.9 Radial stress distribution in a rotating annular Stodola disc with the free-free boundary condition for **(a)** MAT-1 **(b)** MAT-2 **(c)** MAT-3 **(d)** MAT-4

It can be observed from the above plots that the uniform-thickness disc with s = 0, experiences the maximum radial stress and as the taper parameter is increased, the radial stress decreases accordingly and is least for a taper parameter of s = 1.

It can be seen that unlike in the case of linearly-tapered discs with the free-free boundary condition, where irrespective of the linear taper parameter n (i.e., the taper angle) and the material of the disc, the locus of the point experiencing the maximum radial stress remains fixed at the geometric mean radius of the disc (which in the present case is 53.67 *mm*), the locus of the point experiencing the maximum stress in rotating annular Stodola disc with the free-free boundary condition tends to shift towards the arithmetic mean radius of the disc (which in this case is 72 *mm*) with the increasing value of the Stodola taper parameter s.

The following Tables 2.26 - 2.29 show the maximum radial stress and the percentage decrease in the maximum radial stress with the Stodola taper parameter s for rotating annular Stodola discs with the free-free boundary condition and made up of different materials. Also, in the below Tables 2.26 - 2.29, the percentage decrease in the maximum stress is calculated according to the following formula:

$$\text{Percentage decrease in the stress} = \frac{(\text{Maximum stress value for } s = 0) - (\text{Maximum stress value for } s = i)}{\text{Maximum stress value for } s = 0} * 100 \quad (2.28)$$

where, i = 0.2, 0.4, …, 1.0.

Rotating annular Stodola disc made of Polycarbonate material (MAT-1) and with the free-free boundary condition					
Maximum radial stress corresponding to $s = 0$ is equal to 4.69 *MPa*					
Stodola taper parameter value	$s = 0.2$	$s = 0.4$	$s = 0.6$	$s = 0.8$	$s = 1.0$
Maximum radial stress (in *MPa*)	4.472	4.252	4.046	3.888	3.73
% decrease in the stress	4.630	9.336	9.898	13.432	17.014

Table 2.26 Percentage decrease in the maximum radial stress with the Stodola taper parameter s in a rotating annular Stodola disc made of Polycarbonate material (MAT-1) and with the free-free boundary condition

Rotating annular Stodola disc made of Glass-Fiber Reinforced Plastic material (MAT-2) and with the free-free boundary condition					
Maximum radial stress corresponding to $s = 0$ is equal to 7.677 *MPa*					
Stodola taper parameter value	$s = 0.2$	$s = 0.4$	$s = 0.6$	$s = 0.8$	$s = 1.0$
Maximum radial stress (in *MPa*)	7.386	7.075	6.751	6.421	6.18
% decrease in the stress	3.793	7.832	12.054	11.032	14.332

Table 2.27 Percentage decrease in the maximum radial stress with the Stodola taper parameter s in a rotating annular Stodola disc made of Glass-Fiber Reinforced Plastic material (MAT-2) and with the free-free boundary condition

Rotating annular Stodola disc made of Graphite-Fiber Reinforced Plastic material (MAT-3) and with the free-free boundary condition					
Maximum radial stress corresponding to $s = 0$ is equal to 6.582 *MPa*					
Stodola taper parameter value	$s = 0.2$	$s = 0.4$	$s = 0.6$	$s = 0.8$	$s = 1.0$
Maximum radial stress (in *MPa*)	6.348	6.095	5.826	5.547	5.31
% decrease in the stress	3.552	7.401	11.482	15.728	13.568

Table 2.28 Percentage decrease in the maximum radial stress with the Stodola taper parameter s in a rotating annular Stodola disc made of Graphite-Fiber Reinforced Plastic material (MAT-3) and with the free-free boundary condition

Rotating annular Stodola disc made of Nylon-6 composite material (MAT-4) and with the free-free boundary condition					
Maximum radial stress corresponding to $s = 0$ is equal to 5.4 *MPa*					
Stodola taper parameter value	$s = 0.2$	$s = 0.4$	$s = 0.6$	$s = 0.8$	$s = 1.0$
Maximum radial stress (in *MPa*)	5.153	4.930	4.753	4.572	4.39
% decrease in the stress	4.584	6.409	9.776	13.205	16.665

Table 2.29 Percentage decrease in the maximum radial stress with the Stodola taper parameter s in a rotating annular Stodola disc made of Nylon-6 composite material (MAT-4) and with the free-free boundary condition

It can be seen from the above Tables 2.26 - 2.29 that for the rotating discs made of MAT-1, MAT-2 and MAT-4, the percentage decrease in the maximum value of the radial stress, increases with the increase in the value of the Stodola taper parameter and is highest for the taper parameter value of $s = 1$. However, for the rotating disc made of MAT-3, the percentage decrease in the maximum value of the radial stress is maximum for the Stodola taper parameter value of $s = 0.8$.

The following Figures 2.10(a), (b), (c) and (d) shows the circumferential stress distributions in rotating annular Stodola discs with the free-free boundary condition for different values of the Stodola taper parameter s for an isotropic material and various orthotropic materials.

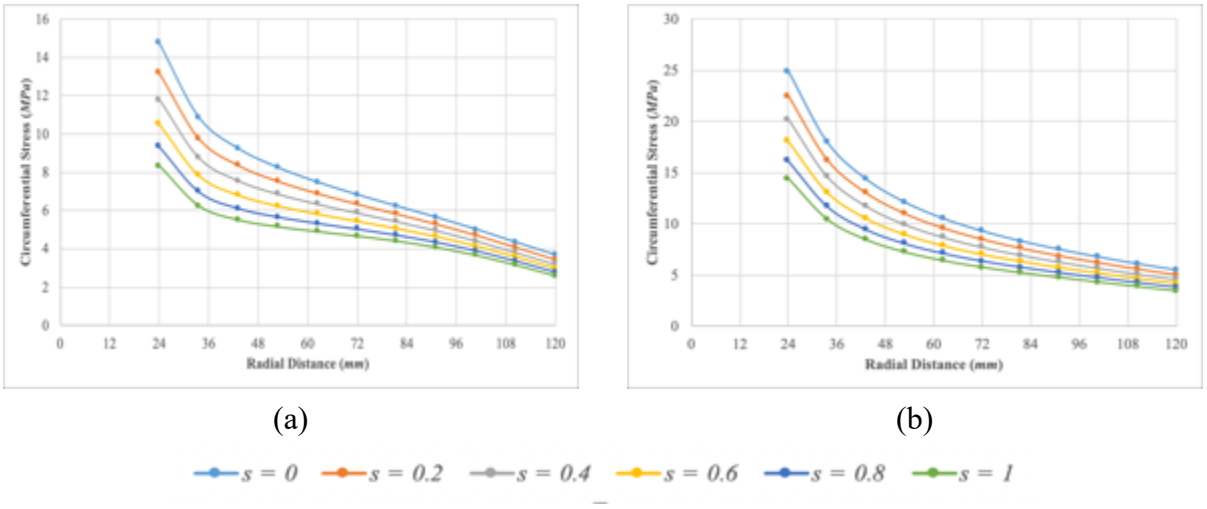

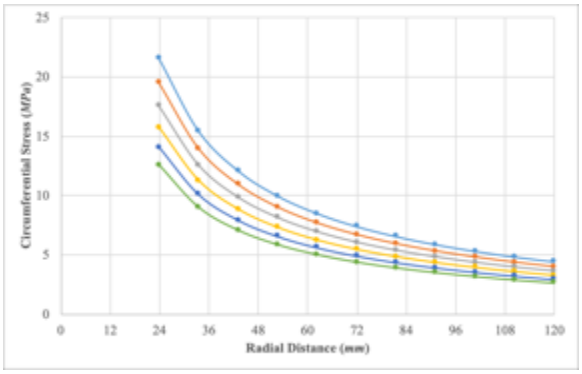

(c)

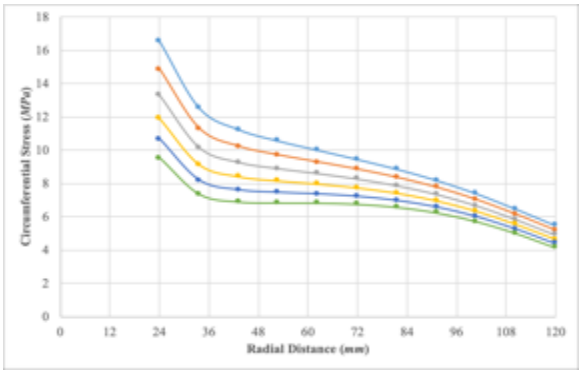

(d)

Figure 2.10 Circumferential stress distributions in a rotating annular Stodola disc with the free-free boundary condition for **(a)** MAT-1 **(b)** MAT-2 **(c)** MAT-3 **(d)** MAT-4

It can be observed from the above Figures 2.10 (a), (b), (c) and (d) that similar to the radial stress distributions, the uniform-thickness disc experiences the maximum circumferential stress and as the taper parameter is increased, the stress decreases accordingly and is least for a taper parameter value of $s = 1$. It is also clear from the above plots that similar to the circumferential stress distributions in the linearly-tapered discs with the free-free boundary condition, the locus of the point experiencing the maximum circumferential stress does not change with the increasing value of taper parameter in Stodola discs with the free-free boundary condition.

The following Tables 2.30 - 2.33 show the maximum circumferential stress and the percentage decrease in the maximum circumferential stress with the Stodola taper parameter s for rotating annular Stodola discs with the free-free boundary condition and made up of different materials. Also, in the below Tables 2.30 to 2.33, the percentage decrease in the maximum circumferential stress is calculated from the Equation (2.28).

Rotating annular Stodola disc made of Polycarbonate material (MAT-1) and with the free-free boundary condition					
Maximum circumferential stress corresponding to $s = 0$ is equal to 14.748 *MPa*					
Stodola taper parameter value	$s = 0.2$	$s = 0.4$	$s = 0.6$	$s = 0.8$	$s = 1.0$
Maximum circumferential stress (in *MPa*)	13.197	11.782	10.500	9.348	8.320
% decrease in the stress	10.516	20.115	28.805	36.617	43.592

Table 2.30 Percentage decrease in the maximum circumferential stress with the Stodola taper parameter s in a rotating annular Stodola disc made of Polycarbonate material (MAT-1) and with the free-free boundary condition

Rotating annular Stodola disc made of Glass-Fiber Reinforced Plastic material (MAT-2) and with the free-free boundary condition					
Maximum circumferential stress corresponding to $s = 0$ is equal to 24.87 *MPa*					
Stodola taper parameter value	$s = 0.2$	$s = 0.4$	$s = 0.6$	$s = 0.8$	$s = 1.0$
Maximum circumferential stress (in *MPa*)	22.447	20.178	18.076	16.147	14.4
% decrease in the stress	9.745	18.866	27.317	35.073	42.126

Table 2.31 Percentage decrease in the maximum circumferential stress with the Stodola taper parameter s in a rotating annular Stodola disc made of Glass-Fiber Reinforced Plastic material (MAT-2) and with the free-free boundary condition

Rotating annular Stodola disc made of Graphite-Fiber Reinforced Plastic material (MAT-3) and with the free-free boundary condition					
Maximum circumferential stress corresponding to $s = 0$ is equal to 21.537 *MPa*					
Stodola taper parameter value	$s = 0.2$	$s = 0.4$	$s = 0.6$	$s = 0.8$	$s = 1.0$
Maximum circumferential stress (in *MPa*)	19.485	17.548	15.74	14.071	12.5
% decrease in the stress	9.531	18.522	26.913	34.664	41.751

Table 2.32 Percentage decrease in the maximum circumferential stress with the Stodola taper parameter s in a rotating annular Stodola disc made of Graphite-Fiber Reinforced Plastic material (MAT-3) and with the free-free boundary condition

Rotating annular Stodola disc made of Nylon-6 composite material (MAT-4) and with the free-free boundary condition					
Maximum circumferential stress corresponding to $s = 0$ is equal to 16.544 *MPa*					
Stodola taper parameter value	$s = 0.2$	$s = 0.4$	$s = 0.6$	$s = 0.8$	$s = 1.0$
Maximum circumferential stress (in *MPa*)	14.845	13.299	11.903	10.64	9.53
% decrease in the stress	10.272	19.615	28.053	35.629	42.39

Table 2.33 Percentage decrease in the maximum circumferential stress with the Stodola taper parameter s in a rotating annular Stodola disc made of Nylon-6 composite material (MAT-4) and with the free-free boundary condition

It can be seen from the above Tables 2.30 - 2.33 that the percentage decrease in the maximum circumferential stress in the rotating disc made up of Polycarbonate material (MAT-1) is maximum for a taper parameter value of $s = 1$ and is equal to 43.592 %.

The following Figures 2.11(a), (b), (c) and (d) show the radial displacement distributions in a rotating annular Stodola disc with the free-free boundary condition for different values of the Stodola taper parameter s for an isotropic material and various orthotropic materials.

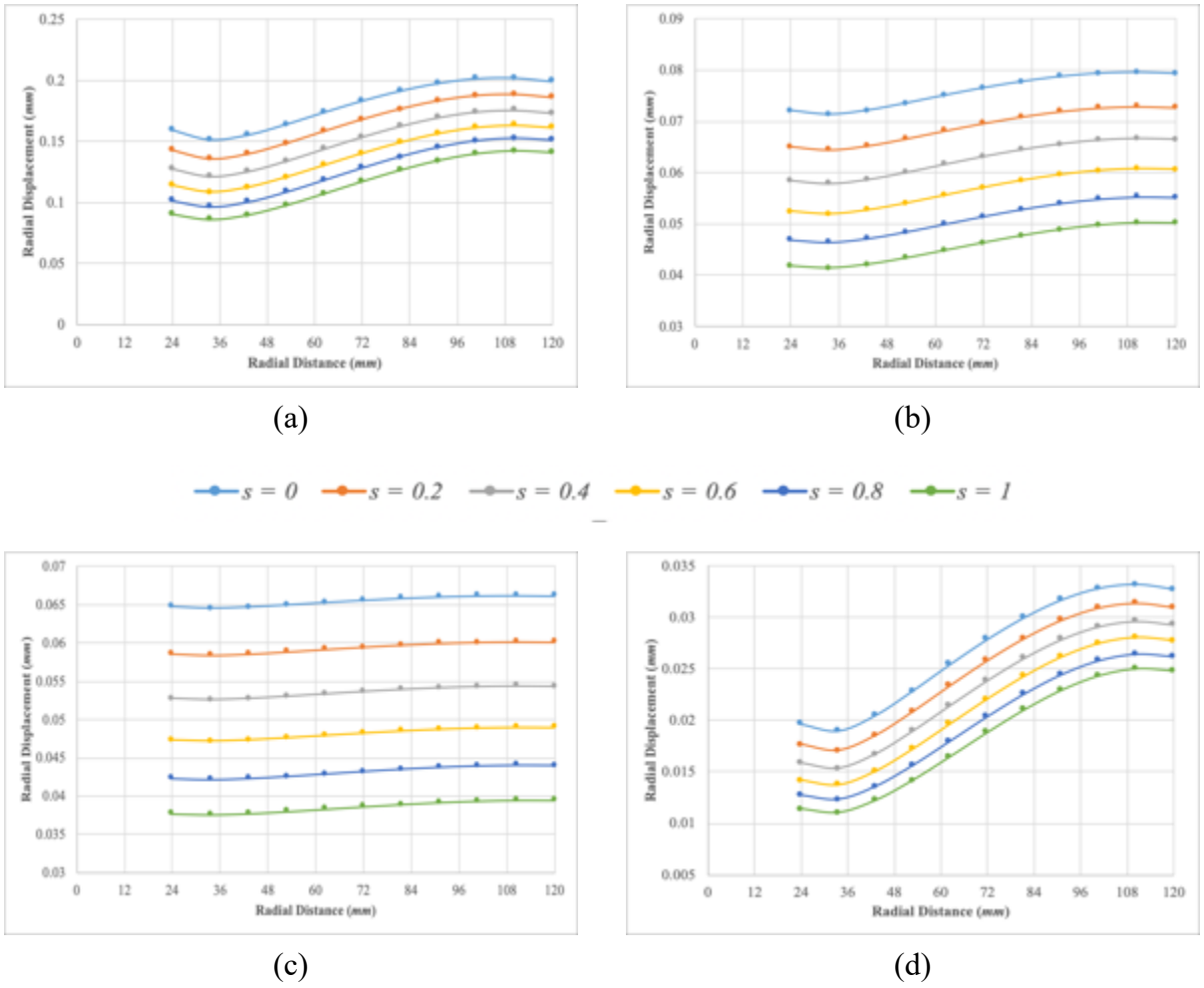

Figure 2.11 Radial displacement distributions in a rotating annular Stodola disc with the free-free boundary condition for **(a)** MAT-1 **(b)** MAT-2 **(c)** MAT-3 **(d)** MAT-4

It can be observed from the above plots that similar to the radial stress and the circumferential stress distributions, the uniform-thickness disc is subjected to maximum radial displacement and as the taper parameter is increased, the displacement decreases accordingly and is least for a taper parameter value of $s = 1$.

The following Tables 2.34 - 2.37 show the maximum radial displacement and the percentage decrease in the maximum radial displacement with the Stodola taper parameter s for rotating annular Stodola discs with the free-free boundary condition and made up of different materials. Also, in the below Tables 2.34 - 2.37, the percentage decrease in the value of the maximum radial displacement is calculated according to the following formula:

$$\text{Percentage decrease in the displacement} = \frac{(\text{Maximum displacement for } s = 0) - (\text{Maximum displacement for } s = i)}{\text{Maximum displacement for } s = 0} * 100 \quad (2.29)$$

where, $i = 0.2, 0.4, \ldots, 1.0$.

Rotating annular Stodola disc made of Polycarbonate material (MAT-1) and with the free-free boundary condition					
Maximum radial displacement corresponding to $s = 0$ is equal to 0.202 *mm*					
Stodola taper parameter value	$s = 0.2$	$s = 0.4$	$s = 0.6$	$s = 0.8$	$s = 1.0$
Maximum radial displacement (in *mm*)	0.18852	0.17563	0.16359	0.15241	0.14
% decrease in the displacement	6.77365	13.145	19.098	24.631	29.745

Table 2.34 Percentage decrease in the maximum radial displacement with the Stodola taper parameter s in a rotating annular Stodola disc made of Polycarbonate material (MAT-1) and with the free-free boundary condition

Rotating annular Stodola disc made of Glass-Fiber Reinforced Plastic material (MAT-2) and with the free-free boundary condition					
Maximum radial displacement corresponding to $s = 0$ is equal to 0.07956 *mm*					
Stodola taper parameter value	$s = 0.2$	$s = 0.4$	$s = 0.6$	$s = 0.8$	$s = 1.0$
Maximum radial displacement (in *mm*)	0.072906	0.06661	0.06072	0.05525	0.05
% decrease in the displacement	8.369	16.28	23.684	30.555	36.875

Table 2.35 Percentage decrease in the maximum radial displacement with the Stodola taper parameter s in a rotating annular Stodola disc made of Glass-Fiber Reinforced Plastic material (MAT-2) and with the free-free boundary condition

Rotating annular Stodola disc made of Graphite-Fiber Reinforced Plastic material (MAT-3) and with the free-free boundary condition					
Maximum radial displacement corresponding to $s = 0$ is equal to 0.0662 *mm*					
Stodola taper parameter value	$s = 0.2$	$s = 0.4$	$s = 0.6$	$s = 0.8$	$s = 1.0$
Maximum radial displacement (in *mm*)	0.06015	0.05441	0.04904	0.04406	0.04
% decrease in the displacement	9.163	17.829	25.938	33.448	40.337

Table 2.36 Percentage decrease in the maximum radial displacement with the Stodola taper parameter s in a rotating annular Stodola disc made of Graphite-Fiber Reinforced Plastic material (MAT-3) and with the free-free boundary condition

Rotating annular Stodola disc made of Nylon-6 composite material (MAT-4) and with the free-free boundary condition					
Maximum radial displacement corresponding to $s = 0$ is equal to 0.03321 *mm*					
Stodola taper parameter value	$s = 0.2$	$s = 0.4$	$s = 0.6$	$s = 0.8$	$s = 1.0$
Maximum radial displacement (in *mm*)	0.03138	0.02965	0.02802	0.02648	0.03
% decrease in the displacement	5.490	10.704	15.630	20.265	24.608

Table 2.37 Percentage decrease in the maximum radial displacement with the Stodola taper parameter s in a rotating annular Stodola disc made of Nylon-6 composite material (MAT-3) and with the free-free boundary condition

It can be seen from the above Tables 2.34 - 2.37 that irrespective of the material of the disc, the percentage decrease in the maximum value of the radial displacement increases with the increasing value of the Stodola taper parameter and is highest for a taper parameter value of $s = 1$. Furthermore, the rotating disc made up of Graphite-Fiber Reinforced Plastic material (MAT-3) has the maximum percentage decrease (40.34%) in the amount of maximum radial displacement as compared with the discs made of other materials taken into consideration.

2.4.2.2 Effect of the degree of orthotropy (λ) on the elastic response

The following Figures 2.12 and 2.13 show the variation of the maximum radial stress and maximum circumferential stress in a rotating annular Stodola disc for the free-free boundary condition, with the degree of orthotropy of the material of the disc for different values of the Stodola taper parameter *s*.

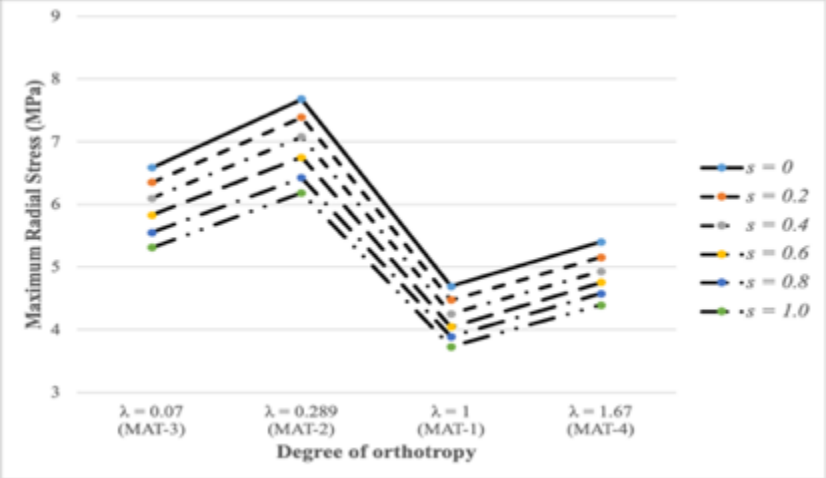

Figure 2.12 Effect of degree of orthotropy on the maximum radial stress in a rotating annular Stodola disc for different values of the Stodola taper parameter *s* and for the free-free boundary condition

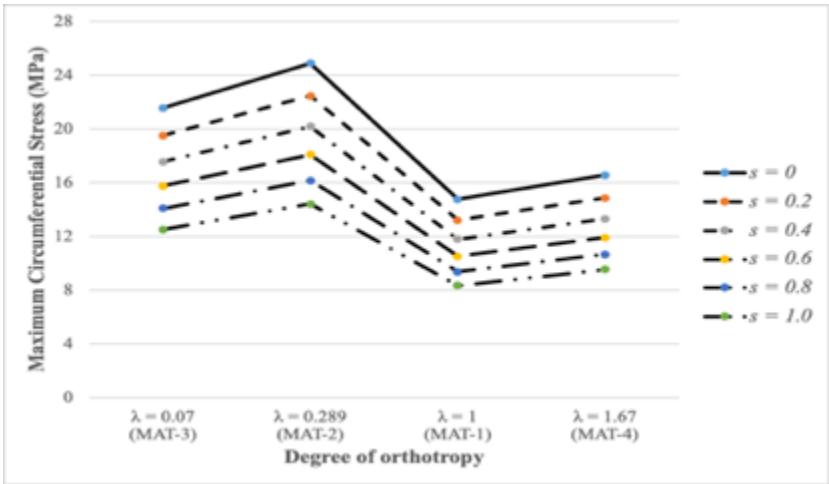

Figure 2.13 Effect of degree of orthotropy on the maximum circumferential stress in a rotating annular Stodola disc for different values of the Stodola taper parameter *s* and for the free-free boundary condition

It can be seen from the above Figures 2.12 and 2.13 that irrespective of the Stodola taper parameter *s*, the rotating discs made of MAT-2 with λ = 0.289 experiences the maximum radial and circumferential stresses while the disc made up of MAT-1 with λ = 1.0, experiences the minimum amount of radial and circumferential stresses.

The following Figure 2.14 shows the variation of the maximum radial displacement in a rotating annular Stodola disc for the free-free boundary condition with the degree of orthotropy of the material of the disc for different values of the Stodola taper parameter *s*.

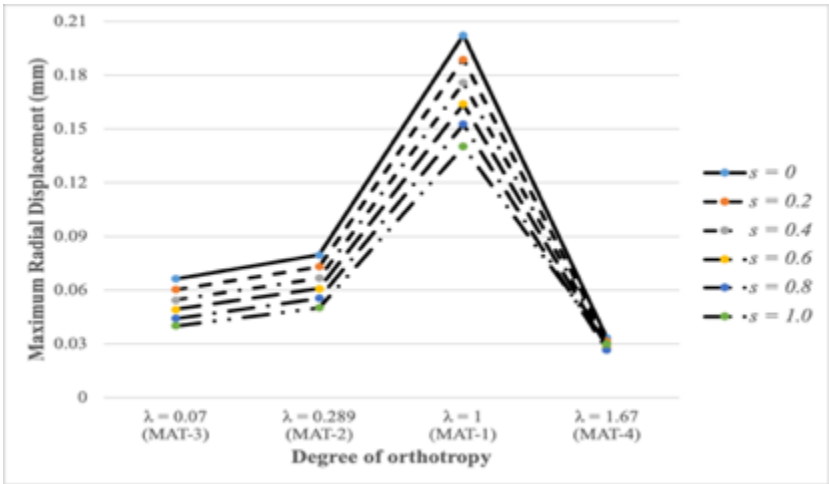

Figure 2.14 Effect of degree of orthotropy on the maximum radial displacement in a rotating annular Stodola disc for different values of the Stodola taper parameter *s* for the free-free boundary condition

It can be seen from the above Figure 2.14 that irrespective of the taper parameter of the disc, the radial displacement increases with the increasing value of the degree of orthotropy λ of the material of the disc till it reaches unity. Also, the radial displacement is maximum in a rotating annular Stodola disc made of isotropic material (MAT-1, λ = 1.0) for the free-free boundary condition as compared with the rotating discs made of other materials.

Furthermore, the value of maximum radial displacement decreases when the degree of orthotropy of the material of the disc is greater than unity and is the least for a disc made of MAT-4 with λ = 1.67.

2.4.3 Rotating annular linearly-tapered disc with the clamped-free boundary condition

This sub-section deals with the parametric study on the elastic response of rotating annular linearly-tapered disc with the clamped-free boundary condition. The effect of linear taper

parameter (n) and the effect of the degree of orthotropy (λ) of the material of the disc on the radial stress and circumferential stress distributions and the radial displacement distributions are studied. Graphical results for the stress and displacement distributions are presented and the percentage change in the maximum stress and displacement values are calculated for rotating annular linearly-tapered discs made up of an isotropic material (MAT-1) and various orthotropic materials.

2.4.3.1 Effect of the linear taper parameter (n) on the elastic response

The following Figures 2.15 (a), (b), (c) and (d) show the radial stress distributions in a rotating annular linearly-tapered disc with the clamped-free boundary condition for different values of the linear taper parameter n for an isotropic material and various orthotropic materials.

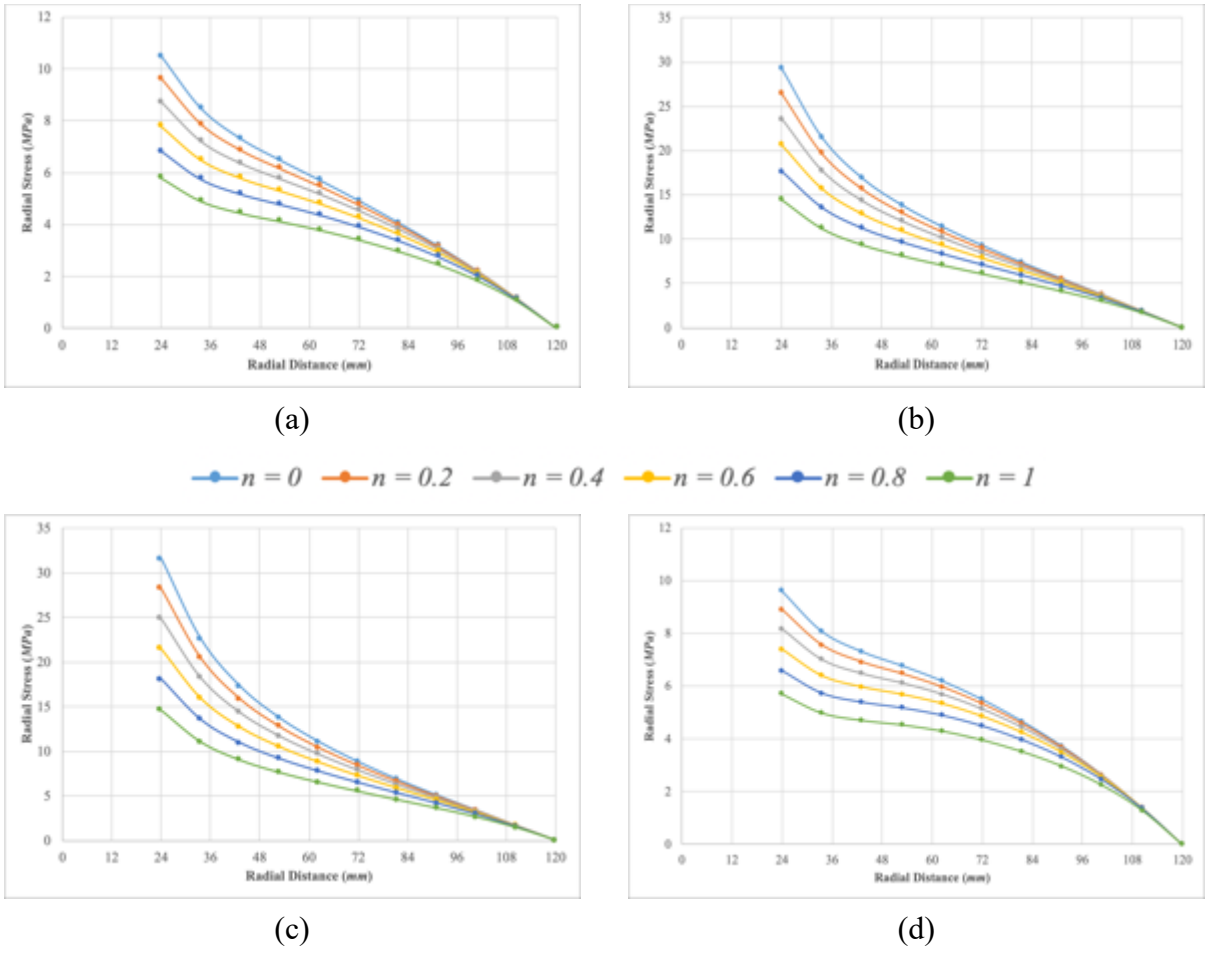

Figure 2.15 Radial stress distributions in a rotating annular linearly-tapered disc with the clamped-free boundary condition for **(a)** MAT-1 **(b)** MAT-2 **(c)** MAT-3 **(d)** MAT-4

It can be observed from the above plots that the uniform-thickness discs with $n = 0$, experience the maximum radial stress and as the taper parameter is increased, the radial stress decreases accordingly and is the least for a taper parameter value of $n = 1$.

It is known that for an annular uniform-thickness disc rotating at a constant speed with the clamped-free boundary condition, the radial stress is always maximum at the hub of the disc at which it is clamped and tends to zero at its outer end. For a disc of given geometric properties as mentioned earlier in the verification section, the radial stress is maximum at the inner radius of the disc i.e., at 24 *mm*. Also, the locus of the point experiencing the maximum radial stress does not change with the increasing value of the taper parameter n. i.e., for the clamped-free boundary condition, the radial stress in a rotating annular linearly-tapered disc is always maximum at the hub of the disc i.e., at the inner radius of the annular disc. This observation holds true irrespective of the material of the disc.

The following Tables 2.38 - 2.41 show the maximum radial stress and the percentage decrease in the maximum radial stress with the linear taper parameter n for rotating annular linearly-tapered discs with the clamped-free boundary condition and made up of different materials. Since the uniform-thickness disc is subjected to the maximum amount of radial stress, the value of the maximum radial stress in the uniform-thickness disc is considered as a benchmark while calculating the percentage difference. Also, in the below Tables 2.38 - 2.41, the percentage decrease in the maximum radial stress is calculated according to the formula given in the Equation (2.26).

Rotating annular linearly-tapered disc made of Polycarbonate material (MAT-1) and with the clamped-free boundary condition					
Maximum radial stress corresponding to $n = 0$ is equal to 10.457 *MPa*					
Linear taper parameter value	$n = 0.2$	$n = 0.4$	$n = 0.6$	$n = 0.8$	$n = 1.0$
Maximum radial stress (in *MPa*)	9.602	8.713	7.788	6.817	5.791
% decrease in the stress	8.181	16.673	25.525	34.806	44.621

Table 2.38 Percentage decrease in the maximum radial stress with the linear taper parameter n in a rotating annular linearly-tapered disc made of Polycarbonate material (MAT-1) and with the clamped-free boundary condition

Rotating annular linearly-tapered disc made of Glass-Fiber Reinforced composite material (MAT-2) and with the clamped-free boundary condition					
Maximum radial stress corresponding to $n = 0$ is equal to 29.199 *MPa*					
Linear taper parameter value	$n = 0.2$	$n = 0.4$	$n = 0.6$	$n = 0.8$	$n = 1.0$
Maximum radial stress (in *MPa*)	26.405	23.543	20.605	17.581	14.456
% decrease in the stress	9.57	19.372	29.434	39.789	50.491

Table 2.39 Percentage decrease in the maximum radial stress with the linear taper parameter n in a rotating annular linearly-tapered disc made of Glass-Fiber Reinforced composite material (MAT-2) and with the clamped-free boundary condition

Rotating annular linearly-tapered disc made of Graphite-Fiber Reinforced composite material (MAT-3) and with the clamped-free boundary condition					
Maximum radial stress corresponding to $n = 0$ is equal to 31.542 *MPa*					
Linear taper parameter value	$n = 0.2$	$n = 0.4$	$n = 0.6$	$n = 0.8$	$n = 1.0$
Maximum radial stress (in *MPa*)	28.222	24.871	21.485	18.06	14.59
% decrease in the stress	10.518	21.143	31.879	42.739	53.73

Table 2.40 Percentage decrease in the maximum radial stress with the linear taper parameter n in a rotating annular linearly-tapered disc made of Graphite-Fiber Reinforced composite material (MAT-3) and with the clamped-free boundary condition

Rotating annular linearly-tapered disc made of Nylon-6 composite material (MAT-4) and with the clamped-free boundary condition					
Maximum radial stress corresponding to $n = 0$ is equal to 9.607 *MPa*					
Linear taper parameter value	$n = 0.2$	$n = 0.4$	$n = 0.6$	$n = 0.8$	$n = 1.0$
Maximum radial stress (in *MPa*)	8.905	8.170	7.397	6.577	5.697
% decrease in the stress	7.309	14.955	23.0	31.534	40.697

Table 2.41 Percentage decrease in the maximum radial stress with the linear taper parameter n in a rotating annular linearly-tapered disc made of Nylon-6 composite material (MAT-4) and with the clamped-free boundary condition

It can be seen from the above Tables 2.38 - 2.41 that the percentage decrease in the maximum value of the radial stress in the rotating disc made up of Graphite-Fiber Reinforced

Plastic material (MAT-3) is maximum for a linear taper parameter value of $n = 1$ and is equal to 53.73 %. Also, from the Tables 2.39 and 2.40, it is observed that for the linear taper parameter value of $n = 1$, the maximum radial stress in the rotating annular linearly-tapered discs made up of MAT-3 and MAT-2 and with the clamped-free boundary condition, reduces to half of the maximum radial stress induced in the uniform-thickness disc made up of MAT-3 and MAT-2 respectively, and with the clamped-free boundary condition.

The following Figures 2.16(a), (b), (c) and (d) show the circumferential stress distributions in a rotating annular linearly-tapered disc with the clamped-free boundary condition for different values of the linear taper parameter n for an isotropic material and various orthotropic materials.

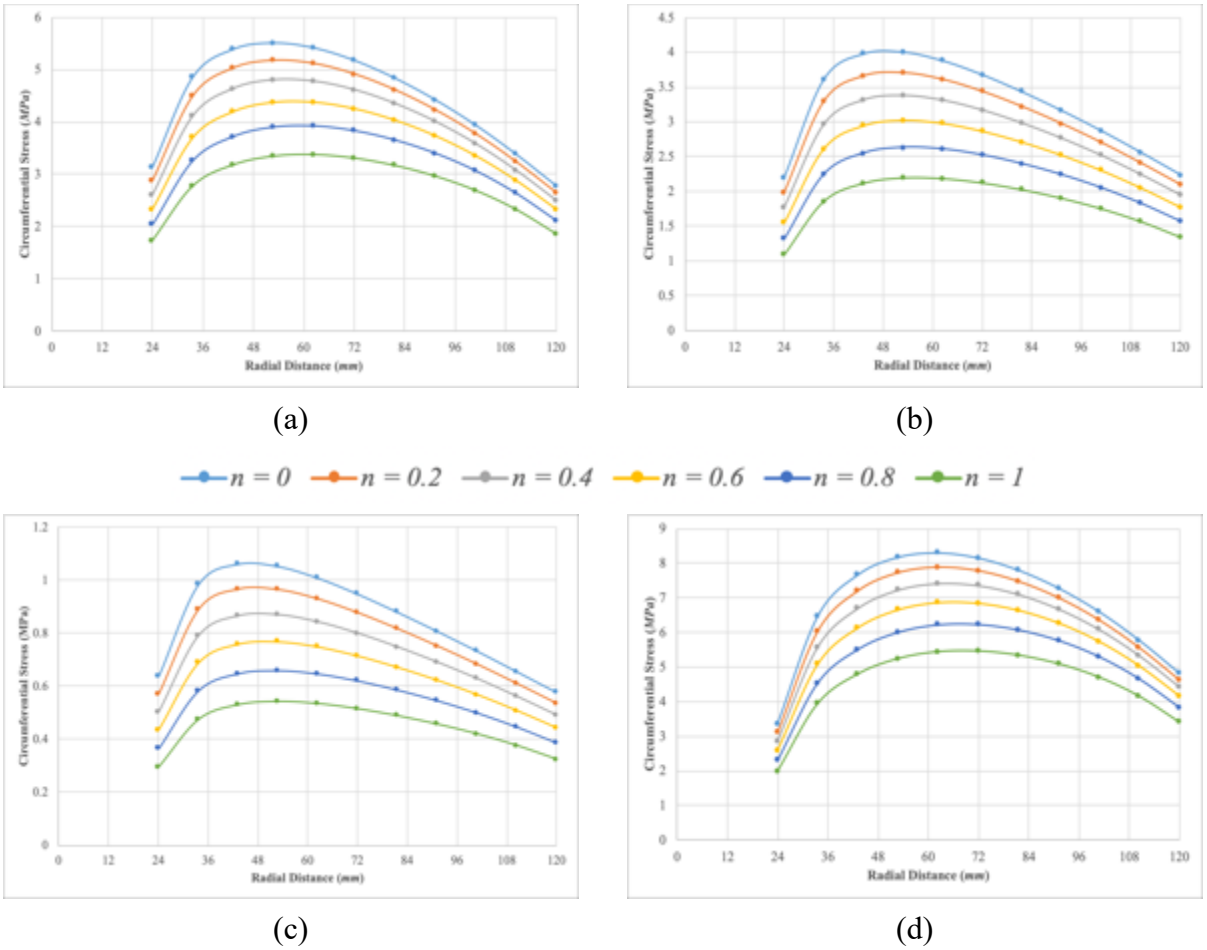

Figure 2.16 Circumferential stress distributions in a rotating annular linearly-tapered disc with the clamped-free boundary condition for **(a)** MAT-1 **(b)** MAT-2 **(c)** MAT-3 **(d)** MAT-4

It can be observed from the above Figure 2.16 that the uniform-thickness discs with $n = 0$, experience the maximum circumferential stress and as the taper parameter is increased, the circumferential stress decreases accordingly and is the least for a taper parameter value of $n = 1$.

It is known that for an annular uniform-thickness disc rotating at a constant speed with the clamped-free boundary condition, the circumferential stress is always maximum at the geometric mean radius of the rotating disc which is 53.67 *mm* in the present case. Also, the locus of the point experiencing the maximum circumferential stress does not change with the increasing value of the taper parameter *n*. i.e., for the clamped-free boundary condition, the circumferential stress in a rotating annular linearly-tapered disc is always maximum at the geometric mean radius of the disc. This observation holds true irrespective of the material of the disc.

The following Tables 2.42 - 2.45 show the maximum circumferential stress and the percentage decrease in the maximum circumferential stress with the linear taper parameter *n* for rotating annular linearly-tapered discs with the clamped-free boundary condition and made up of different materials. Also, in the below Tables 2.42 - 2.45, the percentage decrease in the maximum circumferential stress is calculated according to the formula given in the Equation (2.26).

Rotating annular linearly-tapered disc made of Polycarbonate material (MAT-1) and with the clamped-free boundary condition					
Maximum circumferential stress corresponding to $n = 0$ is equal to 5.51*MPa*					
Linear taper parameter value	$n = 0.2$	$n = 0.4$	$n = 0.6$	$n = 0.8$	$n = 1.0$
Maximum circumferential stress (in *MPa*)	5.173	4.798	4.376	3.899	3.351
% decrease in the stress	6.119	12.931	20.575	29.239	39.182

Table 2.42 Percentage decrease in the maximum circumferential stress with the linear taper parameter *n* in a rotating annular linearly-tapered disc made of Polycarbonate material (MAT-1) and with the clamped-free boundary condition

Rotating annular linearly-tapered disc made of Glass-Fiber Reinforced composite material (MAT-2) and with the clamped-free boundary condition					
Maximum circumferential stress corresponding to $n = 0$ is equal to 4.007 *MPa*					
Linear taper parameter value	$n = 0.2$	$n = 0.4$	$n = 0.6$	$n = 0.8$	$n = 1.0$
Maximum circumferential stress (in *MPa*)	3.704	3.377	3.02	2.628	2.195
% decrease in the stress	7.543	15.719	24.630	34.403	45.206

Table 2.43 Percentage decrease in the maximum circumferential stress with the linear taper parameter n in a rotating annular linearly-tapered disc made of Glass-Fiber Reinforced composite material (MAT-2) and with the clamped-free boundary condition

Rotating annular linearly-tapered disc made of Graphite-Fiber Reinforced composite material (MAT-3) and with the clamped-free boundary condition					
Maximum circumferential stress corresponding to $n = 0$ is equal to 1.053 *MPa*					
Linear taper parameter value	$n = 0.2$	$n = 0.4$	$n = 0.6$	$n = 0.8$	$n = 1.0$
Maximum circumferential stress (in *MPa*)	0.963	0.869	0.767	0.65	0.541
% decrease in the stress	8.456	17.456	27.072	37.394	48.534

Table 2.44 Percentage decrease in the maximum circumferential stress with the linear taper parameter n in a rotating annular linearly-tapered disc made of Graphite-Fiber Reinforced composite material (MAT-3) and with the clamped-free boundary condition

Rotating annular linearly-tapered disc made of Nylon-6 composite material (MAT-4) and with the clamped-free boundary condition					
Maximum circumferential stress corresponding to $n = 0$ is equal to 8.308 *MPa*					
Linear taper parameter value	$n = 0.2$	$n = 0.4$	$n = 0.6$	$n = 0.8$	$n = 1.0$
Maximum circumferential stress (in *MPa*)	7.894	7.420	6.870	6.22	5.443
% decrease in the stress	4.980	10.685	17.302	25.101	34.477

Table 2.45 Percentage decrease in the maximum circumferential stress with the linear taper parameter n in a rotating annular linearly-tapered disc made of Nylon-6 composite material (MAT-4) and with the clamped-free boundary condition

It can be seen from the above Tables 2.42 - 2.45 that the percentage decrease in the maximum value of the circumferential stress in the rotating disc made up of Graphite-Fiber Reinforced Plastic material (MAT-3) is maximum for a linear taper parameter value of $n = 1$ as compared with the percentage decrease in the maximum circumferential stress in the rotating discs made up of other materials, and is equal to 48.534 %.

The following Figures 2.17(a), (b), (c) and (d) show the radial displacement distributions in rotating annular linearly-tapered discs with the clamped-free boundary condition for different values of the linear taper parameter n for an isotropic material and various orthotropic materials.

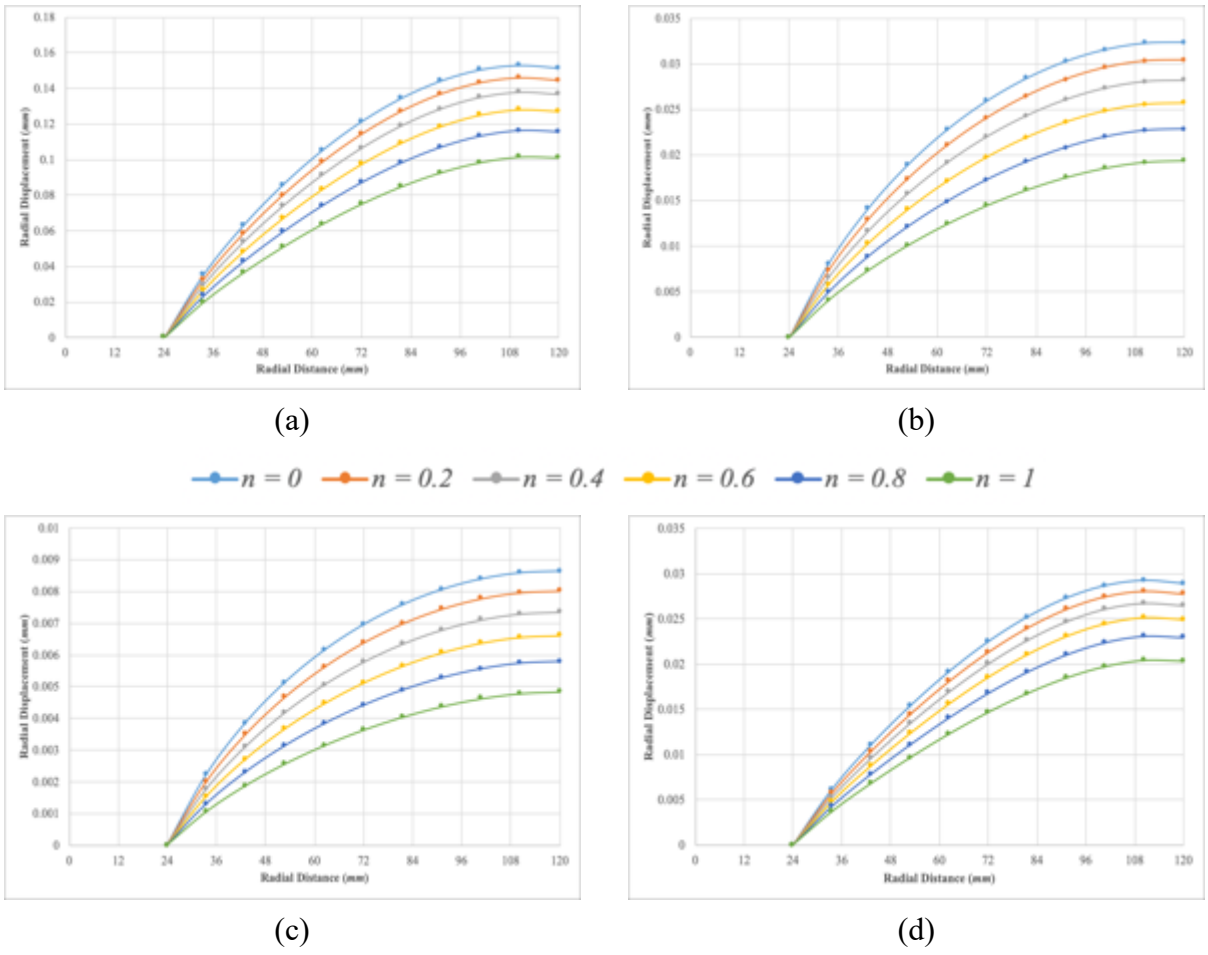

Figure 2.17 Radial displacement distributions in a rotating annular linearly-tapered disc with the clamped-free boundary condition for **(a)** MAT-1 **(b)** MAT-2 **(c)** MAT-3 **(d)** MAT-4

It can be observed from the above plots that the uniform-thickness disc is subjected to maximum radial displacement and as the taper parameter is increased, the displacement decreases accordingly and is least for a taper parameter value of $n = 1$.

It is known that for an annular disc rotating at a constant speed with the clamped-free boundary condition, there does not exists any displacement at the inner radius of the disc at which it is clamped. The radial displacement increases with the increase in radial distance from the center of the disc and is maximum at the outer periphery of the rotating disc. It can also be seen from the above plots that the radial displacement distributions are maximum for the rotating disc made of Polycarbonate material (MAT-1) as compared with the rotating disc made up of other materials that are considered in the present study.

The following Tables 2.46 - 2.49 show the maximum radial displacement and the percentage decrease in the maximum radial displacement with the linear taper parameter n for rotating annular linearly-tapered discs with the clamped-free boundary condition and made up of different materials. Also, in the below Tables 2.46 - 2.49, the percentage decrease in the maximum radial displacement is calculated according to the formula given in the Equation (2.27).

Rotating annular linearly-tapered disc made of Polycarbonate material (MAT-1) and with the clamped-free boundary condition					
Maximum radial displacement corresponding to $n = 0$ is equal to 0.1513 *mm*					
Linear taper parameter value	$n = 0.2$	$n = 0.4$	$n = 0.6$	$n = 0.8$	$n = 1.0$
Maximum radial displacement (in *mm*)	0.1444	0.13643	0.12701	0.11555	0.10094
% decrease in the displacement	4.551	9.82	16.046	23.622	33.276

Table 2.46 Percentage decrease in the maximum radial displacement with the linear taper parameter n in a rotating annular linearly-tapered disc made of Polycarbonate material (MAT-1) and with the clamped-free boundary condition

Rotating annular linearly-tapered disc made of Glass-Fiber Reinforced composite material (MAT-2) and with the clamped-free boundary condition					
Maximum radial displacement corresponding to $n = 0$ is equal to 0.0324 *mm*					
Linear taper parameter value	$n = 0.2$	$n = 0.4$	$n = 0.6$	$n = 0.8$	$n = 1.0$
Maximum radial displacement (in *mm*)	0.03042	0.02821	0.02572	0.02284	0.01942
% decrease in the displacement	6.11	12.917	20.611	29.486	40.06

Table 2.47 Percentage decrease in the maximum radial displacement with the linear taper parameter n in a rotating annular linearly-tapered disc made of Glass-Fiber Reinforced composite material (MAT-2) and with the clamped-free boundary condition

Rotating annular linearly-tapered disc made of Graphite-Fiber Reinforced composite material (MAT-3) and with the clamped-free boundary condition					
Maximum radial displacement corresponding to $n = 0$ is equal to 0.008642 *mm*					
Linear taper parameter value	$n = 0.2$	$n = 0.4$	$n = 0.6$	$n = 0.8$	$n = 1.0$
Maximum radial displacement (in *mm*)	0.008	0.007356	0.00662	0.00579	0.00484
% decrease in the displacement	7.124	14.871	23.395	32.932	43.897

Table 2.48 Percentage decrease in the maximum radial displacement with the linear taper parameter n in a rotating annular linearly-tapered disc made of Graphite-Fiber Reinforced composite material (MAT-3) and with the clamped-free boundary condition

Rotating annular linearly-tapered disc made of Nylon-6 composite material (MAT-4) and with the clamped-free boundary condition					
Maximum radial displacement corresponding to $n = 0$ is equal to 0.0292 *mm*					
Linear taper parameter value	$n = 0.2$	$n = 0.4$	$n = 0.6$	$n = 0.8$	$n = 1.0$
Maximum radial displacement (in *mm*)	0.0281	0.02677	0.02515	0.02312	0.02045
% decrease in the displacement	3.862	8.430	13.964	20.898	30.054

Table 2.49 Percentage decrease in the maximum radial displacement with the linear taper parameter n in a rotating annular linearly-tapered disc made of Nylon-6 composite material (MAT-4) and with the clamped-free boundary condition

It can be seen from the above Tables 2.46 - 2.49 that the percentage decrease in the maximum radial displacement in the rotating disc made up of Graphite-Fiber Reinforced Plastic material (MAT-3) is maximum for a linear taper parameter value of n = 1 when compared with the percentage decrease in the maximum radial displacement in the rotating discs made up of other materials for the same value of the linear taper parameter, and is equal to 43.9 %.

2.4.3.2 Effect of the degree of orthotropy (λ) on the elastic response

The following Figure 2.18 shows the variation of the maximum radial stress in a rotating annular linearly-tapered disc with the degree of orthotropy of the material of the disc for the different values of the linear taper parameter n and for the clamped-free boundary condition.

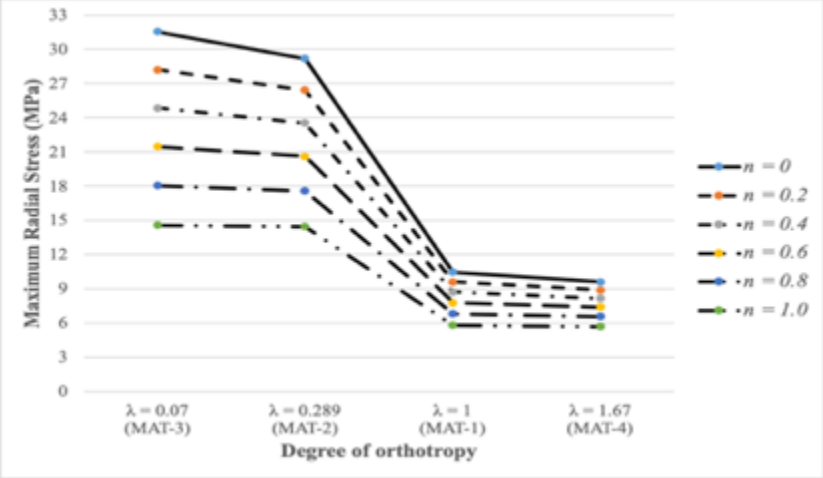

Figure 2.18 Effect of degree of orthotropy on the maximum radial stress in a rotating annular linearly-tapered disc for different values of the linear taper parameter n and for the clamped-free boundary condition

It can be seen from the above Figure 2.18 that irrespective of the linear taper parameter n, the rotating linearly-tapered disc made up of MAT-3 with λ = 0.07 and with the clamped-free boundary condition is subjected to the maximum radial stress and as the value of the degree of orthotropy of the material increases, the radial stress decreases and is the lowest for the linearly-tapered disc made up of MAT-4 with λ = 1.67. Therefore, it can be concluded that for a rotating disc with the clamped-free boundary condition, the more the degree of the orthotropy of the material of the disc is, the less the amount of radial stress induced in the disc will be.

Since for the present case, $\lambda_{MAT-3} < \lambda_{MAT-2} < \lambda_{MAT-1} < \lambda_{MAT-4}$, therefore the decreasing order of the maximum radial stress is given as ${\sigma_r^{max}}_{MAT-3} > {\sigma_r^{max}}_{MAT-2} > {\sigma_r^{max}}_{MAT-1} > {\sigma_r^{max}}_{MAT-4}$.

The following Figure 2.19 shows the variation of the maximum circumferential stress in a rotating annular linearly-tapered disc with the degree of orthotropy of the material of the disc for the different values of the linear taper parameter *n* and for the clamped-free boundary condition.

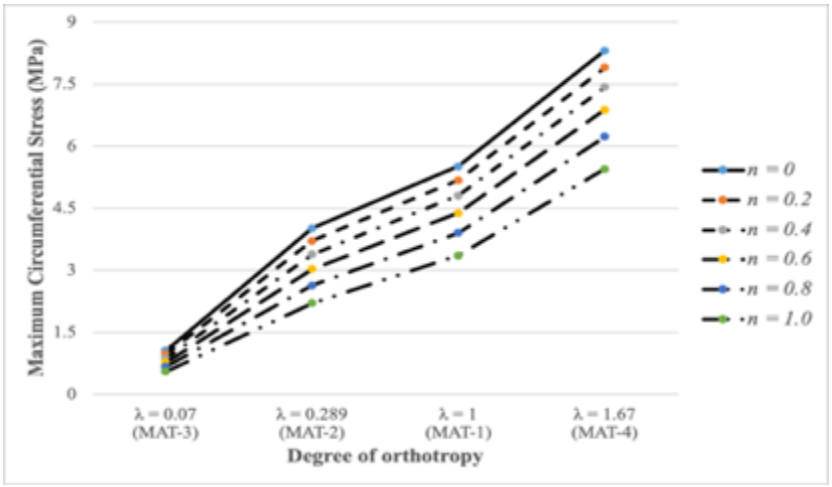

Figure 2.19 Effect of degree of orthotropy on the maximum circumferential stress in a rotating annular linearly-tapered disc for different values of the linear taper parameter *n* and for the clamped-free boundary condition

It can be seen from the above Figure 2.19 that irrespective of the linear taper parameter *n*, the rotating linearly-tapered disc made up of MAT-4 with λ = 1.67 and with the clamped-free boundary condition is subjected to the maximum circumferential stress and as the value of the degree of orthotropy of the material decreases, the circumferential stress decreases and is the lowest for the linearly-tapered disc made up of MAT-3 with λ = 0.07. Therefore, it can be concluded that for a rotating disc with the clamped-free boundary condition, the more the degree of the orthotropy of the material of the disc is, the more the amount of circumferential stress induced in the disc will be.

Since for the present case, $\lambda_{MAT-3} < \lambda_{MAT-2} < \lambda_{MAT-1} < \lambda_{MAT-4}$, therefore the increasing order of the maximum circumferential stress is given as ${\sigma_\theta^{max}}_{MAT-3} < {\sigma_\theta^{max}}_{MAT-2} < {\sigma_\theta^{max}}_{MAT-1} < {\sigma_\theta^{max}}_{MAT-4}$.

The following Figure 2.20 shows the variation of the maximum radial displacement in a rotating annular linearly-tapered disc with the degree of orthotropy of the material of the disc for the different values of the linear taper parameter *n* and for the clamped-free boundary condition.

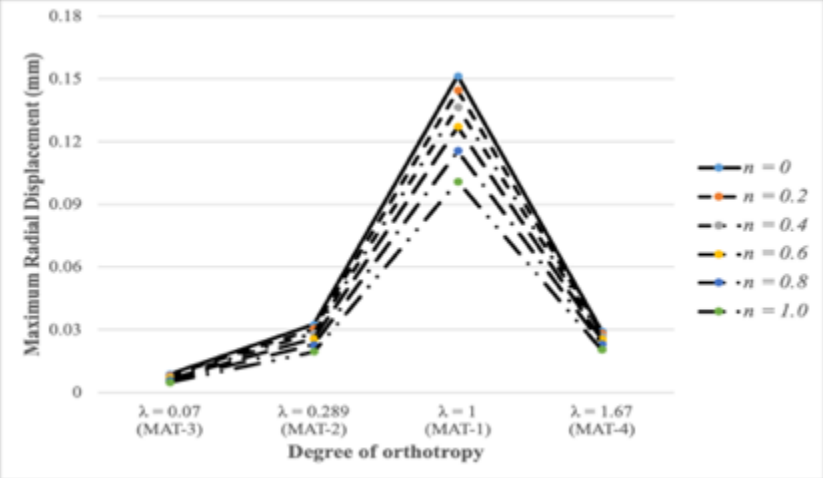

Figure 2.20 Effect of degree of orthotropy on the maximum radial displacement in a rotating annular linearly-tapered disc for different values of the linear taper parameter *n* and for the clamped-free boundary condition

It can be seen from the above Figure 2.20 that irrespective of the value of the linear taper parameter, the radial displacement in a rotating annular linearly-tapered disc with the clamped-free boundary condition increases with the increasing value of the degree of orthotropy λ of the material of the disc till it reaches unity. This variation of displacement is similar to the case of radial displacement distributions in a linearly-tapered disc with the free-free boundary condition, where the displacements are maximum in a rotating annular linearly-tapered disc made up of Polycarbonate material (MAT-1, λ = 1.0) as compared with the rotating discs made of other materials.

Furthermore, the value of maximum radial displacement decreases as the degree of orthotropy of the material of the disc is greater than unity i.e., for a disc made up of MAT-4 with λ = 1.67. Therefore, it can be said that irrespective of the boundary condition, the radial displacement is always maximum in a rotating disc made up of an isotropic material (Polycarbonate material, in the present case).

2.4.4 Rotating annular Stodola disc with the clamped-free boundary condition

This sub-section deals with the parametric study on the elastic response of rotating annular Stodola discs with the clamped-free boundary condition. The effect of Stodola taper parameter (s) and the effect of the degree of orthotropy (λ) of the material of the disc on the radial stress and circumferential stress distributions and the radial displacement distributions are studied. Graphical results for the stress and displacement distributions are presented and the percentage change in the maximum stress and displacement values are calculated for rotating annular linearly-tapered discs made up of an isotropic material (MAT-1) and various orthotropic materials.

2.4.4.1 Effect of the Stodola taper parameter (s) on the elastic response

The following Figures 2.21(a), (b), (c) and (d) show the radial stress distributions in rotating annular Stodola discs with the clamped-free boundary condition for different values of the taper parameter s for an isotropic material and various orthotropic materials.

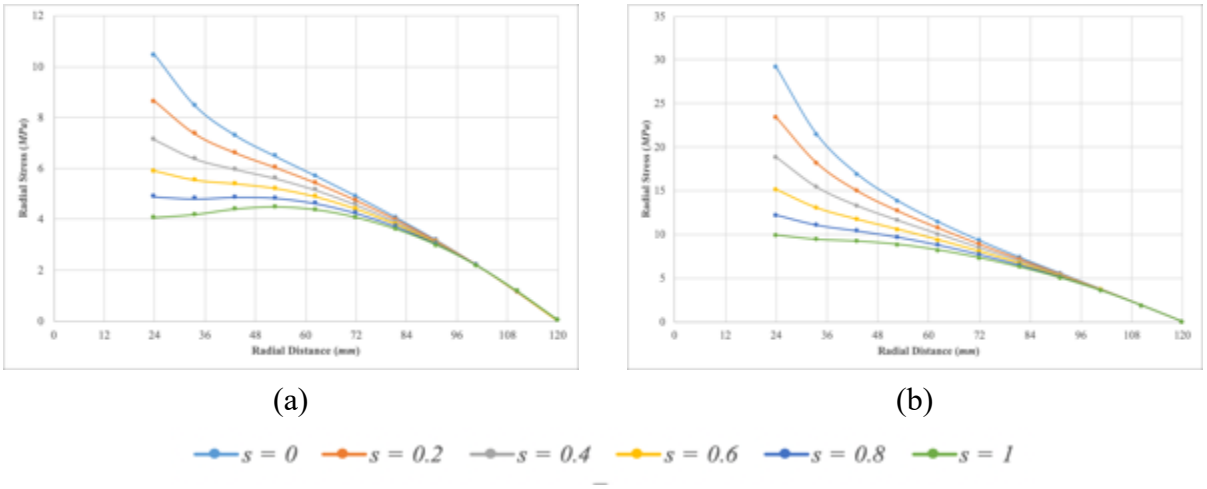

(a) (b)

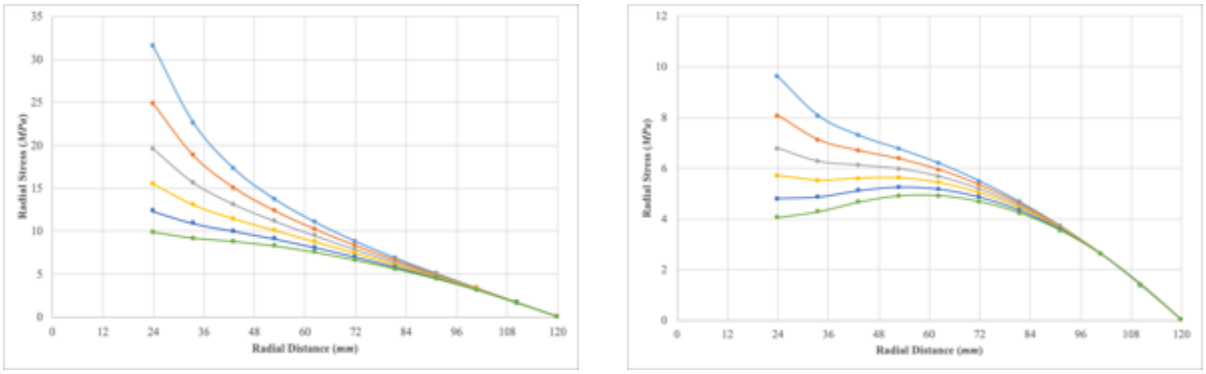

(c) (d)

Figure 2.21 Radial stress distribution in a rotating annular Stodola disc with the clamped-free boundary condition for **(a)** MAT-1 **(b)** MAT-2 **(c)** MAT-3 **(d)** MAT-4

It can be observed from the above Figures 2.21(a), (b), (c) and (d) that similar to the radial stress distributions in the linearly-tapered discs with the clamped-free boundary condition, the radial stress in the Stodola discs also decreases with the increasing value of the Stodola taper parameter s and the stress is least for a taper parameter value of $s = 1$.

Also, as it is known that for a rotating annular uniform-thickness disc with the clamped-free boundary condition, the maximum radial stress is always induced at the hub of the disc at which it is clamped. However, in the case of a rotating annular Stodola disc with the clamped-free boundary condition, the locus of the point experiencing the maximum radial stress changes with the increasing value of the taper parameter. As the taper parameter is increased, the locus of the point experiencing the maximum radial stress tends to shift towards the geometric mean radius of the clamped-free disc which is 53.67 *mm* in this case. The above observation is independent of the degree of orthotropy of the material of the disc. i.e., the observation is true regardless of the material of the rotating disc.

The following Tables 2.50 - 2.53 show the maximum radial stress and the percentage decrease in the maximum radial stress with the Stodola taper parameter s for rotating annular Stodola discs with the clamped-free boundary condition and made up of different materials. Also, in the below Tables 2.50 - 2.53, the percentage decrease in the maximum radial stress is calculated according to the formula given in the Equation (2.28).

Rotating annular Stodola disc made up of Polycarbonate material (MAT-1) and with the clamped-free boundary condition					
Maximum radial stress corresponding to $s = 0$ is equal to 10.457 *MPa*					
Stodola taper parameter value	$s = 0.2$	$s = 0.4$	$s = 0.6$	$s = 0.8$	$s = 1.0$
Maximum radial stress (in *MPa*)	8.633	7.128	5.891	4.879	4.473
% decrease in the stress	17.442	31.834	43.66	53.344	57.22

Table 2.50 Percentage decrease in the maximum radial stress with the Stodola taper parameter s in a rotating annular Stodola disc made of Polycarbonate material (MAT-1) and with the clamped-free boundary condition

Rotating annular Stodola disc made up of Glass-Fiber Reinforced Plastic material (MAT-2) and with the clamped-free boundary condition					
Maximum radial stress corresponding to $s = 0$ is equal to 29.199 *MPa*					
Stodola taper parameter value	$s = 0.2$	$s = 0.4$	$s = 0.6$	$s = 0.8$	$s = 1.0$
Maximum radial stress (in *MPa*)	23.438	18.826	15.146	12.215	9.883
% decrease in the stress	19.730	35.524	48.12	58.167	66.152

Table 2.51 Percentage decrease in the maximum radial stress with the Stodola taper parameter s in a rotating annular Stodola disc made of Glass-Fiber Reinforced Plastic material (MAT-2) and with the clamped-free boundary condition

Rotating annular Stodola disc made of Graphite-Fiber Reinforced Plastic material (MAT-3) and with the clamped-free boundary condition					
Maximum radial stress corresponding to $s = 0$ is equal to 31.542 *MPa*					
Stodola taper parameter value	$s = 0.2$	$s = 0.4$	$s = 0.6$	$s = 0.8$	$s = 1.0$
Maximum radial stress (in *MPa*)	24.823	19.583	15.498	12.312	9.824
% decrease in the stress	21.302	37.914	50.86	60.967	68.853

Table 2.52 Percentage decrease in the maximum radial stress with the Stodola taper parameter s in a rotating annular Stodola disc made of Graphite-Fiber Reinforced Plastic material (MAT-3) and with the clamped-free boundary condition

Rotating annular Stodola disc made of Nylon-6 composite material (MAT-4) and with the clamped-free boundary condition					
Maximum radial stress corresponding to $s = 0$ is equal to 9.607 *MPa*					
Stodola taper parameter value	$s = 0.2$	$s = 0.4$	$s = 0.6$	$s = 0.8$	$s = 1.0$
Maximum radial stress (in *MPa*)	8.076	6.788	5.711	5.257	4.923
% decrease in the stress	15.93	29.33	40.556	45.27	48.758

Table 2.53 Percentage decrease in the maximum radial stress with the Stodola taper parameter s in a rotating annular Stodola disc made of Nylon-6 composite material (MAT-4) and with the clamped-free boundary condition

It can be seen from the above Tables 2.50 - 2.53 that the percentage decrease in the maximum radial stress in the rotating disc made up of Graphite-Fiber Reinforced Plastic material (MAT-3) and with the clamped-free boundary condition is maximum for a Stodola taper parameter value of $s = 1$ and is equal to 68.85 %.

Recalling the thickness reduction ratio values of the tapered discs from the Table 2.4, it is clear that for the linear taper parameter value of $n = 1$ and the Stodola taper parameter value of $s = 1$, the thickness of the disc at its outer radius is the same and is equal to 0.48 *mm*. On comparing the percentage decrease in the maximum radial stress in rotating annular linearly-tapered discs from the Tables 2.38 - 2.41 with the percentage decrease in the maximum radial stress in rotating annular Stodola discs from the Tables 2.50 - 2.53 corresponding to n and s equal to 1, it can be seen that the percentage decrease in the maximum radial stress is more for the case of rotating annular Stodola discs.

Therefore, it can be said that regardless of the material of the disc, for the same thickness reduction ratio value of $\bar{h} = 0.2$, the radial stress is always lower in a rotating annular Stodola disc as compared with the rotating annular linearly-tapered disc.

The following Figures 2.22(a), (b), (c) and (d) shows the circumferential stress distributions in a rotating annular Stodola disc with the clamped-free boundary condition for different values of the Stodola taper parameter s for an isotropic material and various orthotropic materials.

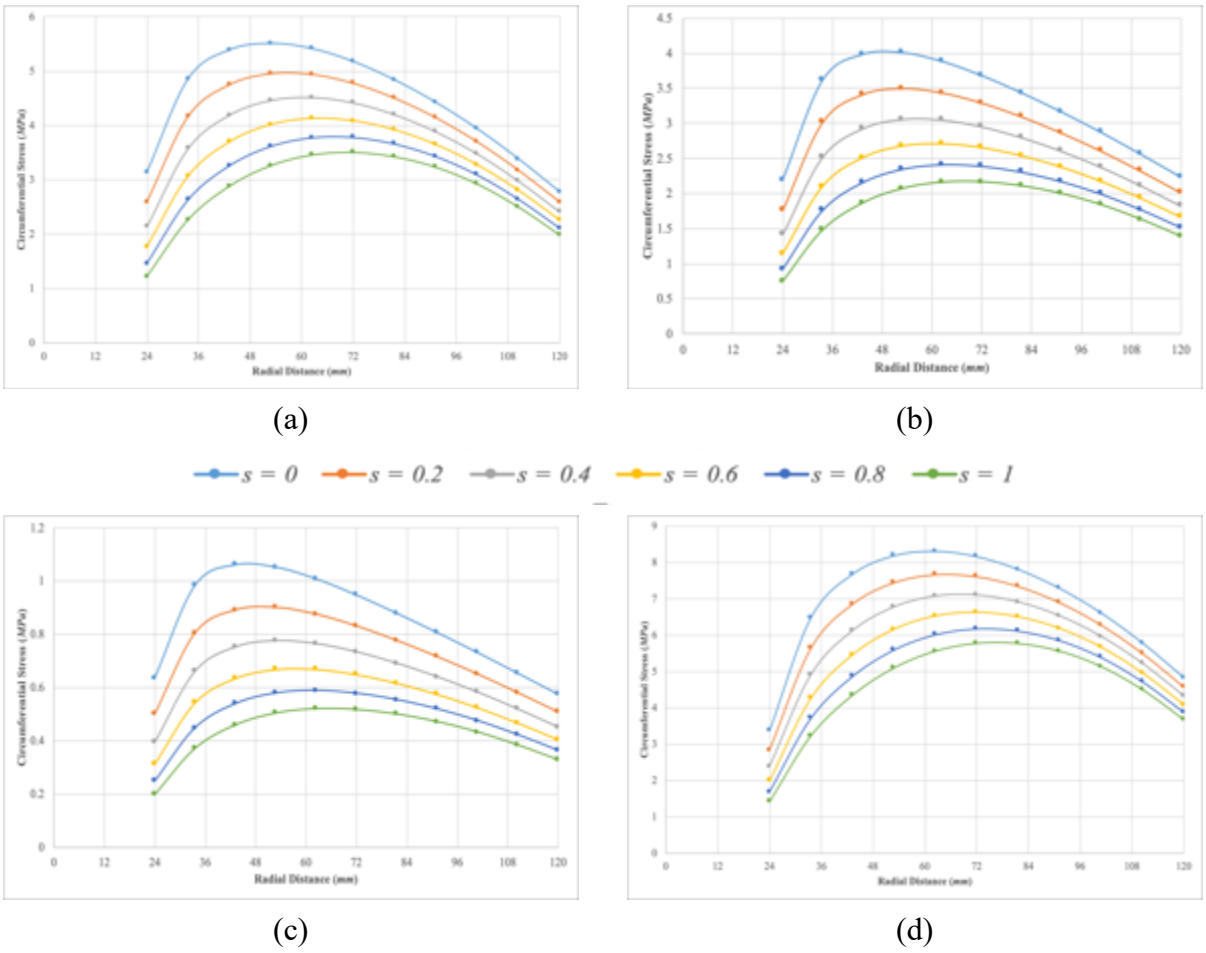

Figure 2.22 Circumferential stress distributions in a rotating annular Stodola disc with the clamped-free boundary condition for **(a)** MAT-1 **(b)** MAT-2 **(c)** MAT-3 **(d)** MAT-4

As it is known that for a rotating annular uniform-thickness disc with the clamped-free boundary condition, the maximum circumferential stress is always induced at the geometric mean radius of the disc which is 53.67 *mm* in the present case. However, in the case of a rotating annular Stodola disc with the clamped-free boundary condition, the locus of the point experiencing the maximum circumferential stress changes with the increasing value of the taper parameter of the disc. As the taper parameter is increased, the locus of the point experiencing the maximum circumferential stress tends to shift towards the arithmetic mean radius of the clamped-free disc (which is 72 *mm* in the present case).

The following Tables 2.54 - 2.57 show the maximum circumferential stress and the percentage decrease in the maximum circumferential stress with the Stodola taper parameter *s* for

rotating annular Stodola discs with the clamped-free boundary condition and made up of different materials that are considered in the present study. Also, in the below Tables 2.54 - 2.57, the percentage decrease in the maximum circumferential stress is calculated according to the formula given in the Equation (2.28).

Rotating annular Stodola disc made of Polycarbonate material (MAT-1) and with the clamped-free boundary condition					
Maximum circumferential stress corresponding to $s = 0$ is equal to 5.51 *MPa*					
Stodola taper parameter value	$s = 0.2$	$s = 0.4$	$s = 0.6$	$s = 0.8$	$s = 1.0$
Maximum circumferential stress (in *MPa*)	4.958	4.462	4.017	3.619	3.264
% decrease in the stress	10.014	19.025	27.104	34.325	40.765

Table 2.54 Percentage decrease in the maximum circumferential stress with the Stodola taper parameter s in a rotating annular Stodola disc made of Polycarbonate material (MAT-1) and with the clamped-free boundary condition

Rotating annular Stodola disc made of Glass-Fiber Reinforced Plastic material (MAT-2) and with the clamped-free boundary condition					
Maximum circumferential stress corresponding to $s = 0$ is equal to 4.007 *MPa*					
Stodola taper parameter value	$s = 0.2$	$s = 0.4$	$s = 0.6$	$s = 0.8$	$s = 1.0$
Maximum circumferential stress (in *MPa*)	3.497	3.056	2.708	2.413	2.162
% decrease in the stress	12.725	23.723	32.398	39.760	46.03

Table 2.55 Percentage decrease in the maximum circumferential stress with the Stodola taper parameter s in a rotating annular Stodola disc made of Glass-Fiber Reinforced Plastic material (MAT-2) and with the clamped-free boundary condition

Rotating annular Stodola disc made of Graphite-Fiber Reinforced Plastic material (MAT-3) and with the clamped-free boundary condition					
Maximum circumferential stress corresponding to $s = 0$ is equal to 1.053 *MPa*					
Stodola taper parameter value	$s = 0.2$	$s = 0.4$	$s = 0.6$	$s = 0.8$	$s = 1.0$
Maximum circumferential stress (in *MPa*)	0.901	0.775	0.669	0.588	0.520
% decrease in the stress	14.321	26.339	36.389	44.046	50.575

Table 2.56 Percentage decrease in the maximum circumferential stress with the Stodola taper parameter s in a rotating annular Stodola disc made of Graphite-Fiber Reinforced Plastic material (MAT-3) and with the clamped-free boundary condition

Rotating annular Stodola disc made of Nylon-6 composite material (MAT-4) and with the clamped-free boundary condition					
Maximum circumferential stress corresponding to $s = 0$ is equal to 8.308 *MPa*					
Stodola taper parameter value	$s = 0.2$	$s = 0.4$	$s = 0.6$	$s = 0.8$	$s = 1.0$
Maximum circumferential stress (in *MPa*)	7.665	7.098	6.621	6.179	5.770
% decrease in the stress	7.739	14.562	20.299	25.619	30.541

Table 2.57 Percentage decrease in the maximum circumferential stress with the Stodola taper parameter s in a rotating annular Stodola disc made of Nylon-6 composite material (MAT-4) and with the clamped-free boundary condition

It can be seen from the above Tables 2.54 - 2.57 that the percentage decrease in the maximum circumferential stress in the rotating disc made up of Graphite-Fiber Reinforced Plastic material (MAT-3) and with the clamped-free boundary condition is maximum for a Stodola taper parameter value of $s = 1$ and is equal to 50.58 %.

On comparing the percentage decrease in the maximum circumferential stress in rotating annular linearly-tapered discs from the Tables 2.42 - 2.45 with the percentage decrease in the maximum circumferential stress in rotating annular Stodola discs from the Tables 2.54 - 2.57 corresponding to n and s equal to 1, it can be seen that the percentage decrease in the maximum circumferential stress is more for rotating annular Stodola discs made up of MAT-1, MAT-2 and

MAT-3. However, for the rotating disc made up of MAT-4 and with the clamped-free boundary condition, the percentage decrease in the maximum circumferential stress corresponding to *n* and *s* equal to 1 is more in the case of linearly-tapered disc.

The following Figures 2.23(a), (b), (c) and (d) show the radial displacement distributions in a rotating annular Stodola disc with the clamped-free boundary condition for different values of the Stodola taper parameter *s* for an isotropic material and various orthotropic materials.

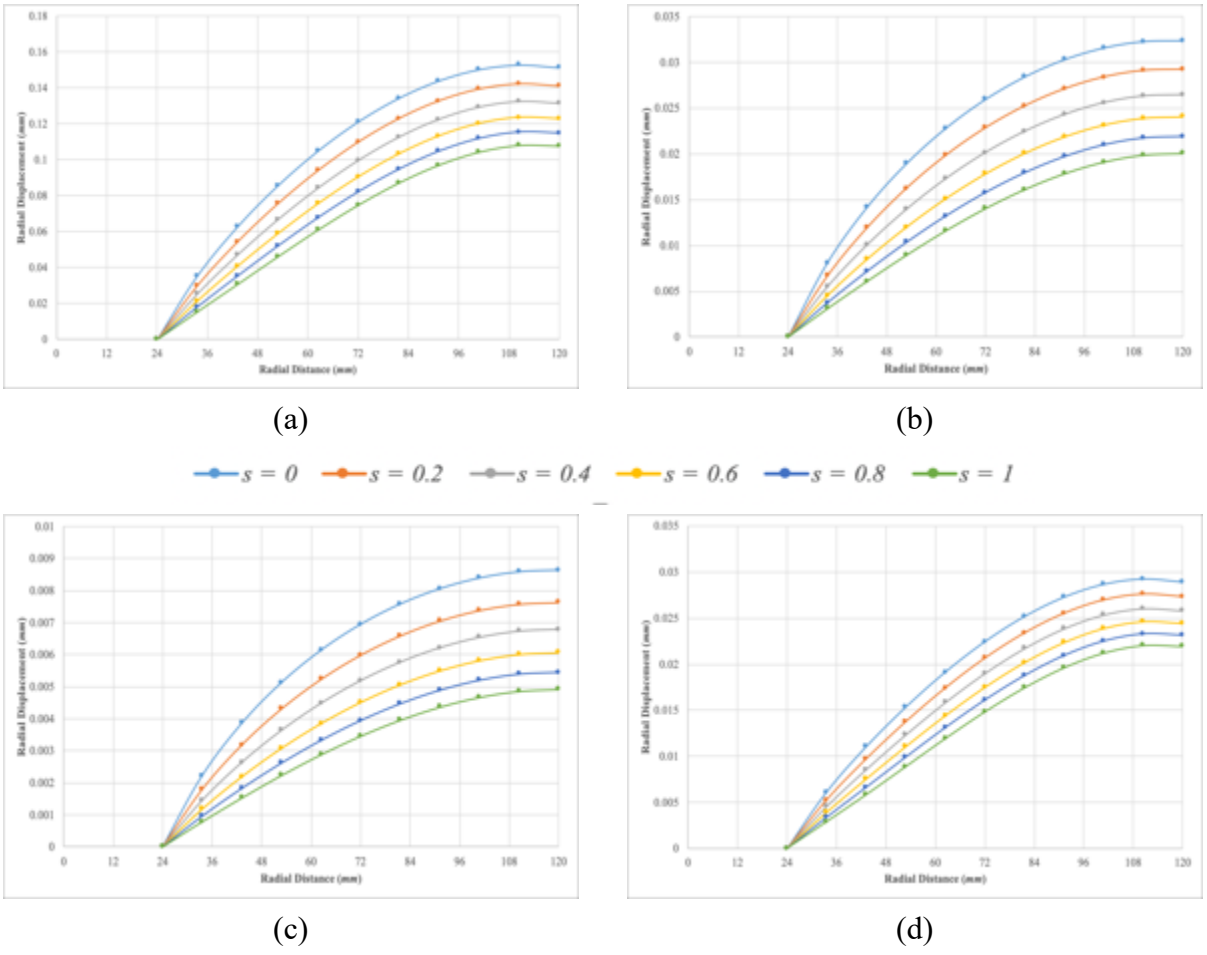

Figure 2.23 Radial displacement distributions in a rotating annular Stodola disc with the clamped-free boundary condition for **(a)** MAT-1 **(b)** MAT-2 **(c)** MAT-3 **(d)** MAT-4

It can be observed from the above Figures 2.23(a), (b), (c) and (d) that the uniform-thickness disc is subjected to maximum amount of radial displacement and as the taper parameter is increased, the displacement decreases accordingly and is least for a taper parameter value of *s* =

1. It can also be seen from the above plots that similar to the radial displacement distributions in the linearly-tapered disc with the clamped-free boundary condition, the radial displacement in the rotating annular Stodola disc is also maximum for the case of a rotating disc made of Polycarbonate material (MAT-1) as compared with the rotating disc made up of other materials that are considered in the present study.

The following Tables 2.58 - 2.61 show the maximum radial displacement and the percentage decrease in the maximum radial displacement with the Stodola taper parameter s for rotating annular Stodola discs with the clamped-free boundary condition and made up of different materials. Also, in the below Tables 2.58 - 2.61, the percentage decrease in the radial displacement is calculated according to the formula given in the Equation (2.29).

Rotating annular Stodola disc made of Polycarbonate material (MAT-1) and with the clamped-free boundary condition					
Maximum radial displacement corresponding to $s = 0$ is equal to 0.1513 *mm*					
Stodola taper parameter value	$s = 0.2$	$s = 0.4$	$s = 0.6$	$s = 0.8$	$s = 1.0$
Maximum radial displacement (in *mm*)	0.14092	0.13145	0.12280	0.11493	0.10776
% decrease in the displacement	6.849	13.112	18.826	24.0311	28.769

Table 2.58 Percentage decrease in the maximum radial displacement with the Stodola taper parameter s in a rotating annular Stodola disc made of Polycarbonate material (MAT-1) and with the clamped-free boundary condition

Rotating annular Stodola disc made of Glass-Fiber Reinforced Plastic material (MAT-2) and with the clamped-free boundary condition					
Maximum radial displacement corresponding to $s = 0$ is equal to 0.0324 *mm*					
Stodola taper parameter value	$s = 0.2$	$s = 0.4$	$s = 0.6$	$s = 0.8$	$s = 1.0$
Maximum radial displacement (in *mm*)	0.02924	0.02647	0.02405	0.02193	0.02007
% decrease in the displacement	9.748	18.284	25.756	32.298	38.035

Table 2.59 Percentage decrease in the maximum radial displacement with the Stodola taper parameter s in a rotating annular Stodola disc made of Glass-Fiber Reinforced Plastic material (MAT-2) and with the clamped-free boundary condition

Rotating annular Stodola disc made of Graphite-Fiber Reinforced Plastic material (MAT-3) and with the clamped-free boundary condition					
Maximum radial displacement corresponding to $s = 0$ is equal to 0.008642 *mm*					
Stodola taper parameter value	$s = 0.2$	$s = 0.4$	$s = 0.6$	$s = 0.8$	$s = 1.0$
Maximum radial displacement (in *mm*)	0.00764	0.006792	0.006071	0.005455	0.004928
% decrease in the displacement	11.585	21.405	29.754	36.878	42.978

Table 2.60 Percentage decrease in the maximum radial displacement with the Stodola taper parameter *s* in a rotating annular Stodola disc made of Graphite-Fiber Reinforced Plastic material (MAT-3) and with the clamped-free boundary condition

Rotating annular Stodola disc made of Nylon-6 composite material (MAT-4) and with the clamped-free boundary condition					
Maximum radial displacement corresponding to $s = 0$ is equal to 0.0292 *mm*					
Stodola taper parameter value	$s = 0.2$	$s = 0.4$	$s = 0.6$	$s = 0.8$	$s = 1.0$
Maximum radial displacement (in *mm*)	0.02759	0.02606	0.02463	0.02330	0.02206
% decrease in the displacement	5.609	10.856	15.75	20.304	24.535

Table 2.61 Percentage decrease in the maximum radial displacement with the Stodola taper parameter *s* in a rotating annular Stodola disc made of Nylon-6 composite material (MAT-4) and with the clamped-free boundary condition

It can be seen from the above Tables 2.58 - 2.61 that the percentage decrease in the maximum radial displacement in the rotating disc made up of Graphite-Fiber Reinforced Plastic material (MAT-3) is maximum for a Stodola taper parameter value of $s = 1$ as compared with the percentage decrease in the maximum radial displacement in the rotating discs made up of other materials for the same value of the Stodola taper parameter, and the maximum percentage decrease is equal to 42.9 %.

On comparing the percentage decrease in the maximum radial displacement in rotating annular linearly-tapered discs from the Tables 2.46 - 2.49 with the percentage decrease in the maximum radial displacement in rotating annular Stodola discs from the Tables 2.58 - 2.61 corresponding to *n* and *s* equal to 1, it can be seen that the percentage decrease in the maximum

radial displacement is more for the case of linearly-tapered discs when compared with the Stodola discs.

2.4.4.2 Effect of the degree of orthotropy (λ) on the elastic response

The following Figure 2.24 shows the variation of the maximum radial stress in a rotating annular Stodola disc with the degree of orthotropy of the material of the disc for the different values of the Stodola taper parameter *s* and for the clamped-free boundary condition.

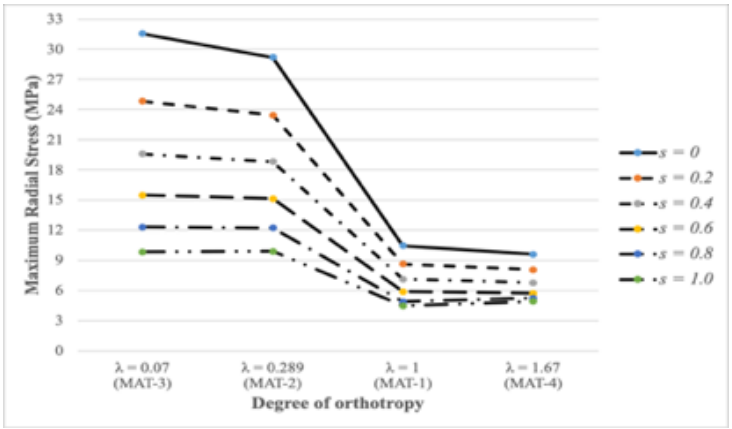

Figure 2.24 Effect of degree of orthotropy on the maximum radial stress in a rotating annular Stodola disc for different values of the taper parameter *s* and for the clamped-free boundary condition

It can be seen from the above Figure 2.24 that irrespective of the value of the Stodola taper parameter *s*, the rotating annular Stodola disc made up of MAT-3 with $\lambda = 0.07$ with the clamped-free boundary condition is subjected to the maximum amount of the radial stress and as the value of the degree of orthotropy of the material increases, the radial stress decreases and is the lowest for the Stodola disc made up of MAT-4 with $\lambda = 1.67$. This variation of the maximum radial stress in a rotating annular Stodola disc with the degree of orthotropy of the material of the disc is similar to the variation of the maximum radial stress in a rotating annular linearly-tapered disc with the clamped-free boundary condition.

The following Figure 2.25 shows the variation of the maximum circumferential stress in a rotating annular Stodola disc with the degree of orthotropy of the material of the disc for the different values of the Stodola taper parameter *s* and for the clamped-free boundary condition.

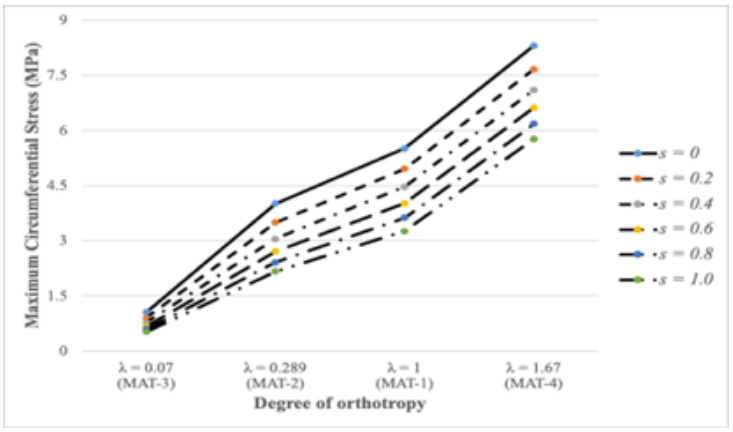

Figure 2.25 Effect of degree of orthotropy on the maximum circumferential stress in a rotating annular Stodola disc for different values of the taper parameter *s* and for the clamped-free boundary condition

It can be seen from the above Figure 2.25 that irrespective of the value of the Stodola taper parameter *s*, the rotating annular Stodola disc made up of MAT-4 with λ = 1.67 and with the clamped-free boundary condition is subjected to the maximum amount of circumferential stress and as the value of the degree of orthotropy of the material decreases, the circumferential stress decreases and is the lowest for the Stodola disc made up of MAT-3 with λ = 0.07. This variation of the maximum circumferential stress in a rotating annular Stodola disc with the degree of orthotropy of the material of the disc is similar to the variation of the maximum circumferential stress in a rotating annular linearly-tapered disc with the clamped-free boundary condition.

The following Figure 2.26 shows the variation of the maximum radial displacement in a rotating annular Stodola disc with the degree of orthotropy of the material of the disc for the different values of the Stodola taper parameter *s* and for the clamped-free boundary condition.

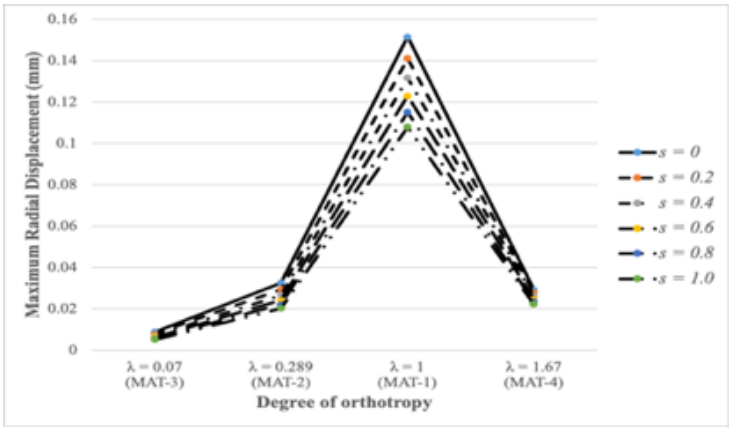

Figure 2.26 Effect of degree of orthotropy on the maximum radial displacement in a rotating annular Stodola disc for different values of the taper parameter *s* and for the clamped-free boundary condition

It can be seen from the above Figure 2.28 that irrespective of the value of the Stodola taper parameter *s*, the radial displacement in a rotating annular Stodola disc with the clamped-free boundary condition increases with the increasing order of the degree of orthotropy λ of the material of the disc till it reaches unity.

This variation of displacement with the degree of orthotropy of the material of the disc is similar to the variation of radial displacement in a linearly-tapered disc with the clamped-free boundary condition, where the displacement is maximum in a rotating annular linearly-tapered disc made of Polycarbonate material (MAT-1, $\lambda = 1.0$) as compared with the rotating discs made of other materials. Furthermore, the value of maximum radial displacement decreases when the degree of orthotropy of the material of the disc is greater than unity i.e., for a disc made of MAT-4 with $\lambda = 1.67$.

2.5 Conclusion

In this chapter, the elastic response of rotating annular linearly-tapered and Stodola discs made up of an isotropic material and various orthotropic materials is presented. Finite-element-like modification of the rotating disc is shown in sub-section 2.2.1. In sub-section 2.2.4, the Rayleigh-Ritz method based on the total potential energy of the rotating disc is used to determine the elastic response of the rotating tapered discs. In section 2.3, the results obtained for the elastic response of the tapered disc using the Rayleigh-Ritz method are validated with the results obtained for the same using the closed-form analytical solutions that are available in the literature and also with the solution obtained using the finite element analysis software ANSYS®. A convergence study is presented in the sub-section 2.3.1 to demonstrate the dependence of accuracy of the obtained results for the elastic response of rotating annular tapered discs on the number of divisions of the tapered disc. In section 2.4, a parametric study is conducted to investigate the effects of the linear taper and Stodola taper parameters *n* and *s* respectively, and the degree of orthotropy (λ) on the radial stresses and circumferential stresses and the radial displacements in rotating annular tapered discs with the free-free and clamped-free boundary conditions. A summary of observations is as follows:

- The accuracy of the results obtained for the elastic response of the rotating disc using the Rayleigh-Ritz method with finite-element-like modification is dependent on the number of divisions of the tapered disc.
- Tapering has a significant effect on the stress state of the rotating disc. The higher the taper parameter value of the rotating disc (which in turn is the representation of the taper angle) is, the lesser the radial and circumferential stresses induced in the disc will be. The same observation holds true for the distribution of radial displacements in the disc.
- Irrespective of the values of the taper parameters n and s, for the rotating annular linearly-tapered and Stodola discs with the clamped-free boundary condition, the lower the degree of orthotropy of the material of the disc is, the higher the radial stress induced in the disc will be and the lower the circumferential stress induced in the disc will be.
- Tapering the disc has no effect on the loci of the points experiencing the maximum radial and circumferential stresses in the case of a rotating annular linearly-tapered disc with the free-free and the clamped-free boundary conditions.
- Irrespective of the material properties, for a Stodola disc with the clamped-free boundary condition, tapering has a significant effect on the loci of the points that experience maximum radial and circumferential stresses. As the taper angle is increased, the locus of the point experiencing the maximum radial stress tends to shift from the hub of the disc to its geometric mean radius point while the locus of the point exposed to the maximum circumferential stress shifts from the geometric mean radius point to the arithmetic mean radius point of the disc.
- For the same thickness reduction ratio value of $\bar{h} = 0.2$ (i.e., when the thickness of the disc at its outer radius is 0.48 mm), the maximum radial stress and the maximum radial displacement are always lower in the rotating annular linearly-tapered disc with the free-free boundary condition as compared with the rotating annular Stodola disc with the free-free boundary condition, while the maximum circumferential stress is higher in the rotating annular linearly-tapered disc
- For the same thickness reduction ratio value of $\bar{h} = 0.2$, the maximum radial stress and the maximum circumferential stress is always higher in the rotating annular linearly-tapered disc as compared with the rotating annular Stodola disc with the clamped-free boundary

condition, while the maximum radial displacement is higher in the rotating annular Stodola disc with the clamped-free boundary condition.

Chapter 3

Elastic response of rotating annular uniform-thickness discs made of fiber-reinforced composite materials

3.1 Introduction

Rotating disc finds its application in engineering structures such as in the aircraft engines, gas turbines, flywheels and brakes in the automobile system. The selection of material for such applications is principally based on its ability to bear strength. However, strength alone is not always enough, since in aircrafts or many other structures a great penalty accompanies weight. It is obvious that an aircraft must be as light as possible, since it must be able to fly. This situation leads to the use of FRP (Fiber Reinforced Plastic) composite materials, since they have high stiffness, high strength and high toughness often comparable with structural metal alloys. Furthermore, they provide these properties at substantially less weight than metals. i.e., their specific strength and modulus per unit weight is near four to five times than that of steel and aluminium, thereby making the overall structure lighter.

This chapter presents the formulation to determine the elastic response of rotating annular uniform-thickness discs made up of fiber-reinforced composite materials by using the Rayleigh-Ritz method based on the Classical Laminate Theory (CLT) in cylindrical coordinate system. The radial displacements, the in-plane stresses and the radial and circumferential stress variations through the thickness in a rotating annular uniform-thickness fiber-reinforced composite disc with the clamped-free boundary condition are computed. Approximate functions for the radial, circumferential and the transverse displacement functions in polar coordinates are assumed. An approximate solution is developed for the radial, circumferential and transverse displacements and the stress distributions in the laminated disc that is clamped at the hub, and it is compared with the solutions obtained for the same using the finite element analysis software ANSYS®. The finite element analysis is performed using SOLID185 and SHELL181 elements. A comprehensive parametric study is conducted to investigate the effect of fiber orientation, radius ratio, rotational velocity and laminate configuration on the stress distributions and the radial displacement

distributions in rotating annular uniform-thickness composite discs with the clamped-free boundary condition.

3.2 Classical Laminate Theory in polar coordinates [56]

There are various theories that can be used in evaluating the stress distribution and dynamic response of a structural component such as the first order shear deformation theory (also known as the Mindlin-Reissner theory), second order shear deformation theory and so on. The Classical Laminate Theory (CLT) is commonly used to analyze the strains, displacements and stresses that are developed due to mechanical or thermal loading in thin laminated structures. The classical theory of laminates uses a first order model, and the following assumptions are made in order to analyze the structure under consideration.

a. The thickness of the laminate, h should be much smaller than any other characteristic dimension of the laminate.
b. The displacements (radial and circumferential in the present case) i.e., u_r and u_θ are assumed to be linear functions of the thickness coordinate z. i.e., no warping takes place in the laminate.
c. The transverse shear strains are zero. i.e., $\gamma_{rz} = \gamma_{\theta z} = 0$
d. The laminate consists of orthotropic plies bonded together, with the principal material axes of the plies oriented along arbitrary directions with respect to the *x-y* plane, and each orthotropic ply should obey Hooke's law.

Following the above made assumptions in the Classical Laminate Theory, the displacement field in cylindrical coordinate system is written as:

$$u_r(r,\theta,z) = u_r^o(r,\theta) - z\frac{\partial w_o(r,\theta)}{\partial r} \tag{3.1}$$

$$u_\theta(r,\theta,z) = u_\theta^o(r,\theta) - z\frac{\partial w_o(r,\theta)}{\partial r} \tag{3.2}$$

$$w(r,\theta,z) = w_o(r,\theta) \tag{3.3}$$

In the above Equations (3.1) - (3.3), u_r, u_θ and w are the radial, circumferential and the transverse displacements of a point in the *k*-th ply of the laminated disc. u_r^o, u_θ^o and w_o are the corresponding displacements in the mid-plane of the laminated disc and z is the position of the point in the *k*-th ply in the laminate. Owing to the rotational symmetry of the disc, the above Equations (3.1 - 3.3) can be reduced to:

$$u_r(r,z) = u_r^o(r) - z\frac{dw_o(r)}{dr} \tag{3.4}$$

$$u_\theta(r,z) = u_\theta^o(r) - z\frac{dw_o(r)}{dr} \tag{3.5}$$

$$w(r) = w_o(r) \tag{3.6}$$

3.2.1 Expression for the strain field

Under the axisymmetric loading and plane stress condition, by making use of the assumptions made in the Classical Laminate Theory, the strain field in condensed form in the cylindrical coordinate system is written as [57]:

$$\{\varepsilon\} = \{\varepsilon_m\} + \{\varepsilon_f\} \tag{3.7}$$

where $\{\varepsilon\}$ represents the strain matrix that contains the radial strain, circumferential strain and in-plane shear strain at any point inside the rotating disc, and is the superposition of the mid-plane strain matrix $\{\varepsilon_m\}$ and the flexural strain matrix $\{\varepsilon_f\}$, if any. In expanded form, the above Equation (3.7) can be written as:

$$\begin{Bmatrix} \varepsilon_{rr} \\ \varepsilon_{\theta\theta} \\ \gamma_{r\theta} \end{Bmatrix} = \begin{Bmatrix} \varepsilon_{rr}^o \\ \varepsilon_{\theta\theta}^o \\ \gamma_{r\theta}^o \end{Bmatrix} + \begin{Bmatrix} \varepsilon_{rr}^f \\ \varepsilon_{\theta\theta}^f \\ \gamma_{r\theta}^f \end{Bmatrix} \tag{3.8}$$

where, ε_{rr}, $\varepsilon_{\theta\theta}$ and $\gamma_{r\theta}$ are the radial, circumferential and in-plane shear strains respectively, ε_{rr}^o, $\varepsilon_{\theta\theta}^o$ and $\gamma_{r\theta}^o$ are the corresponding strains at the mid plane and ε_{rr}^f, $\varepsilon_{\theta\theta}^f$ and $\gamma_{r\theta}^f$

are the flexural strains. The strain-displacement relations according to the Classical Laminate Theory in cylindrical coordinate system are given as:

$$\varepsilon_{rr}^{o} = \frac{du_r^o(r)}{dr} \tag{3.9}$$

$$\varepsilon_{rr}^{f} = -z\frac{d^2w(r)}{dr^2} \tag{3.10}$$

$$\gamma_{r\theta}^{o} = \left(\frac{du_\theta^o(r)}{dr} - \frac{u_\theta^o(r)}{r}\right) \tag{3.11}$$

$$\varepsilon_{\theta\theta}^{o} = \frac{u_r^o(r)}{r} \tag{3.12}$$

$$\varepsilon_{\theta\theta}^{f} = -z\frac{dw(r)}{rdr} \tag{3.13}$$

$$\gamma_{r\theta}^{f} = -2z\frac{d}{dr}\left(\frac{dw(r)}{rd\theta}\right) \tag{3.14}$$

Since for the axisymmetric components, the variation with respect to θ is neglected, therefore, in the above Equation (3.14), the flexural shear strain $\gamma_{r\theta}^{f}$ vanishes i.e., $\gamma_{r\theta}^{f} = 0$.

3.2.2 Expression for the stress field

Using the stress-strain relations in the Classical Laminate Theory, the stresses in the *k*-th ply of the rotating disc are given as:

$$\begin{Bmatrix} \sigma_{rr} \\ \sigma_{\theta\theta} \\ \tau_{r\theta} \end{Bmatrix}_k = \overline{[Q]}_k \begin{Bmatrix} \varepsilon_{rr} \\ \varepsilon_{\theta\theta} \\ \gamma_{r\theta} \end{Bmatrix}_k \tag{3.15}$$

where, σ_{rr}, $\sigma_{\theta\theta}$ and $\tau_{r\theta}$ are the radial, circumferential and the in-plane shear stresses in the *k*-th ply of the rotating disc respectively and $\overline{[Q]}_k$ is the transformed reduced stiffness matrix of the *k*-th ply in the laminated disc, given as:

$$\overline{[Q]}_k = \begin{bmatrix} \overline{Q_{11}} & \overline{Q_{12}} & \overline{Q_{16}} \\ \overline{Q_{12}} & \overline{Q_{22}} & \overline{Q_{26}} \\ \overline{Q_{16}} & \overline{Q_{26}} & \overline{Q_{66}} \end{bmatrix}_k \tag{3.16}$$

In the above Equation (3.16), $\overline{Q_{ij}}$ *i, j* = 1,2 and 6 are the elements of the transformed reduced stiffness matrix of the material of the disc and are expressed according to the following relations [2]:

$$\overline{Q_{11}} = Q_{11}cos^4\theta + Q_{22}sin^4\theta + 2(Q_{12} + 2Q_{66})sin^2\theta cos^2\theta \tag{3.17}$$

$$\overline{Q_{12}} = (Q_{11} + Q_{22} - 4Q_{66})sin^2\theta cos^2\theta + Q_{12}(sin^4\theta + cos^4\theta) \tag{3.18}$$

$$\overline{Q_{16}} = (Q_{11} - Q_{12} - 2Q_{66})sin\theta cos^3\theta + (Q_{11} - Q_{22} + 2Q_{66})sin^3\theta cos\theta \tag{3.19}$$

$$\overline{Q_{22}} = Q_{11}sin^4\theta + Q_{22}cos^4\theta + 2(Q_{12} + 2Q_{66})sin^2\theta cos^2\theta \tag{3.20}$$

$$\overline{Q_{26}} = (Q_{11} - Q_{12} - 2Q_{66})cos\theta sin^3\theta + (Q_{11} - Q_{22} + 2Q_{66})cos^3\theta sin\theta \tag{3.21}$$

$$\overline{Q_{66}} = [Q_{11} + Q_{22} - 2(Q_{12} + Q_{66})]sin^2\theta cos^2\theta + Q_{66}(sin^4\theta + cos^4\theta) \tag{3.22}$$

where, Q_{ij} *i, j* = 1, 2 and 6 are the elements of the reduced stiffness matrix of the material of the disc given by Equation (2.10) and θ is the angle of fiber orientation in the ply. Using the strain-displacement relations given in Equations (3.9) - (3.14), the stress-strain relation given in Equation (3.15) and using the Equation (3.16), the stresses in the *k*-th ply of the rotating disc can be written as:

$$\begin{Bmatrix} \sigma_{rr} \\ \sigma_{\theta\theta} \\ \tau_{r\theta} \end{Bmatrix}_k = \begin{bmatrix} \overline{Q_{11}} & \overline{Q_{12}} & \overline{Q_{16}} \\ \overline{Q_{12}} & \overline{Q_{22}} & \overline{Q_{26}} \\ \overline{Q_{16}} & \overline{Q_{26}} & \overline{Q_{66}} \end{bmatrix}_k \begin{Bmatrix} \dfrac{du_r^o(r)}{dr} - z\dfrac{d^2w(r)}{dr^2} \\ \dfrac{u_r^o(r)}{r} - z\dfrac{dw(r)}{rdr} \\ \dfrac{du_\theta^o(r)}{dr} - \dfrac{u_\theta^o(r)}{r} \end{Bmatrix}_k \tag{3.23}$$

3.3 Formulation for the total potential energy

As discussed previously in the section (2.2), the total potential energy of a rotating annular disc is the sum of the strain energy and the potential energy originated from the centrifugal loading of the disc. The following Figure 3.1 shows an annular uniform-thickness disc made up of orthotropic plies that are bonded together, and with the cylindrical coordinate system. r_i and r_o are the inner and the outer radii of the annular disc respectively, h is the total thickness of the disc and t is the thickness of an individual ply in the laminated disc.

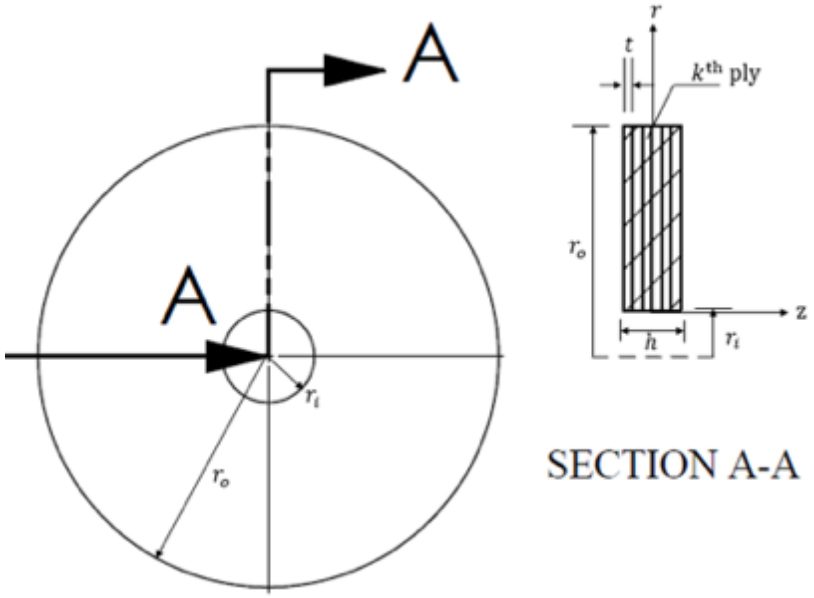

Figure 3.1 Annular uniform-thickness laminated disc with the cylindrical coordinate system

Recalling the strain energy density (i.e., the strain energy per unit volume), U_o, given in the Equation (2.6), it is written as:

$$U_o = \frac{1}{2}[\sigma][\varepsilon] \tag{3.24}$$

where, $[\sigma] = [\sigma_{rr}\ \sigma_{\theta\theta}\ \tau_{r\theta}]$ and $[\varepsilon] = [\varepsilon_{rr}\ \varepsilon_{\theta\theta}\ \gamma_{r\theta}]^T$.

Therefore, using Equation (3.23) and the strain-displacement relations given above in the Equations (3.9) – (3.14), the strain energy of the k-th ply in the laminated disc, denoted by U_k, can be given as:

U_k

$$= \frac{1}{2}\int_{r_i}^{r_o}\int_{0}^{2\pi}\int_{\frac{-t_k}{2}}^{\frac{t_k}{2}} \left\{ \begin{bmatrix} \overline{Q_{11}} & \overline{Q_{12}} & \overline{Q_{16}} \\ \overline{Q_{12}} & \overline{Q_{22}} & \overline{Q_{26}} \\ \overline{Q_{16}} & \overline{Q_{26}} & \overline{Q_{66}} \end{bmatrix}_k \begin{Bmatrix} \frac{du_r^o(r)}{dr} - z\frac{d^2w(r)}{dr^2} \\ \frac{u_r^o(r)}{r} - z\frac{dw(r)}{rdr} \\ \frac{du_\theta^o(r)}{dr} - \frac{u_\theta^o(r)}{r} \end{Bmatrix}_k \right\}^T \begin{Bmatrix} \frac{du_r^o(r)}{dr} - z\frac{d^2w(r)}{dr^2} \\ \frac{u_r^o(r)}{r} - z\frac{dw(r)}{rdr} \\ \frac{du_\theta^o(r)}{dr} - \frac{u_\theta^o(r)}{r} \end{Bmatrix}_k dz.rd\theta.dr \quad (3.25)$$

Subsequently, for a disc of total thickness h, the strain energy of an annular uniform-thickness laminated disc, denoted by U can be given as

U

$$= \frac{1}{2}\sum_{k=1}^{N}\int_{r_i}^{r_o}\int_{0}^{2\pi}\int_{\frac{-t_k}{2}}^{\frac{t_k}{2}} \left\{ \begin{bmatrix} \overline{Q_{11}} & \overline{Q_{12}} & \overline{Q_{16}} \\ \overline{Q_{12}} & \overline{Q_{22}} & \overline{Q_{26}} \\ \overline{Q_{16}} & \overline{Q_{26}} & \overline{Q_{66}} \end{bmatrix}_k \begin{Bmatrix} \frac{du_r^o(r)}{dr} - z\frac{d^2w(r)}{dr^2} \\ \frac{u_r^o(r)}{r} - z\frac{dw(r)}{rdr} \\ \frac{du_\theta^o(r)}{dr} - \frac{u_\theta^o(r)}{r} \end{Bmatrix}_k \right\}^T \begin{Bmatrix} \frac{du_r^o(r)}{dr} - z\frac{d^2w(r)}{dr^2} \\ \frac{u_r^o(r)}{r} - z\frac{dw(r)}{rdr} \\ \frac{du_\theta^o(r)}{dr} - \frac{u_\theta^o(r)}{r} \end{Bmatrix}_k dz.rd\theta.d \quad (3.26)$$

where, N is the number of plies in the laminated disc and t_k is the thickness of the k-th ply in the laminated disc. Since for the present case, the thickness of every ply is the same, therefore, $t_1 = t_2 = \ldots = t_N = t$. Upon expanding and then rearranging the above Equation (3.26), the strain energy of a rotating annular uniform-thickness laminated disc can be given as:

$$\mathrm{U} = \frac{1}{2}\int_{0}^{2\pi}\int_{r_i}^{r_o} \begin{Bmatrix} \frac{du_r^o(r)}{dr} \\ \frac{u_r^o(r)}{r} \\ \frac{du_\theta^o(r)}{dr} - \frac{u_\theta^o(r)}{r} \\ -\frac{d^2w(r)}{dr^2} \\ -\frac{dw(r)}{rdr} \\ 0 \end{Bmatrix}^T \begin{bmatrix} A_{11} & A_{12} & A_{16} & B_{11} & B_{12} & B_{16} \\ A_{12} & A_{22} & A_{26} & B_{12} & B_{22} & B_{26} \\ A_{16} & A_{26} & A_{66} & B_{16} & B_{26} & B_{66} \\ B_{11} & B_{12} & B_{16} & D_{11} & D_{12} & D_{16} \\ B_{12} & B_{22} & B_{26} & D_{12} & D_{22} & D_{26} \\ B_{16} & B_{26} & B_{66} & D_{16} & D_{26} & D_{66} \end{bmatrix} \begin{Bmatrix} \frac{du_r^o(r)}{dr} \\ \frac{u_r^o(r)}{r} \\ \frac{du_\theta^o(r)}{dr} - \frac{u_\theta^o(r)}{r} \\ -\frac{d^2w(r)}{dr^2} \\ -\frac{dw(r)}{rdr} \\ 0 \end{Bmatrix} rdrd\theta \quad (3.27)$$

where, A_{ij}, B_{ij} and D_{ij}, i, j = 1,2 and 6, are the elements of the laminate stiffness matrix commonly referred to as the ABD matrix of the composite material, and are expressed as:

$$A_{ij} = \sum_{k=1}^{N} (z_k - z_{k-1}) \overline{Q_{ij}}_k \tag{3.28}$$

$$B_{ij} = \frac{1}{2} \sum_{k=1}^{N} (z_k^2 - z_{k-1}^2) \overline{Q_{ij}}_k \tag{3.29}$$

$$D_{ij} = \frac{1}{3} \sum_{k=1}^{N} (z_k^3 - z_{k-1}^3) \overline{Q_{ij}}_k \tag{3.30}$$

The potential energy originated from the centrifugal loading of the disc denoted by V, remains the same as given in the Equation (2.17) and can be re-written as:

$$\mathrm{V} = -h \int_{\frac{-1}{2}}^{\frac{1}{2}} \int_{0}^{2\pi} \int_{r_i}^{r_o} \rho \omega^2 r u_r(r) dr.rd\theta.dz \tag{3.31}$$

where, ρ is the density of the fiber-reinforced composite material, $u_r(r)$ is the radial displacement of the laminated disc and ω is the angular velocity of rotation. The potential energy of the rotating annular uniform-thickness laminated disc, denoted by Π, is then given as the sum of the strain energy and the potential energy originated from the centrifugal loading of the disc, which were derived in Equations (3.27) and (3.31) respectively, i.e., $\Pi = \mathrm{U} + \mathrm{V}$

3.4 Solution by Rayleigh-Ritz Method

Let the displacements in the radial, circumferential and transverse directions be expressed in terms of algebraic polynomial series in cylindrical coordinates given as:

$$u_r^o(r) = n_r \sum_{j=0}^{m_1} a_j r^j \tag{3.32}$$

$$u_\theta^o(r) = n_\theta \sum_{j=0}^{m_2} b_j r^j \tag{3.33}$$

$$w_o(r) = n_w \sum_{j=0}^{m_3} c_j r^j \tag{3.34}$$

where, n_r, n_θ and n_w are the constraint functions that together with the assumed shape functions satisfy the geometric boundary conditions. a_j, b_j and c_j are the constant coefficients and r is the radial coordinate. m_1, m_2 and m_3 are the total number of terms in the assumed displacement functions that are required to correctly estimate the elastic response of the rotating disc with m_1, m_2 and $m_3 \in Z^+$ (positive integer). For the present case, $m_1 = m_2 = m_3 = 7$. i.e., a total of 8 terms are assumed in each of the radial, circumferential and transverse displacement functions. The following Table 3.1 shows the constraint functions used for the clamped-free boundary condition.

Constraint functions	Clamped-Free
$n_r = n_\theta = n_w$	$(r - r_i)$

Table 3.1 Constraint functions for the clamped-free boundary condition

The obtained potential energy is then minimized with respect to each set of assumed coefficients in the radial, circumferential and transverse displacement functions so as to obtain the closest approximation of the elastic response of the rotating annular uniform-thickness disc made up of fiber-reinforced composite materials and with the clamped-free boundary condition. i.e.,

$$\frac{\partial \Pi}{\partial a_j} = 0 \tag{3.35}$$

$$\frac{\partial \Pi}{\partial b_j} = 0 \tag{3.36}$$

$$\frac{\partial \Pi}{\partial c_j} = 0 \tag{3.37}$$

The above Equations (3.35) - (3.37) represent a set of algebraic equations that are solved to yield the coefficients a_j, b_j and c_j. A MATLAB® code is developed to determine the values of these coefficients, which are then used to obtain the required deformations and the stress distributions in the rotating annular uniform-thickness fiber-reinforced composite disc with the clamped-free boundary condition.

3.5 Finite Element Model

The finite element modeling of the rotating annular uniform-thickness fiber-reinforced composite disc with the clamped-free boundary condition has been carried out in ANSYS® R19.2. The rotating disc has been clamped at the inner edge and is rotating at a constant angular velocity of 1000 *rad/s* i.e., 9554.14 *rpm*. The modelling of the disc has been carried out using the SOLID185 and SHELL181 elements in ANSYS® Composite Prepost (ACP Pre) module. The geometry, node locations and the element coordinate system for the SOLID185 and SHELL181 elements has been shown in Appendix A.

The following Figures 3.2 and 3.3 show the mesh and the elements of a disc modelled using SOLID185 and SHELL181 elements respectively.

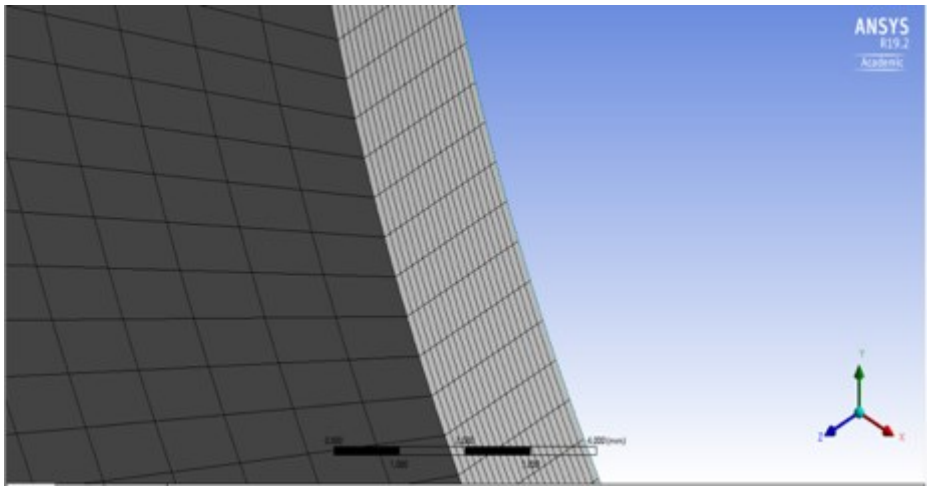

Figure 3.2 Modelling of a uniform-thickness disc in ANSYS® using SOLID185 element

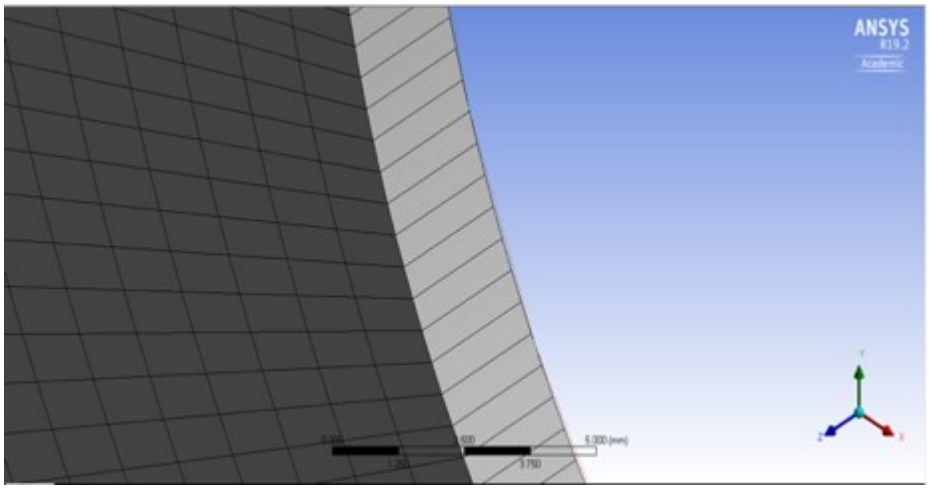

Figure 3.3 Modelling of a uniform-thickness disc in ANSYS® using SHELL181 element

It can be clearly seen from the above Figures 3.2 and 3.3 that the disc modelled using the SOLID185 element has elements that are layered on top of each other in the laminated disc whereas for the disc modelled using the SHELL181 element, with only one element through the thickness, a single element covers up the total thickness of the laminated disc. i.e., for a disc of given thickness and containing '*N*' number of plies, there would be '*N*' number of SOLID185 elements through the thickness of the disc, at any given radial distance. However, for a disc with the given same thickness and containing the same number of plies *N*, there would be only one SHELL181 element through the thickness of the disc, at any given radial distance.

The following Figure 3.4 shows a rotating annular uniform-thickness disc in ANSYS® R19.2. The disc has been clamped at its inner boundary represented by a fixed support A and is rotating at a constant angular velocity about the z-axis as represented by a rotation symbol B.

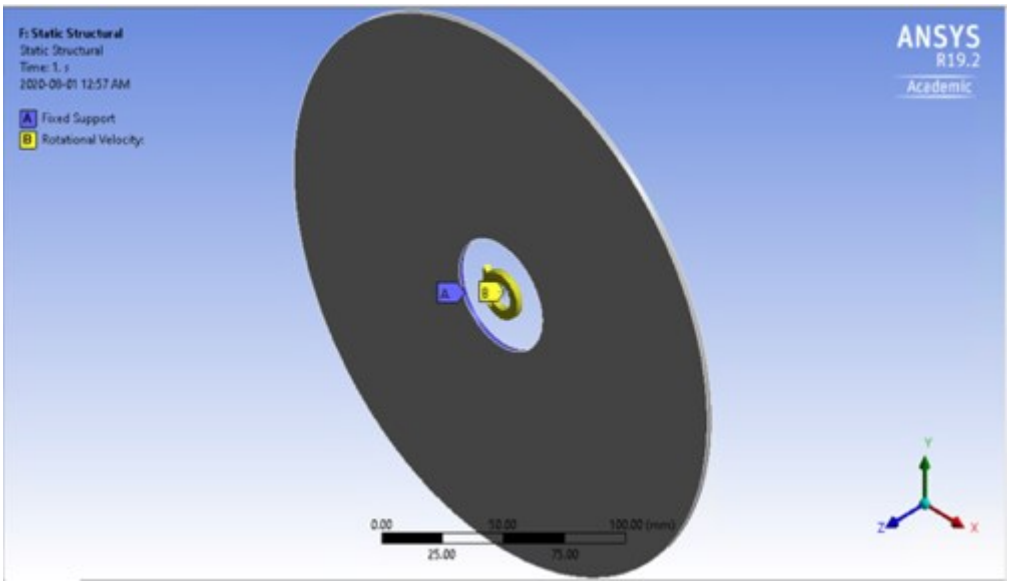

Figure 3.4 Static structural analysis setting of a rotating annular uniform-thickness disc with the clamped-free boundary condition in ANSYS® R19.2

The following steps have been adopted in the finite element modelling of the rotating annular uniform-thickness laminated disc in ANSYS®.

- The large deflection option is turned off during the analysis as it accounts for the change in the stiffness of the material when it deforms.
- The mesh size of the structure is set to a minimum value of 0.5 *mm* along with face meshing (quadrilateral type) feature turned on, since it is required to represent the

proper orientation of fibers in the prepreg. The triangular type face meshing is not recommended for the analysis of rotating fiber-reinforced composite structures.

The following Figures 3.5 (a), (b) and 3.6 (a), (b) show the mesh and the fiber orientation generated using the triangular type face meshing and the quadrilateral type face meshing respectively, for a $[0]_{20}$ uni-directional laminated disc in ANSYS®.

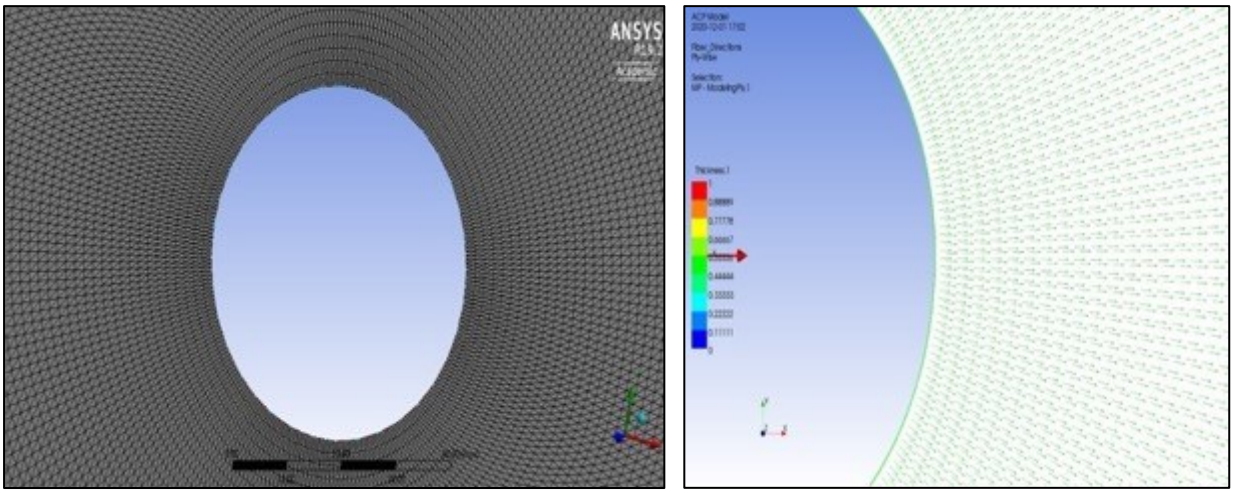

(a) (b)

Figure 3.5 (a) Mesh and **(b)** Fiber orientation generated using triangular type face meshing for a $[0]_{20}$ uni-directional laminated disc in ANSYS®

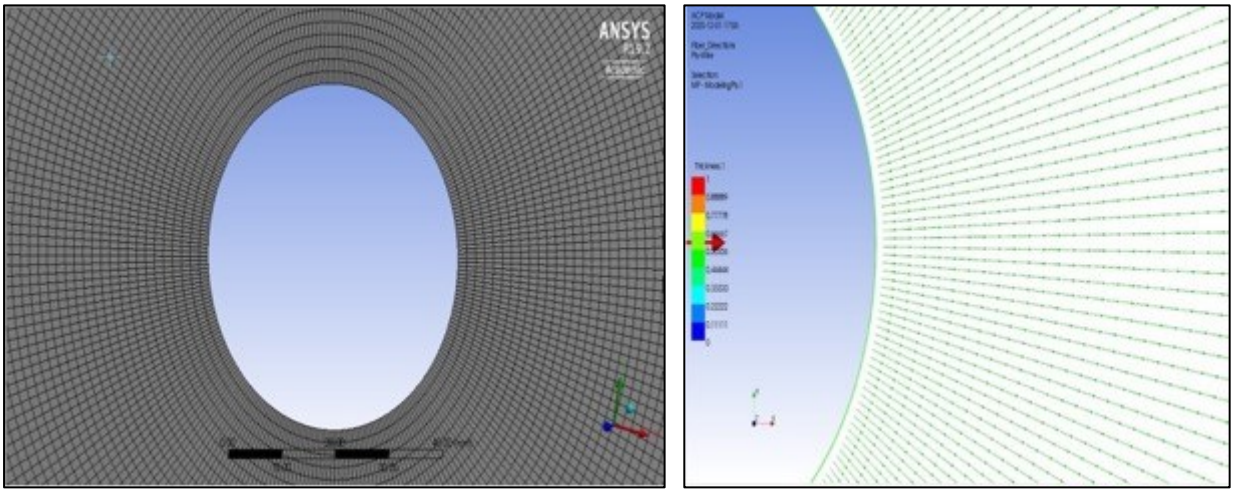

(a) (b)

Figure 3.6 (a) Mesh and **(b)** Fiber orientation generated using quadrilateral type face meshing for a $[0]_{20}$ uni-directional laminated disc in ANSYS®

It can be seen from the above Figures 3.5 (a) and 3.6 (a) that the meshes of the annular disc generated using triangular type face meshing and that generated using quadrilateral type face meshing are not identical, wherein the former, the mesh consists of right-angled face split triangles

(having a diagonal of 0.707 *mm*) and in the latter, the mesh consists of equally sized squares (a special case of lower symmetry quadrilaterals having each side equal to 0.5 *mm*).

Figures 3.5 (b) and 3.6 (b) represent the fiber orientation (as shown by green arrows) developed in the NCT-301 prepreg for a $[0]_{20}$ uni-directional laminated disc using triangular type face meshing and quadrilateral type face meshing respectively. It can be noted from the Figure 3.6 (b) that the fibers are not properly aligned along the radial direction for the disc modelled using right-angled face split triangles, while the fibers in the NCT-301 prepreg are accurately aligned along the radial direction of the disc that is modelled using quadrilateral face meshing, as shown in the Figure 3.6(b). Therefore, for the finite element analysis of structures made up of fiber-reinforced composite materials, quadrilateral type face meshing is preferred over the triangular type face meshing.

3.6 Verification

In this section, the elastic response of a rotating annular uniform-thickness laminated disc made up of fiber-reinforced composite material and with the clamped-free boundary condition, that is obtained using the Rayleigh-Ritz method based on the potential energy is verified with the elastic response obtained for the same using the finite element analysis software ANSYS®. The verification has been done using 300,160 SOLID185 elements and 15,008 SHELL181 elements. The rotating disc has an inner radius of r_i = 24 *mm*, an outer radius of r_o = 120 *mm*, a total thickness of h = 2.4 *mm* with an individual ply thickness of t = 0.12 *mm* and it is rotating at a constant angular velocity of ω = 1000 *rad/s* i.e., 9554.14 *rpm*. The individual plies in the laminated disc are made of a Graphite-Fiber Reinforced Plastic material (NCT-301 prepreg), the material properties of which are given in the following Table 3.2.

Graphite-Fiber Reinforced Plastic (NCT-301) prepreg [58]	
E_1 = 113.9 *GPa*	ν_{12} = 0.288
E_2 = 7.985 *GPa*	ν_{13} = 0.288
E_3 = 7.985 *GPa*	ν_{21} = 0.018
G_{12} = 3.138 *GPa*	G_{23} = 2.852 *GPa*
G_{13} = 3.138 *GPa*	$\rho = 1480\ Kg/m^3$

Table 3.2 Material properties of Graphite-Fiber Reinforced Plastic NCT-301 prepreg

The following Tables 3.3 – 3.7 show the comparison of the radial and circumferential stress distributions, radial displacement distributions and the radial and circumferential strain distributions in a rotating annular uniform-thickness laminated disc obtained using the Rayleigh-Ritz method based on the total potential energy of the rotating disc with the distributions obtained for the same using the finite element software ANSYS®. The comparison of the elastic response has been carried out for laminated discs with $[0]_{20}$ and $[45]_{20}$ configurations and made up of Graphite-Fiber Reinforced Plastic material (NCT-301) for the clamped-free boundary condition.

Radial stress distribution, σ_r (in *MPa*)						
Radial distance in *mm* from the center of the disc	Laminate configuration					
	$[0]_{20}$			$[45]_{20}$		
	Rayleigh-Ritz Solution	ANSYS® Solution (SOLID185)	ANSYS® Solution (SHELL181)	Rayleigh-Ritz Solution	ANSYS® Solution (SOLID185)	ANSYS® Solution (SHELL181)
24.0	31.644	30.535	30.645	12.128	11.586	11.91
33.6	22.545	22.585	22.575	10.086	10.118	10.091
43.2	17.268	17.288	17.285	8.892	8.9137	8.8996
52.8	13.715	13.711	13.709	7.956	7.9592	7.9501
62.4	11.000	11.002	11.0	7.041	7.0457	7.0394
72.0	8.764	8.7704	8.7691	6.086	6.0951	6.0906
81.6	6.819	6.8181	6.8172	5.070	5.0716	5.0683
91.2	5.030	5.0247	5.0241	3.960	3.9584	3.956
100.8	3.316	3.3194	3.3189	2.742	2.7455	2.7437
110.4	1.655	1.6549	1.6547	1.427	1.4269	1.4257
120.0	0.00	1.47e-05	1.47e-06	0	1.28e-4	1.31e-6

Table 3.3 Comparison of the radial stress distributions obtained using the Rayleigh-Ritz method for a rotating annular uniform-thickness laminated disc made up of Graphite-Fiber Reinforced Plastic material (NCT-301) for the clamped-free boundary condition, with the distributions obtained for the same using ANSYS®

Circumferential stress distribution, σ_θ (in *MPa*)						
Radial distance in *mm* from the center of the disc	Laminate configuration					
	$[0]_{20}$			$[45]_{20}$		
	Rayleigh-Ritz Solution	ANSYS® Solution (SOLID185)	ANSYS® Solution (SHELL181)	Rayleigh-Ritz Solution	ANSYS® Solution (SOLID185)	ANSYS® Solution (SHELL181)
24.0	0.6389	0.6566	0.62464	5.1405	5.6576	5.0709
33.6	0.9839	0.98237	0.98548	6.6830	6.6592	6.6815
43.2	1.0622	1.0611	1.0637	7.0884	7.0761	7.0911
52.8	1.0531	1.0517	1.0538	7.0713	7.0571	7.0676
62.4	1.0084	1.0072	1.0089	6.8143	6.8043	6.812
72.0	0.9478	0.94698	0.94834	6.4009	6.3957	6.4016
81.6	0.8798	0.87891	0.87999	5.8711	5.8646	5.8693
91.2	0.8074	0.80652	0.80734	5.2372	5.23	5.2339
100.8	0.7320	0.7313	0.73188	4.5049	4.5009	4.5041
110.4	0.6545	0.65392	0.65427	3.6875	3.6829	3.6856
120.0	0.5748	0.5798	0.57785	2.7796	2.8439	2.8384

Table 3.4 Comparison of the circumferential stress distributions obtained using the Rayleigh-Ritz method for a rotating annular uniform-thickness laminated disc made up of Graphite-Fiber Reinforced Plastic material (NCT-301) for the clamped-free boundary condition, with the distributions obtained for the same using ANSYS®

Radial displacement distribution, u_r (in mm)						
Radial distance in mm from the center of the disc	Laminate configuration					
	$[0]_{20}$			$[45]_{20}$		
	Rayleigh-Ritz Solution	ANSYS® Solution (SOLID185)	ANSYS® Solution (SHELL181)	Rayleigh-Ritz Solution	ANSYS® Solution (SOLID185)	ANSYS® Solution (SHELL181)
24.0	0	0	0	0	0	0
33.6	0.00222	0.002219	0.0022227	0.00905	0.008903	0.009035
43.2	0.00386	0.003857	0.0038603	0.01604	0.015935	0.016039
52.8	0.00513	0.005129	0.0051322	0.02185	0.021758	0.021845
62.4	0.00614	0.0061405	0.0061437	0.02674	0.026654	0.02673
72.0	0.00695	0.006948	0.0069512	0.03078	0.03071	0.030778
81.6	0.00758	0.007580	0.0075838	0.03398	0.033917	0.033978
91.2	0.00806	0.008058	0.0080618	0.03631	0.036247	0.036304
100.8	0.00839	0.008391	0.0083944	0.03770	0.037638	0.037692
110.4	0.00858	0.008583	0.0085869	0.03808	0.038021	0.038072
120.0	0.00864	0.008638	0.0086423	0.03738	0.037327	0.037376

Table 3.5 Comparison of the radial displacement distributions obtained using the Rayleigh-Ritz method for a rotating annular uniform-thickness laminated disc made up of Graphite-Fiber Reinforced Plastic material (NCT-301) for the clamped-free boundary condition, with the distributions obtained for the same using ANSYS®

Radial strain distribution, ε_{rr} (in mm/mm)						
Radial distance in *mm* from the center of the disc	Laminate configuration					
	$[0]_{20}$			$[45]_{20}$		
	Rayleigh-Ritz Solution	ANSYS® Solution SOLID185	ANSYS® Solution SHELL181	Rayleigh-Ritz Solution	ANSYS® Solution SOLID185	ANSYS® Solution SHELL181
24.0	0.0002762	0.000260	0.000267	0.001113	0.0010785	0.001090
33.6	0.0001954	0.000195	0.000196	0.0008116	0.0008158	0.0008121
43.2	0.0001489	0.000149	0.000150	0.0006588	0.0006616	0.0006594
52.8	0.0001177	0.000117	0.000117	0.000555	0.0005557	0.0005543
62.4	9.403e-05	9.404e-005	9.404e-005	0.000464	0.000465	0.0004645
72.0	7.455e-05	7.460e-005	7.460e-005	0.000377	0.000378	0.000377
81.6	5.764e-05	5.764e-005	5.764e-005	0.000288	0.000289	0.000288
91.2	4.212e-05	4.208e-005	4.208e-005	0.000194	0.000194	0.000194
100.8	2.726e-05	2.730e-005	2.73e-005	9.3198e-05	9.3706e-05	9.3359e-05
110.4	1.288e-05	1.288e-005	1.289e-005	-1.5201e-05	-1.5023e-05	-1.5296e-05
120.0	-1.58e-06	-1.71e-07	-1.54e-07	-1.32e-04	-1.21e-04	-1.20e-04

Table 3.6 Comparison of the radial strain distributions obtained using the Rayleigh-Ritz method for a rotating annular uniform-thickness laminated disc made up of Graphite-Fiber Reinforced Plastic material (NCT-301) for the clamped-free boundary condition, with the distributions obtained for the same using ANSYS®

Hoop strain distribution, $\varepsilon_{\theta\theta}$ (in *mm*/*mm*)						
Radial distance in *mm* from the center of the disc	Laminate configuration					
	$[0]_{20}$			$[45]_{20}$		
	Rayleigh-Ritz Solution	ANSYS® Solution (SOLID185)	ANSYS® Solution (SHELL181)	Rayleigh-Ritz Solution	ANSYS® Solution (SOLID185)	ANSYS® Solution (SHELL181)
24.0	0	9.37e-13	0	0	8.12e-11	0
33.6	6.62e-05	6.58e-05	6.59e-05	0.000269	0.000265	0.000268
43.2	8.93e-05	8.91e-05	8.92e-05	0.000371	0.000368	0.000371
52.8	9.71e-05	9.70e-05	9.70e-05	0.000413	0.000412	0.000413
62.4	9.84e-05	9.82e-05	9.83e-05	0.000428	0.000427	0.000428
72.0	9.65e-05	9.64e-05	9.64e-05	0.000427	0.000426	0.000427
81.6	9.29e-05	9.28e-05	9.28e-05	0.000416	0.000415	0.000416
91.2	8.83e-05	8.82e-05	8.831e-05	0.000398	0.000397	0.000398
100.8	8.32e-05	8.31e-05	8.3205e-05	0.000374	0.000373	0.000373
110.4	7.77e-05	7.76e-05	7.7721e-05	0.000344	0.000344	0.000344
120.0	7.20e-05	7.19e-05	7.1985e-05	0.000311	0.000310	0.000311

Table 3.7 Comparison of the circumferential strain distributions obtained using the Rayleigh-Ritz method for a rotating annular uniform-thickness laminated disc made up of Graphite-Fiber Reinforced Plastic material (NCT-301) for the clamped-free boundary condition, with the distributions obtained for the same using ANSYS®

It can be seen from the above Tables 3.3 – 3.7 that the results obtained for the elastic response of a rotating annular uniform-thickness laminated disc made up of Graphite-Fiber Reinforced Plastic material and with the clamped-free boundary condition, using the Rayleigh-Ritz method involving the Classical Laminate Theory are in good agreement with the results obtained for the same using the finite element analysis software ANSYS®.

The following Tables 3.8 – 3.12 show the average percentage differences between the results obtained for the elastic response using the Rayleigh-Ritz method and ANSYS® SOLID185

element solution, and that obtained using the Rayleigh-Ritz method and ANSYS® SHELL181 element solution. Also, in the below Tables 3.8 – 3.12, the average percentage difference has been calculated using the following formula:

$$\text{Average percentage difference} = \frac{\sum_{i=1}^{T} \frac{(\text{R} - \text{R solution}) - \text{ANSYS}^{1,2}\ \text{solution}}{(\text{R} - \text{R solution})}}{\text{T}} * 100 \tag{3.38}$$

In the above Equation (3.38), R-R solution stands for the Rayleigh-Ritz solution and $\text{ANSYS}^{1,2}$ refers to ANSYS® SOLID185 solution and SHELL181 solution respectively and T is the number of sampling points taken along the radial direction of the disc. For the present case, T = 11.

Average percentage difference in the results obtained for the radial stress distribution, σ_r		
Laminate configuration of the disc	Rayleigh-Ritz solution and ANSYS® SOLID185 solution	Rayleigh-Ritz solution and ANSYS® SHELL181 solution
$[0]_{20}$	0.3768	0.3399
$[45]_{20}$	0.4994	0.2175

Table 3.8 Average percentage difference in the results obtained for the radial stress distributions in a rotating annular uniform-thickness laminated disc made up of Graphite-Fiber Reinforced Plastic material for the clamped-free boundary condition

Average percentage difference in the results obtained for the circumferential stress distribution, σ_θ		
Laminate configuration of the disc	Rayleigh-Ritz solution and ANSYS® SOLID185 solution	Rayleigh-Ritz solution and ANSYS® SHELL181 solution
$[0]_{20}$	0.4211	0.3016
$[45]_{20}$	1.0435	0.1522

Table 3.9 Average percentage difference in the results obtained for the circumferential stress distributions in a rotating annular uniform-thickness laminated disc made up of Graphite-Fiber Reinforced Plastic material for the clamped-free boundary condition

Average percentage difference in the results obtained for the radial displacement distribution, u_r		
Laminate configuration of the disc	Rayleigh-Ritz solution and ANSYS® SOLID185 solution	Rayleigh-Ritz solution and ANSYS® SHELL181 solution
$[0]_{20}$	0.0249	0.0437
$[45]_{20}$	0.3699	0.0285

Table 3.10 Average percentage difference in the results obtained for the radial displacement distributions in a rotating annular uniform-thickness laminated disc made up of Graphite-Fiber Reinforced Plastic material for the clamped-free boundary condition

Average percentage difference in the results obtained for the radial strain distribution, ε_{rr}		
Laminate configuration of the disc	Rayleigh-Ritz solution and ANSYS® SOLID185 solution	Rayleigh-Ritz solution and ANSYS® SHELL181 solution
$[0]_{20}$	0.641	0.488
$[45]_{20}$	0.6102	0.2955

Table 3.11 Average percentage difference in the results obtained for the radial strain distributions in a rotating annular uniform-thickness laminated disc made up of Graphite-Fiber Reinforced Plastic material for the clamped-free boundary condition

Average percentage difference in the results obtained for the radial strain distributions, $\varepsilon_{\theta\theta}$		
Laminate configuration of the disc	Rayleigh-Ritz solution and ANSYS® SOLID185 solution	Rayleigh-Ritz solution and ANSYS® SHELL181 solution
$[0]_{20}$	0.1552	0.0932
$[45]_{20}$	0.3422	0.0581

Table 3.12 Average percentage difference in the results obtained for the circumferential strain distributions in a rotating annular uniform-thickness laminated disc made up of Graphite-Fiber Reinforced Plastic material for the clamped-free boundary condition

It can be seen from the Tables 3.8 – 3.12 that, the average percentage difference between the results obtained for the elastic response of the rotating annular uniform-thickness laminated disc is much lower for the case of R-R solution and ANSYS® SHELL181 solution as compared to the results obtained for the same in the case of R-R solution and ANSYS® SOLID185 solution. Therefore, it can be said that the SHELL181 element is best suited for the elastic analysis of thin to moderately-thick structures.

3.7 Parametric Study

In this section, a thorough parametric study is conducted to study the effects of fiber orientation, beta value of the disc (i.e., the radius ratio of the disc which is the ratio of the inner radius of the disc to its outer radius), rotational velocity and laminate configuration on the stress distributions and the radial displacement distributions in a rotating annular uniform-thickness composite disc with the clamped-free boundary condition. The disc is made up of Graphite-Fiber Reinforced Plastic (NCT-301) material, the material properties of which have been mentioned earlier in the Table 3.2.

3.7.1 Laminated disc made up of unidirectional plies

This sub-section presents the parametric study on the elastic response of rotating annular uniform-thickness discs made up of Graphite-Fiber Reinforced Plastic material with uni-directional laminate configuration for the clamped-free boundary condition. The effects of fiber orientation in the uni-directional laminated disc configuration, radius ratio and the rotational velocity on the radial stress and circumferential stress distributions, and on the radial displacement distribution in rotating annular uniform-thickness composite discs are studied. Graphical results for the stress and displacement distributions are presented and the percentage change in the maximum stress and maximum displacement values with respect to the fiber orientation in the uni-directional laminated disc are calculated.

Uni-directional laminated discs are made when the fibers in each and every ply in the laminated disc are oriented at the same angle i.e., $+\theta$ or $-\theta$. In the present study, the uni-directional laminated disc configurations considered are of the $[+\theta]_{20}$ ply group. i.e., from $[0]_{20}$

to $[90]_{20}$. These uni-directional layups help prevent the coupling between the stretching, bending and/or twisting in the laminate. i.e., the coupling stiffness matrix [B] is zero in all of the unidirectional layups. Furthermore, the laminates with $[0]_{20}$ and $[90]_{20}$ configurations (commonly referred to as single orthotropic layer referred to its principal directions), also have the elements A_{16}, A_{26} of the stretching stiffness matrix [A] and the elements D_{16}, D_{26} of the bending stiffness matrix [D] equal to zero. i.e., there is no tension-shear coupling (due to the elements A_{16} and A_{26}) and no bending-twisting coupling (due to the elements D_{16} and D_{26}) in the laminate.

3.7.1.1 Effect of fiber orientation on the elastic response of uni-directional laminated discs

The effect of fiber orientation on the stress distributions and the radial displacement distribution in a rotating annular uniform-thickness composite disc with uni-directional configuration is studied. The rotating disc has the same geometric properties as mentioned in the validation section. i.e., the disc has an inner radius of r_i = 24 *mm*, an outer radius of r_o = 120 *mm*, thickness of h = 2.4 *mm* with an individual ply thickness of t = 0.12 *mm,* and is rotating at a constant angular velocity of ω = 1000 *rad/s* i.e., 9554.14 *rpm*.

The following Figure 3.7 shows the radial stress distribution in a rotating annular uniform-thickness fiber-reinforced composite disc with uni-directional configuration ranging from $[0]_{20}$ to $[90]_{20}$ and for the clamped-free boundary condition.

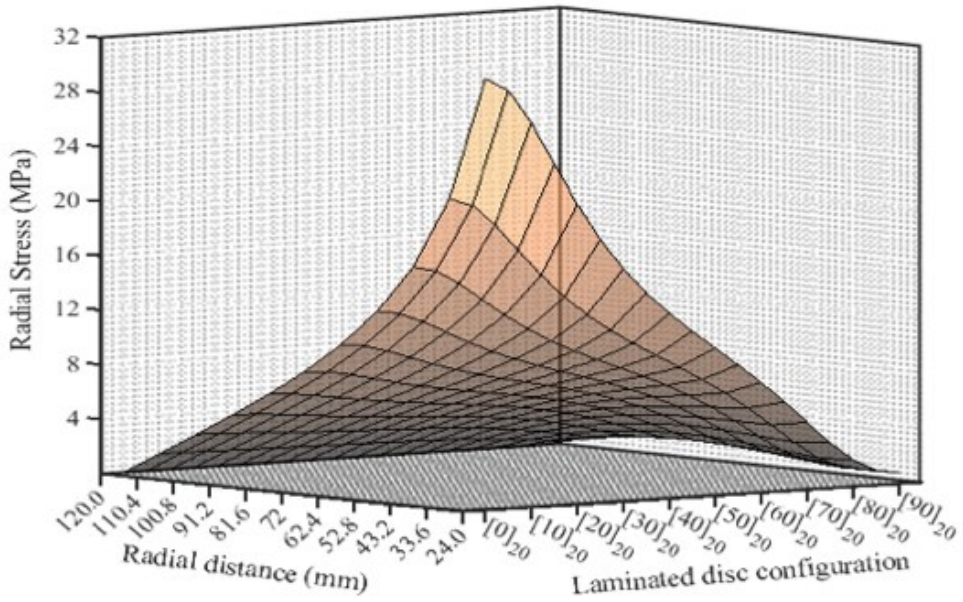

Figure 3.7 Radial stress distribution in a rotating annular uniform-thickness fiber-reinforced composite disc with uni-directional configuration and for the clamped-free boundary condition

It can be seen from the above Figure 3.7 that the $[0]_{20}$ and the $[90]_{20}$ laminated discs experience the maximum and the minimum amounts of radial stress respectively. Since the fibers in the $[0]_{20}$ laminated disc are aligned along the radial direction of the disc, and it is known that the fibers are strongest in the direction of their length, therefore, in the $[0]_{20}$ laminated disc, there is minimum radial displacement and correspondingly higher radial stress. The stress decreases with the increasing angle of fiber orientation in the ply and is the least for the $[90]_{20}$ laminated disc.

The following Table 3.13 shows the maximum radial stress and the percentage decrease in the maximum radial stress with the fiber orientation in the case of a rotating annular uniform-thickness composite disc with uni-directional configuration and for the clamped-free boundary condition. Since the $[0]_{20}$ laminated disc is subjected to the maximum amount of radial stress, the value of the maximum radial stress in the $[0]_{20}$ laminated disc is considered as a benchmark while calculating the percentage decrease in the stress. Also, in the below Table 3.13, the percentage decrease in the maximum radial stress is calculated according to the following formula:

$$\text{Percentage decrease in the maximum radial stress} = \frac{(\text{Maximum stress value for } \theta = 0°) - (\text{Maximum stress value for } \theta = \text{N}°)}{\text{Maximum stress value for } \theta = 0°} * 100 \quad (3.39)$$

where, N = 10, 20, …, 90.

Rotating annular uniform-thickness fiber-reinforced composite disc made up of Graphite-Fiber Reinforced Plastic (NCT-301) material and with the clamped-free boundary condition									
Maximum radial stress corresponding to $\theta = 0°$ is equal to 31.645 MPa									
Fiber orientation angle (in *degrees*)	10	20	30	40	50	60	70	80	90
Maximum radial stress (in *MPa*)	28.176	21.973	17.039	13.558	10.78	8.03	4.9	2.581	1.59
% decrease in the stress	10.9	30.56	46.15	57.15	65.93	74.6	84.4	91.8	94.9

Table 3.13 Percentage decrease in the maximum radial stress with the fiber orientation angle in a rotating annular uniform-thickness fiber-reinforced composite disc with uni-directional configuration and for the clamped-free boundary condition

It can be seen from the above Table 3.13 that the percentage decrease in the maximum value of the radial stress, increases with the increase in the value of the fiber orientation angle and the decrease in stress is the highest for $\theta = 90°$, and is equal to 94.9% ~ 95%.

It is known that for a rotating annular uniform-thickness disc with the clamped-free boundary condition, the radial stress is always maximum at the hub of the disc at which it is clamped and tends to zero at its outer periphery. The above statement holds good in the case of rotating annular uniform-thickness disc made up of isotropic or orthotropic materials. The locus of the point experiencing the maximum radial stress changes with the fiber orientation in the case of a rotating annular uniform-thickness fiber-reinforced composite disc with uni-directional configuration and for the clamped-free boundary condition.

The following Figure 3.8 shows the variation of the locus of the point experiencing the maximum amount of radial stress with the fiber orientation in a rotating annular uniform-thickness fiber-reinforced composite disc with uni-directional configuration and for the clamped-free boundary condition.

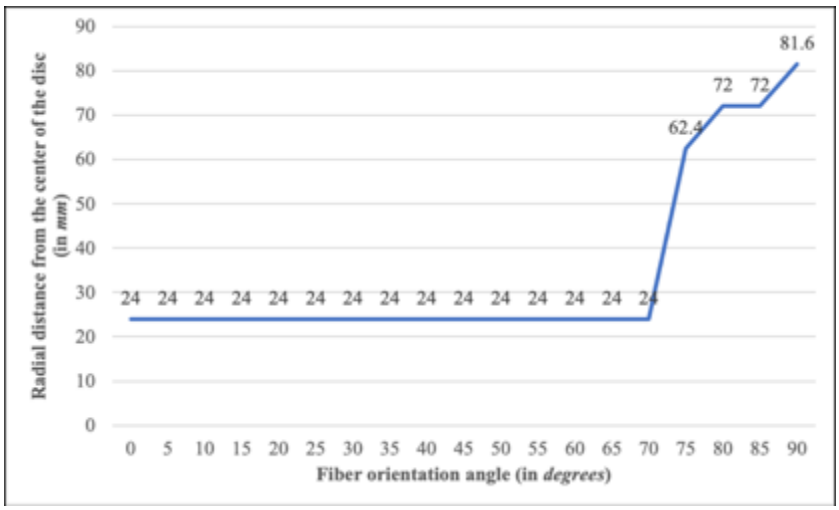

Figure 3.8 Variation of the locus of the point experiencing the maximum radial stress with the fiber orientation angle in a rotating annular uniform-thickness fiber-reinforced composite disc with uni-directional configuration and for the clamped-free boundary condition

It can be seen from the above Figure 3.8 that for the uni-directional composite disc with fiber orientations from 0° to 70°, the radial stress is maximum at the inner radius of the disc (which is 24 *mm* in the present case). Thereafter, as the fiber orientation angle is increased from 70° to 85°, the locus of the point experiencing the maximum radial stress in the uni-directional composite

disc tends to shift towards the arithmetic mean radius of the disc (which is 72 *mm* in the present case). For a disc having the fibers aligned circumferentially i.e., for the disc with fiber orientation of 90°, the radial stress is maximum at a radial distance of 81.6 *mm* from the center of the disc. This variation of the locus of the point experiencing the maximum radial stress can be best represented by a 6th degree polynomial equation, given as:

$$r_{RS}^{max} = a_6\theta^6 + a_5\theta^5 + a_4\theta^4 + a_3\theta^3 + a_2\theta^2 + a_1\theta + 24.00 \quad (3.40)$$

where, r_{RS}^{max} is the radial distance (in *mm*) at which the maximum radial stress is induced, θ is the fiber orientation (in *degrees*) and $a_1, a_2 \ldots a_6$ are unknown coefficients that depend on the geometric and material properties of the rotating disc.

The following Figure 3.9 shows the circumferential stress distribution in a rotating annular uniform-thickness fiber-reinforced composite disc with uni-directional configuration ranging from $[0]_{20}$ to $[90]_{20}$ and for the clamped-free boundary condition.

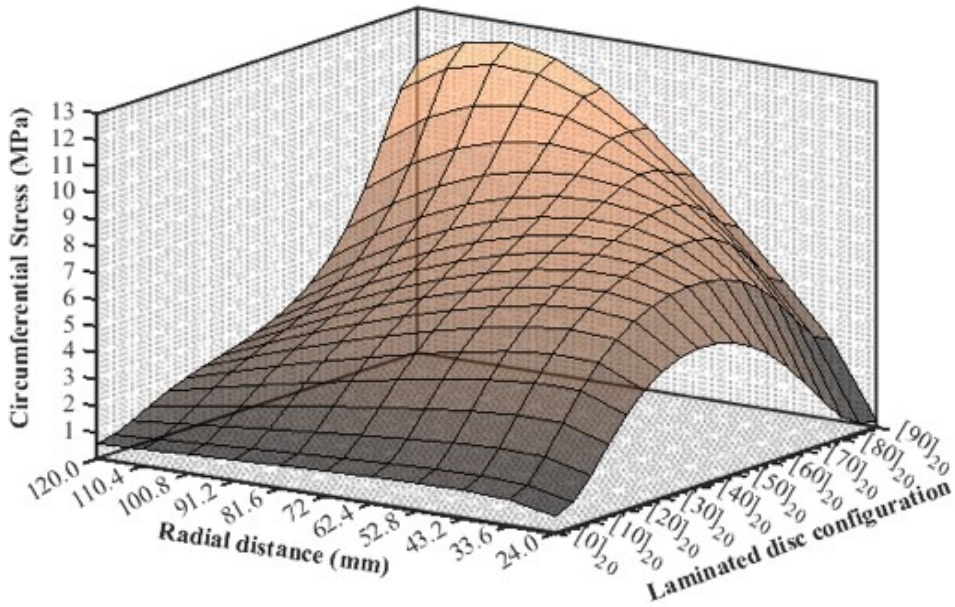

Figure 3.9 Circumferential stress distribution in a rotating annular uniform-thickness fiber-reinforced composite disc with uni-directional configuration and for the clamped-free boundary condition

It can be seen from the above Figure 3.9 that the $[0]_{20}$ and the $[90]_{20}$ laminated discs experience the minimum and maximum amounts of circumferential stress respectively. Since the fibers in the $[90]_{20}$ laminated disc are aligned along the circumferential direction of the disc,

therefore, in the $[90]_{20}$ laminated disc, there is least circumferential displacement and correspondingly higher circumferential stress. The stress decreases with the decreasing angle of fiber orientation and is the least for the $[0]_{20}$ laminated disc.

The following Table 3.14 shows the maximum circumferential stress and the percentage decrease in the maximum circumferential stress with the fiber orientation angle in the case of a rotating annular uniform-thickness composite disc with uni-directional configuration and for the clamped-free boundary condition. Since the $[90]_{20}$ laminated disc is subjected to the maximum amount of circumferential stress, the value of the maximum circumferential stress in the $[90]_{20}$ laminated disc is considered as a benchmark while calculating the percentage decrease in the circumferential stress. Also, in the below Table 3.14, the percentage decrease in the maximum circumferential stress is calculated according to the following formula:

$$\text{Percentage decrease in the maximum circumferential stress} = \frac{(\text{Maximum stress value for } \theta = 90°) - (\text{Maximum stress value for } \theta = \text{N}°)}{\text{Maximum stress value for } \theta = 90°} * 100 \quad (3.41)$$

where, N = 80, 70, …, 0.

Rotating annular uniform-thickness fiber-reinforced composite disc made up of Graphite-Fiber Reinforced Plastic (NCT-301) material and with the clamped-free boundary condition									
Maximum circumferential stress corresponding to $\theta = 90°$ is equal to 12.233 MPa									
Fiber orientation angle (in *degrees*)	80	70	60	50	40	30	20	10	0
Maximum circumferential stress (in *MPa*)	10.58	8.975	8.057	7.427	6.756	5.775	4.22	2.2	1.06
% decrease in the stress	13.5	26.6	34.1	39.28	44.7	52.8	65.5	82.0	91.3

Table 3.14 Percentage decrease in the maximum circumferential stress with the fiber orientation angle in a rotating annular uniform-thickness fiber-reinforced composite disc with uni-directional configuration and for the clamped-free boundary condition

It can be seen from the above Table 3.14 that the percentage decrease in the maximum value of the circumferential stress, increases with the decrease in the value of the fiber orientation angle and the decrease in stress is the highest for $\theta = 0°$, and is equal to 91.3%

It is known that for a rotating annular uniform-thickness disc with the clamped-free boundary condition, the circumferential stress is always maximum at the geometric mean radius of the disc. The above statement holds good in the case of a rotating annular uniform-thickness disc made up of isotropic or orthotropic materials. The locus of the point experiencing the maximum circumferential stress changes with the fiber orientation in the case of a rotating annular uniform-thickness fiber-reinforced composite disc with uni-directional configuration and for the clamped-free boundary condition.

The following Figure 3.10 shows the variation of the locus of the point experiencing the maximum amount of circumferential stress with the fiber orientation in a rotating annular uniform-thickness fiber-reinforced composite disc with uni-directional configuration for the clamped-free boundary condition.

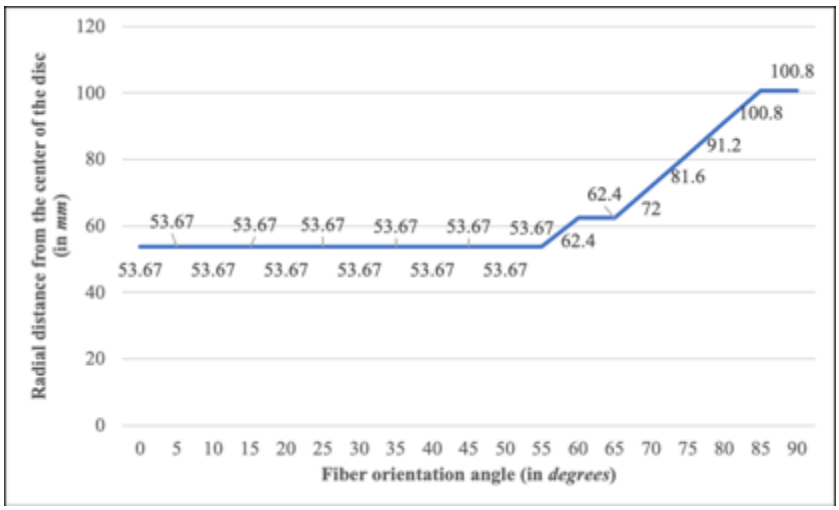

Figure 3.10 Variation of the locus of the point experiencing the maximum circumferential stress with the fiber orientation angle in a rotating annular uniform-thickness fiber-reinforced composite disc with uni-directional configuration and for the clamped-free boundary condition

It can be seen from the above Figure 3.10 that for the uni-directional composite disc with fiber orientations from 0° to 55°, the circumferential stress is maximum at the geometric mean radius of the disc (which is 53.67 *mm* in the present case). Thereafter, as the fiber orientation angle is increased from 55° to 90°, the locus of the point experiencing the maximum circumferential

stress in the uni-directional composite disc tends to shift towards the outer radius of the disc. For a disc having the fibers aligned circumferentially i.e., for the disc with the fiber orientation of 90°, the circumferential stress is maximum at a radial distance of 100.8 *mm* from the center of the disc. This variation of the locus of the point experiencing the maximum circumferential stress can be best represented by a 5th degree polynomial equation, given as:

$$r_{CS}^{max} = b_5\theta^5 + b_4\theta^4 + b_3\theta^3 + b_2\theta^2 + b_1\theta + 53.677 \tag{3.42}$$

where, r_{CS}^{max} is the radial distance (in *mm*) at which the maximum circumferential stress is induced, θ is the fiber orientation (in *degrees*) and b_1, b_2, …, b_5 are unknown coefficients that depend on the geometric and material properties of the disc.

The following Figure 3.11 shows the radial displacement distribution in a rotating annular uniform-thickness fiber-reinforced composite disc with uni-directional configuration ranging from $[0]_{20}$ to $[90]_{20}$ and for the clamped-free boundary condition.

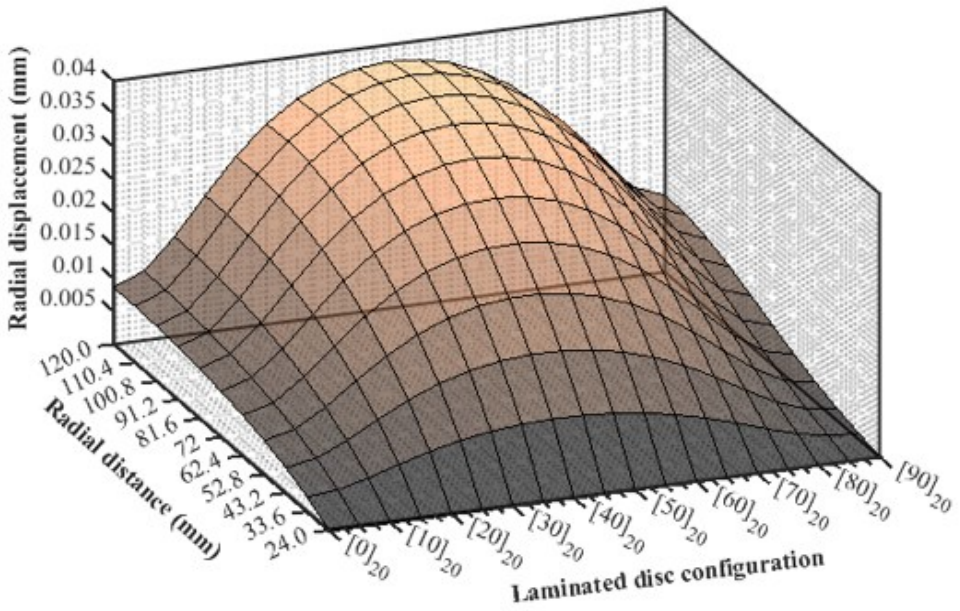

Figure 3.11 Radial displacement distribution in a rotating annular uniform-thickness fiber-reinforced composite disc with uni-directional configuration and for clamped-free boundary condition

It is clear with the clamped-free boundary condition that, there does not exist any radial displacement at the hub of the disc at which it is clamped, and the displacement is maximum at the outer periphery of the disc (which is the free end). It can be seen from the above Figure 3.11 that, there is the least amount of radial displacement in the $[0]_{20}$ laminated disc and the displacement increases with the increasing angle of fiber orientation up to $+45°$. The $[45]_{20}$ laminated disc experiences the maximum radial displacement and then the displacement tends to decrease with the increasing angle of fiber orientation till $90°$.

The cause for such low radial displacement in the $[0]_{20}$ and $[90]_{20}$ laminated discs is due to the fact that in the $[0]_{20}$ laminated disc, the fibers are aligned along the radial direction of the disc, and it is known that the fibers are strongest in the direction of their length, thereby causing resistance to deformation while in the $[90]_{20}$ laminated disc, the fibers are aligned circumferentially in the disc subsequently making the disc stiffer in the circumferential direction.

The following Table 3.15 shows the maximum radial displacement and the percentage decrease in the maximum radial displacement with the fiber orientation angle in the case of a rotating annular uniform-thickness composite disc with uni-directional configuration and for the clamped-free boundary condition. Since the $[45]_{20}$ laminated disc is subjected to the maximum amount of radial displacement, the value of the maximum radial displacement in the $[45]_{20}$ laminated disc is considered as a benchmark while calculating the percentage decrease in the displacement. Also, in the below Table 3.15, the percentage decrease in the maximum radial displacement is calculated according to the following formula:

$$\text{Percentage decrease in the maximum radial displacement} = \frac{(\text{Maximum displacement for } \theta = 45°) - (\text{Maximum displacement for } \theta = \text{N}°)}{\text{Maximum displacement value for } \theta = 45°} * 100 \quad (3.43)$$

where, N = [0, 40] U [50, 90]

Rotating annular uniform-thickness fiber-reinforced composite disc made up of Graphite-Fiber Reinforced Plastic (NCT-301) material and with the clamped-free boundary condition										
Maximum radial displacement corresponding to $\theta = 45°$ is equal to 0.0374 *mm*										
Fiber orientation (in *degrees*)	0	10	20	30	40	50	60	70	80	90
Maximum radial displacement (in 10^{-3} *mm*)	8.64	15.07	26.04	33.54	36.95	37.06	34	27.4	17.7	11.6
% decrease in the displacement	76.8	59.7	30.3	10.3	1.17	0.87	8.9	26.7	52.7	69.0

Table 3.15 Percentage decrease in the maximum radial displacement with the fiber orientation angle in a rotating annular uniform-thickness fiber-reinforced composite disc with uni-directional configuration and for the clamped-free boundary condition

It can be seen from the above Table 3.15 that the percentage decrease in the maximum value of the radial displacement is the highest for $\theta = 0°$, and is equal to 76.8%

The following Figures 3.12 and 3.13 show the radial strain and the circumferential strain distributions in a rotating annular uniform-thickness fiber-reinforced composite disc with uni-directional configurations ranging from $[0]_{20}$ to $[90]_{20}$ and for the clamped-free boundary condition.

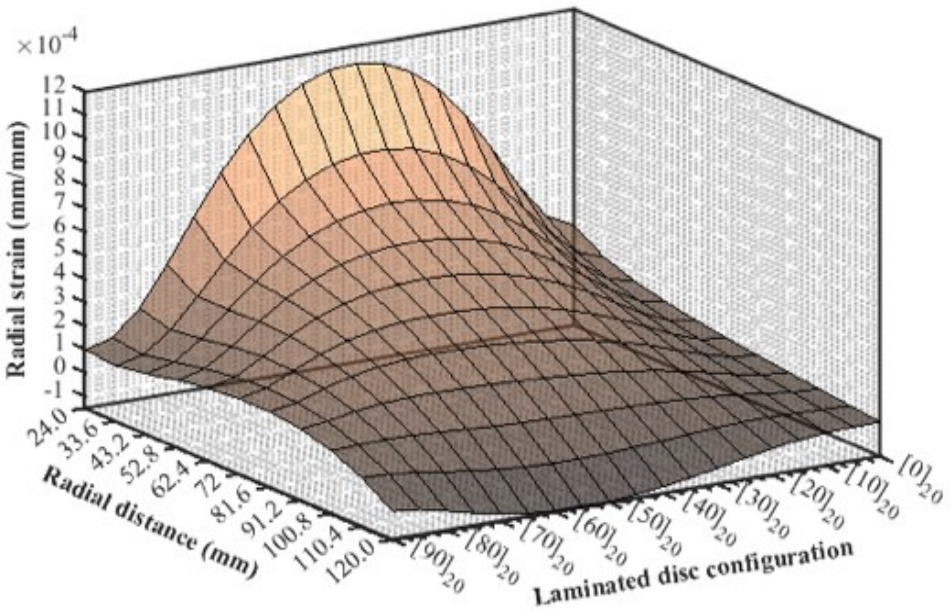

Figure 3.12 Radial strain distribution in a rotating annular uniform-thickness fiber-reinforced composite disc with uni-directional configuration and for the clamped-free boundary condition

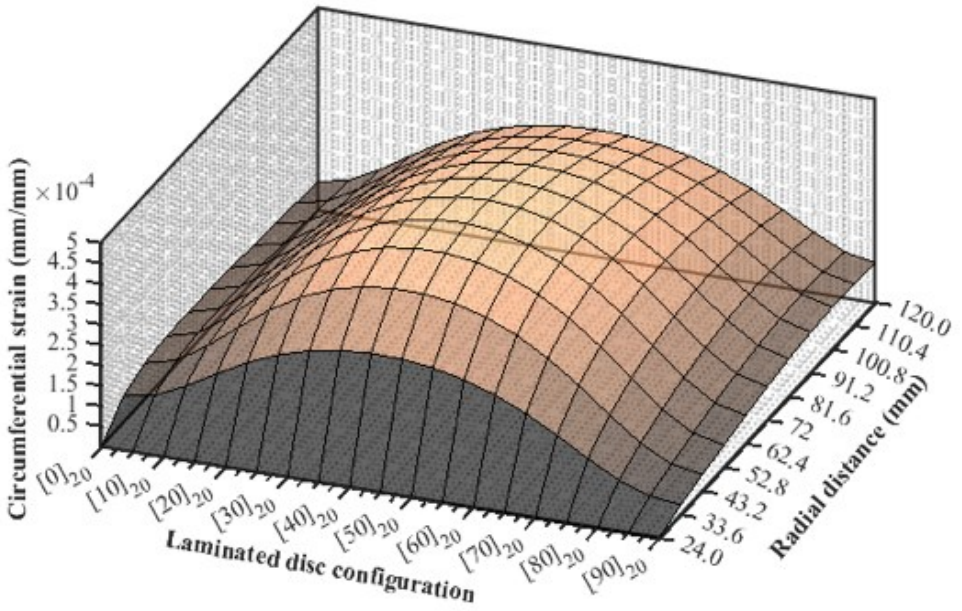

Figure 3.13 Circumferential strain distribution in a rotating annular uniform-thickness fiber-reinforced composite disc with uni-directional configuration and for the clamped-free boundary condition

It can be seen from the above Figures 3.12 and 3.13 that similar to the distributions of radial displacement, the same trend can be seen in the distribution of the radial and the circumferential strains. i.e., both the strains are minimum in the $[0]_{20}$ laminated disc and are maximum in the $[45]_{20}$ laminated disc with the clamped-free boundary condition.

3.7.1.2 Effect of radius ratio on the elastic response of uni-directional laminated discs

The effect of radius ratio on the radial and circumferential stress distributions and on the radial displacement distribution in a rotating annular uniform-thickness fiber-reinforced composite disc with uni-directional configuration is studied. The variations of maximum radial and circumferential stresses and the maximum radial displacement with the fiber orientation are studied for the rotating annular uniform-thickness discs with the beta values of 0.2, 0.25 and 0.3.

The disc has a fixed outer radius of r_o = 120 *mm*, thickness of h = 2.4 *mm* with an individual ply thickness of t = 0.12 *mm,* and it is rotating at a constant angular velocity of ω = 1000 *rad/s* i.e., 9554.14 *rpm*. The inner radius of the disc is dependent on the beta value taken into consideration and is given in the following Table 3.16.

Beta value (β)	Inner radius (r_i) in mm	Outer radius (r_0) in mm
0.2	24	120
0.25	30	
0.3	36	

Table 3.16 Inner radius values of the rotating disc corresponding to different beta values

The following Table 3.17 shows the variation with the fiber orientation angle of the maximum radial stress in a rotating annular uniform-thickness uni-directional laminated disc with the clamped-free boundary condition for the beta values of 0.2, 0.25 and 0.3.

Maximum radial stress (in *MPa*) in a rotating annular uniform-thickness fiber-reinforced composite disc made up of Graphite-Fiber Reinforced Plastic (NCT-301) material and with the clamped-free boundary condition										
Fiber orientation angle (in *degrees*)	0	10	20	30	40	50	60	70	80	90
β = 0.2	31.64	28.17	21.97	17.03	13.55	10.78	8.03	4.9	2.581	1.59
β = 0.25	25.80	23.54	19.27	15.64	12.95	10.72	8.425	5.606	2.624	1.597
β = 0.3	21.65	20.13	17.11	14.40	12.31	10.53	8.627	6.146	3.134	1.582

Table 3.17 Variation of maximum radial stress (in *MPa*) with the fiber orientation angle in a rotating annular uniform-thickness uni-directional laminated disc with the clamped-free boundary condition for different values of radius ratio

The following Figure 3.14 shows the variation with the fiber orientation angle of the maximum radial stress in a rotating annular uniform-thickness uni-directional laminated disc with the clamped-free boundary condition for the beta values of 0.2, 0.25 and 0.3.

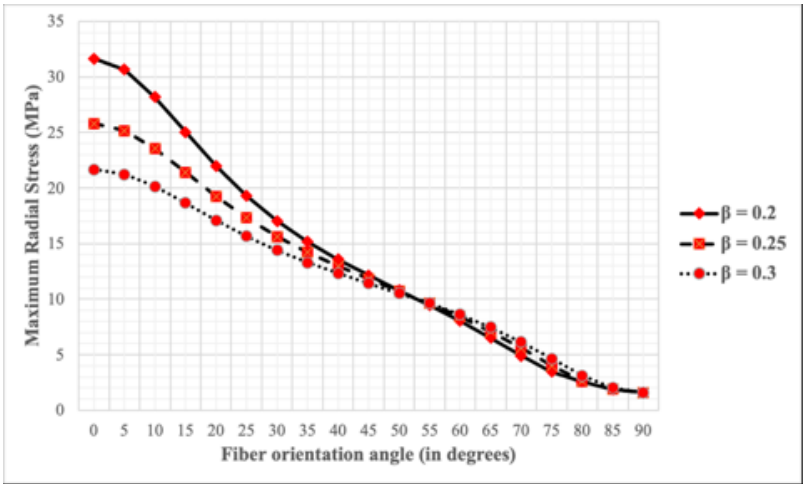

Figure 3.14 Variation of maximum radial stress with the fiber orientation angle in a rotating annular uniform-thickness uni-directional laminated disc with the clamped-free boundary condition for different values of radius ratio

It can be seen from the above Table 3.17 and Figure 3.14 that irrespective of the fiber orientation angle, the maximum radial stress in a rotating annular uniform-thickness fiber-reinforced composite disc with uni-directional configuration and with the clamped-free boundary condition, decreases with the increasing value of the radius ratio up to the fiber orientation angle of 50°. From the fiber orientation angle of 50° to 90°, the maximum radial stress tends to relatively-slightly increase with the increasing beta value of the rotating disc.

The following Table 3.18 shows the variation with the fiber orientation angle of the maximum circumferential stress in a rotating annular uniform-thickness uni-directional laminated disc with the clamped-free boundary condition for the beta values of 0.2, 0.25 and 0.3.

Maximum circumferential stress (in *MPa*) in a rotating annular uniform-thickness uni-directional composite disc made up of Graphite-Fiber Reinforced Plastic (NCT-301) material and with the clamped-free boundary condition										
Fiber orientation angle (in *degrees*)	0	10	20	30	40	50	60	70	80	90
$\beta = 0.2$	1.06	2.2	4.22	5.75	6.75	7.34	8.06	8.97	10.58	12.23
$\beta = 0.25$	0.85	1.80	3.64	5.16	6.20	6.95	7.69	8.77	10.52	12.22
$\beta = 0.3$	0.685	1.5	3.15	4.61	5.65	6.46	7.27	8.48	10.41	12.12

Table 3.18 Variation of maximum circumferential stress (in *MPa*) with the fiber orientation angle in a rotating annular uniform-thickness uni-directional laminated disc with the clamped-free boundary condition for different values of radius ratio

The following Figure 3.15 shows the variation with the fiber orientation angle of the maximum circumferential stress in a rotating annular uniform-thickness uni-directional laminated disc with the clamped-free boundary condition for the beta values of 0.2, 0.25 and 0.3.

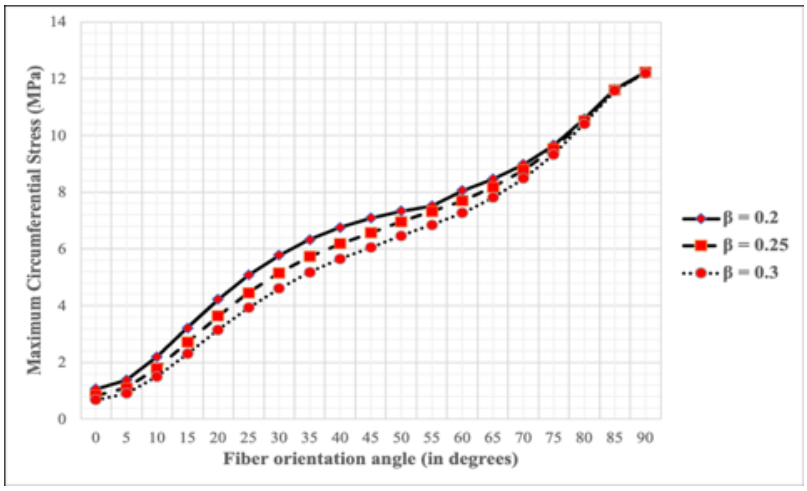

Figure 3.15 Variation of maximum circumferential stress with the fiber orientation angle in a rotating annular uniform-thickness uni-directional laminated disc with the clamped-free boundary condition for different values of radius ratio

It can be seen from the above Table 3.18 and Figure 3.15 that irrespective of the fiber orientation angle, the maximum circumferential stress in a rotating annular uniform-thickness fiber-reinforced composite disc with uni-directional configuration and with the clamped-free boundary condition, decreases with the increasing beta value of the rotating disc.

The following Table 3.19 shows the variation with the fiber orientation angle of the maximum radial displacement in a rotating annular uniform-thickness uni-directional laminated disc with the clamped-free boundary condition for the beta values of 0.2, 0.25 and 0.3.

Maximum radial displacement (in $10^{-3}mm$) in a rotating annular uniform-thickness fiber-reinforced composite disc made up of Graphite-Fiber Reinforced Plastic (NCT-301) material and with the clamped-free boundary condition										
Fiber orientation angle (in *degrees*)	0	10	20	30	40	50	60	70	80	90
$\beta = 0.2$	8.64	15.07	26.04	33.54	36.95	34.03	27.4	17.69	11.56	8.64
$\beta = 0.25$	7.29	12.97	23.26	31.07	35.15	33.64	27.48	17.75	11.55	7.29
$\beta = 0.3$	6.15	11.12	20.49	28.12	32.44	32.13	26.79	17.65	11.54	6.15

Table 3.19 Variation of maximum radial displacement (in *mm*) with the fiber orientation angle in a rotating annular uniform-thickness uni-directional laminated disc with the clamped-free boundary condition for different values of radius ratio

The following Figure 3.16 shows the variation with the fiber orientation angle of the maximum radial displacement in a rotating annular uniform-thickness uni-directional laminated disc with the clamped-free boundary condition for the beta values of 0.2, 0.25 and 0.3.

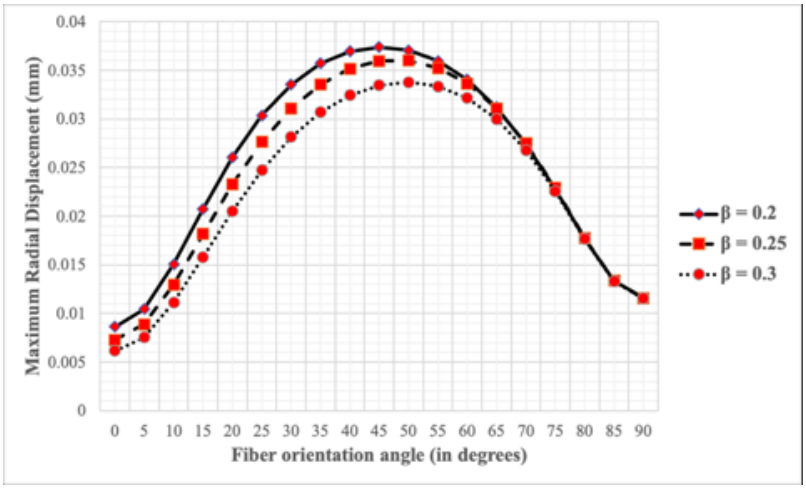

Figure 3.16 Variation of maximum radial displacement with the fiber orientation angle in a rotating annular uniform-thickness uni-directional laminated disc with the clamped-free boundary condition for different values of radius ratio

It can be seen from the above Table 3.19 and Figure 3.16 that irrespective of the fiber orientation angle, the maximum radial displacement in a rotating annular uniform-thickness fiber-reinforced composite disc with uni-directional configuration and with the clamped-free boundary condition, decreases with the increasing beta value of the rotating disc.

3.7.1.3 Effect of rotational speed on the elastic response of uni-directional laminated discs

The effect of rotational speed on the radial and circumferential stress distributions and on the radial displacement distribution in a rotating annular uniform-thickness uni-directional laminated disc with the clamped-free boundary condition is studied.

The rotating disc has the same geometric properties as mentioned in the validation section. i.e., the disc has an inner radius of r_i = 24 *mm*, an outer radius of r_o = 120 *mm*, thickness of h = 2.4 *mm* with an individual ply thickness of t = 0.12 *mm*.

The following Figures 3.17 and 3.18 show the variation with the fiber orientation angle of the maximum radial stress and the maximum circumferential stress in a rotating annular uniform-thickness uni-directional laminated disc with a beta value of 0.2 and with the clamped-free boundary condition for the rotational speeds of 1000, 1500 and 2000 *rad/s*.

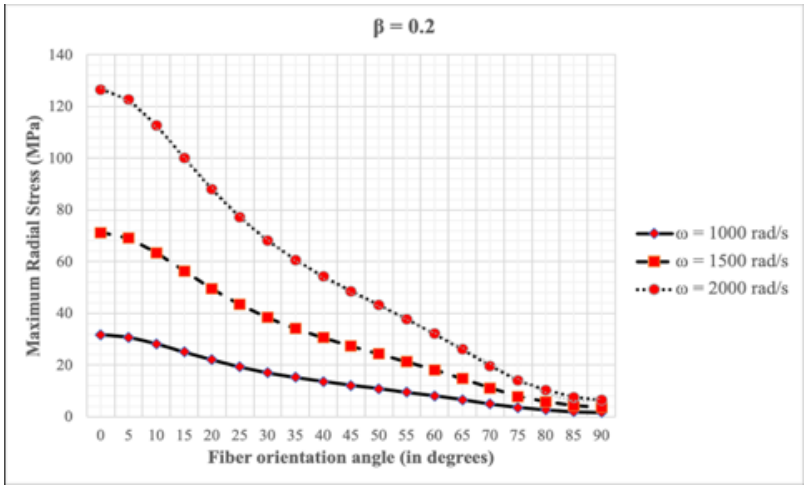

Figure 3.17 Variation of maximum radial stress with the fiber orientation angle in a rotating annular uniform-thickness uni-directional laminated disc with the clamped-free boundary condition for different rotational speeds

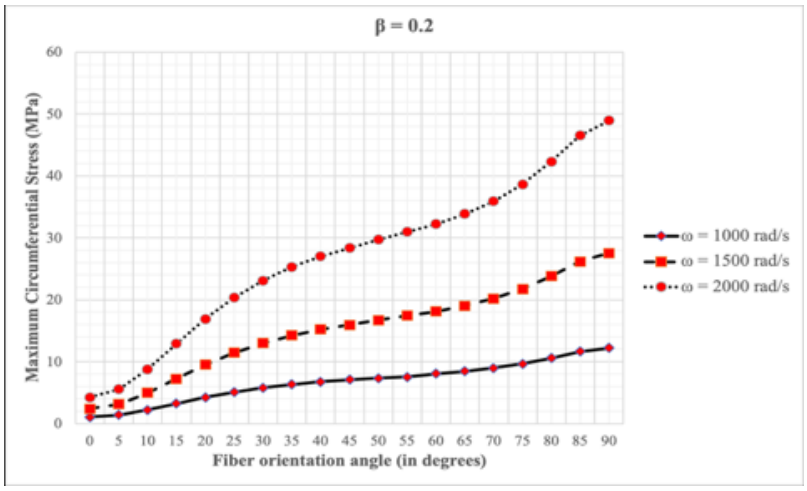

Figure 3.18 Variation of maximum circumferential stress with the fiber orientation angle in a rotating annular uniform-thickness uni-directional laminated disc with the clamped-free boundary condition for different rotational speeds

It can be seen from the above Figures 3.17 and 3.18 that irrespective of the fiber orientation angle, the maximum radial stress and the maximum circumferential stress in a rotating annular uniform-thickness uni-directional laminated disc with the clamped-free boundary condition increase with the increase in the rotational speed.

The following Tables 3.20 and 3.21 show the rate of increase and the percentage increase in the maximum radial stress and the maximum circumferential stress for the rotational speeds of 1000, 1500 and 2000 *rad/s*. Also, in the following Tables, the rate of increase of the stress and the percentage increase in the stress are calculated according to the following formula:

$$\text{Rate of increase of the stress } (m_n) = \frac{\text{Maximum stress value corresponding to } \omega_{n+1} - \text{Maximum stress value corresponding to } \omega_n}{\omega_{n+1} - \omega_n} \quad (3.44)$$

$$\%\text{ increase in the stress } (\eta_n) = \frac{\text{Maximum stress value corresponding to } \omega_{n+1} - \text{Maximum stress value corresponding to } \omega_n}{\text{Maximum stress value corresponding to } \omega_{n+1}} * 100 \quad (3.45)$$

Rotating annular uniform-thickness fiber-reinforced composite disc made up of Graphite-Fiber Reinforced Plastic (NCT-301) material and with the clamped-free boundary condition							
Fiber orientation angle (in *degrees*)	Maximum radial stress (in *MPa*) corresponding to different rotational speeds			Rate of increase of the radial stress		% increase in the maximum radial stress	
	$\omega_1 =$ 1000 *rad/s*	$\omega_2 =$ 1500 *rad/s*	$\omega_3 =$ 2000 *rad/s*	m_1	m_2	η_1	η_2
0	31.645	71.2	126.578	0.079	0.111	55.55	43.75
5	30.67	69.008	122.681	0.077	0.107	55.56	43.75
10	28.176	63.396	112.704	0.07	0.099	55.56	43.75
15	25.043	56.347	100.17	0.063	0.088	55.56	43.75
20	21.974	49.44	87.894	0.055	0.077	55.55	43.75
25	19.288	43.398	77.152	0.048	0.068	55.56	43.75
30	17.04	38.339	68.158	0.043	0.06	55.55	43.75
35	15.163	34.117	60.652	0.038	0.053	55.56	43.75
40	13.559	30.508	54.236	0.034	0.047	55.56	43.75
45	12.128	27.288	48.512	0.03	0.042	55.56	43.75
50	10.781	24.257	43.123	0.027	0.038	55.56	43.75
55	9.438	21.236	37.752	0.024	0.033	55.56	43.75
60	8.033	18.074	32.132	0.02	0.028	55.55	43.75
65	6.521	14.671	26.083	0.016	0.023	55.55	43.75
70	4.906	11.039	19.624	0.012	0.017	55.56	43.75
75	3.48	7.832	13.924	0.009	0.012	55.57	43.75
80	2.581	5.808	10.325	0.006	0.009	55.56	43.75
85	1.876	4.221	7.503	0.005	0.007	55.56	43.74
90	1.595	3.589	6.381	0.004	0.006	55.56	43.75

Table 3.20 Variation of maximum radial stress (in *MPa*), rate of increase of the stress and the percentage increase in the maximum radial stress with the fiber orientation angle in a rotating annular uniform-thickness uni-directional laminated disc with the clamped-free boundary condition for different rotational speeds

Rotating annular uniform-thickness fiber-reinforced composite disc made up of Graphite-Fiber Reinforced Plastic (NCT-301) material and with the clamped-free boundary condition							
Fiber orientation angle (in *degrees*)	Maximum circumferential stress (in *MPa*) corresponding to different rotational speeds			Rate of increase of the circumferential stress		% increase in the maximum circumferential stress	
	$\omega_1 = 1000$ *rad/s*	$\omega_2 = 1500$ *rad/s*	$\omega_3 = 2000$ *rad/s*	m_1	m_2	η_1	η_2
0	1.062	2.39	4.249	0.003	0.004	55.56	43.75
5	1.382	3.109	5.527	0.003	0.005	55.55	43.75
10	2.199	4.949	8.798	0.006	0.008	55.57	43.75
15	3.224	7.253	12.895	0.008	0.011	55.55	43.75
20	4.22	9.495	16.88	0.011	0.015	55.56	43.75
25	5.078	11.426	20.313	0.013	0.018	55.56	43.75
30	5.775	12.994	23.1	0.014	0.02	55.56	43.75
35	6.326	14.233	25.304	0.016	0.022	55.55	43.75
40	6.756	15.201	27.024	0.017	0.024	55.56	43.75
45	7.088	15.949	28.354	0.018	0.025	55.56	43.75
50	7.339	16.712	29.71	0.019	0.026	56.09	43.75
55	7.515	17.42	30.968	0.02	0.027	56.86	43.75
60	8.057	18.13	32.231	0.02	0.028	55.56	43.75
65	8.462	19.039	33.848	0.021	0.03	55.55	43.75
70	8.975	20.193	35.899	0.022	0.031	55.55	43.75
75	9.657	21.729	38.629	0.024	0.034	55.56	43.75
80	10.581	23.807	42.324	0.026	0.037	55.56	43.75
85	11.634	26.176	46.535	0.029	0.041	55.55	43.75
90	12.233	27.524	48.932	0.031	0.043	55.56	43.75

Table 3.21 Variation of maximum circumferential stress (in *MPa*), rate of increase of the stress and the percentage increase in the maximum circumferential stress with the fiber orientation angle in a rotating annular uniform-thickness uni-directional laminated disc with the clamped-free boundary condition for different rotational speeds

It can be seen from the above Tables 3.20 and 3.21 that irrespective of the fiber orientation angle, the rates of increase of the maximum radial stresses and the maximum circumferential stresses do not have the same value. i.e., the increase of the maximum radial stress and the maximum circumferential stress is non-linear with the increase in the rotational speed. Furthermore, the value of the slopes are higher for the fiber orientation angles for which the radial stress and circumferential stress are maximum. i.e., the rate of increase of the radial stress is maximum for the fiber orientation angle of 0° while the rate of increase of the circumferential stress is maximum for the fiber orientation angle of 90°.

The following Figure 3.19 shows the variation with the fiber orientation angle of the maximum radial displacement in a rotating annular uniform-thickness uni-directional laminated disc with a beta value of 0.2 and with the clamped-free boundary condition for the rotational speeds of 1000, 1500 and 2000 *rad/s*.

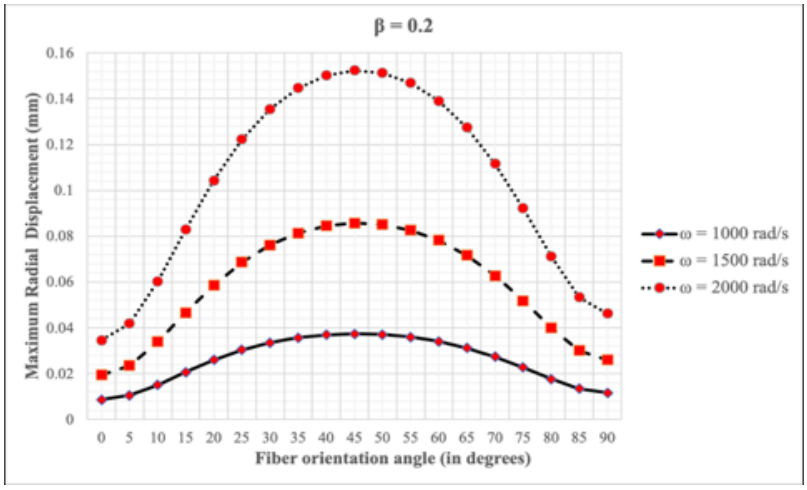

Figure 3.19 Variation of maximum radial displacement with the fiber orientation angle in a rotating annular uniform-thickness uni-directional laminated disc with the clamped-free boundary condition for different rotational speeds

It can be seen from the above Figure 3.19 that similar to the variation of the maximum radial stress and the maximum circumferential stress, the maximum radial displacement also increases with the increase in the rotational speed. The following Table 3.22 shows the rate of increase of the radial displacement and the percentage increase in the maximum radial displacement for the rotational speeds of 1000, 1500 and 2000 *rad/s*. Also, in the following Table, the rate of increase and the percentage increase are calculated according to the following formula:

Rate of increase of the displacement (m_n)

$$= \frac{\text{Maximum displacement value corresponding to } \omega_{n+1} - \text{Maximum displacement value corresponding to } \omega_n}{\omega_{n+1} - \omega_n} \quad (3.46)$$

% increase in the displacement (η_n) =

$$\frac{\text{Maximum displacement value corresponding to } \omega_{n+1} - \text{Maximum displacement value corresponding to } \omega_n}{\text{Maximum displacement value corresponding to } \omega_{n+1}} * \quad (3.47)$$

100

Rotating annular uniform-thickness fiber-reinforced composite disc made up of Graphite-Fiber Reinforced Plastic (NCT-301) material and with the clamped-free boundary condition							
Fiber orientation angle (in *degrees*)	Maximum radial displacement (in *mm*) corresponding to different rotational speeds			Rate of increase of the radial displacement		% increase in the maximum radial displacement	
	$\omega_1 = 1000$ *rad/s*	$\omega_2 = 1500$ *rad/s*	$\omega_3 = 2000$ *rad/s*	m_1	m_2	η_1	η_2
0	0.0086	0.0194	0.0346	2.16e-05	3.03e-05	55.56	43.75
5	0.0105	0.0235	0.0419	2.62e-05	3.66e-05	55.55	43.75
10	0.0151	0.0339	0.0603	3.77e-05	5.28e-05	55.57	43.75
15	0.0207	0.0466	0.0829	5.18e-05	7.26e-05	55.55	43.75
20	0.026	0.0586	0.1044	6.51e-05	9.17e-05	55.56	43.75
25	0.0304	0.0687	0.1222	7.68e-05	1.07e-04	55.56	43.75
30	0.0335	0.0762	0.1355	8.54e-05	1.19e-04	55.56	43.75
35	0.0357	0.0814	0.1447	9.14e-05	1.27e-04	55.55	43.75
40	0.0369	0.0845	0.1502	9.51e-05	1.31e-04	55.56	43.75
45	0.0374	0.0857	0.1523	9.66e-05	1.33e-04	55.56	43.75
50	0.0371	0.0851	0.1513	9.61e-05	1.32e-04	56.09	43.75
55	0.036	0.0826	0.1469	9.34e-05	1.29e-04	56.86	43.75
60	0.034	0.0782	0.1391	8.84e-05	1.22e-04	55.56	43.75
65	0.0312	0.0717	0.1274	8.09e-05	1.11e-04	55.55	43.75
70	0.0274	0.0628	0.1116	7.08e-05	9.77e-05	55.55	43.75
75	0.0227	0.0519	0.0922	5.83e-05	8.07e-05	55.56	43.75
80	0.0177	0.04	0.0711	4.46e-05	6.22e-05	55.56	43.75
85	0.0134	0.0301	0.0534	3.34e-05	4.68e-05	55.55	43.75
90	0.0116	0.026	0.0462	2.89e-05	4.05e-05	55.56	43.75

Table 3.22 Variation of maximum radial displacement (in *mm*), rate of increase of the displacement and the percentage increase in the maximum radial displacement with the fiber orientation angle in a rotating annular uniform-thickness uni-directional laminated disc with the clamped-free boundary condition for different rotational speeds

It can be seen from the above Table 3.22 that irrespective of the fiber orientation angle, the rates of increase of the maximum radial displacement (m_1 and m_2) are not identical. i.e., the increase of the maximum radial displacement is non-linear with the increase in the rotational speed. Furthermore, the value of the slope is the highest for the fiber orientation angle for which the radial displacement is maximum. That is the rate of increase of the radial displacement is maximum for the fiber orientation angle of 45°.

3.7.2 Cross-ply laminated discs

This sub-section presents the parametric study on the elastic response of rotating annular uniform-thickness discs made up of Graphite-Fiber Reinforced Plastic material with various cross-ply laminate configurations and for the clamped-free boundary condition. The relative effects of the $0°$ plies and the radius ratio on the radial stress and circumferential stress distributions and on the radial displacement distributions, and the effect of the modelling element on the radial stress and circumferential stress variations through the thickness in rotating annular uniform-thickness fiber-reinforced composite discs with various cross-ply configurations are studied. Graphical results for the stress and displacement distributions are presented and the percentage changes in the maximum stress and maximum displacement values with the number of $0°$ plies in the cross-ply laminated disc are calculated.

A cross-ply laminate is made of layers whose principal directions are oriented alternatively at $0°$ or $90°$ to the reference directions of the laminate. Since, the thickness of each ply in the laminate is equal (which is 0.12 *mm* in the present case), therefore these laminates can be called as regular cross-ply laminates. Such types of laminates are characterized by the total number of plies (*N*) and by the total number of plies oriented at $0°$, denoted by N_0 in the laminate, provided $N = N_0 + N_{90}$, where N_{90} are the total number of plies oriented at $90°$ in the laminate. Here *N* is taken to be 20.

Note that when N_0 = 20, it corresponds to the $[0]_{20}$ laminated disc in which only the fibers sustain the radial load and when N_{90} = 20, it corresponds to the $[90]_{20}$ laminated disc in which only the matrix (resin) should sustain the radial loads which can result in failure even at low rotating speed. Therefore, for high-speed applications, the selection of optimum cross-ply laminated disc is required.

3.7.2.1 Relative effect of 0° plies on the elastic response of cross-ply laminated discs

The relative effect of the 0° plies on the elastic response (i.e., the radial and circumferential stress distributions and the radial displacement distribution) of a rotating annular uniform-thickness cross-ply laminated disc with a beta value of 0.2 and with the clamped-free boundary condition is studied. The rotating disc has the same geometric dimensions as mentioned in the validation section. i.e., the disc has an inner radius of r_i = 24 *mm*, an outer radius of r_o = 120 *mm*, a total thickness of h = 2.4 *mm* with an individual ply thickness of t = 0.12 *mm,* and it is rotating at constant angular velocity of ω = 1000 *rad/s* i.e., 9554.14 *rpm*.

In the cross-ply configurations considered below in the Table 3.23 i.e., the configurations ranging from $[0_9/90]_s$ to $[0/90_9]_s$, there is no stretching-bending coupling since the coupling stiffness matrix, [B] is zero.

Cross-ply configuration	Number of 0° plies (N_0)	Total number of plies (N)
$[0_9/90]_s$	18	20
$[0_8/90_2]_s$	16	
$[0_7/90_3]_s$	14	
$[0_6/90_4]_s$	12	
$[0_5/90_5]_s$	10	
$[0_4/90_6]_s$	8	
$[0_3/90_7]_s$	6	
$[0_2/90_8]_s$	4	
$[0/90_9]_s$	2	

Table 3.23 Number of 0° plies corresponding to various cross-ply configurations considered in the present study

The following Tables 3.24 and 3.25 show the effect of the 0° plies on the radial stress distributions in the 0° ply and the 90° ply respectively, of a rotating annular uniform-thickness fiber-reinforced composite disc for various cross-ply configurations considered in the present study and mentioned above in the Table 3.23.

Radial stress distributions (σ_r, in *MPa*) in the 0° ply of a rotating annular uniform-thickness disc with various cross-ply configurations									
Radial distance in *mm* from the center of the disc	Number of 0° plies (N_o) in the cross-ply laminated disc								
	18	16	14	12	10	8	6	4	2
24.0	31.003	30.272	29.425	28.420	27.197	25.660	23.653	20.902	16.92
33.6	22.188	21.785	21.318	20.767	20.094	19.245	18.120	16.533	14.08
43.2	17.156	17.035	16.902	16.751	16.574	16.351	16.050	15.590	14.74
52.8	13.771	13.846	13.946	14.078	14.253	14.487	14.802	15.221	15.73
62.4	11.156	11.349	11.589	11.894	12.288	12.812	13.530	14.560	16.11
72.0	8.969	9.220	9.530	9.922	10.429	11.106	12.050	13.447	15.70
81.6	7.035	7.298	7.623	8.034	8.567	9.284	10.296	11.830	14.42
91.2	5.224	5.461	5.754	6.124	6.607	7.260	8.192	9.630	12.15
100.8	3.461	3.638	3.857	4.135	4.498	4.991	5.702	6.813	8.815
110.4	1.730	1.820	1.932	2.074	2.259	2.511	2.872	3.437	4.452
120.0	-3.7e-3	-4.1e-4	-4.3e-3	-5.2e-5	-5.7e-5	-6.3e-7	-6.8e-7	-7.1e-9	-9.4e-9

Table 3.24 Radial stress distributions in the 0° ply of a rotating annular uniform-thickness composite disc for various cross-ply configurations and for the clamped-free boundary condition

Radial stress distributions (σ_r, in *MPa*) in the 90° ply of a rotating annular uniform-thickness disc with various cross-ply configurations									
Radial distance in *mm* from the center of the disc	Number of 0° plies (N_o) in the cross-ply laminated disc								
	18	16	14	12	10	8	6	4	2
24.0	2.173	2.122	2.063	1.992	1.906	1.799	1.658	1.465	1.186
33.6	1.695	1.664	1.627	1.585	1.532	1.466	1.379	1.256	1.067
43.2	1.392	1.380	1.366	1.351	1.333	1.310	1.280	1.234	1.155
52.8	1.172	1.174	1.178	1.183	1.191	1.202	1.216	1.235	1.254
62.4	0.992	1.003	1.018	1.037	1.061	1.094	1.140	1.205	1.303
72.0	0.835	0.851	0.872	0.898	0.932	0.978	1.042	1.137	1.291
81.6	0.692	0.710	0.733	0.761	0.798	0.849	0.920	1.028	1.212
91.2	0.556	0.573	0.593	0.620	0.655	0.702	0.770	0.874	1.057
100.8	0.422	0.434	0.451	0.471	0.498	0.535	0.588	0.672	0.822
110.4	0.289	0.296	0.304	0.316	0.330	0.351	0.380	0.426	0.509
120.0	0.153	0.152	0.151	0.149	0.148	0.145	0.141	0.132	0.109

Table 3.25 Radial stress distributions in the 90° ply of a rotating annular uniform-thickness composite disc for various cross-ply configurations and for the clamped-free boundary condition

It can be seen from the above Tables 3.24 and 3.25 that the radial stress distributions in the $0°$ and the $90°$ ply are higher in the cross-ply disc having 18 plies oriented at $0°$ in comparison to the other cross-ply discs. i.e., the radial stresses are maximum for the disc with the maximum number of $0°$ plies i.e., for $N_o = 18$ in $[0_9/90]_s$ and as the number of $0°$ plies are reduced by replacing them with the $90°$ plies, the radial stress distributions decreases accordingly, and is the least for the $[0/90_9]_s$ laminated disc with $N_o = 2$.

The following Tables 3.26 and 3.27 show the rates of change of the radial stresses in the $0°$ ply and the $90°$ ply i.e., the slope of the radial stress distributions at any radial coordinate for the above considered values of N_o (i.e., from $N_o = 18$ to $N_o = 2$). Also, in the following Tables, the rate of change of the radial stress is calculated according to the following formula:

Rate of change of the radial stress, ${}_{N_o-2}^{N_o}m_i^R$) =

$$\frac{\text{Maximum stress value corresponding to } N_o - \text{Maximum stress value corresponding to } N_o - 2}{2} \quad (3.48)$$

In the above Equation (3.48), the superscript *R* after the base, represents the rate of change of the radial stress and the subscript $i = 0$ refers to the 0° ply and $i = 90$ refers to the 90° ply in the cross-ply laminated disc.

Rates of change of the radial stresses in the 0° ply of a rotating annular uniform-thickness disc with various cross-ply configurations								
Radial distance in *mm* from the center of the disc	Rate of change of the radial stress							
	${}_{16}^{18}m_0^R$	${}_{14}^{16}m_0^R$	${}_{12}^{14}m_0^R$	${}_{10}^{12}m_0^R$	${}_{8}^{10}m_0^R$	${}_{6}^{8}m_0^R$	${}_{4}^{6}m_0^R$	${}_{2}^{4}m_0^R$
24.0	-0.366	-0.423	-0.503	-0.612	-0.769	-1.004	-1.376	-1.991
33.6	-0.201	-0.233	-0.276	-0.336	-0.425	-0.563	-0.794	-1.227
43.2	-0.06	-0.066	-0.075	-0.088	-0.112	-0.15	-0.23	-0.425
52.8	0.037	0.05	0.066	0.088	0.117	0.158	0.21	0.255
62.4	0.096	0.12	0.153	0.197	0.262	0.359	0.515	0.775
72.0	0.126	0.155	0.196	0.254	0.339	0.472	0.698	1.127
81.6	0.132	0.163	0.206	0.267	0.359	0.506	0.767	1.295
91.2	0.119	0.147	0.185	0.242	0.327	0.466	0.719	1.26
100.8	0.089	0.11	0.139	0.182	0.247	0.356	0.556	1.001
110.4	0.045	0.056	0.071	0.093	0.126	0.181	0.283	0.508
120.0	0.002	-0.002	0.002	0	0	0	0	0

Table 3.26 Rates of change of the radial stresses in the 0° ply of a rotating annular uniform-thickness composite disc for various cross-ply configurations and for the clamped-free boundary condition

Rates of change of the radial stresses in the 90° ply of a rotating annular uniform-thickness disc with various cross-ply configurations								
Radial distance in *mm* from the center of the disc	Rate of change of the radial stress							
	${}^{18}_{16}m^{R}_{90}$	${}^{16}_{14}m^{R}_{90}$	${}^{14}_{12}m^{R}_{90}$	${}^{12}_{10}m^{R}_{90}$	${}^{10}_{8}m^{R}_{90}$	${}^{8}_{6}m^{R}_{90}$	${}^{6}_{4}m^{R}_{90}$	${}^{4}_{2}m^{R}_{90}$
24.0	-0.026	-0.029	-0.036	-0.043	-0.054	-0.071	-0.096	-0.14
33.6	-0.016	-0.019	-0.021	-0.027	-0.033	-0.044	-0.062	-0.095
43.2	-0.006	-0.007	-0.008	-0.009	-0.012	-0.015	-0.023	-0.04
52.8	0.001	0.002	0.003	0.004	0.005	0.007	0.01	0.009
62.4	0.005	0.008	0.009	0.012	0.017	0.023	0.033	0.049
72.0	0.008	0.011	0.013	0.017	0.023	0.032	0.048	0.077
81.6	0.009	0.012	0.014	0.019	0.026	0.036	0.054	0.092
91.2	0.008	0.01	0.014	0.018	0.024	0.034	0.052	0.092
100.8	0.006	0.009	0.01	0.014	0.019	0.027	0.042	0.075
110.4	0.004	0.004	0.006	0.007	0.011	0.015	0.023	0.042
120.0	-0.001	-0.001	-0.001	-0.001	-0.002	-0.002	-0.004	-0.012

Table 3.27 Rates of change of the radial stresses in the 90° ply of a rotating annular uniform-thickness composite disc for various cross-ply configurations and for the clamped-free boundary condition

In the above Tables 3.26 and 3.27, a positive value of the rate of change indicates that the stress has increased and a negative value indicates that the stress has decreased with the decreasing value of N_o. It can be seen that the rate of change of the radial stress in the 0° and the 90° plies is non-linear with the decreasing value of N_o. Furthermore, it can also be seen that up to the radial distance of 43.2 *mm*, the rates of change of the radial stresses in the 0° and the 90° plies have a negative value, i.e., up to the radial distance of 43.2 *mm* from the center of the disc, the radial stresses in the 0° and the 90° plies decreases with the decreasing value of N_o. From the radial distance of 52.8 *mm* to 120 *mm*, the radial stresses in the 0° and the 90° plies increases with the decreasing value of N_o, however, the increase in the stress is not that significant.

The following Tables 3.28 and 3.29 show the percentage decrease in the maximum radial stress in the 0° and the 90° ply of a rotating annular uniform-thickness composite disc for various cross-ply configurations considered in the present study. Since the cross-ply disc with $N_o = 18$ is subjected to the maximum amount of radial stress, the value of the maximum radial stress in the cross-ply disc with $N_o = 18$ is considered as a benchmark while calculating the percentage decrease in the stress.

Rotating annular uniform-thickness cross-ply laminated disc made up of Graphite-Fiber Reinforced Plastic (NCT-301) material and with the clamped-free boundary condition								
Maximum radial stress in the 0° ply corresponding to $N_o = 18$ is equal to 31.003 *MPa*								
Number of 0° plies (N_o)	16	14	12	10	8	6	4	2
Maximum radial stress (in *MPa*)	30.272	29.425	28.420	27.197	25.660	23.653	20.902	16.92
% decrease in the stress	2.35	5.09	8.331	12.276	17.232	23.70	32.581	45.415

Table 3.28 Percentage decrease in the maximum radial stress in the 0° ply of a rotating annular uniform-thickness composite disc for various cross-ply configurations and for the clamped-free boundary condition

Rotating annular uniform-thickness cross-ply laminated disc made up of Graphite-Fiber Reinforced Plastic (NCT-301) material and with the clamped-free boundary condition								
Maximum radial stress in the 90° ply corresponding to $N_o = 18$ is equal to 2.173 *MPa*								
Number of 0° plies (N_o)	16	14	12	10	8	6	4	2
Maximum radial stress (in *MPa*)	2.122	2.063	1.992	1.906	1.799	1.658	1.465	1.303
% decrease in the stress	2.35	5.09	8.331	12.276	17.232	23.70	32.581	40.05

Table 3.29 Percentage decrease in the maximum radial stress in the 90° ply of a rotating annular uniform-thickness composite disc for various cross-ply configurations and for the clamped-free boundary condition

It can be seen from the above Tables 3.28 and 3.29 that except for the cross-ply disc with $N_o = 2$, the values of the percentage decrease in the maximum radial stresses in the 0° and the 90°

plies of a rotating annular uniform-thickness composite disc for various cross-ply configurations and for the clamped-free boundary condition are the same.

The following Tables 3.30 and 3.31 show the relative effect of the 0° plies on the circumferential stress distributions in the 0° and the 90° ply respectively of a rotating annular uniform-thickness composite disc for various cross-ply configurations considered in the present study.

Circumferential stress distributions (σ_θ, in *MPa*) in the 0° ply of a rotating annular uniform-thickness disc with various cross-ply configurations									
Radial distance in *mm* from the center of the disc	Number of 0° plies (N_o) in the cross-ply laminated disc								
	18	16	14	12	10	8	6	4	2
24.0	0.626	0.611	0.594	0.573	0.549	0.518	0.477	0.422	0.341
33.6	0.966	0.947	0.924	0.898	0.865	0.824	0.770	0.695	0.581
43.2	1.048	1.033	1.016	0.996	0.971	0.940	0.899	0.841	0.748
52.8	1.044	1.035	1.025	1.014	1.001	0.984	0.962	0.931	0.878
62.4	1.004	1.001	0.997	0.994	0.991	0.988	0.984	0.979	0.969
72.0	0.947	0.948	0.950	0.953	0.958	0.965	0.977	0.994	1.022
81.6	0.882	0.886	0.891	0.898	0.908	0.923	0.945	0.979	1.035
91.2	0.811	0.816	0.823	0.832	0.846	0.864	0.891	0.934	1.008
100.8	0.735	0.741	0.748	0.758	0.771	0.789	0.817	0.860	0.936
110.4	0.657	0.661	0.667	0.675	0.686	0.701	0.724	0.759	0.822
120.0	0.576	0.578	0.580	0.585	0.590	0.599	0.611	0.630	0.661

Table 3.30 Circumferential stress distributions in the 0° ply of a rotating annular uniform-thickness composite disc for various cross-ply configurations and for the clamped-free boundary condition

Circumferential stress distributions (σ_θ, in *MPa*) in the 90° ply of a rotating annular uniform-thickness disc with different cross-ply configurations									
Radial distance in *mm* from the center of the disc	Number of 0° plies (N_o) in the cross-ply laminated disc								
	18	16	14	12	10	8	6	4	2
24.0	0.626	0.611	0.594	0.573	0.549	0.518	0.4776	0.422	0.341
33.6	7.888	7.718	7.521	7.288	7.004	6.646	6.175	5.521	4.549
43.2	10.418	10.234	10.022	9.771	9.466	9.082	8.574	7.861	6.768
52.8	11.274	11.124	10.954	10.755	10.515	10.214	9.817	9.252	8.360
62.4	11.404	11.302	11.189	11.060	10.908	10.721	10.476	10.129	9.561
72.0	11.177	11.121	11.062	11.001	10.934	10.858	10.765	10.639	10.425
81.6	10.758	10.740	10.727	10.722	10.727	10.745	10.784	10.853	10.966
91.2	10.226	10.237	10.258	10.295	10.354	10.443	10.582	10.803	11.182
100.8	9.621	9.650	9.693	9.756	9.848	9.983	10.184	10.503	11.058
110.4	8.965	9.001	9.053	9.127	9.232	9.384	9.609	9.965	10.589
120.0	8.270	8.304	8.353	8.422	8.520	8.660	8.869	9.197	9.767

Table 3.31 Circumferential stress distributions in the 90° ply of a rotating annular uniform-thickness composite disc for various cross-ply configurations and for the clamped-free boundary condition

It can be seen from the above Tables 3.30 and 3.31 that the circumferential stresses in both of the 0° ply and the 90° ply are higher for the cross-ply discs with N_0 = 18 and the stress decreases as the 0° plies are replaced with the 90° plies till there are 6 plies oriented at 0° in the cross-ply disc i.e., till $N_0 = 6$. On further increasing the 90° plies, the circumferential stresses in both the 0° ply and the 90° ply increases till there are 2 plies left with 0° in the cross-ply disc. i.e., till $N_0 = 2$.

The following Tables 3.32 and 3.33 show the rates of change of the circumferential stresses in the 0° ply and the 90° ply i.e. the slope of the circumferential stress distributions at any radial coordinate for the above considered values of N_o (i.e., from $N_o = 18$ to $N_o = 2$). Also, in the following Tables, the rate of change of the circumferential stress is calculated according to the following formula:

Rate of change of the circumferential stress, ${}_{N_o-2}^{N_o}m_i^C$) =

$$\frac{\text{Maximum stress value corresponding to } N_o - \text{Maximum stress value corresponding to } N_o - 2}{2} \quad (3.49)$$

In the above Equation (3.49), the superscript *C* after the base, represents the rate of change of the circumferential stress and the subscript $i = 0$ refers to the 0° ply and $i = 90$ refers to the 90° ply in the cross-ply laminated disc.

Rates of change of the circumferential stresses in the 0° ply of a rotating annular uniform-thickness disc with various cross-ply configurations								
Radial distance in *mm* from the center of the disc	Rate of change of the circumferential stress							
	${}_{16}^{18}m_0^C$	${}_{14}^{16}m_0^C$	${}_{12}^{14}m_0^C$	${}_{10}^{12}m_0^C$	${}_{8}^{10}m_0^C$	${}_{6}^{8}m_0^C$	${}_{4}^{6}m_0^C$	${}_{2}^{4}m_0^C$
24.0	-0.008	-0.009	-0.011	-0.012	-0.016	-0.021	-0.028	-0.041
33.6	-0.01	-0.012	-0.013	-0.017	-0.021	-0.027	-0.038	-0.057
43.2	-0.008	-0.008	-0.01	-0.013	-0.016	-0.021	-0.029	-0.047
52.8	-0.005	-0.005	-0.005	-0.007	-0.008	-0.011	-0.016	-0.027
62.4	-0.002	-0.002	-0.002	-0.002	-0.002	-0.002	-0.003	-0.005
72.0	0.001	0.001	0.002	0.003	0.004	0.006	0.009	0.014
81.6	0.002	0.003	0.004	0.005	0.008	0.011	0.017	0.028
91.2	0.002	0.004	0.005	0.007	0.009	0.014	0.022	0.037
100.8	0.003	0.004	0.005	0.007	0.009	0.014	0.022	0.038
110.4	0.002	0.003	0.004	0.006	0.007	0.012	0.018	0.032
120.0	0.001	0.001	0.003	0.003	0.005	0.006	0.01	0.016

Table 3.32 Rates of change of the circumferential stresses in the 0° ply of a rotating annular uniform-thickness composite disc for various cross-ply configurations and for the clamped-free boundary condition

Rates of change of the circumferential stresses in the 90° ply of a rotating annular uniform-thickness disc with various cross-ply configurations								
Radial distance in *mm* from the center of the disc	Rate of change of the circumferential stress							
	${}^{18}_{16}m^{C}_{90}$	${}^{16}_{14}m^{C}_{90}$	${}^{14}_{12}m^{C}_{90}$	${}^{12}_{10}m^{C}_{90}$	${}^{10}_{8}m^{C}_{90}$	${}^{8}_{6}m^{C}_{90}$	${}^{6}_{4}m^{C}_{90}$	${}^{4}_{2}m^{C}_{90}$
24.0	-0.008	-0.009	-0.011	-0.012	-0.016	-0.02	-0.028	-0.041
33.6	-0.085	-0.099	-0.117	-0.142	-0.179	-0.236	-0.327	-0.486
43.2	-0.092	-0.106	-0.126	-0.153	-0.192	-0.254	-0.357	-0.547
52.8	-0.075	-0.085	-0.099	-0.12	-0.151	-0.199	-0.283	-0.446
62.4	-0.051	-0.056	-0.064	-0.076	-0.093	-0.123	-0.174	-0.284
72.0	-0.028	-0.03	-0.031	-0.034	-0.038	-0.047	-0.063	-0.107
81.6	-0.009	-0.006	-0.003	0.003	0.009	0.02	0.034	0.056
91.2	0.005	0.01	0.019	0.029	0.045	0.07	0.111	0.19
100.8	0.015	0.021	0.032	0.046	0.067	0.1	0.16	0.278
110.4	0.018	0.026	0.037	0.052	0.076	0.113	0.178	0.312
120.0	0.017	0.024	0.035	0.049	0.07	0.105	0.164	0.285

Table 3.33 Rates of change of the circumferential stresses in the 90° ply of a rotating annular uniform-thickness composite disc for various cross-ply configurations and for the clamped-free boundary condition

In the above Tables 3.32 and 3.33, a positive value of slope indicates that the circumferential stress has increased and a negative value of slope indicates that the stress has decreased with the decreasing value of N_o. It can be seen that the rate of change of the circumferential stress in the $0°$ and the $90°$ plies is non-linear with the decreasing value of N_o. Furthermore, it can also be seen that for the $0°$ ply, the rates of change of the circumferential stresses have a negative value up to the radial distance of 62.4 *mm* while for the $90°$ ply, the rates of change of the circumferential stresses have a negative value up to the radial distance of 72 *mm*. That is, the circumferential stress in the $0°$ ply decreases with the decreasing value of N_o up to a radial distance of 62.4 *mm* while the circumferential stress in the $90°$ ply decreases with the decreasing value of N_o up to a radial distance of 72 *mm* from the center of the disc.

The following Tables 3.34 and 3.35 show the percentage change in the maximum circumferential stress in the 0° and the 90° ply of a rotating annular uniform-thickness composite disc for various cross-ply configurations considered in the present study. Since the cross-ply disc with $N_o = 18$ is subjected to the maximum amount of circumferential stress, the value of the maximum circumferential stress in the cross-ply disc with $N_o = 18$ is considered as a benchmark while calculating the percentage decrease in the stress.

Rotating annular uniform-thickness cross-ply laminated disc made up of Graphite-Fiber Reinforced Plastic (NCT-301) material and with the clamped-free boundary condition								
Maximum circumferential stress in the 0° ply corresponding to $N_o = 18$ is equal to 1.048 *MPa*								
Number of 0° plies (N_o)	16	14	12	10	8	6	4	2
Maximum circumferential stress (in *MPa*)	1.035	1.025	1.014	1.001	0.988	0.984	0.994	1.035
% decrease in the stress	1.16	2.11	3.2	4.48	5.69	6.03	5.10	1.24

Table 3.34 Percentage decrease in the maximum circumferential stress in the 0° ply of a rotating annular uniform-thickness composite disc for various cross-ply configurations and for the clamped-free boundary condition

Rotating annular uniform-thickness cross-ply laminated disc made up of Graphite-Fiber Reinforced Plastic (NCT-301) material and with the clamped-free boundary condition								
Maximum circumferential stress in the 90° ply corresponding to $N_o = 18$ is equal to 11.404 *MPa*								
Number of 0° plies (N_o)	16	14	12	10	8	6	4	2
Maximum circumferential stress (in *MPa*)	11.302	11.189	11.06	10.934	10.858	10.784	10.853	11.182
% decrease in the stress	0.886	1.88	3.011	4.12	4.78	5.43	4.831	1.946

Table 3.35 Percentage decrease in the maximum circumferential stress in the 90° ply of a rotating annular uniform-thickness composite disc for various cross-ply configurations and for the clamped-free boundary condition

The following Table 3.36 shows the relative effect of the 0° plies on the radial displacement distributions in a rotating annular uniform-thickness composite disc for various cross-ply configurations that are considered in the present study.

Radial displacement distributions (u_r, in $10^{-3}mm$) in a rotating annular uniform-thickness disc with various cross-ply configurations									
Radial distance in *mm* from the center of the disc	Number of 0° plies (N_o) in the cross-ply laminated disc								
	18	16	14	12	10	8	6	4	2
24.0	0	0	0	0	0	0	0	0	0
33.6	2.18	2.14	2.08	2.02	1.94	1.84	1.7	1.52	1.25
43.2	3.8	3.73	3.65	3.56	3.44	3.3	3.11	2.85	2.44
52.8	5.07	5	4.92	4.83	4.72	4.57	4.39	4.12	3.71
62.4	6.09	6.03	5.97	5.9	5.81	5.7	5.56	5.36	5.03
72.0	6.91	6.88	6.83	6.79	6.74	6.69	6.62	6.52	6.36
81.6	7.56	7.55	7.53	7.52	7.52	7.52	7.54	7.56	7.61
91.2	8.06	8.06	8.08	8.1	8.14	8.2	8.3	8.45	8.71
100.8	8.41	8.43	8.46	8.51	8.59	8.7	8.86	9.12	9.58
110.4	8.61	8.64	8.69	8.76	8.86	9	9.21	9.54	10.12
120.0	8.67	8.7	8.75	8.83	8.93	9.08	9.3	9.65	10.26

Table 3.36 Radial displacement distributions in a rotating annular uniform-thickness composite disc with various cross-ply configurations and for the clamped-free boundary condition

It can be seen from the above Table 3.36 that the maximum value of radial displacement (i.e., the displacement at the outer periphery of the rotating disc) is the least for a cross-ply disc with N_0 = 18 in comparison to the other cross-ply discs, and as the number of 0° plies are reduced by replacing them with the 90° plies, the displacement increases accordingly and is maximum for the cross-ply disc with N_0 = 2. i.e., the radial displacement is maximum for the $[0/90_9]_s$ laminated disc. The cause for such a variation in the radial displacement can be explained by the fact that the

fibers are strong in the direction of their length, therefore the laminated disc containing a higher number of 0° plies will not deform much. The $[0/90_9]_s$ laminated disc has only 2 plies oriented at 0° and therefore, it has less restriction to deformation in the radial direction as compared to the $[0_9/90]_s$ laminated disc which has 18 plies oriented at 0°.

3.7.2.2 Effect of radius ratio on the elastic response of cross-ply laminated discs

The effect of radius ratio on the radial and circumferential stress distributions and on the radial displacement distribution in a rotating annular uniform-thickness fiber-reinforced composite discs with various cross-ply configurations and with the clamped-free boundary condition is studied. The variation of maximum radial and circumferential stresses and the maximum radial displacements with the number of 0° plies in the cross-ply laminated discs are studied for the beta values of 0.2, 0.25 and 0.3. The rotating disc has a fixed outer radius of r_o = 120 *mm*, thickness of h = 2.4 *mm* with an individual ply thickness of t = 0.12 *mm,* and is rotating at constant angular velocity of ω = 1000 *rad/s* i.e., 9554.14 *rpm*. The inner radius of the disc is dependent on the beta value taken into consideration which has been mentioned earlier in the Table 3.16.

The following Figure 3.20 shows the variation of the maximum radial stress in a rotating annular uniform-thickness cross-ply laminated disc with varying number of 0° plies corresponding to the various cross-ply configurations considered in the present study for beta values of 0.2, 0.25 and 0.3.

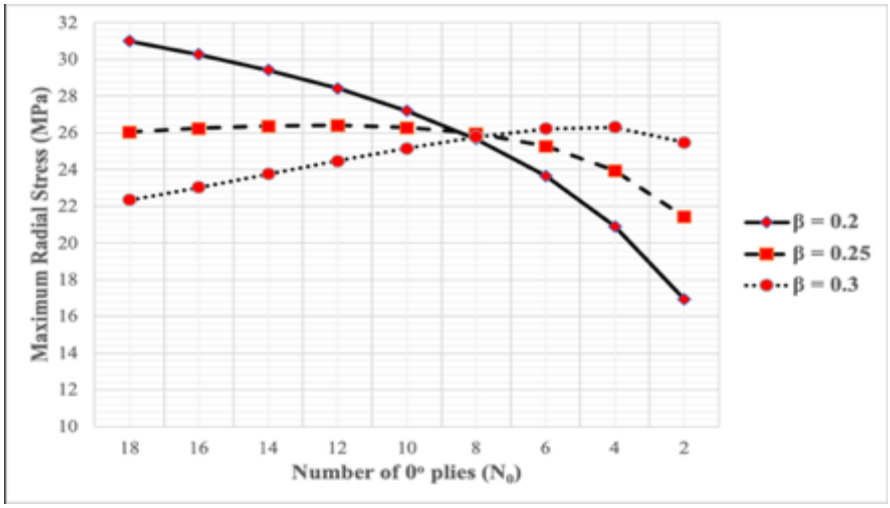

Figure 3.20 Variation of the maximum radial stress with the number of 0° plies in a rotating annular uniform-thickness cross-ply laminated disc with the clamped-free boundary condition for different values of radius ratio

The following observations can be made from the variation of the maximum radial stress with the number of 0° plies in a rotating annular uniform-thickness cross-ply laminated disc with the clamped-free boundary condition for the beta values of 0.2, 0.25 and 0.3, shown above in the Figure 3.20:

- For a cross-ply laminated disc with a beta value of 0.2, the maximum radial stress decreases with the decreasing number of 0° plies (N_0).
- For a cross-ply laminated disc with a beta value of 0.25 and with N_0 = 18 up to N_0 = 10, the maximum radial stress increases with the decrease in N_0 and then, the stress tends to decrease till N_0 = 2. However, the increase of the stress till N_0 = 10 is not that significant.
- For a cross-ply laminated disc with a beta value of 0.3 and with N_0 = 18 up to N_0 = 4, the maximum radial stress increases with the decrease in N_0 and then the stress decreases till N_0 = 2. However, the decrease in the stress from $N_0 = 4$ to N_0 = 2, is not that significant when compared with the cross-ply laminated discs with beta values of 0.25 and 0.2.
- For the cross-ply discs with $N_0 = 8$, the maximum radial stress is almost the same in cross-ply discs with beta values of 0.2, 0.25 and 0.3.

The following Figure 3.21 shows the variation of the maximum circumferential stress in a rotating annular uniform-thickness cross-ply laminated disc with varying number of 0° plies corresponding to various cross-ply configurations considered in the present study for beta values of 0.2, 0.25 and 0.3.

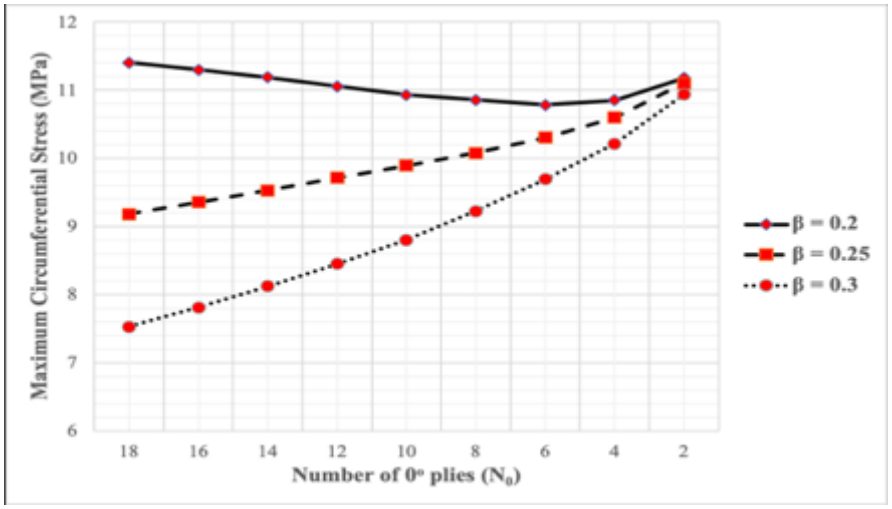

Figure 3.21 Variation of the maximum circumferential stress with the number of 0° plies in a rotating annular uniform-thickness cross-ply laminated disc with the clamped-free boundary condition for different values of radius ratio

The following observations can be made from the variation of the maximum circumferential stress with the number of 0° plies in a rotating annular uniform-thickness cross-ply laminated disc with the clamped-free boundary condition for the beta values of 0.2, 0.25 and 0.3, shown above in the Figure 3.21:

- Irrespective of the number of 0° plies, the maximum amount of circumferential stress decreases with the increasing beta value of the cross-ply laminated disc. However, for the cross-ply disc with $N_0 = 2$, the decrease in the maximum circumferential stress with the increasing beta value of the disc is not that significant.
- For a cross-ply laminated disc with a beta value of 0.2 and with N_0 = 18 up to N_0 = 6, the maximum circumferential stress decreases with the decrease in N_0 and then, the stress increases for the discs with N_0 = 4 up to N_0 = 2.
- For the discs with beta values of 0.25 and 0.3, the maximum circumferential stress increases with the decrease in N_0.

The following Figure 3.22 shows the variation of the maximum radial displacement in a rotating annular uniform-thickness cross-ply laminated disc with varying number of 0° plies corresponding to various cross-ply configurations considered in the present study for beta values of 0.2, 0.25 and 0.3.

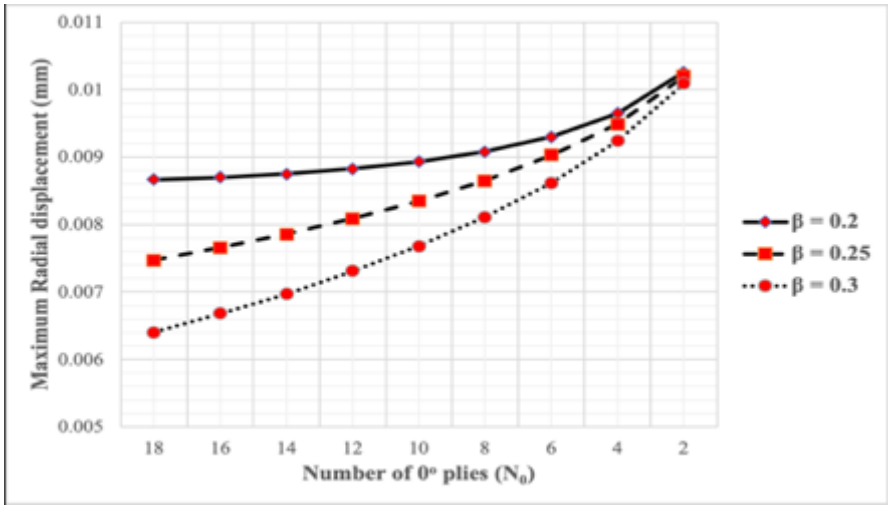

Figure 3.22 Variation of the maximum radial displacement with the number of 0° plies in a rotating annular uniform-thickness cross-ply laminated disc with the clamped-free boundary condition for different values of radius ratio

The following observations can be made from the variation of the maximum radial displacement with the number of 0° plies in a rotating annular uniform-thickness cross-ply laminated disc with the clamped-free boundary condition for the beta values of 0.2, 0.25 and 0.3, shown above in the Figure 3.22:

- Irrespective of the number of 0° plies, the maximum radial displacement decreases with the increasing beta value of the disc. However, for the cross-ply disc with $N_0 = 2$, the decrease in the maximum radial displacement with the increasing beta value of the disc is not that significant.
- Irrespective of the beta value, the maximum radial displacement in a rotating annular uniform-thickness cross-ply laminated disc increases with the decrease in N_0.

3.7.2.3 Influence of modelling element on the stress distributions in cross-ply laminated discs

It is important to study the stress variations through the thickness in a laminated disc made of plies oriented at different angles (such as angle-ply laminates, cross-ply laminates or quasi-isotropic laminates). For illustrative purpose, the following Figure 3.23 shows the radial stress distributions through the thickness at the hub of a rotating annular uniform-thickness cross-ply laminated disc with $[0_7/90_3]_s$ configuration and with the clamped-free boundary condition. The

variation of the radial stress has been obtained using ANSYS® ACP Post for (a) SHELL181 element and (b) SOLID185 element.

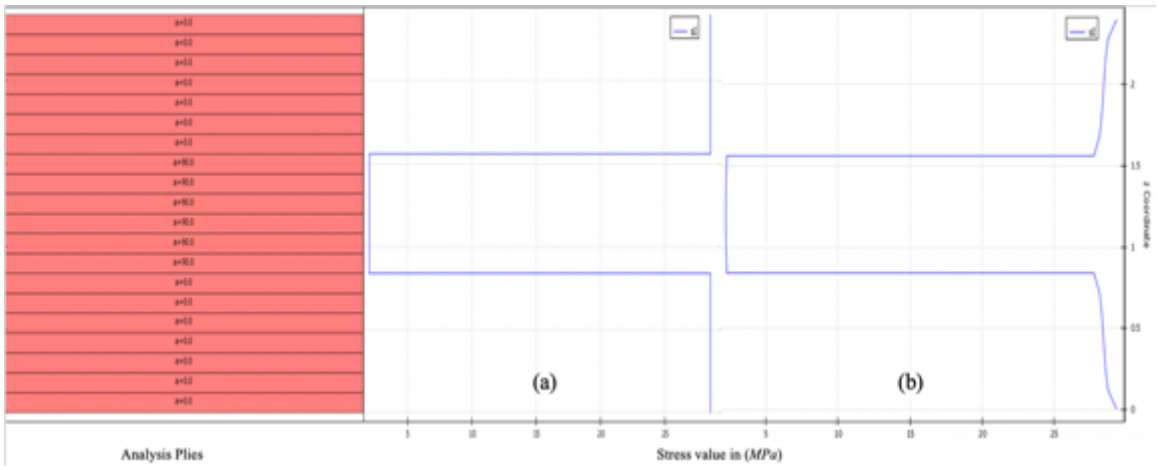

Figure 3.23 Radial stress distribution through the thickness at the hub of a rotating annular uniform-thickness cross-ply disc with $[0_7/90_3]_s$ configuration and with the clamped-free boundary condition obtained using ANSYS® ACP Post for (a) SHELL181 element and (b) SOLID185 element

It can be seen from the above Figure 3.23 that the results obtained for the radial stress distributions through the thickness at the hub of the disc, at which it is clamped, using the SOLID185 and SHELL181 elements in a cross-ply laminated disc are not identical, where in the results obtained using SOLID185 element, there is a slight variation of radial stress along the thickness of the rotating disc in the plies oriented at both 0° and 90°, but in the results for the radial stress variation using the SHELL181 element, the radial stress is constant along the plies oriented at the same angle. i.e., even if the top 7 layers (as measured from the mid plane of the disc) are oriented at 0°, the value of stress is not constant along the thickness of the plies if the analysis is done using the SOLID185 element in ANSYS®.

The following Figure 3.24 shows the circumferential stress distributions through the thickness at the hub of a rotating annular uniform-thickness cross-ply laminated disc with $[0_7/90_3]_s$ configuration and with the clamped-free boundary condition. The variation of the circumferential stress has been obtained using ANSYS® ACP Post for (a) SHELL181 element and (b) SOLID185 element.

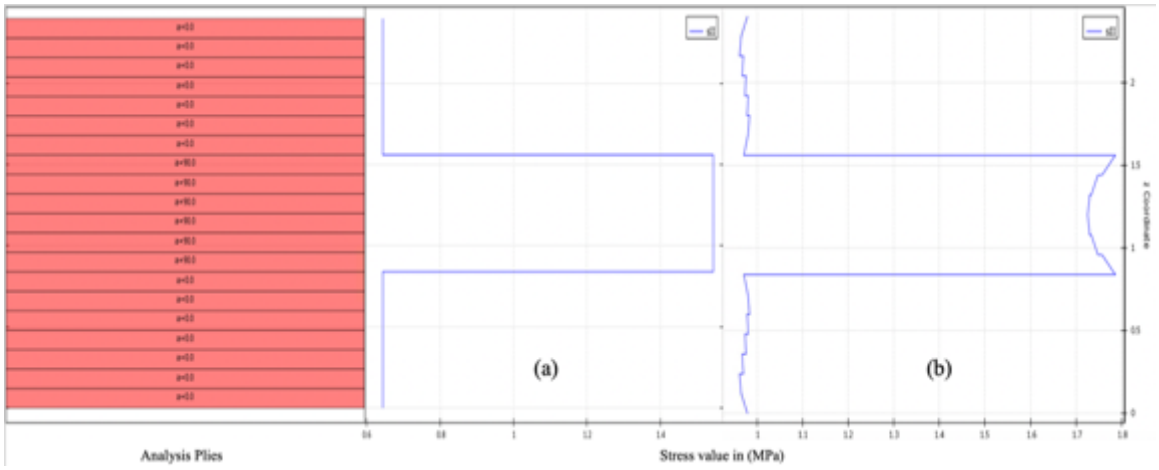

Figure 3.24 Circumferential stress distribution through the thickness at the hub of a rotating annular uniform-thickness cross-ply disc with $[0_7/90_3]_s$ configuration and with the clamped-free boundary condition obtained using ANSYS® ACP Post for (a) SHELL181 element and (b) SOLID185 element

The same observation can be seen in the above Figure 3.24, where the 6 plies (3 top and 3 bottom as measured from the mid plane of the disc) that are oriented at 90°, the circumferential stress in this case also varies along the thickness of the plies if the analysis is performed using SOLID185 element. But for the analysis done using SHELL181 element, the circumferential stress is constant along the thickness of the plies that are oriented at the same angle. This observation regarding the distribution of the radial stress and the circumferential stress through the thickness holds true for every cross-ply configurations of the rotating annular uniform-thickness fiber-reinforced composite discs that are taken into consideration for the present study.

The cause for such kind of variations in the stresses can be explained by the fact that the SOLID185 is a layered element, i.e., for a disc of given thickness and containing '*N*' number of plies, there would be '*N*' number of SOLID185 elements throughout the thickness of the disc, at any given radial distance. Since for the present case, there are 20 plies in the uniform-thickness composite disc, therefore, there are 20 SOLID185 elements throughout the thickness of the disc at any given radial distance, as shown earlier in the Figure 3.2. For the same disc with the same thickness and the same number of plies (i.e., 20) there is only one SHELL181 element throughout the thickness of the disc at any given radial distance, as shown earlier in the Figure 3.3. During the static structural analysis of the rotating disc, the SOLID185 element of *k*-th ply of the laminated disc has contact with the adjacent SOLID185 elements of the (*k*-1)-th and (*k*+1)-th plies, thereby interfering with the deformations of the element through the thickness and as a result causing the

stress to vary even in the plies that are oriented at the same angle. SHELL181 element does not contribute to the interference with the deformations, since a single SHELL element covers up the entire thickness of the laminated disc.

Furthermore, the SHELL181 element has equations built in to calculate the bending behavior since each node has rotational degrees of freedom to represent bending. SOLID185 element does not have rotational degrees of freedom i.e., the element only possesses displacement degrees of freedom, so a single layer of the element cannot represent bending accurately. Many SOLID elements through the thickness are required to accurately capture the bending behavior and match the results obtained from a SHELL element model of the same component.

3.7.3 Symmetrically-balanced laminated discs

This sub-section presents the parametric study on the elastic response of rotating annular uniform-thickness discs made up of Graphite-Fiber Reinforced Plastic material with various symmetrically-balanced configurations and for the clamped-free boundary condition. The effects of different laminate configuration and the radius ratio on the radial stress and circumferential stress distributions and on the radial displacement distribution in rotating annular uniform-thickness fiber-reinforced composite discs are studied. A laminated disc is said to be symmetrically-balanced if it satisfies the following two conditions:

- For every ply oriented at $+\theta$, there should be a ply oriented at $-\theta$ in the laminate.
- The plies located symmetrically about the middle plane, should have the same orientation, same thickness and be made of the same material.

For the present study, the various symmetrically-balanced configurations of the rotating annular uniform-thickness disc considered are: LC(1): $[(0/90)_5]_s$, LC(2): $[(\pm 45)_5]_s$, LC(3): $[0_2/(\pm 45)_4]_s$ and LC(4): $[(0/90/\pm 45)_2/(0/90)]_s$.

For the above-considered configurations of the laminated disc, the components A_{16} and A_{26} are zero. i.e., there is no tension-shear coupling and also the coupling matrix [B] is zero. i.e., there is no stretching-bending coupling in the laminated disc. It means that if the disc is only exposed to forces in its radial direction, then it has zero midplane curvatures and it also prevents the disc from twisting due to thermal loads.

3.7.3.1 Effect of radius ratio on the elastic response of symmetrically-balanced laminated discs

The effect of radius ratio on the radial and circumferential stress distributions and on the radial displacement distribution in a rotating annular uniform-thickness fiber-reinforced composite disc with various symmetrically-balanced configurations and for the clamped-free boundary condition is studied for the beta values of 0.2, 0.25 and 0.3.

The rotating disc has a fixed outer radius of r_o = 120 *mm*, thickness of h = 2.4 *mm* with an individual ply thickness of t = 0.12 *mm,* and is rotating at a constant angular velocity of ω = 1000 *rad/s* i.e., 9554.14 *rpm*. The inner radius of the disc is dependent on the beta value taken into consideration which has been mentioned earlier in the Table 3.16.

The following Figure 3.25 shows the effect of the radius ratio on the maximum radial stress in a rotating annular uniform-thickness disc with various symmetrically-balanced configurations and for the clamped-free boundary condition.

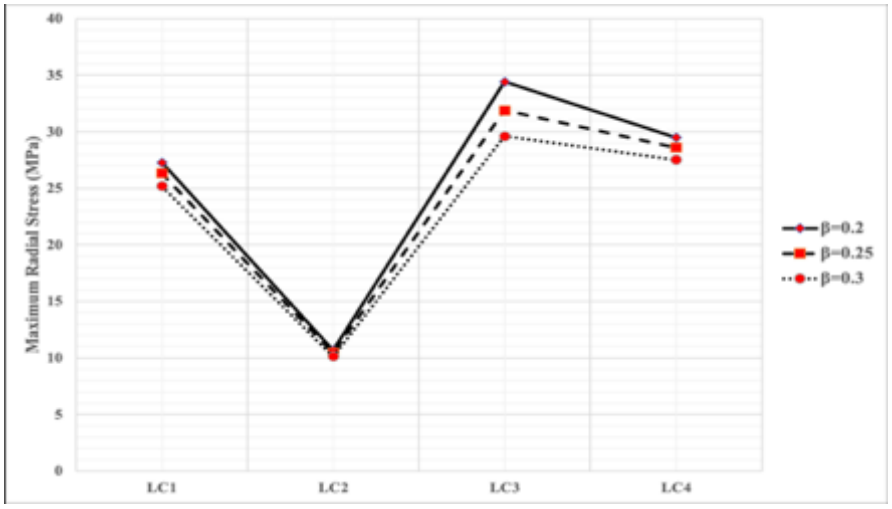

Figure 3.25 Effect of radius ratio on the maximum radial stress in a rotating annular uniform-thickness disc for various symmetrically-balanced configurations and for the clamped-free boundary condition

The following observations can be made from the effect of radius ratio on the maximum radial stress in a rotating annular uniform-thickness fiber-reinforced composite disc with various symmetrically-balanced configurations and with the clamped-free boundary condition for the beta values of 0.2, 0.25 and 0.3, shown above in the Figure 3.25:

- Irrespective of the beta value i.e., the radius ratio of the disc, the rotating disc with LC3 ($[0_2/(\pm 45)_4]_s$) configuration experiences the maximum amount of radial stress while the rotating disc with LC2 ($[(\pm 45)_5]_s$) configuration experiences the minimum amount of radial stress.
- Irrespective of the configuration of the laminated disc, the radial stress decreases with the increasing beta value of the disc. However, for the laminated disc with LC2 configuration, the decrease in the maximum radial stress with the increasing beta value of the disc is not that significant.

The following Figure 3.26 shows the effect of radius ratio on the maximum circumferential stress in a rotating annular uniform-thickness disc with various symmetrically-balanced configurations and for the clamped-free boundary condition.

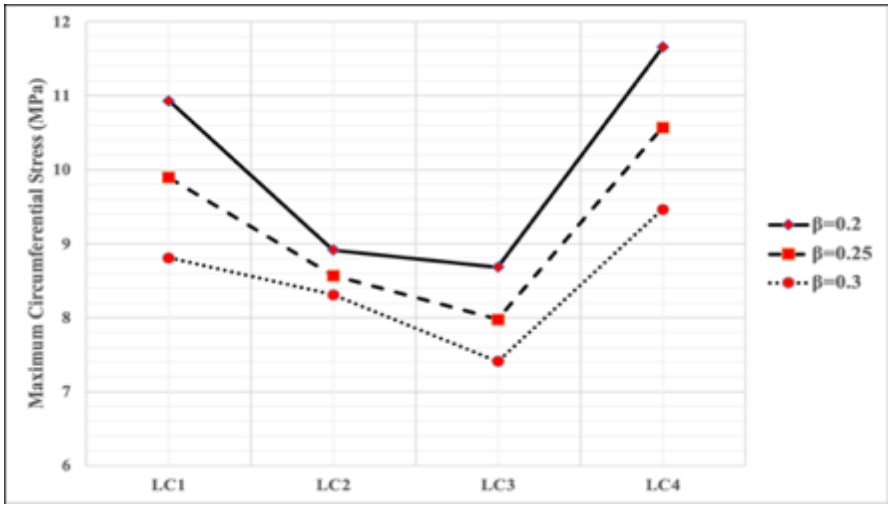

Figure 3.26 Effect of radius ratio on the maximum circumferential stress in a rotating annular uniform-thickness disc for various symmetrically-balanced configurations and for the clamped-free boundary condition

The following observations can be made from the effect of radius ratio on the maximum circumferential stress in a rotating annular uniform-thickness fiber-reinforced composite disc with various symmetrically-balanced configurations and with the clamped-free boundary condition for the beta values of 0.2, 0.25 and 0.3, shown above in the Figure 3.26:

- Irrespective of the beta value of the disc, the rotating disc with LC4 ($[(0/90/\pm 45)_2/(0/90)]_s$) configuration experiences the maximum amount of

circumferential stress while the rotating disc with LC3 ($[0_2/(\pm 45)_4]_s$) configuration experiences the minimum amount of circumferential stress.

- Irrespective of the configuration of the laminated disc, the circumferential stress decreases with the increasing beta value of the disc.

The following Figure 3.27 shows the effect of radius ratio on the maximum radial displacement in a rotating annular uniform-thickness disc with various symmetrically-balanced configurations and for the clamped-free boundary condition.

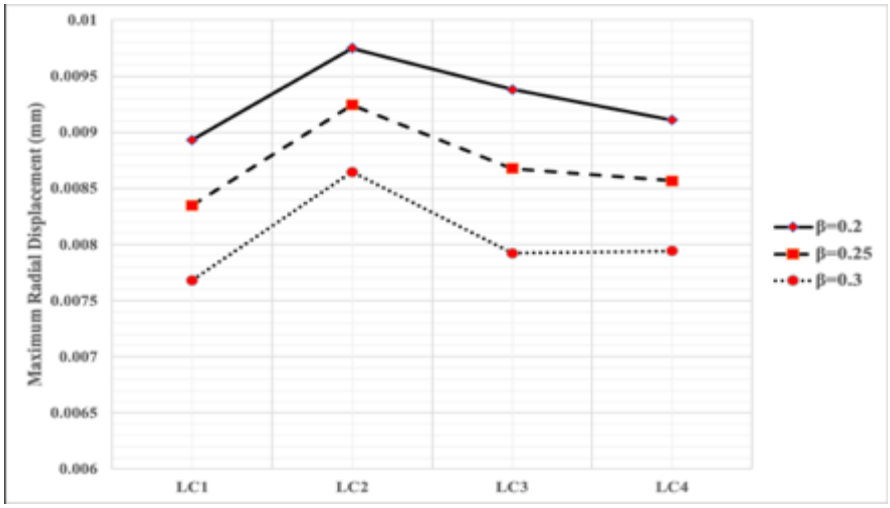

Figure 3.27 Effect of radius ratio on the maximum radial displacement in a rotating annular uniform-thickness disc for various symmetrically-balanced configurations and for the clamped-free boundary condition

The following observations can be made from the effect of radius ratio on the maximum radial displacement in a rotating annular uniform-thickness fiber-reinforced composite disc with various symmetrically-balanced configurations and with the clamped-free boundary condition for the beta values of 0.2, 0.25 and 0.3, shown above in the Figure 3.27:

- Irrespective of the beta value of the disc, the rotating disc with LC2 ($[(\pm 45)_5]_s$) configuration experiences the maximum amount of radial displacement and the rotating disc with LC1 ($[(0/90)_5]_s$) configuration experiences the minimum amount of radial displacement.
- Irrespective of the configuration of the laminated disc, the radial displacement decreases with the increasing beta value of the disc.

3.7.3.2 Effect of laminate configuration on the shear stress distribution

The effect of laminate configuration on the in-plane shear stress distribution in a rotating annular uniform-thickness fiber-reinforced composite disc with various symmetrically-balanced configurations is studied for the beta values of 0.2, 0.25 and 0.3. In all of the symmetrically-balanced configurations considered in the present study, except for LC1, there are some plies in which the fibers are oriented at $\pm 45°$. The presence of such plies in the laminated disc influences the presence of shear stress in the disc.

The following Table 3.37 shows the comparison of the results obtained for the in-plane shear stress distributions in a rotating annular uniform-thickness fiber-reinforced composite disc for various symmetrically-balanced configurations (except for LC1) using the Rayleigh-Ritz method, with the results obtained for the same using ANSYS® (SHELL181 element solution).

Shear stress distributions ($\tau_{r\theta}$, in *MPa*) in a rotating annular uniform-thickness disc with various symmetrically-balanced configurations and with the clamped-free boundary condition						
Radial distance in *mm* from the center of the disc	Laminate configuration					
	LC2		LC3		LC4	
	Rayleigh-Ritz Solution	ANSYS® Solution (SHELL181)	Rayleigh-Ritz Solution	ANSYS® Solution (SHELL181)	Rayleigh-Ritz Solution	ANSYS® Solution (SHELL181)
24.0	8.360	8.088	8.209	7.992	7.032	6.857
33.6	8.004	7.850	7.795	7.639	6.781	6.634
43.2	7.561	7.434	7.236	7.118	6.473	6.371
52.8	7.021	6.914	6.625	6.531	6.099	5.964
62.4	6.375	6.290	5.971	5.9	5.654	5.654
72.0	5.631	5.562	5.280	5.225	5.141	5.04
81.6	4.781	4.731	4.544	4.504	4.556	4.493
91.2	3.824	3.795	3.756	3.735	3.896	3.725
100.8	2.763	2.756	2.919	2.913	3.165	3.011
110.4	1.597	1.613	2.026	2.035	2.363	2.376
120.0	0.327	0.477	1.077	0.619	1.488	1.29

Table 3.37 Comparison of the results obtained for the in-plane shear stress distribution in a rotating annular uniform-thickness disc for various symmetrically-balanced configurations and for the clamped-free boundary condition

It can be seen from the above Table 3.37 that the shear stress in a rotating annular uniform-thickness disc with the clamped-free boundary condition for various symmetrically-balanced configurations that are considered in the present study (except for LC1), is always maximum at the hub of the disc at which it is clamped and tends to a minimum value at its outer periphery.

The following Figure 3.28 shows the effect of various symmetrically-balanced laminate configurations on the maximum in-plane shear stress in a rotating annular uniform-thickness fiber-reinforced composite disc with the clamped-free boundary condition for the beta values of 0.2, 0.25 and 0.3.

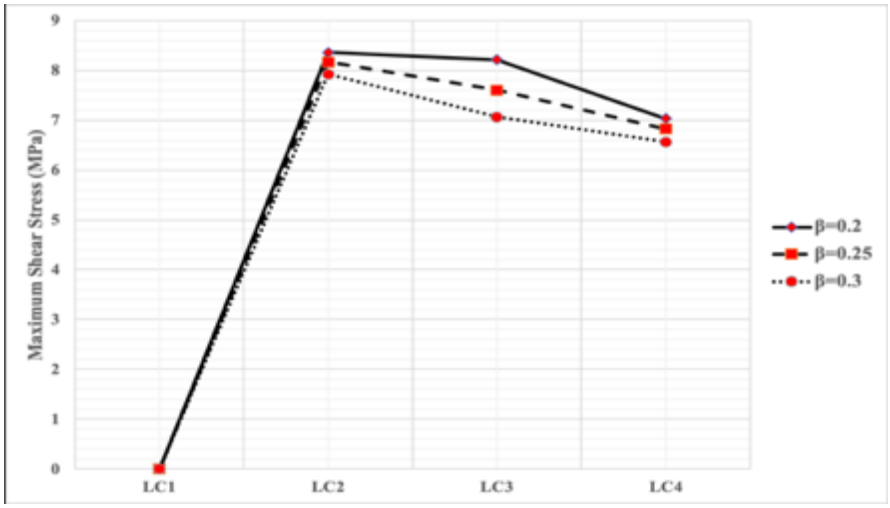

Figure 3.28 Effect of laminate configurations on the maximum in-plane shear stress in a rotating annular uniform-thickness fiber-reinforced composite disc for different values of the radius ratio and for the clamped-free boundary condition

The following observations can be made from the effect of laminate configuration on the maximum in-plane shear stress in a rotating annular uniform-thickness fiber-reinforced composite disc with various symmetrically-balanced configurations and with the clamped-free boundary condition for the beta values of 0.2, 0.25 and 0.3, shown above in the Figure 3.28:

- Irrespective of the beta value of the disc, the rotating disc with LC2 ($[(\pm 45)_5]_s$) configuration is exposed to the maximum amount of shear stress and there is no shear stress induced in the rotating disc with LC1 ($[(0/90)_5]_s$) configuration. This variation can be explained by the presence of plies in which the fibers are oriented at $+45°$ or $-45°$. The disc with LC2 configuration has the maximum number of

these plies i.e., 20, and therefore in comparison to the other configurations, there is maximum shear stress induced in it.

- Irrespective of the configuration of the laminated disc, the shear stress decreases with the increasing beta value of the disc. Also, the decrease in the maximum shear stress with the increasing beta value of the disc is significant for the disc with LC3 configuration.

3.8 Conclusion

In this chapter, the elastic response of rotating annular uniform-thickness discs made up of a fiber-reinforced composite material and with the clamped-free boundary condition is presented. The expressions for the radial and circumferential strains and the corresponding stresses are obtained using the Classical Laminate Theory in cylindrical coordinate system in section 3.2. In section 3.3, the total potential energy of the rotating annular uniform-thickness fiber-reinforced composite disc is derived in terms of the laminate stiffness matrix of the composite material. In section 3.4, the Rayleigh-Ritz method is used to determine the elastic response of the rotating annular composite disc. In section 3.6, the results obtained for the elastic response of the rotating annular composite disc using the Rayleigh-Ritz method are validated with the results obtained for the same using the finite element analysis software ANSYS® (using SOLID185 and SHELL181 elements). A thorough parametric study is conducted in section 3.7 to demonstrate the effects of laminate configurations, fiber orientation and the radius ratio on the radial stress and the circumferential stress distributions and on the radial displacement distributions in a rotating annular uniform-thickness disc made up of Graphite-Fiber Reinforced Plastic material and with the clamped-free boundary condition. A summary of observations is as follows:

- The results obtained for the elastic response of the rotating annular composite disc using the Rayleigh-Ritz method are in good agreement with the results obtained for the same using the finite element analysis software ANSYS® (using SOLID185 and SHELL181 elements). Furthermore, the average percentage difference between the results obtained using the Rayleigh-Ritz method and ANSYS® SHELL181 solution is quite low as compared with the average percentage difference between the results

obtained for the same using the Rayleigh-Ritz method and ANSYS® SOLID185 solution.

- For the laminated disc with uni-directional configurations, the $[0]_{20}$ laminated disc experiences the maximum radial stress while the $[90]_{20}$ laminated disc experiences maximum circumferential stress. The radial displacement is maximum in the $[45]_{20}$ laminated disc and the least for the $[0]_{20}$ laminated disc, since in the latter, the fibers are aligned along the radial direction of the disc causing more resistance to the deformation of the disc.
- For the laminated disc with uni-directional configurations, the loci of the points experiencing the maximum radial stress and the maximum circumferential stress change with the fiber orientation angle. The locus of the point experiencing the maximum radial stress shifts to the arithmetic mean radius of the disc, and the locus of the point experiencing the maximum circumferential stress shifts towards the outer periphery of the disc.
- For cross-ply discs with N_0 = 18 up to N_0 = 8, the radial stress decreases with the increasing beta value of the disc whereas for the discs with N_0 = 6 up to N_0 = 2, the radial stress increases with the increasing beta value of the disc. However, regardless of the number of 0° plies, the circumferential stress and the radial displacement always decreases with the increasing beta value of the cross-ply laminated disc.
- For a cross-ply laminated disc with a beta value of 0.2, the maximum radial stress decreases with the decreasing number of 0° plies. Whereas, for the cross-ply laminated disc with a beta value of 0.25 and with N_0 = 18 up to N_0 = 10, the maximum radial stress increases with the decrease in N_0 and then, the stress tends to decrease and is the lowest for the disc with N_0 = 2. For the cross-ply laminated disc with a beta value of 0.3 and with N_0 = 18 up to N_0 = 4, the maximum radial stress increases with the decrease in N_0 and then the stress decreases for the disc with N_0 = 2.
- For the cross-ply laminated disc with a beta value of 0.2 and with N_0 = 18 up to N_0 = 6, the maximum circumferential stress decreases with the decrease in N_0 and then, the stress increases for the discs with N_0 = 4 to N_0 = 2. For the discs with beta

values of 0.25 and 0.3, the maximum circumferential stress always increases with the decrease in N_0.

- Irrespective of the beta value of the disc, the radial displacement in a rotating annular uniform-thickness cross-ply laminated disc increases with the decreasing number of 0° plies.
- Irrespective of the beta value of the disc, on comparing the responses of the symmetrically-balanced configurations of the laminated disc considered in the present study, the rotating disc with LC3 ($[0_2/(\pm 45)_4]_s$) configuration is exposed to maximum radial stress while the rotating disc with LC4 ($[(0/90/\pm 45)_2/(0/90)]_s$) configuration is exposed to maximum circumferential stress. Also, the radial displacement and the in-plane shear stress are maximum for the disc with LC2 ($[(\pm 45)_5]_s$) configuration.

Chapter 4

Elastic response of rotating annular thickness-tapered discs made of fiber-reinforced composite materials

4.1 Introduction

Laminated disc made up of fiber-reinforced composite material can retain sufficient stiffness and strength while minimizing the structural weight, making the fiber-reinforced composite discs suitable to be used in turbomachinery and aerospace structures. Sometimes, in the application of the fiber-reinforced composite discs, stiffness tailoring is required, i.e., the disc needs to be much stiffer at one location and less stiff at the other location. This stiffness tailoring can be achieved by terminating some of the plies within the laminated structure.

This chapter presents the formulation to determine the elastic response of rotating annular thickness-tapered discs made up of fiber-reinforced composite materials by using the Rayleigh-Ritz method based on the Classical Laminate Theory (CLT) in the cylindrical coordinate system. The radial displacements and the in-plane stresses in a rotating annular thickness-tapered fiber-reinforced composite disc with the clamped-free boundary condition are computed. Approximate functions for the radial, circumferential and transverse displacement functions in cylindrical coordinates are assumed. An approximate solution is developed for the radial, circumferential and transverse displacements and the stress distributions in the laminated disc that is clamped at the hub, and it is compared with the solution obtained for the same using the finite element analysis software ANSYS®. The finite element analysis is performed using the SHELL181 element. A comprehensive parametric study is conducted to investigate the effects of fiber orientation, radius ratio, dropped plies, taper configuration and laminate configuration on the stress distributions and the radial displacement distributions in rotating annular thickness-tapered composite discs with the clamped-free boundary condition.

4.2 Types of thickness-tapered laminated discs

In general, there are three kinds of thickness-tapered laminated discs, namely the externally-tapered, mid-plane tapered and internally-tapered discs.

An externally-tapered laminated disc can be modeled as a combination of N number of annular uniform-thickness circular plies, with each ply having the same inner radius and the same thickness but different outer radius. Therefore, each circular ply in the externally-tapered laminated disc can be considered as a separate uniform-thickness fiber-reinforced composite disc. In a mid-plane tapered disc, the centerline of an individual ply in the laminated disc is not parallel to the mid-plane, rather it is inclined at an arbitrary angle with respect to the mid-plane of the disc.

The internally-tapered discs can be designed and developed in the following three major configurations, shown below in the Figure 4.1.

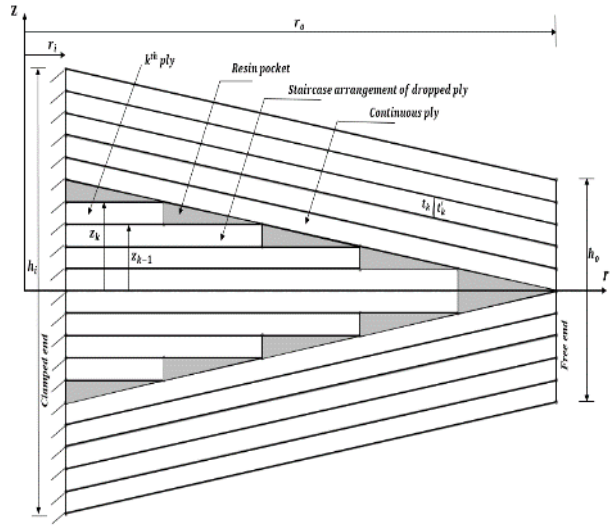

Configuration B: Staircase arrangement

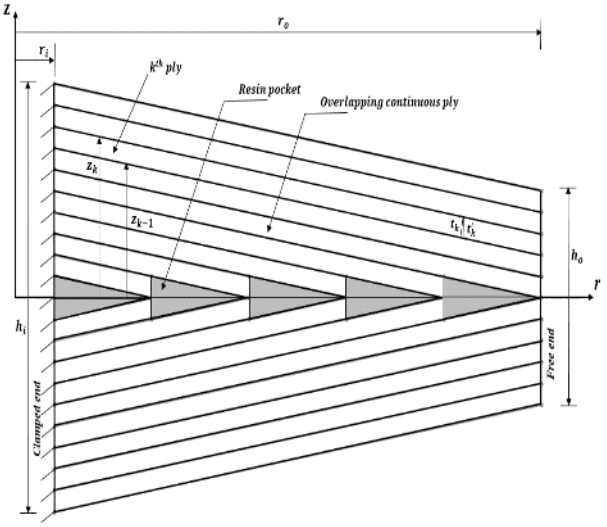

Configuration C: Overlapping continuous plies

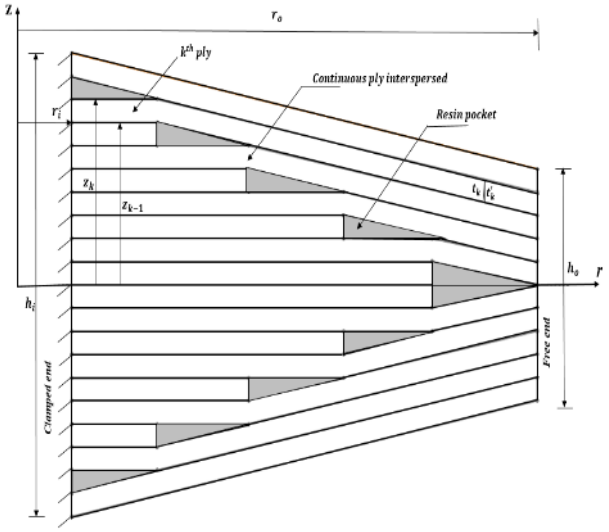

Configuration D: Continuous plies interspersed

Figure 4.1 Right half cross-sectional view of the diametral cut of different configurations of the internally-tapered laminated disc with 10 ply drop-off

In the above Figure 4.1, r_i and r_o are the inner and the outer radii of the thickness-tapered laminated disc, h_i and h_o are the thicknesses of the disc at the hub (at which it is clamped) and at the free end respectively. t_k is the thickness of the *k*-th ply in the thickness-tapered laminated disc. Also, z_k and z_{k-1} are the distances from the mid-plane to the top and bottom surfaces of the *k*-th ply in the thickness-tapered laminated disc, and they can be expressed as:

$$z_k = -\{(r - r_i)tan\varphi\} - \frac{h_i}{2} + (t_k * k) \tag{4.1}$$

$$z_{k-1} = -\{(r - r_i)tan\varphi\} - \frac{h_i}{2} + \{t_k(k-1)\} \tag{4.2}$$

where, $k = [1, N]$, N being the total number of plies in the disc. The above expressions of z_k and z_{k-1} are valid for the three different taper configurations of the laminated disc, shown above in the Figure 4.1. Also, in the above equations, φ is the taper angle of the disc, the value of which depends on the number of dropped plies (δ), and it can be expressed as:

$$\varphi = tan^{-1}\left[\frac{\delta * t_k}{2(r_o - r_i)}\right] \tag{4.3}$$

4.3 Formulation for the total potential energy

As discussed previously in the section 2.2, the total potential energy of a rotating annular disc is the sum of the strain energy and the potential energy originated from the centrifugal loading of the disc.

Recalling the strain energy of an annular uniform-thickness laminated disc obtained previously in the Equation (3.26), it can be re-written as:

$$\mathrm{U} = \frac{1}{2}\sum_{k=1}^{N}\int_{r_i}^{r_o}\int_{0}^{2\pi}\int_{z_{k-1}}^{z_k}\left\{\begin{bmatrix}\overline{Q_{11}} & \overline{Q_{12}} & \overline{Q_{16}}\\ \overline{Q_{12}} & \overline{Q_{22}} & \overline{Q_{26}}\\ \overline{Q_{16}} & \overline{Q_{26}} & \overline{Q_{66}}\end{bmatrix}_k \left\{\begin{matrix}\frac{du_r^o(r)}{dr} - z\frac{d^2w(r)}{dr^2}\\ \frac{u_r^o(r)}{r} - z\frac{dw(r)}{rdr}\\ \frac{du_\theta^o(r)}{dr} - \frac{u_\theta^o(r)}{r}\end{matrix}\right\}_k^T \left\{\begin{matrix}\frac{du_r^o(r)}{dr} - z\frac{d^2w(r)}{dr^2}\\ \frac{u_r^o(r)}{r} - z\frac{dw(r)}{rdr}\\ \frac{du_\theta^o(r)}{dr} - \frac{u_\theta^o(r)}{r}\end{matrix}\right\}_k dz.rd\theta.dr \tag{4.4}$$

The above Equation (4.4) represents the strain energy of an annular uniform-thickness laminated disc made up of fiber-reinforced composite material. For the uniform-thickness disc, $z_k - z_{k-1}$ is the thickness of the *k*-th ply in the laminated disc, also denoted by t_k (which is 0.12 *mm* for the present case). u_r^o, u_θ^o and w are the radial, circumferential and transverse displacements at the mid-plane of the laminated disc.

It is to be noted that in the above Equation (4.4), the $\overline{[Q]}_k$ matrix, which is the transformed reduced stiffness matrix of the *k*-th ply in the uniform-thickness laminated disc, is a function of the fiber orientation angle (θ) and the mechanical properties of the fiber-reinforced composite material. For a ply in the thickness-tapered laminated disc, the transformed reduced stiffness matrix is also a function of the taper angle (φ) in addition to the above-mentioned variables and it can be given as [59]:

$$\overline{[Q]}_k = \left[T_{\sigma\varphi}\right]_k [T_{\sigma\theta}]_k [Q] [T_{\sigma\theta}]_k^T \left[T_{\sigma\varphi}\right]_k^T \tag{4.5}$$

The above Equation (4.5) represents the transformed reduced stiffness matrix of the *k*-th ply in the thickness-tapered laminated disc. $[Q]$ is the reduced stiffness matrix of the fiber-reinforced composite material, $[T_{\sigma\theta}]_k$ is the stress transformation matrix of the *k*-th ply which is a function of the fiber orientation angle θ and $\left[T_{\sigma\varphi}\right]_k$ is the stress transformation matrix of the *k*-th ply which is a function of the taper angle φ. For the case of plane stress, these matrices can be expressed as [59]:

$$[Q] = \begin{bmatrix} Q_{11} & Q_{12} & 0 \\ Q_{12} & Q_{22} & 0 \\ 0 & 0 & Q_{66} \end{bmatrix} \tag{4.6}$$

$$[T_{\sigma\theta}]_k = \begin{bmatrix} cos^2\theta & sin^2\theta & -2cos\theta sin\theta \\ sin^2\theta & cos^2\theta & 2cos\theta sin\theta \\ cos\theta sin\theta & -cos\theta sin\theta & cos^2\theta - sin^2\theta \end{bmatrix}_k \tag{4.7}$$

$$\left[T_{\sigma\varphi}\right]_k = \begin{bmatrix} cos^2\varphi & sin^2\varphi & cos\varphi sin\varphi \\ sin^2\varphi & cos^2\varphi & -cos\varphi sin\varphi \\ -2cos\varphi sin\varphi & 2cos\varphi sin\varphi & cos^2\varphi - sin^2\varphi \end{bmatrix}_k \tag{4.8}$$

It can be seen from the Figure 4.1 that except for the taper configuration C, there are some plies in the taper configurations B and D which are parallel to the mid-plane of the disc. For such plies, $\varphi = 0°$ and as a result, the stress transformation matrix which is a function of the taper angle, $\left[T_{\sigma\varphi}\right]_k$, reduces to an Identity matrix of the order 3x3. Therefore, $\overline{[Q]}_k$ matrix for such plies in the thickness-tapered laminated disc can be given as the same in the Equation (3.16).

In addition to the Graphite Fiber Reinforced Plastic (NCT-301) prepreg plies, there also exist resin pockets in different configurations of the thickness-tapered laminated disc. These resin pockets are developed during the manufacturing of the thickness-tapered laminated disc and are considered to be sandwiched between dropped and continuous plies in the thickness-tapered disc [60]. The material of these resin pockets is generally isotropic. The following Table 4.1 shows the material properties of the resin.

$E = 3.93\ GPa$	$\nu = 0.37$
$\rho_{resin} = 1000\ {}^{Kg}/_{m^3}$	

Table 4.1 Material properties of resin [58]

For a thickness-tapered laminated disc, the total strain energy is the combination of the strain energy of the fiber-reinforced plies (which is NCT-301 in the present case) and the strain energy of the resin pockets.

It is clear that in the case of a uniform-thickness disc, z_k and z_{k-1} are not a function of the radial coordinate *r*, i.e. the distance to the top and the bottom faces of the *k*-th ply from the mid-plane of the disc remain constant along the radius of the disc. Apparently, in the case of a thickness-tapered disc, the distance to the top and the bottom faces of the *k*-th ply from the mid-plane of the disc is not constant, but a function of the radial coordinate. Therefore, upon expanding and then rearranging the above Equation (4.4), the strain energy of the fiber-reinforced plies can be given as:

$$\mathrm{U}_{plies} = \frac{1}{2}\int_0^{2\pi}\int_{r_i}^{r_o} \begin{Bmatrix} \frac{du_r^o(r)}{dr} \\ \frac{u_r^o(r)}{r} \\ \frac{du_\theta^o(r)}{dr} - \frac{u_\theta^o(r)}{r} \\ -\frac{d^2w(r)}{dr^2} \\ -\frac{dw(r)}{rdr} \\ 0 \end{Bmatrix}^T \begin{bmatrix} A_{11}(r) & A_{12}(r) & A_{16}(r) & B_{11}(r) & B_{12}(r) & B_{16}(r) \\ A_{12}(r) & A_{22}(r) & A_{26}(r) & B_{12}(r) & B_{22}(r) & B_{26}(r) \\ A_{16}(r) & A_{26}(r) & A_{66}(r) & B_{16}(r) & B_{26}(r) & B_{66}(r) \\ B_{11}(r) & B_{12}(r) & B_{16}(r) & D_{11}(r) & D_{12}(r) & D_{16}(r) \\ B_{12}(r) & B_{22}(r) & B_{26}(r) & D_{12}(r) & D_{22}(r) & D_{26}(r) \\ B_{16}(r) & B_{26}(r) & B_{66}(r) & D_{16}(r) & D_{26}(r) & D_{66}(r) \end{bmatrix} \begin{Bmatrix} \frac{du_r^o(r)}{dr} \\ \frac{u_r^o(r)}{r} \\ \frac{du_\theta^o(r)}{dr} - \frac{u_\theta^o(r)}{r} \\ -\frac{d^2w(r)}{dr^2} \\ -\frac{dw(r)}{rdr} \\ 0 \end{Bmatrix} rdrd\theta \qquad (4.9)$$

In the above Equation (4.9), U_{plies} represents the strain energy of the fiber-reinforced plies. $A_{ij}(r)$, $B_{ij}(r)$ and $D_{ij}(r)$, *I, j* = 1,2 and 6, are the elements of the laminate stiffness matrix of the thickness-tapered laminated disc and can be calculated from the expressions given in the Equations (3.28) – (3.30).

Since z_k and z_{k-1} for a ply in a thickness-tapered laminated disc are a function of the radial coordinate *r*, therefore, it is required to make use of the expressions of z_k and z_{k-1}, given in the Equations (4.1) and (4.2) into the Equations (3.28) – (3.30) to calculate the elements of the laminate stiffness matrix of the thickness-tapered laminated disc. Subsequently, the elements $A_{ij}(r)$, $B_{ij}(r)$ and $D_{ij}(r)$ in the Equation (4.9) do not have a constant value, rather they are also a function of the radial coordinate *r*.

For the resin pockets in the taper configurations, the $[Q]$ matrix in the Equation (4.5) is replaced with $[Q_{resin}]$, which is the stiffness matrix of the resin material, and it can be given as:

$$[Q_{resin}] = \begin{bmatrix} \frac{E}{1-\nu^2} & \frac{\nu E}{1-\nu^2} & 0 \\ \frac{\nu E}{1-\nu^2} & \frac{E}{1-\nu^2} & 0 \\ 0 & 0 & \frac{E}{2(1+\nu)} \end{bmatrix} \qquad (4.10)$$

where, E and ν are the Young's modulus and the Poisson's ratio of the resin material. Also, for the resin pockets, the fiber orientation angle is set to zero and as a result, the stress transformation matrix which is a function of the fiber orientation angle, $[T_{\sigma\theta}]_k$, reduces to an Identity matrix of the order 3x3. Subsequently, the transformed reduced stiffness matrix of the resin pockets can be given as:

$$\overline{[Q]}_{resin} = [T_{\sigma\varphi}][Q_{resin}][T_{\sigma\varphi}]^T \tag{4.11}$$

Therefore, the strain energy of the resin pockets can be given as:

$$\mathrm{U}_{resin\ pkt} = \frac{1}{2}\sum_{k=1}^{Nr}\int_{r_i+(k-1)L_b}^{r_i+(k)L_b}\int_{0}^{2\pi}\int_{z_{k-1}}^{z_k}\left\{\overline{[Q]}_{resin}\left\{\begin{matrix}\frac{du_r^o(r)}{dr}-z\frac{d^2w(r)}{dr^2}\\ \frac{u_r^o(r)}{r}-z\frac{dw(r)}{rdr}\\ \frac{du_\theta^o(r)}{dr}-\frac{u_\theta^o(r)}{r}\end{matrix}\right\}_k^T\left\{\begin{matrix}\frac{du_r^o(r)}{dr}-z\frac{d^2w(r)}{dr^2}\\ \frac{u_r^o(r)}{r}-z\frac{dw(r)}{rdr}\\ \frac{du_\theta^o(r)}{dr}-\frac{u_\theta^o(r)}{r}\end{matrix}\right\}_k\right. dz.rd\theta.dr \tag{4.12}$$

The above Equation (4.12) represents the strain energy of the resin pockets in the thickness-tapered laminated disc. *Nr* is the total number of resin pockets, L_b is the length of an individual resin pocket along the radius of the disc and z_k and z_{k-1} are the distances to the top and the bottom faces of the resin pocket from the mid-plane of the disc. It is to be noted that the distance to the top and bottom faces of the resin pocket in the thickness-tapered laminated disc is not constant along the radius of the disc, rather a function of the radial coordinate *r*. Therefore, the total strain energy of the thickness-tapered laminated disc, denoted by $U_{tapered}$, can be given as:

$$U_{tapered} = U_{plies} + U_{resin\ pkt} \tag{4.13}$$

Similar to the formulation of the strain energy, the total potential energy originated from the centrifugal loading of the thickness-tapered laminated disc is a combination of the work potential of the fiber-reinforced plies and the work potential of the resin pockets.

Recalling the potential energy originated from the centrifugal loading of the disc from the Equation (3.31), it can be re-written as:

$$V_{plies} = -\sum_{k=1}^{N}\int_{z_{k-1}}^{z_k}\int_{0}^{2\pi}\int_{r_i}^{r_o}\rho\omega^2 r u_r(r)dr.rd\theta.dz \tag{4.14}$$

The above Equation (4.14) represents the potential energy originated from the centrifugal loading of the fiber-reinforced plies. z_k and z_{k-1} are the distances from the mid-plane to the top and the bottom faces of the *k*-th ply in the thickness-tapered laminated disc respectively and are

given by the Equations (4.1) and (4.2). ρ is the density of the fiber-reinforced plies, u_r is the radial displacement of a point in the laminated disc and ω is the angular velocity of rotation.

For the resin pockets in the taper configurations, the density of the fiber-reinforced plies is replaced with the density of the resin, ρ_{resin}. Therefore, the potential energy originated from the centrifugal loading of the resin pockets is given as:

$$V_{resin\,pkt} = -\sum_{k=1}^{Nr} \int_{z_{k-1}}^{z_k} \int_{0}^{2\pi} \int_{r_i+(k-1).L_b}^{r_i+(k).L_b} \rho_{resin}\omega^2 r u_r(r) dr.rd\theta.dz \tag{4.15}$$

Therefore, the total potential energy of the thickness-tapered laminated disc originated from the centrifugal loading, denoted by $V_{tapered}$, can be given as:

$$V_{tapered} = V_{plies} + V_{resin\,pkt} \tag{4.16}$$

The potential energy of the rotating annular thickness-tapered fiber-reinforced composite disc, denoted by Π_T, is then given as the sum of the strain energy and the potential energy originated from the centrifugal loading of the thickness-tapered disc, which were derived in Equations (4.13) and (4.16) respectively, i.e.

$$\Pi_T = U_{tapered} + V_{tapered} \tag{4.17}$$

4.4 Solution by Rayleigh-Ritz Method

The total potential energy of the rotating annular thickness-tapered fiber-reinforced composite disc, obtained above in the section 4.3, is minimized with respect to each set of assumed coefficients in the radial, circumferential and transverse displacement functions, which were given by the Equations (3.32) – (3.34), to obtain the closest approximation of the elastic response of the rotating annular thickness-tapered disc made up of fiber-reinforced composite material and with the clamped-free boundary condition. i.e.

$$\frac{\partial \Pi_T}{\partial a_j} = 0 \tag{4.18}$$

$$\frac{\partial \Pi_T}{\partial b_j} = 0 \tag{4.19}$$

$$\frac{\partial \Pi_T}{\partial c_j} = 0 \tag{4.20}$$

The above Equations (4.18) – (4.20) represent a set of algebraic equations that are solved to yield the coefficients a_j, b_j and c_j. A MATLAB® code is developed to determine the values of these coefficients, which are then used to obtain the required deformations and the stress distributions in the rotating annular thickness-tapered fiber-reinforced composite disc with the clamped-free boundary condition.

4.5 Finite element modeling of the thickness-tapered discs

The finite element modeling of the rotating annular thickness-tapered fiber-reinforced composite disc with the clamped-free boundary condition for the three different taper configurations, shown in the Figure 4.1, has been carried out in ANSYS® R19.2. The following Figure 4.2 shows the cross-sectional view of the diametral cut of the three different taper configurations of the thickness-tapered laminated disc with 10 drop-off plies.

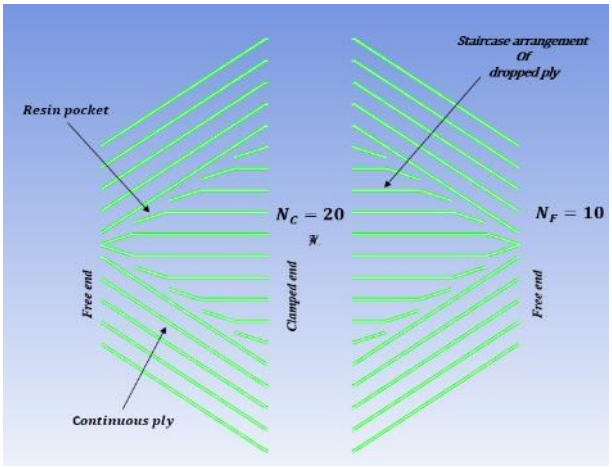

Configuration B: Staircase arrangement

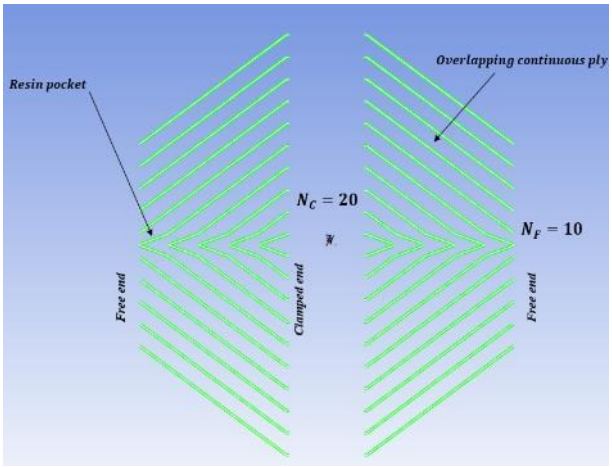

Configuration C: Overlapping continuous plies

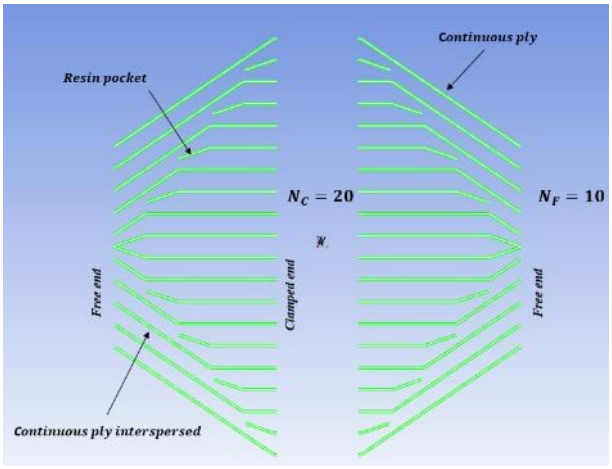

Configuration D: Continuous plies interspersed

Figure 4.2 Cross-sectional view of the diametral cut of a thickness-tapered laminated disc with different taper configurations and with the clamped-free boundary condition in ANSYS® R19.2

The above Figure 4.2 shows the modeling of the three different internal taper configurations of a thickness-tapered fiber-reinforced composite disc in ANSYS® Composite Prepost (ACP Pre). The disc has been clamped at the inner edge and is free to deform at its outer boundary. N_C and N_F represent the number of plies at the clamped end and the free end of the disc respectively.

Since in the present thesis, the rotating annular uniform-thickness laminated disc is considered to be made up of 20 plies, where each ply is made up of a Graphite Fiber-Reinforced Plastic (NCT-301) material, the material properties of which have been mentioned earlier in the Table 3.2, therefore, for the analysis of rotating annular thickness-tapered laminated disc, the disc is considered to be made up of 20 plies at its inner radius (at which the disc is clamped). The number of plies at the free end of the disc is dependent on the number of plies terminated from the structure.

Also, the individual plies in the laminated disc have a thickness of 0.12 *mm*, therefore, the thickness at the hub of the disc is equal to 2.4 *mm* (0.12 *mm* x 20). Consider the Figure 4.2, where, for every taper configuration of the disc, there are only 10 plies at the free end of the disc i.e., irrespective of the taper configuration, the thickness at the free end of the disc is equal to 1.2 *mm* (0.12 *mm* x 10).

The following Table 4.2 shows the thickness at the free end of the disc and the taper angle corresponding to the number of dropped plies in the laminated disc.

Number of plies at the clamped end of the disc	Number of dropped plies (δ)	Thickness at the free end of the disc (in *mm*)	Taper angle, φ (in *degrees*)
20	0	2.40	0.0
	4	1.92	0.143
	8	1.44	0.286
	10	1.20	0.358
	12	0.96	0.430
	16	0.48	0.573

Table 4.2 Taper angle and thickness at the free end of the tapered disc corresponding to the number of dropped plies

Note that in the above Table 4.2, $\delta = 0$ corresponds to the uniform-thickness laminated disc.

4.6 Verification

In this section, the elastic response of a rotating annular thickness-tapered laminated disc made up of Graphite-Fiber Reinforced Plastic material (NCT-301 prepreg) and with the clamped-free boundary condition, that is obtained using the Rayleigh-Ritz method based on the potential energy is compared with the elastic response obtained for the same using the finite element analysis software ANSYS®. It should be noted that to calculate the results for the elastic response of rotating annular thickness-tapered fiber-reinforced composite disc using the Rayleigh-Ritz method, a total of 8 terms are assumed in each of the radial, circumferential and transverse displacement functions, given by the Equations (3.32) – (3.34).

It has been confirmed in section 3.6 that the SHELL181 element is best suited for the elastic analysis of thin to moderately-thick rotating annular discs. Therefore, the verification of the results obtained for the elastic response of a rotating annular thickness-tapered laminated disc has been done using 15,008 SHELL181 elements. The verification of the results for the elastic response has been done for a thickness-tapered laminated disc, the laminate configuration and geometric properties of which are mentioned in the following Table 4.3.

Laminate configuration of the disc at the hub	Number of dropped plies (δ)	Laminate configuration of the disc at its free end	Taper angle of the disc, φ (in *degrees*)
$[0]_{20}$	10	$[0]_{10}$	0.358
Inner radius of the disc, r_i (in mm)	Outer radius of the disc, r_o (in mm)	Angular velocity of rotation, ω (in *rad/s*)	
24	120	1000	
Thickness of the disc at the hub, h_i (in mm)	Thickness of the disc at the free end h_o (in mm)	Taper configurations considered	
2.4	1.2	B and D	

Table 4.3 Laminate configuration and geometric properties of the disc considered for the verification of the results for the elastic response of thickness-tapered laminated disc

The following Tables 4.4 – 4.6 show the comparison of the radial and circumferential stress distributions and the radial displacement distribution in a rotating annular thickness-tapered laminated disc obtained using the Rayleigh-Ritz method, with the distributions obtained for the same using the finite element analysis software ANSYS® (using the SHELL181 element). The comparison of the elastic response has been carried out for the laminated disc with the properties mentioned in the Table 4.3.

Radial stress, σ_r (in *MPa*)				
Radial distance in *mm* from the center of the disc	Taper configuration of the thickness-tapered $[0]_{20}$ laminated disc			
	Configuration B (Staircase arrangement)		Configuration D (Continuous plies interspersed)	
	Rayleigh-Ritz Solution	ANSYS® Solution (SHELL181)	Rayleigh-Ritz Solution	ANSYS® Solution (SHELL181)
24.0	21.493	20.492	21.904	20.435
33.6	16.182	15.651	16.414	15.659
43.2	12.871	12.507	12.842	12.509
52.8	10.542	10.334	10.554	10.335
62.4	8.694	8.63	8.718	8.629
72.0	7.141	7.155	7.19	7.154
81.6	5.798	5.783	5.791	5.783
91.2	4.455	4.435	4.455	4.434
100.8	3.051	3.053	3.049	3.052
110.4	1.588	1.59	1.588	1.589
120.0	0.00	1.31e-05	0.00	1.48e-05

Table 4.4 Comparison of the radial stress distributions obtained using the Rayleigh-Ritz method for a rotating annular thickness-tapered laminated disc made up of Graphite-Fiber Reinforced Plastic material (NCT-301) for the clamped-free boundary condition, with the distributions obtained for the same using ANSYS®

Circumferential stress, σ_θ (in *MPa*)				
Radial distance in *mm* from the center of the disc	Taper configuration of the thickness-tapered $[0]_{20}$ laminated disc			
	Configuration B (Staircase arrangement)		Configuration D (Continuous plies interspersed)	
	Rayleigh-Ritz Solution	ANSYS® Solution (SHELL181)	Rayleigh-Ritz Solution	ANSYS® Solution (SHELL181)
24.0	0.438	0.417	0.442	0.416
33.6	0.687	0.675	0.691	0.675
43.2	0.759	0.746	0.761	0.745
52.8	0.768	0.756	0.771	0.756
62.4	0.740	0.736	0.739	0.736
72.0	0.702	0.703	0.702	0.702
81.6	0.656	0.661	0.657	0.659
91.2	0.607	0.613	0.609	0.612
100.8	0.554	0.56	0.539	0.548
110.4	0.493	0.5	0.488	0.489
120.0	0.433	0.436	0.433	0.436

Table 4.5 Comparison of the circumferential stress distributions obtained using the Rayleigh-Ritz method for a rotating annular thickness-tapered laminated disc made up of Graphite-Fiber Reinforced Plastic material (NCT-301) for the clamped-free boundary condition, with the distributions obtained for the same using ANSYS®

Radial displacement, u_r (in mm)				
Radial distance in mm from the center of the disc	Taper configuration of the thickness-tapered $[0]_{20}$ laminated disc			
	Configuration B (Staircase arrangement)		Configuration D (Continuous plies interspersed)	
	Rayleigh-Ritz Solution	ANSYS® Solution (SHELL181)	Rayleigh-Ritz Solution	ANSYS® Solution (SHELL181)
24.0	0	0	0	0
33.6	0.00151	0.001507	0.00151	0.0015068
43.2	0.00267	0.0026663	0.00266	0.0026667
52.8	0.0036	0.0036061	0.003603	0.0036059
62.4	0.004385	0.0043852	0.004385	0.0043852
72.0	0.005032	0.0050328	0.0050328	0.0050323
81.6	0.00555	0.005559	0.00555	0.0055591
91.2	0.005978	0.0059783	0.00597	0.0059784
100.8	0.00628	0.0062776	0.00629	0.0062771
110.4	0.00645	0.006458	0.00645	0.006457
120.0	0.00652	0.0065169	0.00652	0.0065168

Table 4.6 Comparison of the radial displacement distributions obtained using the Rayleigh-Ritz method for a rotating annular thickness-tapered laminated disc made up of Graphite-Fiber Reinforced Plastic material (NCT-301) for the clamped-free boundary condition, with the distributions obtained for the same using ANSYS®

It can be seen from the above Tables 4.4 – 4.6 that the results obtained for the elastic response of a rotating annular thickness-tapered laminated disc made up of Graphite-Fiber Reinforced Plastic material and with the clamped-free boundary condition, using the Rayleigh-Ritz method involving the Classical Laminate Theory are in good agreement with the results obtained for the same using the finite element analysis software ANSYS®.

The following Tables 4.7 – 4.9 show the average percentage differences between the results obtained for the elastic response using the Rayleigh-Ritz method and ANSYS® SHELL181 element solution. Also, in the below Tables, the average percentage difference has been calculated using the following formula:

$$\text{Average percentage difference} = \frac{\sum_{i=1}^{T} \frac{(\text{R} - \text{R solution}) - \text{ANSYS}^{®}\ \text{SHELL181 solution}}{(\text{R} - \text{R solution})}}{\text{T}} * 100 \quad (4.21)$$

In the above Equation (4.21), R – R solution stands for the Rayleigh-Ritz solution and T is the number of sampling points taken along the radial direction of the disc. For the present case, T = 11.

Average percentage difference in the results obtained for the radial stress, σ_r		
Rayleigh-Ritz solution and ANSYS® SHELL181 solution	Taper configuration of the thickness-tapered disc	
	Configuration B	Configuration D
	1.324	1.66

Table 4.7 Average percentage difference in the results obtained for the radial stress distributions in a rotating annular thickness-tapered laminated disc made up of Graphite-Fiber Reinforced Plastic material for the clamped-free boundary condition

Average percentage difference in the results obtained for the circumferential stress, σ_θ		
Rayleigh-Ritz solution and ANSYS® SHELL181 solution	Taper configuration of the thickness-tapered disc	
	Configuration B	Configuration D
	1.404	1.45

Table 4.8 Average percentage difference in the results obtained for the circumferential stress distributions in a rotating annular thickness-tapered laminated disc made up of Graphite-Fiber Reinforced Plastic material for the clamped-free boundary condition

Average percentage difference in the results obtained for the radial displacement, u_r		
Rayleigh-Ritz solution and ANSYS® SHELL181 solution	Taper configuration of the thickness-tapered disc	
	Configuration B	Configuration D
	0.076	0.11

Table 4.9 Average percentage difference in the results obtained for the radial displacement distributions in a rotating annular thickness-tapered laminated disc made up of Graphite-Fiber Reinforced Plastic material for the clamped-free boundary condition

It can be seen from the above Tables 4.7 – 4.9 that the average percentage difference of the results obtained for the elastic response of a rotating annular thickness-tapered fiber-reinforced composite disc with taper configuration B is comparatively low as compared to the results obtained for the thickness-tapered disc with taper configuration D. Also, it can be noted that the average percentage difference of the results obtained for the elastic response of a rotating annular thickness-tapered fiber-reinforced composite disc, using the Rayleigh-Ritz method and ANSYS SHELL181 element solution, given in the Tables 4.7 – 4.9, is relatively higher as compared to the average percentage difference of the results obtained for the elastic response of a rotating annular thickness-tapered fiber-reinforced composite disc, given in the Tables 3.8 – 3.10.

4.7 Parametric Study

In this section, a comprehensive parametric study is conducted to study the effects of fiber orientation, beta value of the disc, number of dropped plies, taper configuration and laminate configuration on the stress distributions and the radial displacement distribution in a rotating annular thickness-tapered fiber-reinforced composite disc with the clamped-free boundary condition. The disc is made up of Graphite-Fiber Reinforced Plastic (NCT-301) material, the material properties of which have been mentioned earlier in the Table 3.2.

4.7.1 Laminated disc made up of uni-directional plies

This sub-section presents the parametric study on the elastic response of rotating annular thickness-tapered discs made up of Graphite-Fiber Reinforced Plastic material with uni-directional laminate configuration for the clamped-free boundary condition. The effects of the fiber orientation in the uni-directional laminated disc configurations, radius ratio values, taper configurations and numbers of dropped plies on the radial stress and circumferential stress distributions, and on the radial displacement distribution in rotating annular thickness-tapered fiber-reinforced composite discs with the clamped-free boundary condition are studied. Graphical results for the stress and displacement distributions are presented and the percentage changes in the maximum stress and maximum displacement values with the number of dropped plies in the uni-directional laminated disc are calculated.

4.7.1.1 Effect of dropped plies on the elastic response of uni-directional laminated discs

The effect of the number of dropped plies on the radial and circumferential stress distributions, and on the radial displacement distribution in a rotating annular thickness-tapered fiber-reinforced composite disc with uni-directional configuration is studied. To study the effect of dropped plies on the elastic response of uni-directional laminated disc, a rotating disc with a beta value of 0.2 is chosen. Therefore, corresponding to this beta value, the disc has an inner radius of r_i = 24 *mm*, an outer radius of r_o = 120 *mm*, thickness at the hub of h_i = 2.4 *mm* with an individual ply thickness of t_k = 0.12 *mm,* and is rotating at a constant angular velocity of ω = 1000 *rad/s* i.e. 9554.14 *rpm*.

The following Figure 4.3 shows the variation with the number of dropped plies of the maximum radial stress in a rotating annular thickness-tapered uni-directional fiber-reinforced composite disc with the clamped-free boundary condition for different values of the fiber orientation angle ranging from 0° to 90°. The variation of the maximum radial stress has been shown for different taper configurations of the laminated disc considered in the present study.

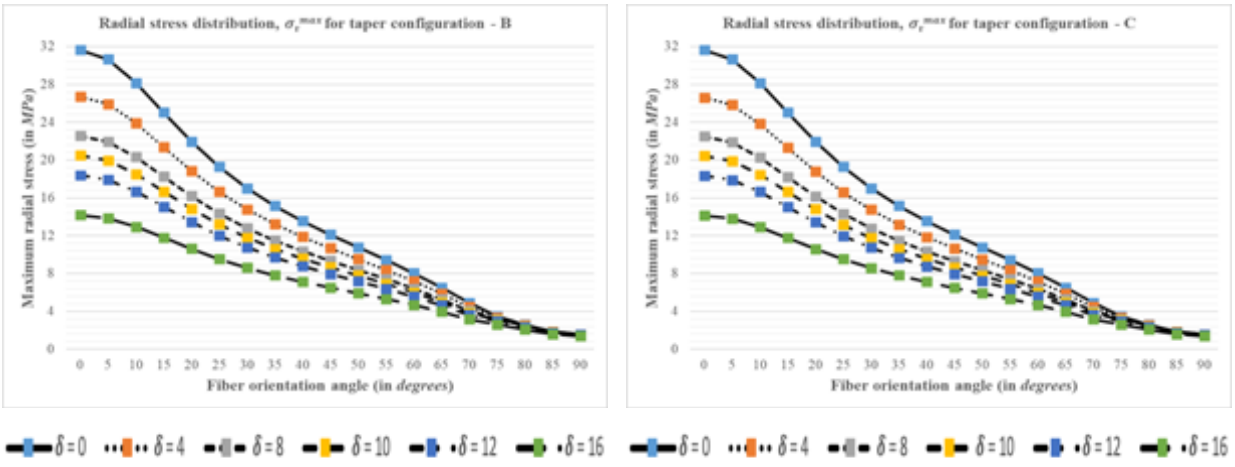

(a) **(b)**

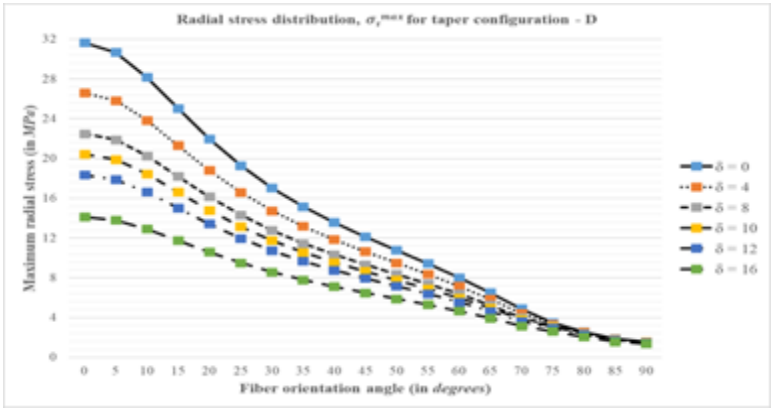

(c)

Figure 4.3 Variation of the maximum radial stress with the number of dropped plies in a rotating annular thickness-tapered uni-directional fiber-reinforced composite disc with the clamped-free boundary condition for **(a)** taper configuration B, **(b)** taper configuration C and **(c)** taper configuration D

In the above Figure 4.3, $\delta = 0$ represents the uniform-thickness laminated disc. It can be seen from the above plots that the uniform-thickness disc ($\delta = 0$) experiences the maximum radial stress and irrespective of the taper configuration, as the number of dropped plies (which in turn is the representation of the taper angle of the disc) is increased, the radial stress decreases accordingly and is the least for a ply drop-off value of 16, i.e. for a taper angle of 0.573°.

The following Tables 4.10 and 4.11 show the variation of the maximum radial stress and the percentage decrease in the maximum radial stress with the number of dropped plies, in a rotating annular thickness-tapered uni-directional laminated disc with taper configuration B and with the clamped-free boundary condition for different values of the fiber orientation angle.

Since the laminated disc with $\delta = 0$ (which is the uniform-thickness laminated disc) is subjected to the maximum amount of radial stress, the value of the maximum radial stress corresponding to $\delta = 0$ is considered as a benchmark while calculating the percentage decrease in the stress. Also, in the below Table 4.11, the percentage decrease in the maximum radial stress is calculated according to the following formula:

$$\text{Percentage decrease in the maximum radial stress } ({}_{i}^{0}\eta_{x}) = \frac{(\text{Maximum stress value for } \delta = 0) - (\text{Maximum stress value for } \delta = i)}{\text{Maximum stress value for } \delta = 0} * 100 \quad (4.22)$$

where, i = 4, 8, 10, 12 and 16, and the subscript x after the base represents the taper configuration considered in the present study.

Maximum radial stress, σ_r^{max} (in *MPa*) in a rotating annular thickness-tapered uni-directional laminated disc with taper configuration B and with the clamped-free boundary condition						
Fiber orientation angle (in *degrees*)	Number of dropped plies (δ)					
	0	4	8	10	12	16
0	31.645	26.688	22.570	20.492	18.4	14.171
5	30.67	25.913	21.948	19.944	17.925	13.836
10	28.176	23.910	20.332	18.517	16.683	12.953
15	25.043	21.374	18.266	16.683	15.079	11.8
20	21.974	18.867	16.204	14.842	13.459	10.618
25	19.288	16.655	14.369	13.196	12	9.543
30	17.04	14.79	12.811	11.794	10.757	8.613
35	15.163	13.22	11.498	10.609	9.701	7.819
40	13.559	11.881	10.367	9.587	8.788	7.129
45	12.128	10.677	9.353	8.669	7.968	6.507
50	10.781	9.538	8.392	7.799	7.190	5.916
55	9.438	8.398	7.428	6.925	6.406	5.317
60	8.033	7.1961	6.408	5.997	5.572	4.676
65	6.521	5.890	5.291	4.977	4.651	3.958
70	4.906	4.479	4.069	3.854	3.629	3.157
75	3.48	3.353	3.186	3.082	2.957	2.620
80	2.581	2.524	2.430	2.369	2.292	2.06
85	1.876	1.855	1.805	1.771	1.726	1.584
90	1.595	1.578	1.543	1.517	1.484	1.372

Table 4.10 Variation of the maximum radial stress (in *MPa*) with the number of dropped plies in a rotating annular thickness-tapered uni-directional laminated disc with taper configuration B and with the clamped-free boundary condition

Percentage decrease in the maximum radial stress in a rotating annular thickness-tapered uni-directional laminated disc with taper configuration B and with the clamped-free boundary condition					
Fiber orientation angle (in *degrees*)	Percentage decrease in the maximum radial stress (${}^{0}_{i}\eta_{B}$)				
	${}^{0}_{4}\eta_{B}$	${}^{0}_{8}\eta_{B}$	${}^{0}_{10}\eta_{B}$	${}^{0}_{12}\eta_{B}$	${}^{0}_{16}\eta_{B}$
0	15.664	28.676	35.243	41.853	55.217
5	15.51	28.436	34.97	41.554	54.885
10	15.138	27.838	34.281	40.789	54.025
15	14.648	27.059	33.38	39.786	52.881
20	14.138	26.257	32.452	38.748	51.676
25	13.65	25.503	31.58	37.768	50.523
30	13.202	24.816	30.782	36.868	49.45
35	12.78	24.169	30.031	36.019	48.429
40	12.375	23.539	29.294	35.182	47.415
45	11.962	22.88	28.52	34.298	46.34
50	11.523	22.151	27.656	33.307	45.125
55	11.018	21.289	26.626	32.118	43.657
60	10.418	20.226	25.342	30.625	41.79
65	9.671	18.859	23.676	28.669	39.303
70	8.701	17.043	21.442	26.022	35.632
75	3.624	8.428	11.428	15.017	24.699
80	2.192	5.814	8.193	11.168	19.888
85	1.078	3.739	5.571	7.963	15.562
90	1.023	3.256	4.862	6.959	13.938

Table 4.11 Variation of the percentage decrease in the maximum radial stress with the number of dropped plies in a rotating annular thickness-tapered uni-directional laminated disc with taper configuration B and with the clamped-free boundary condition

The following Tables 4.12 and 4.13 show the variation of the maximum radial stress and the percentage decrease in the maximum radial stress with the number of dropped plies, in a rotating annular thickness-tapered uni-directional laminated disc with taper configuration C and with the clamped-free boundary condition for different values of the fiber orientation angle. Also, in the below Table 4.13, the percentage decrease in the maximum radial stress is calculated according to the formula given in the Equation (4.22).

Maximum radial stress, σ_r^{max} (in *MPa*) in a rotating annular thickness-tapered uni-directional laminated disc with taper configuration C and with the clamped-free boundary condition						
Fiber orientation angle (in *degrees*)	Number of dropped plies (δ)					
	0	4	8	10	12	16
0	31.645	26.605	22.505	20.435	18.35	14.135
5	30.67	25.833	21.885	19.889	17.87	13.802
10	28.176	23.839	20.275	18.467	16.640	12.922
15	25.043	21.312	18.216	16.639	15.04	11.771
20	21.974	18.813	16.160	14.804	13.425	10.593
25	19.288	16.609	14.331	13.163	11.974	9.521
30	17.04	14.751	12.779	11.766	10.732	8.595
35	15.163	13.191	11.471	10.585	9.680	7.803
40	13.559	11.852	10.344	9.566	8.770	7.116
45	12.128	10.652	9.333	8.651	7.952	6.495
50	10.781	9.518	8.376	7.784	7.176	5.905
55	9.438	8.380	7.414	6.912	6.395	5.308
60	8.033	7.181	6.39	5.986	5.563	4.668
65	6.521	5.878	5.281	4.968	4.643	3.951
70	4.906	4.470	4.062	3.847	3.623	3.157
75	3.48	3.354	3.187	3.082	2.957	2.620
80	2.581	2.524	2.431	2.369	2.292	2.067
85	1.876	1.855	1.806	1.771	1.726	1.584
90	1.595	1.578	1.543	1.517	1.484	1.372

Table 4.12 Variation of the maximum radial stress (in *MPa*) with the number of dropped plies in a rotating annular thickness-tapered uni-directional laminated disc with taper configuration C and with the clamped-free boundary condition

Percentage decrease in the maximum radial stress in a rotating annular thickness-tapered uni-directional laminated disc with taper configuration C and with the clamped-free boundary condition					
Fiber orientation angle (in *degrees*)	Percentage decrease in the maximum radial stress (${}^{0}_{i}\eta_{C}$)				
	${}^{0}_{4}\eta_{C}$	${}^{0}_{8}\eta_{C}$	${}^{0}_{10}\eta_{C}$	${}^{0}_{12}\eta_{C}$	${}^{0}_{16}\eta_{C}$
0	15.926	28.882	35.424	42.011	55.33
5	15.769	28.641	35.15	41.71	54.998
10	15.391	28.039	34.457	40.942	54.136
15	14.898	27.259	33.557	39.94	52.994
20	14.385	26.456	32.628	38.902	51.79
25	13.889	25.696	31.751	37.918	50.635
30	13.432	25.001	30.947	37.013	49.559
35	13	24.347	30.189	36.158	48.535
40	12.585	23.708	29.445	35.315	47.517
45	12.164	23.042	28.665	34.427	46.439
50	11.715	22.307	27.795	33.431	45.221
55	11.203	21.44	26.761	32.238	43.751
60	10.598	20.373	25.475	30.744	41.885
65	9.848	19.006	23.809	28.789	39.401
70	8.88	17.194	21.581	26.15	35.63
75	3.614	8.419	11.432	15.002	24.692
80	2.185	5.81	8.189	11.164	19.882
85	1.087	3.716	5.578	7.967	15.551
90	1.013	3.251	4.835	6.946	13.933

Table 4.13 Variation of the percentage decrease in the maximum radial stress with the number of dropped plies in a rotating annular thickness-tapered uni-directional laminated disc with taper configuration C and with the clamped-free boundary condition

The following Tables 4.14 and 4.15 show the variation of the maximum radial stress and the percentage decrease in the maximum radial stress with the number of dropped plies, in a rotating annular thickness-tapered uni-directional laminated disc with taper configuration D and with the clamped-free boundary condition for different values of the fiber orientation angle. Also, in the below Table 4.15, the percentage decrease in the maximum radial stress is calculated according to the formula given in the Equation (4.22).

Maximum radial stress, σ_r^{max} (in *MPa*) in a rotating annular thickness-tapered uni-directional laminated disc with taper configuration D and with the clamped-free boundary condition						
Fiber orientation angle (in *degrees*)	Number of dropped plies (δ)					
	0	4	8	10	12	16
0	31.645	26.605	22.505	20.435	18.351	14.135
5	30.67	25.834	21.886	19.889	17.878	13.802
10	28.176	23.839	20.276	18.467	16.64	12.922
15	25.043	21.312	18.217	16.639	15.041	11.771
20	21.974	18.813	16.161	14.804	13.426	10.593
25	19.288	16.609	14.332	13.164	11.974	9.521
30	17.04	14.751	12.78	11.767	10.732	8.595
35	15.163	13.192	11.471	10.585	9.680	7.803
40	13.559	11.853	10.344	9.5665	8.77	7.116
45	12.128	10.653	9.333	8.651	7.952	6.495
50	10.781	9.518	8.376	7.784	7.176	5.905
55	9.438	8.380	7.414	6.912	6.395	5.308
60	8.033	7.181	6.396	5.986	5.563	4.668
65	6.521	5.878	5.281	4.968	4.643	3.951
70	4.906	4.47	4.026	3.847	3.623	3.157
75	3.48	3.354	3.187	3.082	2.957	2.620
80	2.581	2.524	2.431	2.369	2.292	2.067
85	1.876	1.855	1.806	1.771	1.726	1.584
90	1.595	1.578	1.543	1.517	1.484	1.372

Table 4.14 Variation of the maximum radial stress (in *MPa*) with the number of dropped plies in a rotating annular thickness-tapered uni-directional laminated disc with taper configuration D and with the clamped-free boundary condition

Percentage decrease in the maximum radial stress in a rotating annular thickness-tapered uni-directional laminated disc with taper configuration D and with the clamped-free boundary condition					
Fiber orientation angle (in *degrees*)	Percentage decrease in the maximum radial stress (${}^{0}_{i}\eta_{D}$)				
	${}^{0}_{4}\eta_{D}$	${}^{0}_{8}\eta_{D}$	${}^{0}_{10}\eta_{D}$	${}^{0}_{12}\eta_{D}$	${}^{0}_{16}\eta_{D}$
0	15.927	28.883	35.424	42.01	55.33
5	15.768	28.64	35.15	41.709	54.998
10	15.393	28.038	34.457	40.943	54.136
15	14.898	27.257	33.557	39.939	52.994
20	14.385	26.454	32.628	38.901	51.79
25	13.889	25.695	31.75	37.92	50.635
30	13.433	25.0	30.945	37.013	49.559
35	12.999	24.349	30.192	36.158	48.535
40	12.582	23.711	29.445	35.315	47.517
45	12.162	23.043	28.665	34.427	46.439
50	11.715	22.307	27.795	33.431	45.221
55	11.204	21.44	26.761	32.238	43.751
60	10.599	20.373	25.475	30.744	41.885
65	9.848	19.006	23.809	28.789	39.401
70	8.879	17.929	21.58	26.15	35.63
75	3.615	8.42	11.431	15.002	24.692
80	2.185	5.812	8.191	11.164	19.882
85	1.087	3.715	5.576	7.967	15.551
90	1.016	3.254	4.834	6.946	13.933

Table 4.15 Variation of the percentage decrease in the maximum radial stress with the number of dropped plies in a rotating annular thickness-tapered uni-directional laminated disc with taper configuration D and with the clamped-free boundary condition

The following observations can be made from the variation of the maximum radial stress and the percentage decrease in the maximum radial stress with the number of dropped plies, in a rotating annular thickness-tapered uni-directional laminated disc with the clamped-free boundary condition for different taper configurations, shown in the Figure 4.3 and Tables 4.10 – 4.15:

- Irrespective of the taper configuration and the number of dropped plies, the maximum radial stress decreases with the increasing value of the fiber orientation

angle. This variation of the maximum radial stress with the fiber orientation angle has been explained about in Chapter 3 (see section 3.7.1.1).

- Irrespective of the fiber orientation angle and the taper configuration of the uni-directional laminated disc, the maximum radial stress decreases with the increasing number of dropped plies. The radial stress is the highest in the uniform-thickness disc with δ = 0 and is the least in the thickness-tapered disc with δ = 16.
- Irrespective of the number of dropped plies and the fiber orientation angle, the thickness-tapered disc with taper configuration B (Staircase arrangement of dropped plies) is subjected to the maximum amount of radial stress as compared to the other taper configurations. Therefore, for the rotating annular thickness-tapered uni-directional laminated disc, it can be deduced that σ_r^{max} (B) > [σ_r^{max} (C) $\cong$ σ_r^{max} (D)], where the letter inside the bracket represents the taper configuration.
- Regardless of the taper configuration and the fiber orientation angle, the percentage decrease in the maximum radial stress increases with the increasing number of dropped plies and the percentage decrease is maximum for the tapered disc with δ = 16. Furthermore, on comparing the percentage decrease in the maximum radial stress corresponding to different taper configurations, it can be noted that irrespective of the fiber orientation angle, the thickness-tapered disc with taper configurations C and D holds the maximum percentage decrease in the radial stress as compared to the disc with taper configuration B.
- Irrespective of the taper configuration and the number of dropped plies, the percentage decrease in the maximum radial stress decreases with the increasing value of the fiber orientation angle, i.e. the percentage decrease is maximum for $\theta = 0°$ and minimum for $\theta = 90°$. In other words, the decrease in the amount of the maximum radial stress with the increasing number of dropped plies becomes less significant with the increasing angle of fiber orientation. For instance, for a disc with δ = 10 and with taper configuration B, the percentage decrease corresponding to $\theta = 0°$ is equal to 35.243 %, while the percentage decrease for a disc with the same number of dropped plies and with the same taper configuration, amounts to only 4.862 %, corresponding to $\theta = 90°$.

The following Figure 4.4 shows the variation with the number of dropped plies of the maximum circumferential stress in a rotating annular thickness-tapered uni-directional fiber-reinforced composite disc with the clamped-free boundary condition for different values of the fiber orientation angle ranging from 0° to 90°. The variation of the maximum circumferential stress has been shown for different taper configurations of the laminated disc considered in the present study.

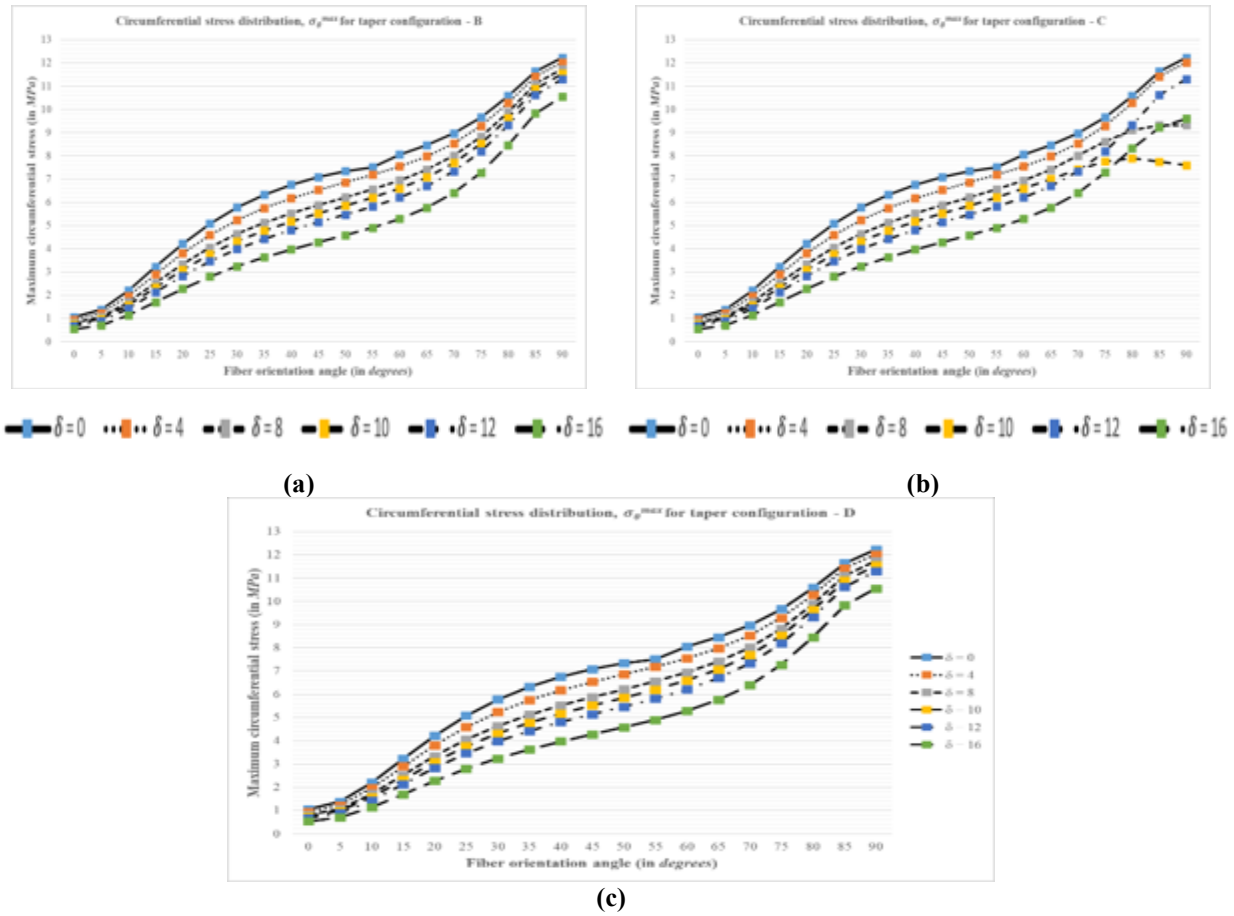

Figure 4.4 Variation of the maximum circumferential stress with the number of dropped plies in a rotating annular thickness-tapered uni-directional fiber-reinforced composite disc with the clamped-free boundary condition for **(a)** taper configuration B, **(b)** taper configuration C and **(c)** taper configuration D

It can be seen from the above Figure 4.4 that the uniform-thickness disc ($\delta = 0$) experiences the maximum amount of circumferential stress and irrespective of the taper configuration, as the number of dropped plies is increased, the circumferential stress decreases accordingly and is the least for a ply drop-off value of 16, i.e., for a taper angle of 0.573°.

The following Tables 4.16 and 4.17 show the variation of the maximum circumferential stress and the percentage decrease in the maximum circumferential stress with the number of

dropped plies, in a rotating annular thickness-tapered uni-directional laminated disc with taper configuration B and with the clamped-free boundary condition for different values of fiber orientation angle. Since the laminated disc with $\delta = 0$ is subjected to the maximum amount of circumferential stress, the value of the maximum circumferential stress corresponding to $\delta = 0$ is considered as a benchmark while calculating the percentage decrease in the stress. Also, in the below Table 4.17, the percentage decrease in the circumferential stress is calculated according to the formula given in the Equation (4.22).

Maximum circumferential stress, σ_θ^{max} (in MPa) in a rotating annular thickness-tapered uni-directional laminated disc with taper configuration B and with the clamped-free boundary condition						
Fiber orientation angle (in *degrees*)	Number of dropped plies (δ)					
	0	4	8	10	12	16
0	1.062	0.94822	0.82247	0.7564	0.68788	0.54182
5	1.382	1.22961	1.06676	0.98121	0.89264	0.70396
10	2.199	1.96424	1.70732	1.57225	1.43256	1.13451
15	3.224	2.8974	2.52841	2.33404	2.13215	1.6999
20	4.22	3.80943	3.34093	3.09307	2.83448	2.27727
25	5.078	4.59553	4.05136	3.76216	3.45917	2.80041
30	5.775	5.23687	4.64037	4.32173	3.98617	3.25013
35	6.326	5.75171	5.12369	4.78505	4.4268	3.63357
40	6.756	6.17321	5.52733	5.17752	4.80444	3.96904
45	7.088	6.53203	5.88192	5.52605	5.14377	4.27701
50	7.339	6.8604	6.21498	5.85819	5.47158	4.58117
55	7.515	7.18797	6.55767	6.20329	5.81567	4.90767
60	8.057	7.55005	6.94206	6.59479	6.21028	5.28907
65	8.462	7.98464	7.40918	7.0741	6.69763	5.76797
70	8.975	8.54282	8.01235	7.69576	7.33315	6.40524
75	9.657	9.28747	8.81781	8.52929	8.18959	7.27901
80	10.581	10.2817	9.88652	9.6334	9.32908	8.46152
85	11.634	11.4205	11.0988	10.8858	10.6216	9.82475
90	12.233	12.0264	11.7387	11.5455	11.3045	10.5513

Table 4.16 Variation of the maximum circumferential stress (in *MPa*) with the number of dropped plies in a rotating annular thickness-tapered uni-directional laminated disc with taper configuration B and with the clamped-free boundary condition

Percentage decrease in the maximum circumferential stress in a rotating annular thickness-tapered uni-directional laminated disc with taper configuration B and with the clamped-free boundary condition					
Fiber orientation angle (in *degrees*)	Percentage decrease in the maximum circumferential stress (${}^{0}_{i}\eta_{B}$)				
	${}^{0}_{4}\eta_{B}$	${}^{0}_{8}\eta_{B}$	${}^{0}_{10}\eta_{B}$	${}^{0}_{12}\eta_{B}$	${}^{0}_{16}\eta_{B}$
0	10.714	22.555	28.776	35.228	48.981
5	11.027	22.81	29.001	35.41	49.062
10	10.676	22.359	28.502	34.854	48.408
15	10.13	21.575	27.604	33.866	47.274
20	9.729	20.831	26.705	32.832	46.036
25	9.501	20.217	25.913	31.879	44.852
30	9.318	19.647	25.165	30.975	43.721
35	9.078	19.006	24.359	30.022	42.561
40	8.626	18.186	23.364	28.886	41.252
45	7.844	17.016	22.037	27.43	39.658
50	6.521	15.316	20.177	25.445	37.578
55	4.352	12.739	17.455	22.613	34.695
60	6.292	13.838	18.148	22.921	34.354
65	5.641	12.442	16.402	20.851	31.837
70	4.815	10.726	14.253	18.294	28.632
75	3.827	8.69	11.678	15.195	24.625
80	2.829	6.563	8.956	11.832	20.031
85	1.835	4.6	6.431	8.702	15.551
90	1.689	4.041	5.62	7.59	13.747

Table 4.17 Variation of the percentage decrease in the maximum circumferential stress with the number of dropped plies in a rotating annular thickness-tapered uni-directional laminated disc with taper configuration B and with the clamped-free boundary condition

The following Tables 4.18 and 4.19 show the variation of the maximum circumferential stress and the percentage decrease in the maximum circumferential stress with the number of dropped plies, in a rotating annular thickness-tapered uni-directional laminated disc with taper configuration C and with the clamped-free boundary condition for different values of the fiber orientation angle. Also, in the below Table 4.19, the percentage decrease in the maximum circumferential stress is calculated according to the formula given in the Equation (4.22).

Maximum circumferential stress, σ_θ^{max} (in MPa) in a rotating annular thickness-tapered uni-directional laminated disc with taper configuration C and with the clamped-free boundary condition						
Fiber orientation angle (in *degrees*)	Number of dropped plies (δ)					
	0	4	8	10	12	16
0	1.062	0.94876	0.82291	0.75689	0.68826	0.54214
5	1.382	1.22959	1.06677	0.98124	0.89268	0.70404
10	2.199	1.96378	1.70693	1.57219	1.43223	1.13433
15	3.224	2.89647	2.52765	2.33389	2.13177	1.69961
20	4.22	3.80832	3.34015	3.09293	2.83426	2.27714
25	5.078	4.59577	4.05148	3.76189	3.45886	2.80025
30	5.775	5.2367	4.6407	4.32128	3.98608	3.25011
35	6.326	5.75216	5.12378	4.78506	4.42683	3.63375
40	6.756	6.1733	5.52738	5.17763	4.80422	3.96871
45	7.088	6.53176	5.88211	5.52571	5.14361	4.27716
50	7.339	6.85954	6.21536	5.85762	5.47145	4.58126
55	7.515	7.18839	6.55745	6.21604	5.81554	4.90769
60	8.057	7.54935	6.94163	6.60207	6.21041	5.28846
65	8.462	7.9847	7.41188	7.00744	6.69736	5.76781
70	8.975	8.54232	8.00955	7.41379	7.33284	6.40498
75	9.657	9.28752	8.61825	7.75369	8.18932	7.28855
80	10.581	10.2824	9.11006	7.89504	9.32916	8.31945
85	11.634	11.4194	9.31847	7.75184	10.6219	9.22888
90	12.233	12.0247	9.31693	7.59524	11.3084	9.60319

Table 4.18 Variation of the maximum circumferential stress (in *MPa*) with the number of dropped plies in a rotating annular thickness-tapered uni-directional laminated disc with taper configuration C and with the clamped-free boundary condition

Percentage decrease in the maximum circumferential stress in a rotating annular thickness-tapered uni-directional laminated disc with taper configuration C and with the clamped-free boundary condition					
Fiber orientation angle (in *degrees*)	Percentage decrease in the maximum circumferential stress ($^{0}_{i}\eta_{C}$)				
	$^{0}_{4}\eta_{C}$	$^{0}_{8}\eta_{C}$	$^{0}_{10}\eta_{C}$	$^{0}_{12}\eta_{C}$	$^{0}_{16}\eta_{C}$
0	10.663	22.513	28.73	35.192	48.951
5	11.028	22.81	28.999	35.407	49.056
10	10.697	22.377	28.504	34.869	48.416
15	10.159	21.599	27.609	33.878	47.283
20	9.755	20.85	26.708	32.837	46.039
25	9.496	20.215	25.918	31.885	44.855
30	9.321	19.642	25.173	30.977	43.721
35	9.071	19.004	24.359	30.022	42.558
40	8.625	18.186	23.362	28.89	41.257
45	7.848	17.013	22.041	27.432	39.656
50	6.533	15.311	20.185	25.447	37.577
55	4.346	12.742	17.285	22.614	34.695
60	6.301	13.843	18.058	22.919	34.362
65	5.641	12.41	17.189	20.854	31.839
70	4.821	10.757	17.395	18.297	28.635
75	3.826	10.756	19.709	15.198	24.526
80	2.822	13.902	25.385	11.831	21.374
85	1.845	19.903	33.369	8.7	20.673
90	1.703	23.838	37.912	7.558	21.498

Table 4.19 Variation of the percentage decrease in the maximum circumferential stress with the number of dropped plies in a rotating annular thickness-tapered uni-directional laminated disc with taper configuration C and with the clamped-free boundary condition

The following Tables 4.20 and 4.21 show the variation of the maximum circumferential stress and the percentage decrease in the maximum circumferential stress with the number of dropped plies, in a rotating annular thickness-tapered uni-directional laminated disc with taper configuration D and with the clamped-free boundary condition for different values of the fiber

orientation angle. Also, in the below Table 4.21, the percentage decrease in the maximum circumferential stress is calculated according to the formula given in the Equation (4.22).

Maximum circumferential stress, σ_θ^{max} (in MPa) in a rotating annular thickness-tapered uni-directional laminated disc with taper configuration D and with the clamped-free boundary condition						
Fiber orientation angle (in *degrees*)	Number of dropped plies (δ)					
	0	4	8	10	12	16
0	1.062	0.94876	0.82291	0.75689	0.68826	0.54214
5	1.382	1.2296	1.0668	0.98124	0.89268	0.70404
10	2.199	1.9638	1.7069	1.57219	1.4322	1.13433
15	3.224	2.8965	2.5277	2.33389	2.1318	1.69961
20	4.22	3.8083	3.3401	3.09293	2.8343	2.27714
25	5.078	4.5958	4.0515	3.7619	3.4589	2.80025
30	5.775	5.2367	4.6407	4.3213	3.98608	3.25011
35	6.326	5.7522	5.1238	4.7851	4.42683	3.63375
40	6.756	6.1733	5.5274	5.1776	4.80422	3.96871
45	7.088	6.5318	5.8821	5.5257	5.14361	4.27716
50	7.339	6.8595	6.2154	5.8576	5.47145	4.58126
55	7.515	7.1884	6.5575	6.2031	5.81554	4.90769
60	8.057	7.5494	6.9416	6.5942	6.21041	5.28846
65	8.462	7.9847	7.4091	7.0734	6.69736	5.76781
70	8.975	8.5423	8.0119	7.6951	7.33284	6.40498
75	9.657	9.2875	8.8169	8.529	8.18932	7.27865
80	10.581	10.282	9.885	9.6337	9.32916	8.46074
85	11.634	11.419	11.099	10.887	10.6219	9.82408
90	12.233	12.025	11.738	11.547	11.305	10.5497

Table 4.20 Variation of the maximum circumferential stress (in *MPa*) with the number of dropped plies in a rotating annular thickness-tapered uni-directional laminated disc with taper configuration D and with the clamped-free boundary condition

Percentage decrease in the maximum circumferential stress in a rotating annular thickness-tapered uni-directional laminated disc with taper configuration D and with the clamped-free boundary condition					
Fiber orientation angle (in *degrees*)	Percentage decrease in the maximum circumferential stress (${}^{0}_{i}\eta_{D}$)				
	${}^{0}_{4}\eta_{D}$	${}^{0}_{8}\eta_{D}$	${}^{0}_{10}\eta_{D}$	${}^{0}_{12}\eta_{D}$	${}^{0}_{16}\eta_{D}$
0	10.663	22.513	28.73	35.192	48.951
5	11.027	22.808	28.999	35.407	49.056
10	10.696	22.378	28.504	34.87	48.416
15	10.158	21.597	27.609	33.877	47.283
20	9.756	20.851	26.708	32.836	46.039
25	9.496	20.215	25.918	31.885	44.855
30	9.321	19.642	25.172	30.977	43.721
35	9.071	19.004	24.358	30.022	42.558
40	8.625	18.185	23.363	28.89	41.257
45	7.847	17.013	22.041	27.432	39.656
50	6.534	15.31	20.185	25.447	37.577
55	4.346	12.741	17.457	22.614	34.695
60	6.3	13.844	18.156	22.919	34.362
65	5.641	12.443	16.41	20.854	31.839
70	4.821	10.731	14.261	18.297	28.635
75	3.826	8.699	11.681	15.198	24.628
80	2.826	6.578	8.953	11.831	20.038
85	1.848	4.599	6.421	8.7	15.557
90	1.7	4.046	5.608	7.586	13.76

Table 4.21 Variation of the percentage decrease in the maximum circumferential stress with the number of dropped plies in a rotating annular thickness-tapered uni-directional laminated disc with taper configuration D and with the clamped-free boundary condition

The following observations can be made from the variation of the maximum circumferential stress and the percentage decrease in the maximum circumferential stress with the number of dropped plies, in a rotating annular thickness-tapered uni-directional laminated disc with the clamped-free boundary condition for different taper configurations, shown in the Figure 4.4 and Tables 4.16 – 4.21:

- Irrespective of the taper configuration and the number of dropped plies, the maximum circumferential stress increases with the increasing value of the fiber orientation angle. This observation holds true for the uniform-thickness disc as well as for the thickness-tapered discs with taper configurations B and D. However, for the disc with taper configuration C, the circumferential stress decreases with the increasing value of the fiber orientation angle from $\theta = 85°$ to $\theta = 90°$ for the disc with $\delta = 8$, and from $\theta = 80°$ to $\theta = 90°$ for the disc with $\delta = 10$. The decrease in the circumferential stress is, however, not that significant.
- Irrespective of the fiber orientation angle and the taper configuration of the uni-directional laminated disc, the maximum circumferential stress decreases with the increasing number of dropped plies. The stress is the highest in the uniform-thickness disc and is the least in the thickness-tapered disc with $\delta = 16$. This observation holds true for the thickness-tapered discs with taper configurations B and D. However, for the disc with taper configuration C and with the fiber orientation angle from $\theta = 75°$ to $\theta = 90°$, the circumferential stress first increases with the increasing number of dropped plies from $\delta = 10$ up to $\delta = 12$. The stress then decreases on further dropping of plies from $\delta = 12$ to $\delta = 16$. Subsequently, the maximum circumferential stress corresponding to $\theta = 90°$ for $\delta = 10$ (which is 7.595 *MPa*) is even lower than the maximum circumferential stress corresponding to $\theta = 90°$ for $\delta = 12$ and 16 (which is 11.308 *MPa* and 9.603 *MPa* respectively).
- For a rotating annular thickness-tapered uni-directional laminated disc with $\delta = 10$ and with the taper configuration C, the increase of circumferential stress with the fiber orientation angle from $65°$ to $75°$ is not that significant and thereafter, as the fiber orientation angle is increased from $\theta = 80°$ to $\theta = 90°$, the circumferential stress decreases with the increasing value of the fiber orientation angle, however, the decrease in the stress is not that significant.
- For a rotating annular thickness-tapered uni-directional laminated disc with $\delta = 10$ and with the taper configuration C, the maximum circumferential stresses corresponding to $\theta = 80°$ up to $\theta = 90°$ (which are 7.895 *MPa*, 7.752 *MPa* and 7.595 *MPa* respectively) are even lower than the maximum circumferential stress corresponding to the same fiber orientation angles for $\delta = 12$ (which are 9.329 *MPa*,

10.622 *MPa* and *11.308* MPa respectively) and for δ = 16 (which are 8.319 *MPa*, 9.23 *MPa* and 9.603 *MPa* respectively). This observation only holds true for a rotating annular thickness-tapered uni-directional laminated disc with taper configuration C.

- Regardless of the taper configuration and the fiber orientation angle, the percentage decrease in the maximum circumferential stress increases with the increasing number of dropped plies and the percentage decrease is maximum for the tapered disc with δ = 16. This observation holds true for the taper configurations B and D. However, for the disc with taper configuration C and with the fiber orientation angle from $\theta = 75°$ up to $\theta = 90°$, the percentage decrease in the circumferential stress is maximum for δ = 10, i.e., ${}_{10}^{0}\eta_C > {}_{12}^{0}\eta_C$ and ${}_{16}^{0}\eta_C$.
- Irrespective of the taper configuration and the number of dropped plies, the percentage decrease in the maximum circumferential stress decreases with the increasing value of the fiber orientation angle, i.e., the percentage decrease is maximum for $\theta = 0°$ and minimum for $\theta = 90°$. This observation holds true for the taper configurations B and D. However, for the taper configuration C, the percentage decrease in the maximum circumferential stress tends to increase with the increase in the fiber orientation angle from $\theta = 85°$ to $\theta = 90°$ for the disc with δ = 8, and from $\theta = 80°$ to $\theta = 90°$ for the disc with δ = 10.

Unlike the variation of the maximum radial stress and the maximum circumferential stress with the number of dropped plies, where, irrespective of the fiber orientation angle and the number of dropped plies, the values of the stresses are not identical corresponding to different taper configurations of the laminated disc, surprisingly, the value of the maximum radial displacement in a rotating annular thickness-tapered uni-directional laminated disc with the clamped-free boundary condition is approximately the same for each of the taper configurations considered in the present study. Therefore, it can be said that for a rotating annular thickness-tapered uni-directional laminated disc with the clamped-free boundary condition, the arrangement of dropped plies within the thickness-tapered disc has a negligible effect on the induced maximum radial displacement in the disc.

The following Figure 4.5 shows the variation with the number of dropped plies of the maximum radial displacement in a rotating annular thickness-tapered uni-directional laminated disc with the clamped-free boundary condition for different values of the fiber orientation angle ranging from 0° to 90°. Since the arrangement of dropped plies has no effect on the maximum radial displacement in the thickness-tapered disc, therefore, the following graph is valid for every taper configuration considered in the present study.

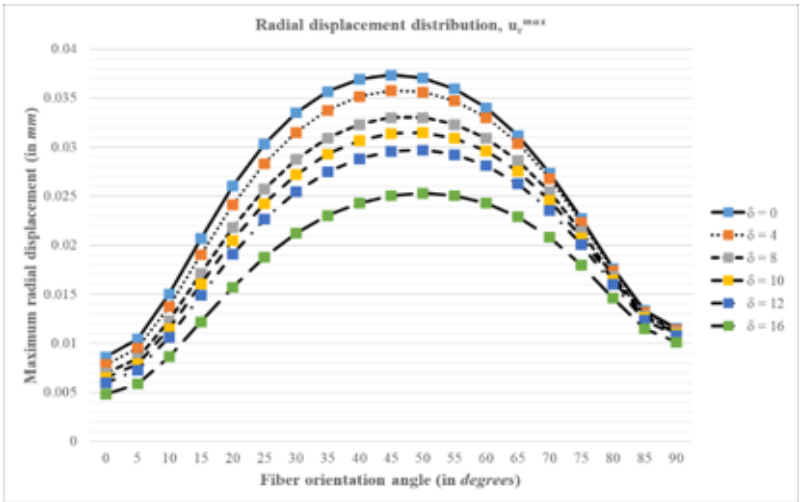

Figure 4.5 Variation of the maximum radial displacement with the number of dropped plies in a rotating annular thickness-tapered uni-directional laminated disc with the clamped-free boundary condition

It can be seen from the above plot that irrespective of the fiber orientation angle, the uniform-thickness disc ($\delta = 0$) experiences the largest value of the maximum radial displacement and as the number of dropped plies is increased, the maximum radial displacement decreases accordingly and is the least for the ply drop-off value of 16.

The following Tables 4.22 and 4.23 show the variation of the maximum radial displacement and the percentage decrease in the maximum radial displacement with the number of dropped plies, in a rotating annular thickness-tapered uni-directional laminated disc with the clamped-free boundary condition, for different values of the fiber orientation angle.

Since irrespective of the fiber orientation angle, the laminated disc with $\delta = 0$ is subjected to the maximum radial displacement, the value of the maximum radial displacement corresponding to $\delta = 0$ is considered as a benchmark while calculating the percentage decrease in the maximum radial displacement. Also, in the below Table 4.23, the percentage decrease in the maximum radial displacement is calculated according to the following formula:

$$\text{Percentage decrease in the maximum radial displacement}({}^{0}_{i}\eta) = \frac{(\text{Maximum displacement value for } \delta = 0) - (\text{Maximum displacement value for } \delta = i)}{\text{Maximum displacement value for } \delta = 0} * 100 \quad (4.23)$$

where, i = 4, 8, 10, 12 and 16.

Maximum radial displacement, u_r^{max} (in mm) in a rotating annular thickness-tapered uni-directional laminated disc with the clamped-free boundary condition						
Fiber orientation angle (in *degrees*)	Number of dropped plies (δ)					
	0	4	8	10	12	16
0	0.00864	0.00786	0.00699	0.00652	0.00601	0.00484
5	0.01046	0.00953	0.00849	0.00792	0.00731	0.0059
10	0.01507	0.01379	0.01234	0.01154	0.01067	0.00866
15	0.02073	0.01908	0.01717	0.0161	0.01494	0.01222
20	0.02604	0.02413	0.02183	0.02053	0.01911	0.01574
25	0.03035	0.02833	0.02576	0.02429	0.02268	0.0188
30	0.03354	0.03153	0.02879	0.02721	0.02547	0.02124
35	0.0357	0.03378	0.03095	0.02933	0.02751	0.02306
40	0.03695	0.03517	0.03234	0.0307	0.02886	0.02432
45	0.03739	0.03579	0.03303	0.03141	0.02959	0.02506
50	0.03706	0.03566	0.03303	0.03149	0.02974	0.02532
55	0.03596	0.03476	0.03235	0.03091	0.02927	0.02508
60	0.03403	0.03305	0.03092	0.02964	0.02815	0.02431
65	0.0312	0.03043	0.02865	0.02756	0.02629	0.02292
70	0.0274	0.02684	0.02547	0.02461	0.0236	0.02083
75	0.02274	0.02236	0.02141	0.02081	0.02008	0.018
80	0.01769	0.01744	0.01687	0.01649	0.01603	0.01464
85	0.01336	0.0132	0.01288	0.01266	0.01238	0.01151
90	0.01156	0.01143	0.01119	0.01102	0.01081	0.01014

Table 4.22 Variation of the maximum radial displacement (in *mm*) with the number of dropped plies in a rotating annular thickness-tapered uni-directional laminated disc with the clamped-free boundary condition

Percentage decrease in the maximum radial displacement in a rotating annular thickness-tapered uni-directional laminated disc with the clamped-free boundary condition					
Fiber orientation angle (in *degrees*)	Percentage decrease in the maximum radial displacement (${}^{0}_{i}\eta$)				
	${}^{0}_{4}\eta$	${}^{0}_{8}\eta$	${}^{0}_{10}\eta$	${}^{0}_{12}\eta$	${}^{0}_{16}\eta$
0	9.028	19.097	24.537	30.44	43.981
5	8.891	18.834	24.283	30.115	43.595
10	8.494	18.115	23.424	29.197	42.535
15	7.959	17.173	22.335	27.931	41.052
20	7.335	16.167	21.16	26.613	39.555
25	6.656	15.124	19.967	25.272	38.056
30	5.993	14.162	18.873	24.061	36.673
35	5.378	13.305	17.843	22.941	35.406
40	4.817	12.476	16.915	21.894	34.181
45	4.279	11.661	15.994	20.861	32.977
50	3.778	10.874	15.03	19.752	31.678
55	3.337	10.039	14.043	18.604	30.256
60	2.88	9.139	12.9	17.279	28.563
65	2.468	8.173	11.667	15.737	26.538
70	2.044	7.044	10.182	13.869	23.978
75	1.671	5.849	8.487	11.697	20.844
80	1.413	4.635	6.783	9.384	17.241
85	1.198	3.593	5.24	7.335	13.847
90	1.125	3.201	4.671	6.488	12.284

Table 4.23 Variation of the percentage decrease in the maximum radial displacement with the number of dropped plies in a rotating annular thickness-tapered uni-directional laminated disc with the clamped-free boundary condition

The following observations can be made from the variation of the maximum radial displacement and the percentage decrease in the maximum radial displacement with the number of dropped plies, in a rotating annular thickness-tapered uni-directional laminated disc with the clamped-free boundary condition, shown in the Figure 4.5 and Tables 4.22 – 4.23:

- Irrespective of the number of dropped plies, the thickness-tapered uni-directional laminated disc with the fiber orientation angle of $\theta = 0°$ is subjected to the least amount of the maximum radial displacement and the maximum radial displacement increases with the increasing angle of fiber orientation up to $+45°$. Thereafter, as the fiber orientation angle is increased, the maximum radial displacement tends to decrease with the increasing angle of fiber orientation till $\theta = 90°$. This variation of the maximum radial displacement with the fiber orientation angle in a rotating annular uniform-thickness uni-directional laminated disc with the clamped-free boundary condition has been explained about in Chapter 3 (see section 3.7.1.1).
- Irrespective of the fiber orientation angle, the maximum radial displacement decreases with the increasing number of dropped plies. The radial displacement is the largest in the uniform-thickness disc and is the least in the thickness-tapered disc with δ = 16.
- Irrespective of the number of dropped plies, the percentage decrease in the maximum radial displacement decreases with the increase in the fiber orientation angle, i.e., the percentage decrease is maximum for $\theta = 0°$ and minimum for $\theta = 90°$. In other words, the decrease in the amount of the maximum radial displacement with the increasing number of dropped plies becomes less significant with the increasing angle of fiber orientation. For instance, for a rotating annular thickness-tapered uni-directional laminated disc with δ = 10, the percentage decrease in the maximum radial displacement corresponding to $\theta = 0°$ is equal to 24.537 %, while the percentage decrease in the displacement for a disc with the same number of dropped plies amounts to only 4.671 %, corresponding to $\theta = 90°$.

4.7.1.2 Effect of radius ratio on the elastic response of uni-directional laminated discs

The effect of radius ratio on the radial and circumferential stress distributions and on the radial displacement distribution in a rotating annular thickness-tapered uni-directional laminated disc with the clamped-free boundary condition is studied for different taper configurations considered in the present thesis. The variations of maximum radial and circumferential stresses and the maximum radial displacement with the fiber orientation angle and with the number of

dropped plies are studied for the rotating annular thickness-tapered uni-directional laminated discs with the beta values of 0.2, 0.25 and 0.3.

The disc has a fixed outer radius of r_o = 120 *mm*, thickness at the hub of h_i = 2.4 *mm* with an individual ply thickness of t_k= 0.12 *mm,* and it is rotating at a constant angular velocity of ω = 1000 *rad/s* i.e. 9554.14 *rpm*. The inner radius of the disc is dependent on the beta value taken into consideration which has been mentioned earlier in the Table 3.16.

The following Figure 4.6 and the Tables 4.24 – 4.26 show the variation with the fiber orientation angle and with the number of dropped plies of the maximum radial stress, in a rotating annular thickness-tapered uni-directional laminated disc with the clamped-free boundary condition for the beta values of 0.2, 0.25 and 0.3. The variation of the maximum radial stress has been shown for different taper configurations of the laminated disc considered in the present study.

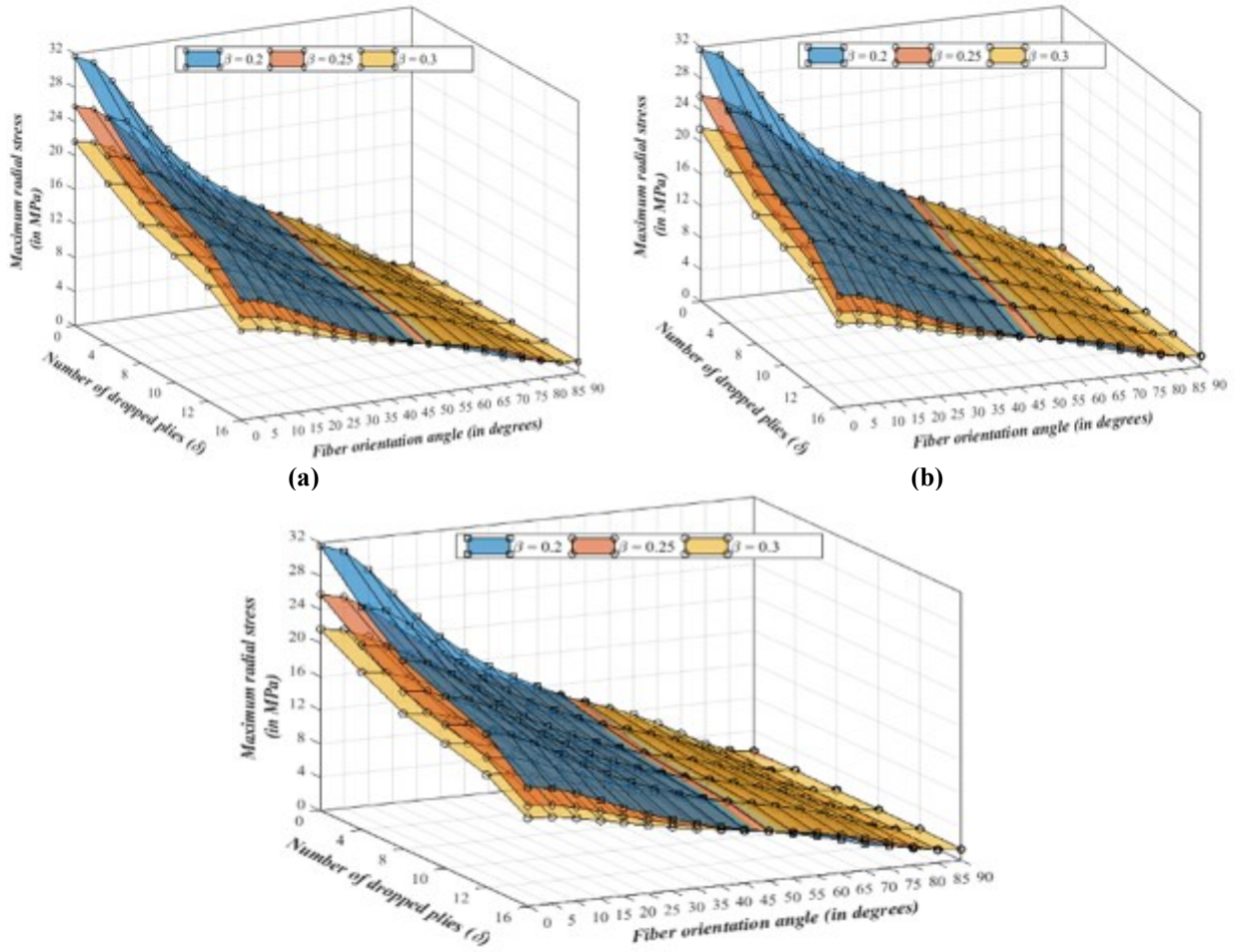

Figure 4.6 Variation of the maximum radial stress with the fiber orientation angle and with the number of dropped plies in a rotating annular thickness-tapered uni-directional laminated disc with different beta values for **(a)** taper configuration B, **(b)** taper configuration C and **(c)** taper configuration D

Maximum radial stress, σ_r^{max} (in *MPa*) in a rotating annular thickness-tapered uni-directional laminated disc with taper configuration B and with the clamped-free boundary condition for different values of radius ratio							
Fiber orientation angle (in *degrees*)	Radius ratio	Number of dropped plies (δ)					
		0	4	8	10	12	16
0	$\beta = 0.2$	31.645	26.688	22.570	20.492	18.400	14.171
	$\beta = 0.25$	25.803	22.150	18.906	17.241	15.54	12.059
	$\beta = 0.3$	21.658	18.861	16.254	14.891	13.48	10.536
10	$\beta = 0.2$	28.176	23.910	20.332	18.517	16.683	12.953
	$\beta = 0.25$	23.545	20.304	17.407	15.914	14.389	11.239
	$\beta = 0.3$	20.131	17.592	15.214	13.967	12.677	9.963
20	$\beta = 0.2$	21.974	18.867	16.204	14.842	13.459	10.618
	$\beta = 0.25$	19.272	16.770	14.499	13.321	12.112	9.594
	$\beta = 0.3$	17.111	15.059	13.115	12.090	11.026	8.771
30	$\beta = 0.2$	17.04	14.790	12.811	11.794	10.757	8.613
	$\beta = 0.25$	15.644	13.729	11.960	11.039	10.090	8.1
	$\beta = 0.3$	14.405	12.764	11.190	10.357	9.49	7.64
40	$\beta = 0.2$	13.559	11.881	10.367	9.587	8.788	7.129
	$\beta = 0.25$	12.955	11.454	10.045	9.309	8.549	6.947
	$\beta = 0.3$	12.316	10.979	9.683	8.994	8.276	6.737
50	$\beta = 0.2$	10.781	9.538	8.392	7.799	7.190	5.916
	$\beta = 0.25$	10.726	9.557	8.445	7.861	7.256	5.974
	$\beta = 0.3$	10.533	9.449	8.389	7.824	7.232	5.957
60	$\beta = 0.2$	8.033	7.196	6.408	5.997	5.572	4.676
	$\beta = 0.25$	8.425	7.581	6.773	6.345	5.9	4.945
	$\beta = 0.3$	8.627	7.804	6.996	6.563	6.106	5.112
70	$\beta = 0.2$	4.906	4.479	4.069	3.854	3.629	3.157
	$\beta = 0.25$	5.606	5.123	4.662	4.415	4.156	3.591
	$\beta = 0.3$	6.146	5.632	5.134	4.863	4.576	3.941
80	$\beta = 0.2$	2.581	2.524	2.430	2.369	2.292	2.067
	$\beta = 0.25$	2.624	2.556	2.45	2.395	2.317	2.089
	$\beta = 0.3$	3.134	2.930	2.748	2.648	2.541	2.299
90	$\beta = 0.2$	1.595	1.578	1.543	1.517	1.484	1.372
	$\beta = 0.25$	1.597	1.583	1.547	1.521	1.487	1.376
	$\beta = 0.3$	1.582	1.596	1.559	1.533	1.499	1.387

Table 4.24 Variation of the maximum radial stress (in *MPa*) with the fiber orientation angle and with the number of dropped plies in a rotating annular thickness-tapered uni-directional laminated disc with taper configuration B and with the clamped-free boundary condition for different values of radius ratio

Maximum radial stress, σ_r^{max} (in *MPa*) in a rotating annular thickness-tapered uni-directional laminated disc with taper configuration C and with the clamped-free boundary condition for different values of radius ratio							
Fiber orientation angle (in *degrees*)	Radius ratio	Number of dropped plies (δ)					
		0	4	8	10	12	16
0	$\beta = 0.2$	31.645	26.605	22.505	20.435	18.351	14.136
	$\beta = 0.25$	25.803	22.085	18.856	17.197	15.507	12.031
	$\beta = 0.3$	21.658	18.802	16.207	14.85	13.45	10.51
10	$\beta = 0.2$	28.176	23.839	20.276	18.467	16.64	12.922
	$\beta = 0.25$	23.545	20.246	17.361	15.874	14.355	11.214
	$\beta = 0.3$	20.131	17.538	15.171	13.929	12.645	9.939
20	$\beta = 0.2$	21.974	18.813	16.161	14.804	13.426	10.594
	$\beta = 0.25$	19.272	16.725	14.463	13.289	12.085	9.573
	$\beta = 0.3$	17.111	15.015	13.08	12.059	10.999	8.751
30	$\beta = 0.2$	17.04	14.751	12.78	11.767	10.733	8.595
	$\beta = 0.25$	15.644	13.695	11.933	11.015	10.069	8.085
	$\beta = 0.3$	14.405	12.73	11.163	10.333	9.469	7.625
40	$\beta = 0.2$	13.559	11.853	10.344	9.566	8.771	7.116
	$\beta = 0.25$	12.955	11.428	10.025	9.291	8.533	6.935
	$\beta = 0.3$	12.316	10.953	9.662	8.975	8.259	6.724
50	$\beta = 0.2$	10.781	9.518	8.376	7.784	7.177	5.906
	$\beta = 0.25$	10.726	9.537	8.429	7.847	7.244	5.964
	$\beta = 0.3$	10.533	9.428	8.372	7.809	7.219	5.947
60	$\beta = 0.2$	8.033	7.182	6.396	5.987	5.563	4.668
	$\beta = 0.25$	8.425	7.567	6.761	6.335	5.89	4.938
	$\beta = 0.3$	8.627	7.787	6.982	6.55	6.095	5.104
70	$\beta = 0.2$	4.906	4.47	4.062	3.847	3.623	3.158
	$\beta = 0.25$	5.606	5.113	4.653	4.407	4.149	3.586
	$\beta = 0.3$	6.146	5.619	5.123	4.853	4.567	3.933
80	$\beta = 0.2$	2.581	2.525	2.431	2.37	2.293	2.068
	$\beta = 0.25$	2.624	2.556	2.459	2.396	2.318	2.09
	$\beta = 0.3$	3.134	2.921	2.739	2.64	2.533	2.292
90	$\beta = 0.2$	1.595	1.579	1.543	1.518	1.484	1.373
	$\beta = 0.25$	1.597	1.583	1.547	1.522	1.488	1.376
	$\beta = 0.3$	1.582	1.597	1.56	1.534	1.5	1.388

Table 4.25 Variation of the maximum radial stress (in *MPa*) with the fiber orientation angle and with the number of dropped plies in a rotating annular thickness-tapered uni-directional laminated disc with taper configuration C and with the clamped-free boundary condition for different values of radius ratio

Maximum radial stress, σ_r^{max} (in *MPa*) in a rotating annular thickness-tapered uni-directional laminated disc with taper configuration D and with the clamped-free boundary condition for different values of radius ratio							
Fiber orientation angle (in *degrees*)	Radius ratio	Number of dropped plies (δ)					
		0	4	8	10	12	16
0	$\beta = 0.2$	31.645	26.605	22.505	20.435	18.351	14.136
	$\beta = 0.25$	25.803	22.085	18.856	17.197	15.507	12.031
	$\beta = 0.3$	21.658	18.802	16.207	14.85	13.45	10.51
10	$\beta = 0.2$	28.176	23.839	20.276	18.467	16.64	12.922
	$\beta = 0.25$	23.545	20.246	17.361	15.874	14.355	11.214
	$\beta = 0.3$	20.131	17.538	15.171	13.929	12.645	9.939
20	$\beta = 0.2$	21.974	18.813	16.161	14.804	13.426	10.594
	$\beta = 0.25$	19.272	16.725	14.463	13.289	12.085	9.573
	$\beta = 0.3$	17.111	15.015	13.08	12.059	10.999	8.751
30	$\beta = 0.2$	17.04	14.751	12.78	11.767	10.733	8.595
	$\beta = 0.25$	15.644	13.695	11.933	11.015	10.069	8.085
	$\beta = 0.3$	14.405	12.73	11.163	10.333	9.469	7.625
40	$\beta = 0.2$	13.559	11.853	10.344	9.567	8.771	7.116
	$\beta = 0.25$	12.955	11.428	10.025	9.291	8.533	6.935
	$\beta = 0.3$	12.316	10.953	9.662	8.976	8.259	6.724
50	$\beta = 0.2$	10.781	9.518	8.376	7.784	7.177	5.906
	$\beta = 0.25$	10.726	9.537	8.429	7.847	7.244	5.964
	$\beta = 0.3$	10.533	9.428	8.372	7.809	7.219	5.947
60	$\beta = 0.2$	8.033	7.182	6.396	5.987	5.563	4.668
	$\beta = 0.25$	8.425	7.567	6.761	6.335	5.89	4.938
	$\beta = 0.3$	8.627	7.787	6.982	6.55	6.095	5.104
70	$\beta = 0.2$	4.906	4.47	4.026	3.847	3.623	3.158
	$\beta = 0.25$	5.606	5.113	4.653	4.407	4.149	3.586
	$\beta = 0.3$	6.146	5.619	5.123	4.853	4.567	3.933
80	$\beta = 0.2$	2.581	2.525	2.431	2.37	2.293	2.068
	$\beta = 0.25$	2.624	2.556	2.459	2.396	2.318	2.09
	$\beta = 0.3$	3.134	2.921	2.739	2.64	2.533	2.292
90	$\beta = 0.2$	1.595	1.579	1.543	1.518	1.484	1.373
	$\beta = 0.25$	1.597	1.583	1.547	1.522	1.488	1.376
	$\beta = 0.3$	1.582	1.597	1.56	1.534	1.5	1.388

Table 4.26 Variation of the maximum radial stress (in *MPa*) with the fiber orientation angle and with the number of dropped plies in a rotating annular thickness-tapered uni-directional laminated disc with taper configuration D and with the clamped-free boundary condition for different values of radius ratio

The following observations can be made from the variation of the maximum radial stress with the fiber orientation angle and with the number of dropped plies, in a rotating annular thickness-tapered uni-directional laminated disc with the clamped-free boundary condition and with different taper configurations for different values of radius ratio, shown in the Figure 4.6 and Tables 4.24 – 4.26:

- For the uniform-thickness uni-directional laminated disc ($\delta = 0$), irrespective of the fiber orientation angle, the maximum radial stress decreases with the increasing beta value of the disc up to the fiber orientation angle of $50°$. From the fiber orientation angle of $50°$ to $90°$, the maximum radial stress tends to relatively-slightly increase with the increasing beta value of the uniform-thickness disc.
- For the thickness-tapered uni-directional laminated discs, irrespective of the taper configuration and the number of dropped plies, the maximum radial stress decreases with the increasing beta value of the disc up to the fiber orientation angle of $40°$. For the tapered disc with a fiber orientation angle of $50°$, the maximum radial stress first tends to relatively-slightly increase with the increasing value of radius ratio from $\beta = 0.2$ to $\beta = 0.25$ and then decreases for $\beta = 0.3$. Thereafter, as the fiber orientation angle is increased from $60°$ to $90°$, the maximum radial stress tends to increase with the increasing beta value of the rotating disc. Also, the increase in the maximum radial stress with the increasing beta value is minimal for the fiber orientation angle of $90°$.

To study the effect of taper configuration on the induced maximum radial stress, a thickness-tapered disc with a specific number of dropped plies, i.e. $\delta = 10$ is chosen for the uni-directional configurations of the laminated disc and the variation of the maximum radial stress with the taper configuration is plotted for different values of radius ratio.

The following Figure 4.7 shows the comparison of the induced maximum radial stress in a rotating annular thickness-tapered uni-directional laminated disc with $\delta = 10$ and with the clamped-free boundary condition for different taper configurations considered in the present study.

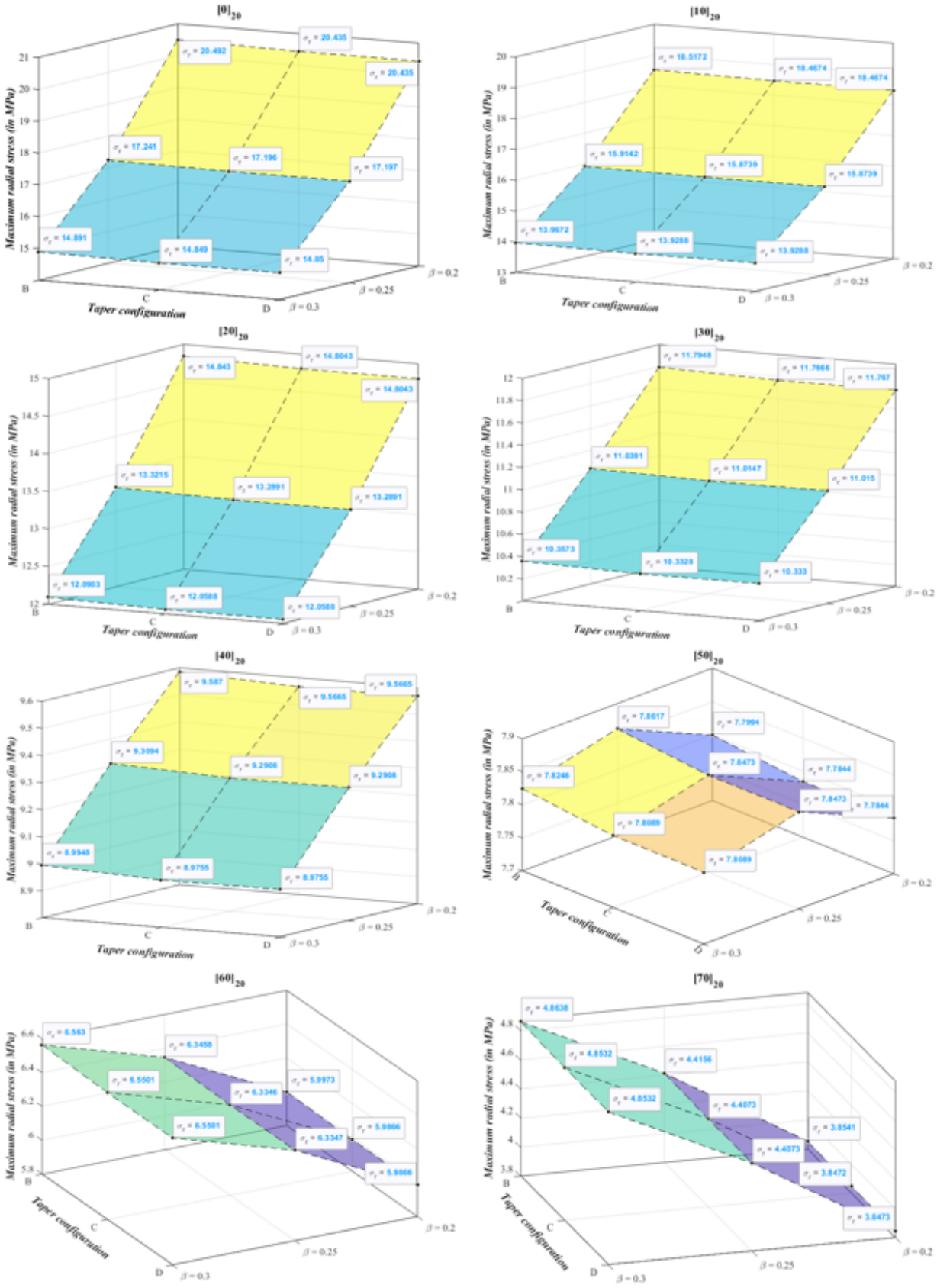
[0]20
[10]20
[20]20
[30]20
[40]20
[50]20
[60]20
[70]20
Maximum radial stress (in MPa)
Taper configuration
B
C
D
β = 0.2
β = 0.25
β = 0.3

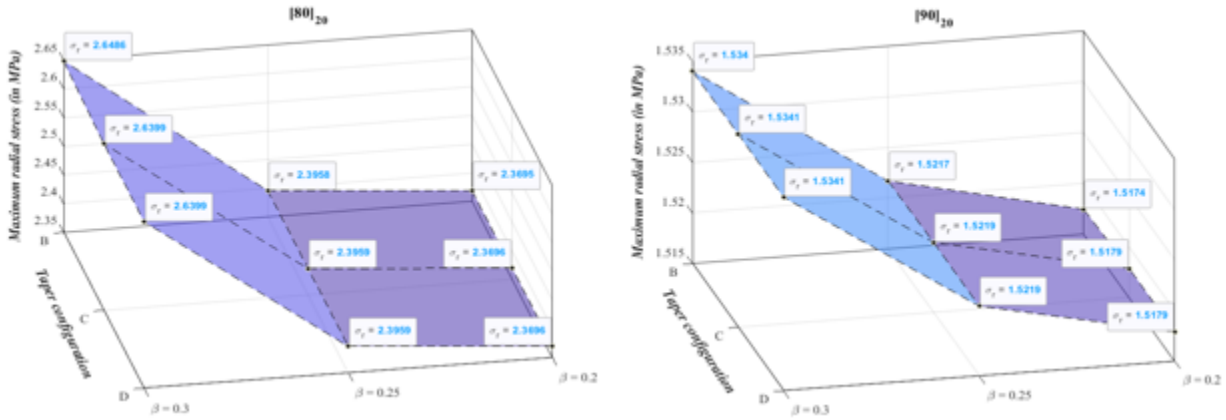

Figure 4.7 Comparison of the induced maximum radial stress corresponding to different taper configurations of a rotating annular thickness-tapered uni-directional laminated disc with 10 ply drop-off and with the clamped-free boundary condition for different values of radius ratio

It can be seen from the above Figure 4.7 that irrespective of the beta value, the rotating annular thickness-tapered uni-directional laminated disc with taper configuration B and with the clamped-free boundary condition experiences a relatively higher amount of the maximum radial stress as compared to the other taper configurations. It can also be seen that irrespective of the taper configuration, the maximum radial stress decreases with the increasing beta value of the disc up to the uni-directional configuration of $[40]_{20}$. For the tapered disc with $[50]_{20}$ laminate configuration, the maximum radial stress first tends to relatively-slightly increase with the increasing value of radius ratio from $\beta = 0.2$ to $\beta = 0.25$ and then it decreases for $\beta = 0.3$. Thereafter, from the laminate configuration of $[60]_{20}$ to $[90]_{20}$, the radial stress tends to increase with the increasing beta value of the rotating disc.

The following Figure 4.8 and Tables 4.27 – 4.29 show the variation with the fiber orientation angle and with the number of dropped plies of the maximum circumferential stress, in a rotating annular thickness-tapered uni-directional laminated disc with the clamped-free boundary condition for the beta values of 0.2, 0.25 and 0.3. The variation of the maximum circumferential stress has been shown for different taper configurations of the laminated disc considered in the present study.

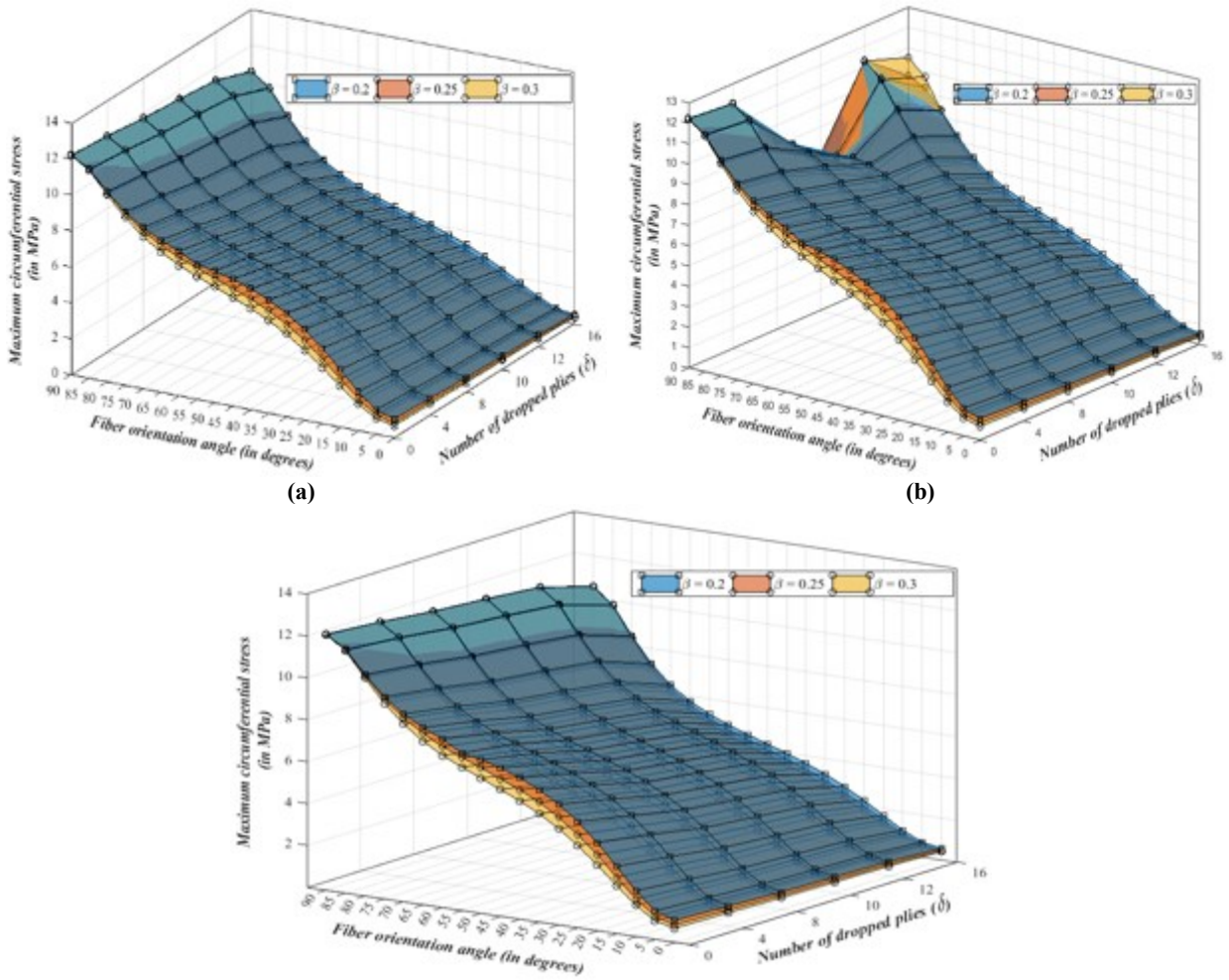

Figure 4.8 Variation of the maximum circumferential stress with the fiber orientation angle and with the number of dropped plies in a rotating annular thickness-tapered uni-directional laminated disc with different beta values for **(a)** taper configuration B, **(b)** taper configuration C and **(c)** taper configuration D

Maximum circumferential stress, σ_θ^{max} (in *MPa*) in a rotating annular thickness-tapered uni-directional laminated disc with taper configuration B and with the clamped-free boundary condition for different values of radius ratio							
Fiber orientation angle (in *degrees*)	Radius ratio	Number of dropped plies (δ)					
		0	4	8	10	12	16
0	$\beta = 0.2$	1.062	0.948	0.822	0.756	0.688	0.542
	$\beta = 0.25$	0.844	0.761	0.668	0.618	0.566	0.45
	$\beta = 0.3$	0.685	0.624	0.554	0.515	0.474	0.38
10	$\beta = 0.2$	2.199	1.964	1.707	1.572	1.433	1.135
	$\beta = 0.25$	1.803	1.622	1.426	1.32	1.209	0.965
	$\beta = 0.3$	1.501	1.364	1.21	1.126	1.036	0.832
20	$\beta = 0.2$	4.22	3.809	3.341	3.093	2.834	2.277
	$\beta = 0.25$	3.635	3.293	2.913	2.708	2.491	2.011
	$\beta = 0.3$	3.152	2.874	2.561	2.389	2.205	1.789
30	$\beta = 0.2$	5.775	5.237	4.64	4.322	3.986	3.25
	$\beta = 0.25$	5.158	4.701	4.193	3.917	3.623	2.963
	$\beta = 0.3$	4.61	4.225	3.792	3.553	3.294	2.7
40	$\beta = 0.2$	6.756	6.173	5.527	5.178	4.804	3.969
	$\beta = 0.25$	6.189	5.69	5.122	4.809	4.471	3.699
	$\beta = 0.3$	5.653	5.224	4.725	4.446	4.141	3.43
50	$\beta = 0.2$	7.339	6.86	6.215	5.858	5.472	4.581
	$\beta = 0.25$	6.958	6.451	5.867	5.539	5.18	4.338
	$\beta = 0.3$	6.462	6.015	5.491	5.192	4.861	4.073
60	$\beta = 0.2$	8.057	7.55	6.942	6.595	6.21	5.289
	$\beta = 0.25$	7.698	7.234	6.666	6.338	5.972	5.083
	$\beta = 0.3$	7.269	6.851	6.327	6.022	5.678	4.83
70	$\beta = 0.2$	8.975	8.543	8.012	7.696	7.333	6.405
	$\beta = 0.25$	8.776	8.362	7.847	7.538	7.183	6.267
	$\beta = 0.3$	8.48	8.092	7.6	7.303	6.958	6.063
80	$\beta = 0.2$	10.581	10.282	9.887	9.633	9.329	8.462
	$\beta = 0.25$	10.522	10.24	9.843	9.592	9.287	8.419
	$\beta = 0.3$	10.407	10.148	9.755	9.504	9.199	8.331
90	$\beta = 0.2$	12.233	12.026	11.739	11.545	11.304	10.551
	$\beta = 0.25$	12.226	12.019	11.732	11.54	11.296	10.543
	$\beta = 0.3$	12.197	11.998	11.711	11.518	11.274	10.518

Table 4.27 Variation of the maximum circumferential stress (in *MPa*) with the fiber orientation angle and with the number of dropped plies in a rotating annular thickness-tapered uni-directional laminated disc with taper configuration B and with the clamped-free boundary condition for different values of radius ratio

Maximum circumferential stress, σ_θ^{max} (in *MPa*) in a rotating annular thickness-tapered uni-directional laminated disc with taper configuration C and with the clamped-free boundary condition for different values of radius ratio							
Fiber orientation angle (in *degrees*)	Radius ratio	Number of dropped plies (δ)					
		0	4	8	10	12	16
0	$\beta = 0.2$	1.062	1.062	0.949	0.823	0.757	0.688
	$\beta = 0.25$	0.844	0.844	0.761	0.669	0.62	0.566
	$\beta = 0.3$	0.685	0.685	0.624	0.554	0.516	0.474
10	$\beta = 0.2$	2.199	2.199	1.964	1.707	1.572	1.432
	$\beta = 0.25$	1.803	1.803	1.622	1.425	1.32	1.209
	$\beta = 0.3$	1.501	1.501	1.364	1.211	1.131	1.036
20	$\beta = 0.2$	4.22	4.22	3.808	3.34	3.093	2.834
	$\beta = 0.25$	3.635	3.635	3.293	2.913	2.708	2.491
	$\beta = 0.3$	3.152	3.152	2.874	2.561	2.39	2.205
30	$\beta = 0.2$	5.775	5.775	5.237	4.641	4.321	3.986
	$\beta = 0.25$	5.158	5.158	4.7	4.194	3.918	3.623
	$\beta = 0.3$	4.61	4.61	4.225	3.792	3.555	3.294
40	$\beta = 0.2$	6.756	6.756	6.173	5.527	5.178	4.804
	$\beta = 0.25$	6.189	6.189	5.691	5.122	4.809	4.471
	$\beta = 0.3$	5.653	5.653	5.224	4.725	4.463	4.141
50	$\beta = 0.2$	7.339	7.339	6.86	6.215	5.858	5.471
	$\beta = 0.25$	6.958	6.958	6.451	5.867	5.552	5.18
	$\beta = 0.3$	6.462	6.462	6.015	5.491	5.205	4.861
60	$\beta = 0.2$	8.057	8.057	7.549	6.942	6.602	6.21
	$\beta = 0.25$	7.698	7.698	7.234	6.665	6.324	5.972
	$\beta = 0.3$	7.269	7.269	6.85	6.344	5.929	5.68
70	$\beta = 0.2$	8.975	8.975	8.542	8.01	7.414	7.333
	$\beta = 0.25$	8.776	8.776	8.361	7.811	7.194	7.183
	$\beta = 0.3$	8.48	8.48	8.091	7.544	6.756	6.958
80	$\beta = 0.2$	10.581	10.581	10.282	9.11	7.895	9.329
	$\beta = 0.25$	10.522	10.522	10.239	8.967	7.837	9.287
	$\beta = 0.3$	10.407	10.407	10.148	8.889	7.452	9.199
90	$\beta = 0.2$	12.233	12.233	12.025	9.317	7.595	11.308
	$\beta = 0.25$	12.226	12.226	12.019	9.189	7.656	11.305
	$\beta = 0.3$	12.197	12.197	11.998	9.286	7.368	11.282

Table 4.28 Variation of the maximum circumferential stress (in *MPa*) with the fiber orientation angle and with the number of dropped plies in a rotating annular thickness-tapered uni-directional laminated disc with taper configuration C and with the clamped-free boundary condition for different values of radius ratio

Maximum circumferential stress, σ_θ^{max} (in *MPa*) in a rotating annular thickness-tapered uni-directional laminated disc with taper configuration D and with the clamped-free boundary condition for different values of radius ratio							
Fiber orientation angle (in *degrees*)	Radius ratio	Number of dropped plies (δ)					
		0	4	8	10	12	16
0	$\beta = 0.2$	1.062	0.949	0.823	0.757	0.688	0.542
	$\beta = 0.25$	0.844	0.761	0.669	0.619	0.566	0.45
	$\beta = 0.3$	0.685	0.624	0.554	0.516	0.474	0.38
10	$\beta = 0.2$	2.199	1.964	1.707	1.572	1.432	1.134
	$\beta = 0.25$	1.803	1.622	1.425	1.32	1.209	0.965
	$\beta = 0.3$	1.501	1.364	1.211	1.126	1.036	0.832
20	$\beta = 0.2$	4.22	3.808	3.34	3.093	2.834	2.277
	$\beta = 0.25$	3.635	3.293	2.913	2.708	2.491	2.011
	$\beta = 0.3$	3.152	2.874	2.561	2.39	2.205	1.789
30	$\beta = 0.2$	5.775	5.237	4.641	4.321	3.986	3.25
	$\beta = 0.25$	5.158	4.7	4.194	3.918	3.623	2.963
	$\beta = 0.3$	4.61	4.225	3.793	3.553	3.294	2.7
40	$\beta = 0.2$	6.756	6.173	5.527	5.178	4.804	3.969
	$\beta = 0.25$	6.189	5.691	5.122	4.809	4.471	3.699
	$\beta = 0.3$	5.653	5.224	4.725	4.445	4.141	3.43
50	$\beta = 0.2$	7.339	6.86	6.215	5.858	5.471	4.581
	$\beta = 0.25$	6.958	6.451	5.867	5.539	5.18	4.338
	$\beta = 0.3$	6.462	6.015	5.491	5.192	4.861	4.073
60	$\beta = 0.2$	8.057	7.549	6.942	6.594	6.21	5.288
	$\beta = 0.25$	7.698	7.234	6.665	6.338	5.972	5.082
	$\beta = 0.3$	7.269	6.85	6.327	6.022	5.678	4.83
70	$\beta = 0.2$	8.975	8.542	8.012	7.695	7.333	6.405
	$\beta = 0.25$	8.776	8.361	7.846	7.538	7.183	6.267
	$\beta = 0.3$	8.48	8.091	7.599	7.302	6.958	6.063
80	$\beta = 0.2$	10.581	10.282	9.885	9.634	9.329	8.461
	$\beta = 0.25$	10.522	10.239	9.844	9.592	9.287	8.419
	$\beta = 0.3$	10.407	10.148	9.754	9.504	9.199	8.331
90	$\beta = 0.2$	12.233	12.025	11.738	11.547	11.305	10.55
	$\beta = 0.25$	12.226	12.019	11.732	11.539	11.296	10.543
	$\beta = 0.3$	12.197	11.998	11.711	11.517	11.274	10.518

Table 4.29 Variation of the maximum circumferential stress (in *MPa*) with the fiber orientation angle and with the number of dropped plies in a rotating annular thickness-tapered uni-directional laminated disc with taper configuration D and with the clamped-free boundary condition for different values of radius ratio

The following observations can be made from the variation of the maximum circumferential stress with the fiber orientation angle and with the number of dropped plies, in a rotating annular thickness-tapered uni-directional laminated disc with different taper configurations and with the clamped-free boundary condition for different values of radius ratio, shown in the Figure 4.8 and Tables 4.27 – 4.29:

- For the uniform-thickness uni-directional laminated disc, irrespective of the fiber orientation angle, the maximum circumferential stress decreases with the increasing beta value of the disc.
- Irrespective of the fiber orientation angle, number of dropped plies and the taper configuration of the thickness-tapered disc, the maximum circumferential stress decreases with the increasing beta value of the disc. This observation holds true for the rotating annular thickness-tapered uni-directional laminated discs with taper configurations B and D. However, for the disc with taper configuration C, this observation is valid only for δ = 4, 8, 10 and 12. For the disc with δ = 16, the maximum circumferential stress first decreases with the increasing beta value of the disc for the fiber orientation angle from $\theta = 0°$ to $\theta = 70°$. Thereafter, as the fiber orientation angle is increased till 90°, the circumferential stress tends to relatively-slightly increase with the increasing beta value of the disc. It should be noted that this observation only holds true for a thickness-tapered disc with δ = 16 and with taper configuration C.

To study the effect of taper configuration on the induced maximum circumferential stress, a thickness-tapered disc with a specific number of dropped plies, i.e. δ = 10 is chosen for the uni-directional configurations of the laminated disc and the variation of the maximum circumferential stress with the taper configuration is plotted for different values of radius ratio. The following Figure 4.9 shows the comparison of the induced maximum circumferential stress in a rotating annular thickness-tapered uni-directional laminated disc with δ = 10 and with the clamped-free boundary condition for different taper configurations considered in the present study.

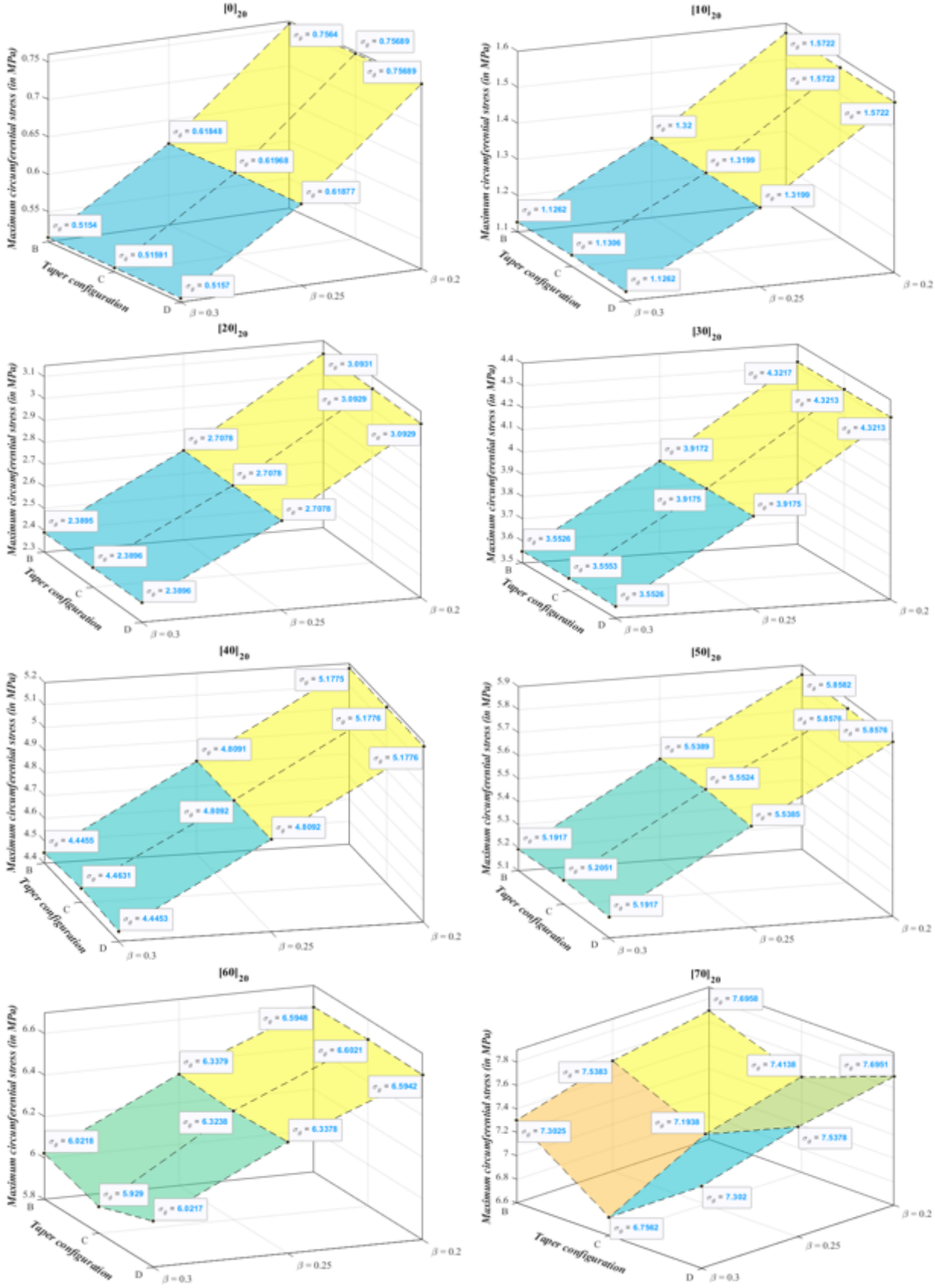
$[0]_{20}$
$[10]_{20}$
$[20]_{20}$
$[30]_{20}$
$[40]_{20}$
$[50]_{20}$
$[60]_{20}$
$[70]_{20}$
Maximum circumferential stress (in MPa)
Taper configuration
B
C
D
$\beta = 0.3$
$\beta = 0.25$
$\beta = 0.2$

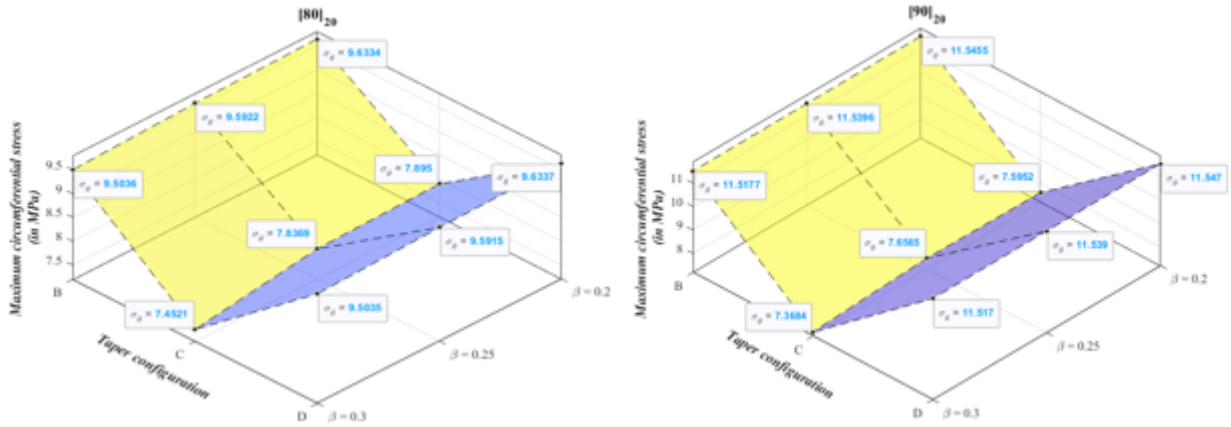

Figure 4.9 Comparison of the induced maximum circumferential stress corresponding to different taper configurations of a rotating annular thickness-tapered uni-directional laminated disc with 10 ply drop-off and with the clamped-free boundary condition for different values of radius ratio

It can be seen from the above Figure 4.9 that irrespective of the beta value, the rotating annular thickness-tapered uni-directional laminated disc with taper configuration C and with the laminate configuration from $[70]_{20}$ to $[90]_{20}$ experiences a significantly lesser amount of circumferential stress as compared to the taper configurations B and D. It can also be seen that for the thickness-tapered disc with $\delta = 10$, irrespective of the taper configuration and the uni-directional laminate configuration, the maximum circumferential stress decreases with the increasing beta value of the thickness-tapered disc.

The following Table 4.30 and Figure 4.10 show the variation with the fiber orientation angle and with the number of dropped plies of the maximum radial displacement, in a rotating annular thickness-tapered uni-directional laminated disc with the clamped-free boundary condition for the beta values of 0.2, 0.25 and 0.3. Note that the following graph for the variation of the maximum radial displacement with the fiber orientation angle and with the number of dropped plies for different beta values is valid for every taper configuration of the thickness-tapered uni-directional laminated disc considered in the present study.

Maximum radial displacement, u_r^{max} (in mm) in a rotating annular thickness-tapered uni-directional laminated disc with the clamped-free boundary condition for different values of radius ratio							
Fiber orientation angle (in *degrees*)	Radius ratio	Number of dropped plies (δ)					
		0	4	8	10	12	16
0	$\beta = 0.2$	0.00864	0.00786	0.00699	0.00652	0.00601	0.00484
	$\beta = 0.25$	0.00729	0.00668	0.00599	0.0056	0.00518	0.0042
	$\beta = 0.3$	0.00615	0.00568	0.00512	0.00481	0.00446	0.00364
10	$\beta = 0.2$	0.01507	0.01379	0.01234	0.01154	0.01067	0.00866
	$\beta = 0.25$	0.01297	0.01194	0.01075	0.01008	0.00934	0.00762
	$\beta = 0.3$	0.01112	0.01029	0.00932	0.00877	0.00815	0.00668
20	$\beta = 0.2$	0.02604	0.02413	0.02183	0.02053	0.01911	0.01574
	$\beta = 0.25$	0.02326	0.0216	0.01962	0.01849	0.01724	0.01423
	$\beta = 0.3$	0.02049	0.01914	0.01746	0.01649	0.01541	0.01276
30	$\beta = 0.2$	0.03354	0.03153	0.02879	0.02721	0.02547	0.02124
	$\beta = 0.25$	0.03107	0.029	0.02654	0.02513	0.02354	0.01966
	$\beta = 0.3$	0.02812	0.02633	0.02418	0.02293	0.02151	0.01799
40	$\beta = 0.2$	0.03695	0.03517	0.03234	0.0307	0.02886	0.02432
	$\beta = 0.25$	0.03515	0.03298	0.03039	0.02887	0.02716	0.0229
	$\beta = 0.3$	0.03244	0.03051	0.02818	0.0268	0.02524	0.02129
50	$\beta = 0.2$	0.03706	0.03566	0.03303	0.03149	0.02974	0.02532
	$\beta = 0.25$	0.03599	0.03398	0.03152	0.03006	0.02839	0.02417
	$\beta = 0.3$	0.03377	0.03194	0.02967	0.02832	0.02677	0.02279
60	$\beta = 0.2$	0.03403	0.03305	0.03092	0.02964	0.02815	0.02431
	$\beta = 0.25$	0.03364	0.032	0.02995	0.02871	0.02727	0.02353
	$\beta = 0.3$	0.03213	0.03058	0.02864	0.02747	0.0261	0.0225
70	$\beta = 0.2$	0.0274	0.02684	0.02547	0.02461	0.0236	0.02083
	$\beta = 0.25$	0.02748	0.02642	0.02507	0.02423	0.02322	0.02048
	$\beta = 0.3$	0.02679	0.02577	0.02444	0.02362	0.02264	0.01993
80	$\beta = 0.2$	0.01769	0.01744	0.01687	0.01649	0.01603	0.01464
	$\beta = 0.25$	0.01775	0.01739	0.01681	0.01644	0.01597	0.01458
	$\beta = 0.3$	0.01765	0.01727	0.01669	0.01632	0.01585	0.01446
90	$\beta = 0.2$	0.01156	0.01143	0.01119	0.01102	0.01081	0.01014
	$\beta = 0.25$	0.01155	0.01142	0.01118	0.01102	0.01081	0.01013
	$\beta = 0.3$	0.01154	0.0114	0.01116	0.011	0.01079	0.01011

Table 4.30 Variation of the maximum radial displacement (in *mm*) with the fiber orientation angle and with the number of dropped plies in a rotating annular thickness-tapered uni-directional laminated disc with the clamped-free boundary condition for different values of radius ratio

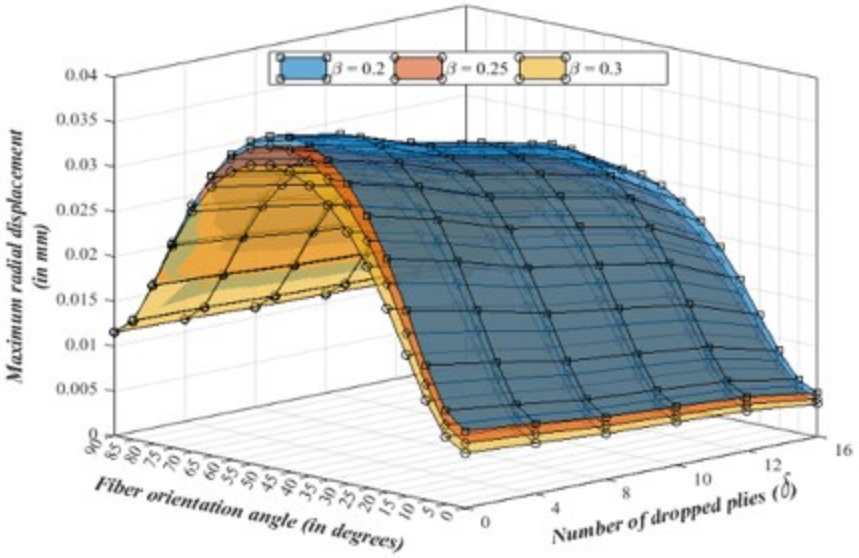

Figure 4.10 Variation of the maximum radial displacement with the fiber orientation angle and with the number of dropped plies in a rotating annular thickness-tapered uni-directional laminated disc with the clamped-free boundary condition for different values of radius ratio

It can be seen from the above Figure 4.10 and Table 4.30 that irrespective of the fiber orientation angle, the maximum radial displacement in the rotating annular thickness-tapered uni-directional laminated disc decreases with the increasing beta value of the disc. However, irrespective of the number of dropped plies, the decrease in the maximum radial displacement with the increasing beta value of the thickness-tapered disc is not that significant for the fiber orientation angle from $\theta = 80°$ to $90°$.

4.7.2 Cross-ply laminated discs

This sub-section presents the parametric study on the elastic response of rotating annular thickness-tapered discs made up of Graphite-Fiber Reinforced Plastic material and with various cross-ply laminate configurations and for the clamped-free boundary condition. The relative effects of $0°$ plies, radius ratio values, numbers of dropped plies and the taper configurations on the radial stress and circumferential stress distributions and on the radial displacement distribution in the rotating annular thickness-tapered fiber-reinforced composite discs with various cross-ply configurations and with the clamped-free boundary condition are studied. The various cross-ply configurations of the laminated disc have been mentioned earlier in the Table 3.23. Graphical

results for the stress and displacement distributions are presented and the percentage changes in the maximum stress and maximum displacement values with the number of dropped plies are calculated for different taper configurations of the cross-ply laminated disc.

4.7.2.1 Effect of dropped plies on the elastic response of cross-ply laminated discs

The effect of dropped plies on the radial and circumferential stress distributions and on the radial displacement distribution in a rotating annular thickness-tapered cross-ply laminated disc with the clamped-free boundary condition is studied for different taper configurations considered in the present thesis. To study the effect of dropped plies on the elastic response of cross-ply laminated disc with varying number of 0° plies, a rotating disc with a beta value of 0.2 is chosen. Therefore, corresponding to this beta value, the disc has an inner radius of r_i = 24 *mm*, an outer radius of r_o = 120 *mm*, thickness at the hub of h_i = 2.4 *mm* with an individual ply thickness of t_k = 0.12 *mm,* and is rotating at a constant angular velocity of ω = 1000 *rad/s* i.e. 9554.14 *rpm*.

The following Figure 4.11 and Tables 4.31 – 4.33 show the variation with the number of dropped plies of the maximum radial stress, in a rotating annular thickness-tapered cross-ply laminated disc with varying number of 0° plies and with the clamped-free boundary condition. The variation of the maximum radial stress has been shown for different taper configurations of the laminated disc considered in the present study.

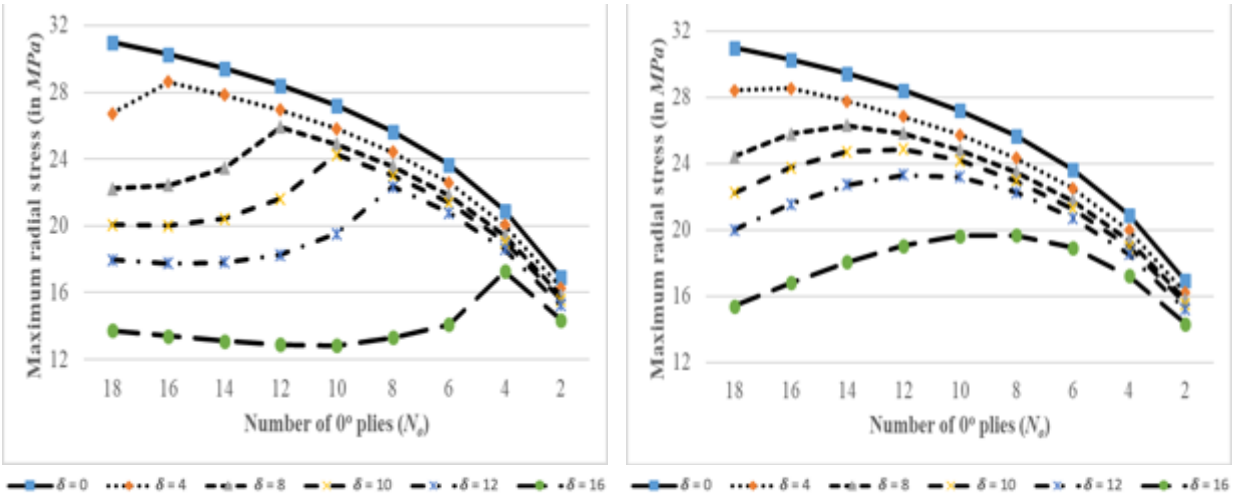

(a) **(b)**

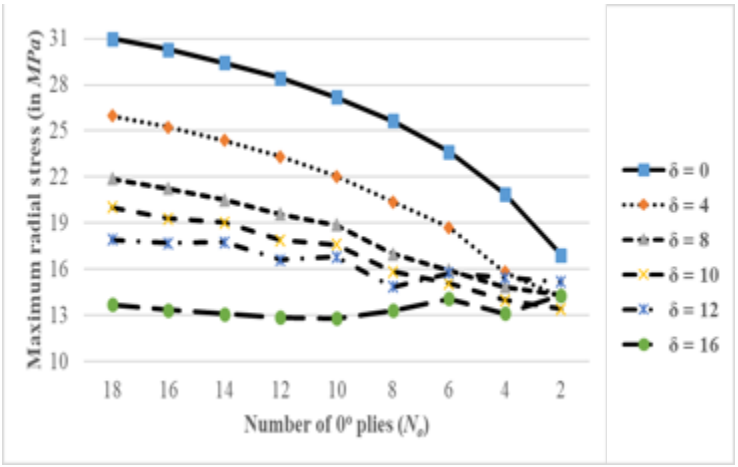

(c)

Figure 4.11 Variation of the maximum radial stress with the number of dropped plies in a rotating annular thickness-tapered cross-ply laminated disc with varying number of 0° plies and with the clamped-free boundary condition for **(a)** taper configuration B, **(b)** taper configuration C and **(c)** taper configuration D

Maximum radial stress, σ_r^{max} (in MPa) in a rotating annular thickness-tapered cross-ply laminated disc with taper configuration B and with the clamped-free boundary condition						
$\beta = 0.2$						
Number of 0° plies (N_o)	Number of dropped plies (δ)					
	0	4	8	10	12	16
18	31.003	26.743	22.218	20.076	17.955	13.741
16	30.273	28.626	22.426	20.018	17.742	13.392
14	29.425	27.853	23.458	20.431	17.806	13.108
12	28.42	26.938	25.922	21.617	18.277	12.896
10	27.197	25.824	24.884	24.271	19.515	12.819
8	25.661	24.423	23.576	23.022	22.349	13.324
6	23.653	22.582	21.852	21.373	20.79	14.1
4	20.902	20.032	19.443	19.06	18.593	17.286
2	16.923	16.281	15.839	15.566	15.242	14.364

Table 4.31 Variation of the maximum radial stress (in MPa) with the number of dropped plies in a rotating annular thickness-tapered cross-ply laminated disc with taper configuration B and with the clamped-free boundary condition for varying number of 0° plies

Maximum radial stress, σ_r^{max} (in MPa) in a rotating annular thickness-tapered cross-ply laminated disc with taper configuration C and with the clamped-free boundary condition						
$\beta = 0.2$						
Number of 0° plies (N_o)	Number of dropped plies (δ)					
	0	4	8	10	12	16
18	31.003	28.415	24.416	22.225	19.985	15.407
16	30.273	28.529	25.805	23.773	21.551	16.787
14	29.425	27.757	26.303	24.713	22.727	18.047
12	28.42	26.844	25.832	24.872	23.323	19.048
10	27.197	25.732	24.796	24.186	23.196	19.638
8	25.661	24.333	23.49	22.939	22.269	19.653
6	23.653	22.496	21.77	21.294	20.713	18.918
4	20.902	19.952	19.367	18.985	18.521	17.22
2	16.923	16.214	15.775	15.503	15.18	14.306

Table 4.32 Variation of the maximum radial stress (in *MPa*) with the number of dropped plies in a rotating annular thickness-tapered cross-ply laminated disc with taper configuration C and with the clamped-free boundary condition for varying number of 0° plies

Maximum radial stress, σ_r^{max} (in MPa) in a rotating annular thickness-tapered cross-ply laminated disc with taper configuration D and with the clamped-free boundary condition						
$\beta = 0.2$						
Number of 0° plies (N_o)	Number of dropped plies (δ)					
	0	4	8	10	12	16
18	31.003	25.967	21.868	20.02	17.907	13.707
16	30.273	25.232	21.224	19.275	17.695	13.359
14	29.425	24.367	20.495	19.041	17.759	13.076
12	28.42	23.324	19.582	17.895	16.605	12.866
10	27.197	22.029	18.877	17.595	16.786	12.79
8	25.661	20.362	16.988	15.841	14.857	13.302
6	23.653	18.704	15.933	15.085	15.751	14.08
4	20.902	15.803	14.855	13.994	15.453	13.133
2	16.923	14.214	14.345	13.403	15.18	14.306

Table 4.33 Variation of the maximum radial stress (in *MPa*) with the number of dropped plies in a rotating annular thickness-tapered cross-ply laminated disc with taper configuration D and with the clamped-free boundary condition for varying number of 0° plies

The following observations can be made from the variation of the maximum radial stress with the number of dropped plies, in a rotating annular thickness-tapered cross-ply laminated disc with varying number of 0° plies and with the clamped-free boundary condition for different taper configurations, shown in the Figure 4.11 and Tables 4.31 – 4.33:

- Irrespective of the taper configuration and the number of 0° plies, the maximum radial stress decreases with the increasing number of dropped plies and is the least for a cross-ply disc with δ = 16. This observation holds true for the thickness-tapered cross-ply discs with taper configurations B and C. However, for the cross-ply disc with taper configuration D, the variation of the maximum radial stress with the increasing number of dropped plies can be elaborated as follows:
  - I. For the cross-ply disc with taper configuration D and with N_o = 18 up to N_o = 8, the maximum radial stress decreases with the increasing number of dropped plies.
  - II. For the cross-ply disc with N_o = 6, the maximum radial stress corresponding to δ = 12 (15.751 *MPa*) is greater than the stress corresponding to δ = 10 (15.085 *MPa*). That is, for the cross-ply disc with 6 plies oriented at 0°, the radial stress increases as the number of dropped plies is increased from 10 to 12.
  - III. For the cross-ply disc with N_o = 4, the maximum radial stress corresponding to δ = 12 (15.453 *MPa*) is greater than the stress corresponding to δ = 8 (14.855 *MPa*) and δ = 10 (13.994 *MPa*). In other words, for the cross-ply disc with 4 plies oriented at 0°, the radial stress increases as the number of dropped plies is increased from 8 to 12.
  - IV. For the cross-ply disc with N_o = 2, the maximum radial stress corresponding to δ = 12 (15.18 *MPa*) is greater than the stresses corresponding to δ = 4, 8 and 10 (which are 14.214 *MPa*, 14.345 *MPa* and 13.403 *MPa* respectively). In other words, for a cross-ply disc with only 2 plies oriented at 0°, the radial stress increases as the number of dropped plies is increased from 4 to 12.
- For the cross-ply disc with δ = 4 and taper configurations B and C, the maximum radial stress first increases with decreasing number of 0° plies from N_o = 18 to N_o = 16, i.e., from 26.743 *MPa* to 28.626 *MPa* for taper configuration B and from

28.415 *MPa* to 28.529 *MPa* for taper configuration C, and then the radial stress decreases with the decreasing number of 0° plies. However, the increase of the radial stress corresponding to N_o = 18 to N_o = 16 for the taper configuration C is not that significant.

- For the cross-ply disc with δ = 8, the maximum radial stress first increases with the decreasing value of N_o from N_o = 18 (22.218 *MPa*) to N_o = 12 (25.922 *MPa*) for taper configuration B, and from N_o = 18 (24.416 *MPa*) to N_o = 14 (26.303 *MPa*) for taper configuration C. The radial stress then decreases with the decreasing number of 0° plies. However, for a cross-ply disc with taper configuration D, irrespective of the number of dropped plies, the maximum radial stress always decreases with the decreasing number of 0° plies.
- For the cross-ply disc with δ = 10, the maximum radial stress first increases with the decreasing value of N_o from N_o = 18 (20.076 *MPa*) to N_o = 10 (24.271 *MPa*) for taper configuration B, and from N_o = 18 (22.225 *MPa*) to N_o = 12 (24.872 *MPa*) for taper configuration C. The radial stress then decreases with the decreasing number of 0° plies till $N_o = 2$.
- For a cross-ply disc with δ = 12, the maximum radial stress first increases with the decreasing value of N_o from N_o = 18 (17.955 *MPa*) to N_o = 8 (22.349 *MPa*) for taper configuration B, and from N_o = 18 (19.985 *MPa*) to N_o = 12 (23.323 *MPa*) for taper configuration C. The radial stress then decreases with the decreasing number of 0° plies till N_o = 2.
- For a cross-ply disc with δ = 16, the maximum radial stress first increases with the decreasing value of N_o from N_o = 18 (13.741 *MPa*) to N_o = 4 (17.286 *MPa*) for taper configuration B, and from N_o = 18 (15.407 *MPa*) to N_o = 8 (19.653 *MPa*) for taper configuration C. The radial stress then decreases with the decreasing number of 0° plies till N_o = 2.

The following Figure 4.12 and Tables 4.34 – 4.36 show the variation with the number of dropped plies of the maximum circumferential stress, in a rotating annular thickness-tapered cross-ply laminated disc with varying number of 0° plies and with the clamped-free boundary condition.

The variation of the maximum circumferential stress has been shown for different taper configurations of the laminated disc considered in the present study.

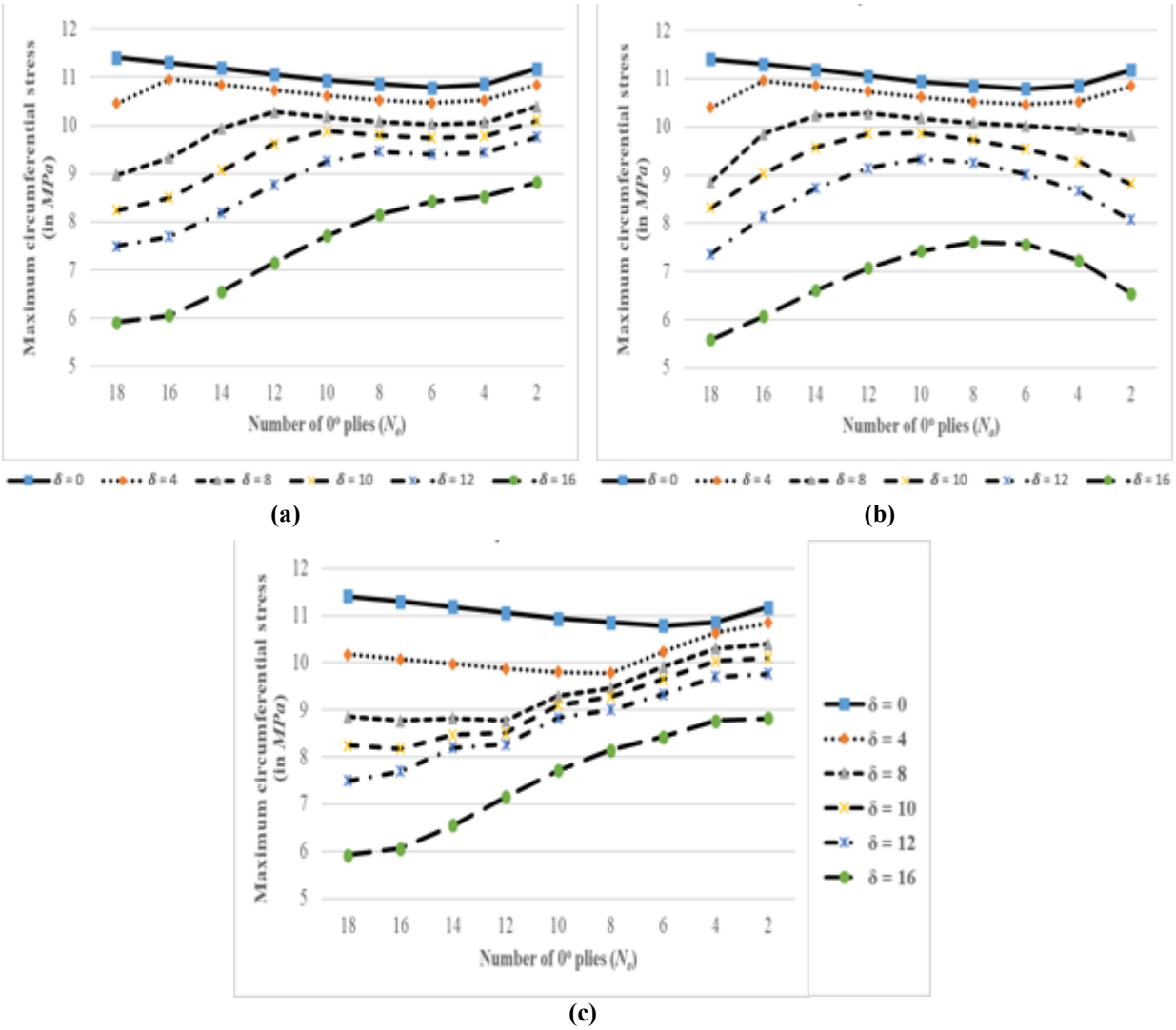

Figure 4.12 Variation of the maximum circumferential stress with the number of dropped plies in a rotating annular thickness-tapered cross-ply laminated disc with varying number of 0° plies and with the clamped-free boundary condition for **(a)** taper configuration B, **(b)** taper configuration C and **(c)** taper configuration D

Maximum circumferential stress, σ_θ^{max} (in MPa) in a rotating annular thickness-tapered cross-ply laminated disc with taper configuration B and with the clamped-free boundary condition						
$\beta = 0.2$						
Number of 0° plies (N_o)	Number of dropped plies (δ)					
	0	4	8	10	12	16
18	11.404	10.455	8.971	8.243	7.497	5.914
16	11.302	10.958	9.329	8.5	7.697	6.059
14	11.189	10.847	9.942	9.065	8.196	6.554
12	11.06	10.734	10.281	9.619	8.777	7.157
10	10.934	10.622	10.175	9.889	9.25	7.714
8	10.858	10.524	10.08	9.798	9.461	8.151
6	10.784	10.468	10.022	9.742	9.406	8.429
4	10.853	10.52	10.068	9.782	9.444	8.532
2	11.182	10.844	10.391	10.104	9.76	8.818

Table 4.34 Variation of the maximum circumferential stress (in *MPa*) with the number of dropped plies in a rotating annular thickness-tapered cross-ply laminated disc with taper configuration B and with the clamped-free boundary condition for varying number of 0° plies

Maximum circumferential stress, σ_θ^{max} (in MPa) in a rotating annular thickness-tapered cross-ply laminated disc with taper configuration C and with the clamped-free boundary condition						
$\beta = 0.2$						
Number of 0° plies (N_o)	Number of dropped plies (δ)					
	0	4	8	10	12	16
18	11.404	10.399	8.851	8.315	7.364	5.589
16	11.302	10.958	9.85	9.028	8.132	6.074
14	11.189	10.847	10.231	9.571	8.727	6.609
12	11.06	10.733	10.281	9.864	9.142	7.077
10	10.934	10.622	10.174	9.873	9.327	7.427
8	10.858	10.524	10.079	9.729	9.254	7.609
6	10.784	10.468	10.019	9.544	9.017	7.567
4	10.853	10.52	9.95	9.278	8.674	7.235
2	11.182	10.843	9.825	8.815	8.08	6.54

Table 4.35 Variation of the maximum circumferential stress (in *MPa*) with the number of dropped plies in a rotating annular thickness-tapered cross-ply laminated disc with taper configuration C and with the clamped-free boundary condition for varying number of 0° plies

Maximum circumferential stress, σ_θ^{max} (in *MPa*) in a rotating annular thickness-tapered cross-ply laminated disc with taper configuration D and with the clamped-free boundary condition						
$\beta = 0.2$						
Number of 0° plies (N_o)	Number of dropped plies (δ)					
	0	4	8	10	12	16
18	11.404	10.169	8.846	8.243	7.498	5.914
16	11.302	10.07	8.765	8.174	7.697	6.059
14	11.189	9.969	8.817	8.464	8.197	6.554
12	11.06	9.875	8.77	8.504	8.268	7.157
10	10.934	9.8	9.294	9.101	8.826	7.713
8	10.858	9.78	9.46	9.276	8.999	8.151
6	10.784	10.234	9.916	9.653	9.327	8.428
4	10.853	10.631	10.309	10.037	9.702	8.767
2	11.182	10.843	10.391	10.104	9.76	8.818

Table 4.36 Variation of the maximum circumferential stress (in *MPa*) with the number of dropped plies in a rotating annular thickness-tapered cross-ply laminated disc with taper configuration D and with the clamped-free boundary condition for varying number of 0° plies

The following observations can be made from the variation of the maximum circumferential stress with the number of dropped plies, in a rotating annular thickness-tapered cross-ply laminated disc with varying number of 0° plies and with the clamped-free boundary condition for different taper configurations, shown in the Figure 4.12 and Tables 4.34 – 4.36:

- Irrespective of the taper configuration and the number of 0° plies, the maximum circumferential stress decreases with the increasing number of dropped plies in a rotating annular thickness-tapered cross-ply laminated disc with the clamped-free boundary condition.
- For the cross-ply disc with $\delta = 4$ and with taper configurations B and C, the maximum circumferential stress first increases with the decreasing value of N_o from $N_o = 18$ to $N_o = 16$, i.e. from 10.455 *MPa* to 10.958 *MPa* for taper configuration B, and from 10.399 *MPa* to 10.958 *MPa* for taper configuration C. The circumferential stress then decreases with the decreasing number of 0° plies till $N_o = 6$. Afterward, as the 0° plies are further reduced, the circumferential stress starts to increase with decreasing value of N_o till $N_o = 2$. Apparently, for the cross-

ply disc with the taper configuration D, the circumferential stress first decreases with the decreasing value of N_o from N_o = 18 (10.169 *MPa*) to N_o = 8 (9.78 *MPa*) and then the stress increases significantly till N_o = 2 (10.843 *MPa*).

- For the cross-ply disc with δ = 8 and taper configuration B, the maximum circumferential stress first increases significantly with the decreasing number of 0° plies from N_o = 18 to N_o = 12, i.e. from 8.971 *MPa* to 10.281 *MPa* and then the stress decreases with the decreasing value of N_o till N_o = 6, however, the decrease in the stress is not that significant. Afterward, the circumferential starts to increase with decreasing value of N_o till N_o = 2 (10.391 *MPa*). For the cross-ply disc with taper configuration C, the circumferential stress increases with the decreasing value of N_o from N_o = 18 (8.851 *MPa*) to N_o = 12 (10.281 *MPa*) and then the stress decreases with decreasing value of N_o till N_o = 2 (9.825 *MPa*). For the disc with taper configuration D, the circumferential stress first relatively-slightly decreases with the decreasing value of N_o from N_o = 18 (8.846 *MPa*) to N_o = 12 (8.77 *MPa*) and then increases significantly till N_o = 2 (10.391 *MPa*).
- For the cross-ply disc with δ = 10 and taper configuration B, the maximum circumferential stress first increases significantly with the decreasing value of N_o from N_o = 18 to N_o = 10, i.e. from 8.243 *MPa* to 9.889 *MPa* and then decreases with the decreasing number of 0° plies till N_o = 6, however, the decrease in stress is not that significant. Afterward, the circumferential stress increases with decreasing value of N_o till N_o = 2 (10.104 *MPa*). For the cross-ply disc with taper configuration C, the circumferential stress first increases with the decreasing value of N_o from N_o = 18 (8.315 *MPa*) to N_o = 10 (9.873 *MPa*) and then the stress decreases with decreasing value of N_o till N_o = 2 (8.815 *MPa*). For the disc with taper configuration D, the circumferential stress relatively-slightly decreases with the decreasing value of N_o from N_o = 18 (8.243 *MPa*) to N_o = 16 (8.174 *MPa*) and then increases significantly till N_o = 2 (10.104 *MPa*).
- For the cross-ply disc with δ = 12 and taper configurations B and D, the maximum circumferential stress increases with the decreasing value of N_o from N_o = 18 to N_o = 2, i.e. from 7.497 *MPa* to 9.76 *MPa* for the taper configuration B, and from 7.498 *MPa* to 9.76 *MPa* for the taper configuration D. For the cross-ply disc with

taper configuration C, the circumferential stress first increases with the decreasing value of N_o from N_o = 18 (7.364 *MPa*) to N_o = 10 (9.327 *MPa*) and then the stress decreases with decreasing value of N_o till N_o = 2 (8.08 *MPa*).

- For the cross-ply disc with δ = 16 and taper configurations B and D, the maximum circumferential stress increases with the decreasing value of N_o from N_o = 18 to N_o = 2, i.e. from 5.914 *MPa* to 8.818 *MPa* for the taper configurations B and D. For the cross-ply disc with the taper configuration C, the circumferential stress first increases with the decreasing value of N_o from N_o = 18 (5.589 *MPa*) to N_o = 8 (7.609 *MPa*) and then the stress decreases with decreasing value of N_o till N_o = 2 (6.54 *MPa*).

The following Figure 4.13 and Tables 4.37 – 4.39 shows the variation with the number of dropped plies of the maximum radial displacement, in a rotating annular thickness-tapered cross-ply laminated disc with varying number of 0° plies and with the clamped-free boundary condition. The variation of the maximum radial displacement has been shown for different taper configurations of the laminated disc considered in the present study.

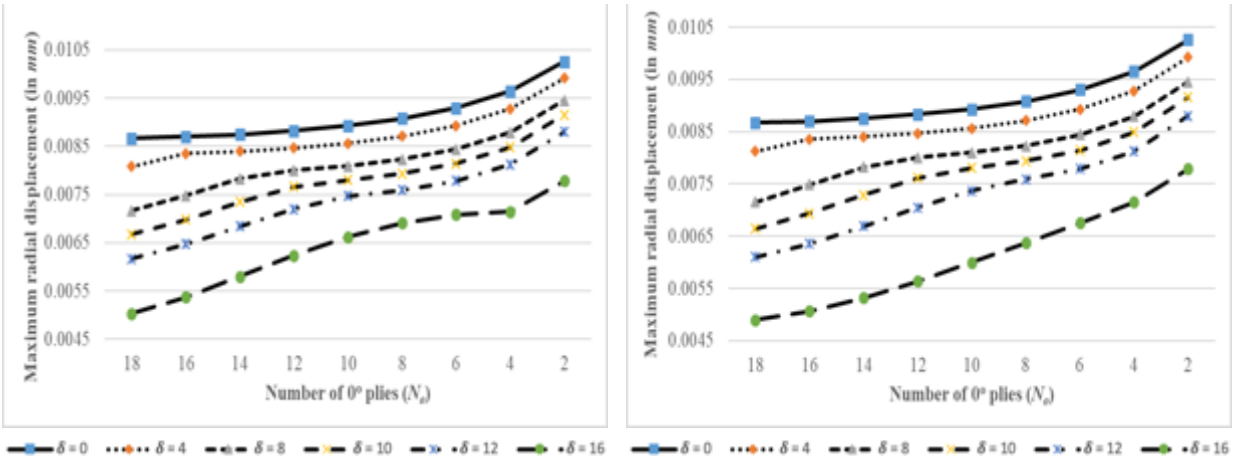

(a) **(b)**

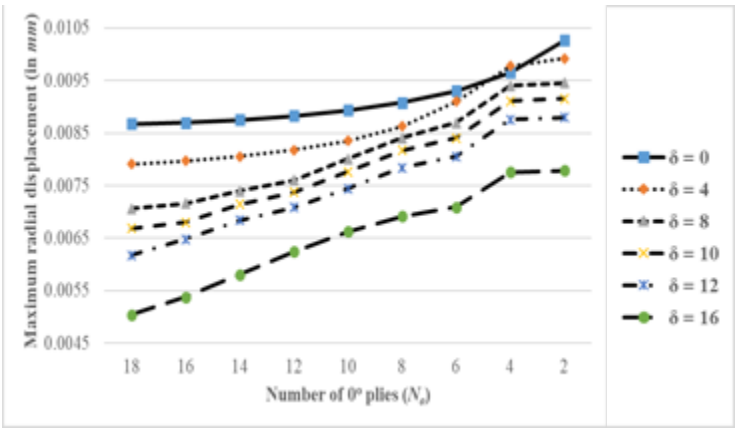

(c)

Figure 4.13 Variation of the maximum radial displacement with the number of dropped plies in a rotating annular thickness-tapered cross-ply laminated disc with varying number of 0° plies and with the clamped-free boundary condition for **(a)** taper configuration B, **(b)** taper configuration C and **(c)** taper configuration D

Maximum radial displacement, u_r^{max} (in mm) in a rotating annular thickness-tapered cross-ply laminated disc with taper configuration B and with the clamped-free boundary condition						
$\beta = 0.2$						
Number of 0° plies (N_o)	Number of dropped plies (δ)					
	0	4	8	10	12	16
18	0.00867	0.00809	0.00716	0.00668	0.00617	0.00504
16	0.0087	0.00835	0.00748	0.00699	0.00648	0.00538
14	0.00875	0.0084	0.00783	0.00735	0.00684	0.0058
12	0.00883	0.00847	0.00801	0.00766	0.0072	0.00624
10	0.00893	0.00857	0.0081	0.00781	0.00748	0.00663
8	0.00908	0.00871	0.00823	0.00794	0.00759	0.00691
6	0.0093	0.00893	0.00844	0.00814	0.00779	0.00709
4	0.00965	0.00928	0.00879	0.00849	0.00813	0.00715
2	0.01026	0.00992	0.00946	0.00916	0.0088	0.00779

Table 4.37 Variation of the maximum radial displacement (in mm) with the number of dropped plies in a rotating annular thickness-tapered cross-ply laminated disc with taper configuration B and with the clamped-free boundary condition for varying number of 0° plies

Maximum radial displacement, u_r^{max} (in mm) in a rotating annular thickness-tapered cross-ply laminated disc with taper configuration C and with the clamped-free boundary condition						
$\beta = 0.2$						
Number of 0° plies (N_o)	Number of dropped plies (δ)					
	0	4	8	10	12	16
18	0.00867	0.00812	0.00715	0.00664	0.00611	0.0049
16	0.0087	0.00835	0.00749	0.00694	0.00635	0.00507
14	0.00875	0.0084	0.00782	0.00729	0.00669	0.00533
12	0.00883	0.00847	0.00801	0.00761	0.00705	0.00564
10	0.00893	0.00857	0.0081	0.00781	0.00737	0.006
8	0.00908	0.00871	0.00823	0.00794	0.00759	0.00638
6	0.0093	0.00893	0.00844	0.00814	0.00779	0.00676
4	0.00965	0.00928	0.00879	0.00849	0.00813	0.00715
2	0.01026	0.00992	0.00946	0.00916	0.0088	0.00779

Table 4.38 Variation of the maximum radial displacement (in *mm*) with the number of dropped plies in a rotating annular thickness-tapered cross-ply laminated disc with taper configuration C and with the clamped-free boundary condition for varying number of 0° plies

Maximum radial displacement, u_r^{max} (in mm) in a rotating annular thickness-tapered cross-ply laminated disc with taper configuration D and with the clamped-free boundary condition						
$\beta = 0.2$						
Number of 0° plies (N_o)	Number of dropped plies (δ)					
	0	4	8	10	12	16
18	0.00867	0.00791	0.00706	0.00668	0.00618	0.00504
16	0.0087	0.00797	0.00716	0.0068	0.00648	0.00538
14	0.00875	0.00805	0.0074	0.00714	0.00684	0.00581
12	0.00883	0.00817	0.0076	0.00738	0.00709	0.00624
10	0.00893	0.00835	0.00801	0.00776	0.00744	0.00663
8	0.00908	0.00863	0.0084	0.00817	0.00784	0.00691
6	0.0093	0.0091	0.0087	0.00841	0.00805	0.00709
4	0.00965	0.00977	0.0094	0.00911	0.00876	0.00776
2	0.01026	0.00992	0.00946	0.00916	0.0088	0.00779

Table 4.39 Variation of the maximum radial displacement (in *mm*) with the number of dropped plies in a rotating annular thickness-tapered cross-ply laminated disc with taper configuration D and with the clamped-free boundary condition for varying number of 0° plies

The following observations can be made from the variation of the maximum radial displacement with the number of dropped plies, in a rotating annular thickness-tapered cross-ply laminated disc with varying number of 0° plies and with the clamped-free boundary condition for different taper configurations, shown in the Figure 4.13 and Tables 4.37 – 4.39:

- Irrespective of the taper configuration and the number of 0° plies, the maximum radial displacement in a rotating annular thickness-tapered cross-ply laminated disc with the clamped-free boundary condition decreases with the increasing number of dropped plies.
- Irrespective of the taper configuration and the number of dropped plies, the maximum radial displacement in a rotating annular thickness-tapered cross-ply laminated disc with the clamped-free boundary condition increases with the decreasing number of 0° plies.
- Irrespective of the number of dropped plies and 0° plies, on comparing the maximum radial displacement corresponding to different taper configurations, it can be observed that the thickness-tapered cross-ply laminated disc with taper configuration C is subjected to the maximum amount of radial displacement. However, the amount of radial displacement is approximately the same corresponding to different taper configurations for a cross-ply disc with $N_o = 2$.

4.7.2.2 Effect of radius ratio on the elastic response of cross-ply laminated discs

The effect of radius ratio on the radial and circumferential stress distributions and on the radial displacement distribution in a rotating annular thickness-tapered cross-ply laminated disc with the clamped-free boundary condition is studied for different taper configurations considered in the present thesis. The variations of the maximum radial and circumferential stresses and the maximum radial displacement with the number of 0° plies and with the number of dropped plies are studied for the rotating annular thickness-tapered cross-ply laminated discs with the beta values of 0.2, 0.25 and 0.3.

The disc has a fixed outer radius of r_o = 120 mm, thickness at the hub of h_i = 2.4 mm with an individual ply thickness of t_k = 0.12 mm, and is rotating at a constant angular velocity of ω =

1000 *rad/s* i.e. 9554.14 *rpm*. The inner radius of the disc is dependent on the beta value taken into consideration which has been mentioned earlier in the Table 3.16.

The following Figure 4.14 shows the variation with the number of dropped plies and with the taper configuration of the maximum radial stress, in a rotating annular thickness-tapered cross-ply laminated disc with varying number of 0° plies and with the clamped-free boundary condition for the above-considered beta values.

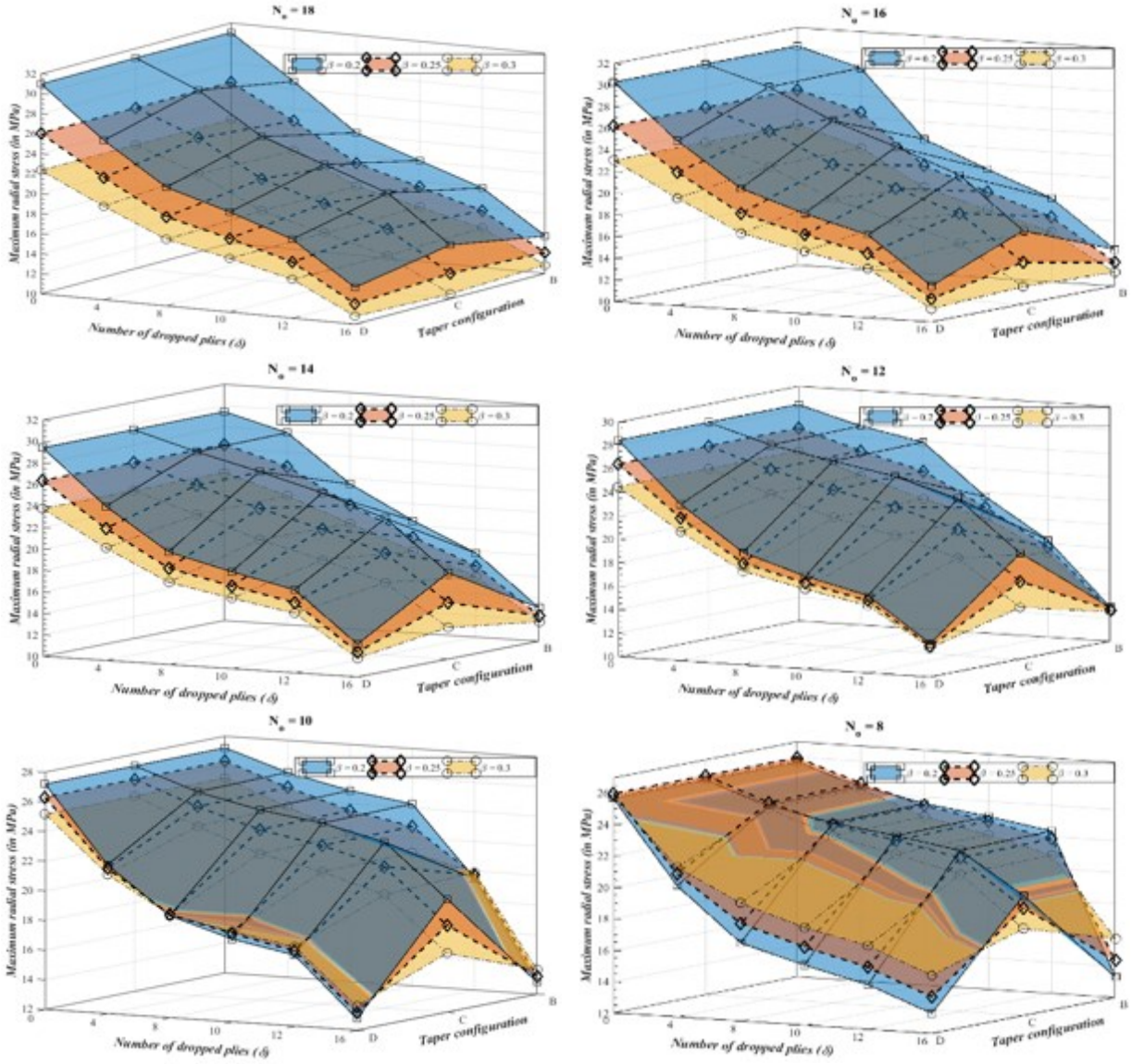

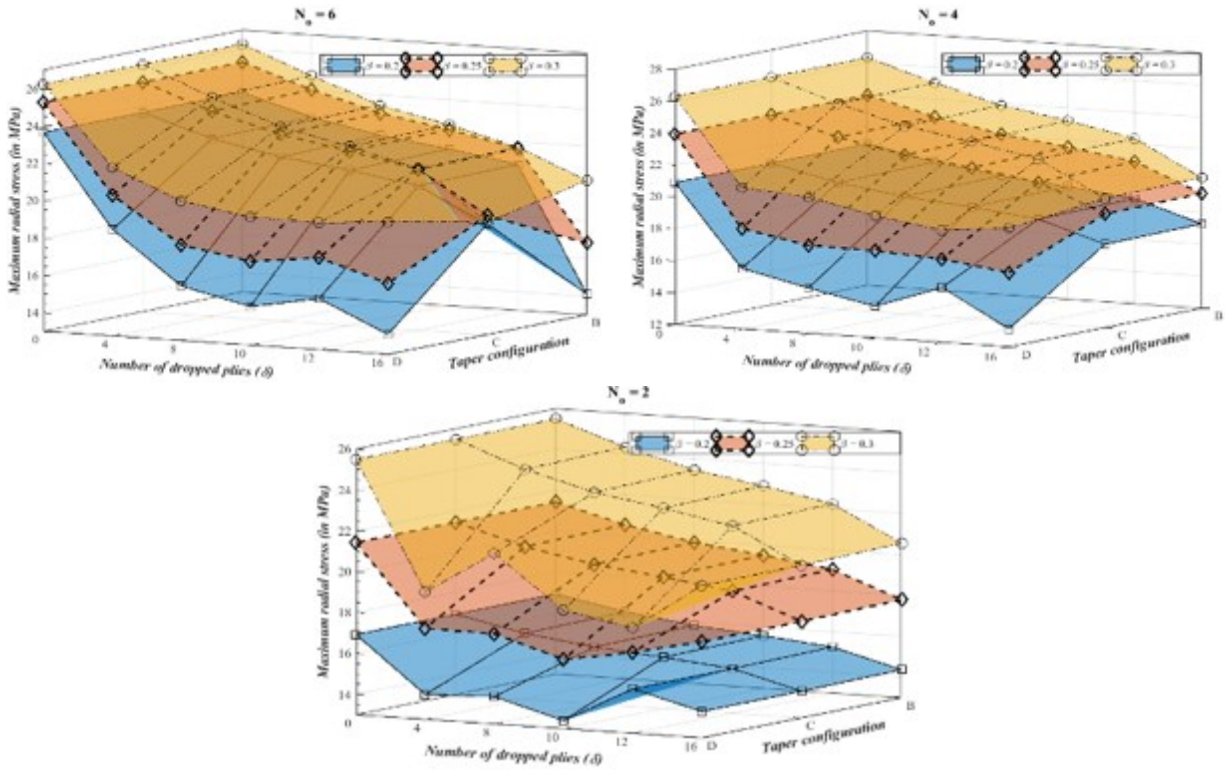

Figure 4.14 Variation of the maximum radial stress with the taper configuration and with the number of dropped plies in a rotating annular thickness-tapered cross-ply laminated disc with varying number of 0° plies and with the clamped-free boundary condition for different values of radius ratio

The following Tables 4.40 – 4.42 show the variation with the number of dropped plies and with the number of 0° plies of the maximum radial stress, in a rotating annular thickness-tapered cross-ply laminated disc with the clamped-free boundary condition for the beta values of 0.2, 0.25 and 0.3. The variation of the maximum radial stress has been shown for the different taper configurations of the laminated disc considered in the present study.

Maximum radial stress, σ_r^{max} (in MPa) in a rotating annular thickness-tapered cross-ply laminated disc with taper configuration B and with the clamped-free boundary condition for different values of radius ratio							
Number of 0° plies (N_o)	Beta value of the disc	Number of dropped plies (δ)					
		0	4	8	10	12	16
18	$\beta = 0.2$	31.003	26.743	22.218	20.076	17.955	13.741
	$\beta = 0.25$	26.041	22.811	19.187	17.43	15.666	12.09
	$\beta = 0.3$	22.334	19.817	16.884	15.425	13.938	10.853
16	$\beta = 0.2$	30.273	28.626	22.426	20.018	17.742	13.392
	$\beta = 0.25$	26.236	24.512	19.948	17.933	15.993	12.193
	$\beta = 0.3$	23.034	21.23	17.961	16.27	14.61	11.265
14	$\beta = 0.2$	29.425	27.853	23.458	20.431	17.806	13.108
	$\beta = 0.25$	26.366	24.708	21.483	18.905	16.609	12.375
	$\beta = 0.3$	23.75	21.98	19.785	17.609	15.613	11.8
12	$\beta = 0.2$	28.42	26.938	25.922	21.617	18.277	12.896
	$\beta = 0.25$	26.402	24.824	23.445	20.706	17.704	12.673
	$\beta = 0.3$	24.468	22.748	21.084	19.841	17.191	12.535
10	$\beta = 0.2$	27.197	25.824	24.884	24.271	19.515	12.819
	$\beta = 0.25$	26.295	24.812	23.536	22.74	19.751	13.204
	$\beta = 0.3$	25.163	23.511	21.928	20.974	19.943	13.664
8	$\beta = 0.2$	25.661	24.423	23.576	23.022	22.349	13.324
	$\beta = 0.25$	25.964	24.598	23.445	22.72	21.862	14.376
	$\beta = 0.3$	25.785	24.224	22.752	21.854	20.817	15.767
6	$\beta = 0.2$	23.653	22.582	21.852	21.373	20.79	14.1
	$\beta = 0.25$	25.269	24.044	23.041	22.405	21.646	16.828
	$\beta = 0.3$	26.233	24.794	23.471	22.656	21.704	20.178
4	$\beta = 0.2$	20.902	20.032	19.443	19.06	18.593	17.286
	$\beta = 0.25$	23.941	22.882	22.057	21.533	20.904	19.191
	$\beta = 0.3$	26.299	25.01	23.883	23.184	22.36	20.178
2	$\beta = 0.2$	16.923	16.281	15.839	15.566	15.242	14.364
	$\beta = 0.25$	21.417	20.535	19.895	19.501	19.037	17.788
	$\beta = 0.3$	25.478	24.343	23.444	22.894	22.252	20.548

Table 4.40 Variation of the maximum radial stress (in MPa) with the number of 0° plies and with the number of dropped plies in a rotating annular thickness-tapered cross-ply laminated disc with taper configuration B and with the clamped-free boundary condition for different values of radius ratio

Maximum radial stress, σ_r^{max} (in MPa) in a rotating annular thickness-tapered cross-ply laminated disc with taper configuration C and with the clamped-free boundary condition for different values of radius ratio							
Number of 0° plies (N_o)	Beta value of the disc	Number of dropped plies (δ)					
		0	4	8	10	12	16
18	$\beta = 0.2$	31.003	28.415	24.416	22.225	19.985	15.407
	$\beta = 0.25$	26.041	23.635	20.154	18.293	16.403	12.566
	$\beta = 0.3$	22.334	20.04	16.971	15.362	13.736	10.51
16	$\beta = 0.2$	30.273	28.529	25.805	23.773	21.551	16.787
	$\beta = 0.25$	26.236	24.434	21.756	19.934	17.984	13.878
	$\beta = 0.3$	23.034	21.156	18.571	16.931	15.205	11.621
14	$\beta = 0.2$	29.425	27.757	26.303	24.713	22.727	18.047
	$\beta = 0.25$	26.366	24.629	22.879	21.321	19.469	15.258
	$\beta = 0.3$	23.75	21.903	19.967	18.466	16.747	12.954
12	$\beta = 0.2$	28.42	26.844	25.832	24.872	23.323	19.048
	$\beta = 0.25$	26.402	24.742	23.369	22.276	20.7	16.624
	$\beta = 0.3$	24.468	22.668	21.01	19.83	18.262	14.419
10	$\beta = 0.2$	27.197	25.732	24.796	24.186	23.196	19.638
	$\beta = 0.25$	26.295	24.729	23.458	22.665	21.522	17.87
	$\beta = 0.3$	25.163	23.426	21.849	20.898	19.637	15.974
8	$\beta = 0.2$	25.661	24.333	23.49	22.939	22.269	19.653
	$\beta = 0.25$	25.964	24.513	23.366	22.643	21.788	18.85
	$\beta = 0.3$	25.785	24.135	22.668	21.774	20.741	17.545
6	$\beta = 0.2$	23.653	22.496	21.77	21.294	20.713	18.918
	$\beta = 0.25$	25.269	23.958	22.96	22.326	21.571	19.365
	$\beta = 0.3$	26.233	24.7	23.382	22.57	21.623	19.002
4	$\beta = 0.2$	20.902	19.952	19.367	18.985	18.521	17.22
	$\beta = 0.25$	23.941	22.796	21.976	21.454	20.828	19.121
	$\beta = 0.3$	26.299	24.91	23.789	23.092	22.272	20.099
2	$\beta = 0.2$	16.923	16.214	15.775	15.503	15.18	14.306
	$\beta = 0.25$	21.417	20.452	19.816	19.424	18.962	17.718
	$\beta = 0.3$	25.478	24.237	23.343	22.796	22.157	20.46

Table 4.41 Variation of the maximum radial stress (in MPa) with the number of 0° plies and with the number of dropped plies in a rotating annular thickness-tapered cross-ply laminated disc with taper configuration C and with the clamped-free boundary condition for different values of radius ratio

Maximum radial stress, σ_r^{max} (in MPa) in a rotating annular thickness-tapered cross-ply laminated disc with taper configuration D and with the clamped-free boundary condition for different values of radius ratio							
Number of 0° plies (N_o)	Beta value of the disc	Number of dropped plies (δ)					
		0	4	8	10	12	16
18	$\beta = 0.2$	31.003	25.967	21.868	20.02	17.907	13.707
	$\beta = 0.25$	26.041	22.228	18.917	17.385	15.628	12.063
	$\beta = 0.3$	22.334	19.363	16.664	15.382	13.902	10.827
16	$\beta = 0.2$	30.273	25.232	21.224	19.275	17.695	13.359
	$\beta = 0.25$	26.236	22.309	18.898	17.325	15.954	12.166
	$\beta = 0.3$	23.034	19.927	17.1	15.762	14.572	11.239
14	$\beta = 0.2$	29.425	24.367	20.495	19.041	17.759	13.076
	$\beta = 0.25$	26.366	22.3	18.987	17.713	16.569	12.348
	$\beta = 0.3$	23.75	20.475	17.68	16.581	15.575	11.774
12	$\beta = 0.2$	28.42	23.324	19.582	17.895	16.605	12.866
	$\beta = 0.25$	26.402	22.157	18.668	17.332	16.159	12.647
	$\beta = 0.3$	24.468	20.976	17.968	16.8	15.765	12.51
10	$\beta = 0.2$	27.197	22.029	18.877	17.595	16.786	12.79
	$\beta = 0.25$	26.295	21.807	18.963	17.976	17.082	13.18
	$\beta = 0.3$	25.163	21.373	18.932	18.107	17.358	13.642
8	$\beta = 0.2$	25.661	20.362	16.988	15.841	14.857	13.302
	$\beta = 0.25$	25.964	21.125	18.234	17	15.972	14.352
	$\beta = 0.3$	25.785	21.554	19.526	18.242	17.337	15.723
6	$\beta = 0.2$	23.653	18.704	15.933	15.085	15.751	14.08
	$\beta = 0.25$	25.269	20.533	18.125	17.5	17.922	16.816
	$\beta = 0.3$	26.233	22.007	20.484	19.864	19.815	20.099
4	$\beta = 0.2$	20.902	15.803	14.855	13.994	15.453	13.133
	$\beta = 0.25$	23.941	18.3	17.533	17.465	17.242	16.662
	$\beta = 0.3$	26.299	20.887	20.56	19.676	19.057	19.46
2	$\beta = 0.2$	16.923	14.214	14.345	13.403	15.18	14.306
	$\beta = 0.25$	21.417	17.452	17.416	16.4	16.962	17.718
	$\beta = 0.3$	25.478	19.237	21.343	18.796	18.159	20.46

Table 4.42 Variation of the maximum radial stress (in MPa) with the number of 0° plies and with the number of dropped plies in a rotating annular thickness-tapered cross-ply laminated disc with taper configuration D and with the clamped-free boundary condition for different values of radius ratio

The following observations can be made from the variation of the maximum radial stress with the number of dropped plies and with the number of 0° plies, in a rotating annular thickness-tapered cross-ply laminated disc with the clamped-free boundary condition and with different taper configurations for the beta values of 0.2, 0.25 and 0.3, shown in the Figure 4.14 and Tables 4.40 – 4.42:

- For the uniform-thickness cross-ply laminated disc with N_o = 18 up to N_o = 10, the maximum radial stress decreases with the increasing beta value of the disc and as the number of 0° plies are reduced from 10 to 2, the radial stress tends to increase with the increasing beta value of the disc. This variation of the maximum radial stress with the increasing beta value of a rotating annular uniform-thickness cross-ply laminated disc has been explained in Chapter 3 (see section 3.7.2.2).
- For the thickness-tapered cross-ply laminated disc with N_o = 18 up to N_o = 12, irrespective of the taper configuration and the number of dropped plies, the radial stress decreases with the increasing beta value of the disc, i.e. $\sigma_r^{max}(for\ \beta = 0.2) > \sigma_r^{max}(for\ \beta = 0.25) > \sigma_r^{max}(for\ \beta = 0.3)$.
- For the thickness-tapered cross-ply laminated disc with N_o = 10, irrespective of the number of dropped plies, the maximum radial stress decreases with the increasing beta value of the disc for taper configuration C. However, for the taper configurations B and D, the trend is not the same. For the disc with taper configuration B, the radial stress first decreases with the increasing beta value of the disc till δ = 10, whereas, for the disc with taper configuration D, the stress decreases with the increasing beta value till δ = 4. Thereafter, as the number of dropped plies is increased to a maximum of δ = 16, the radial stress increases with the increasing beta value of the disc.
- For the thickness-tapered cross-ply laminated disc with N_o = 8, irrespective of the number of dropped plies, the radial stress decreases with the increasing beta value of the disc for the taper configuration C, except for δ = 4 (where, σ_r^{max} corresponding to β = 0.2 is less than the stress corresponding to β = 0.25). For the disc with taper configuration B, the radial stress first decreases with the increasing beta value of the disc till δ = 12. Thereafter, as the number of dropped plies is increased from 12 to 16, the radial stress increases with the increasing beta value

of the disc, whereas, for the disc with the taper configuration D, regardless of the number of dropped plies, the radial stress always increases with the increasing beta value of the disc.

- For the thickness-tapered cross-ply laminated discs with N_o = 6 up to N_o = 2, irrespective of the taper configuration and the number of dropped plies, the radial stress always increases with the increasing beta value of the disc.

To study the effect of taper configuration on the induced maximum radial stress in a rotating annular thickness-tapered cross-ply laminated disc with the clamped-free boundary condition, a disc with a beta value of 0.25 and with some random number of dropped plies and 0° plies is chosen.

The following Table 4.43 shows the comparison of the induced maximum radial stress corresponding to different taper configurations of a rotating annular thickness-tapered cross-ply laminated disc with the clamped-free boundary condition for beta value of 0.25.

Maximum radial stress, σ_r^{max} (in MPa) in a rotating annular thickness-tapered cross-ply laminated disc with the clamped-free boundary condition for different taper configurations				
$\beta = 0.25$				
Number of 0° plies (N_o)	Taper configuration of the disc	Number of dropped plies (δ)		
		4	10	16
14	B	24.708	18.905	12.375
	C	24.629	21.321	15.258
	D	22.3	17.713	12.348
10	B	24.812	22.74	13.204
	C	24.729	22.665	17.87
	D	21.807	17.976	13.18
6	B	24.044	22.405	16.828
	C	23.958	22.326	19.365
	D	20.533	17.5	16.816

Table 4.43 Comparison of the maximum radial stress (in *MPa*) corresponding to different taper configurations of a rotating annular thickness-tapered cross-ply laminated disc with the clamped-free boundary condition for beta value of 0.25

It can be seen from the above Table 4.43 that irrespective of the number of 0° plies and the number of dropped plies, the rotating annular thickness-tapered cross-ply laminated disc with taper configuration D is subjected to the minimum amount of radial stress as compared to the other taper configurations. Also, it can be seen that for lower number of dropped plies, i.e. $\delta = 4$, the cross-ply disc with taper configuration B experiences a slightly higher amount of radial stress in comparison to the disc with taper configuration C. Besides, as the number of dropped plies is increased, i.e. $\delta = 10$ or 16, the cross-ply disc with taper configuration C is subjected to the maximum amount of radial stress.

The following Figure 4.15 shows the variation with the number of dropped plies and with the taper configuration of the maximum circumferential stress, in a rotating annular thickness-tapered cross-ply laminated disc with varying number of 0° plies and with the clamped-free boundary condition for the beta values of 0.2, 0.25 and 0.3.

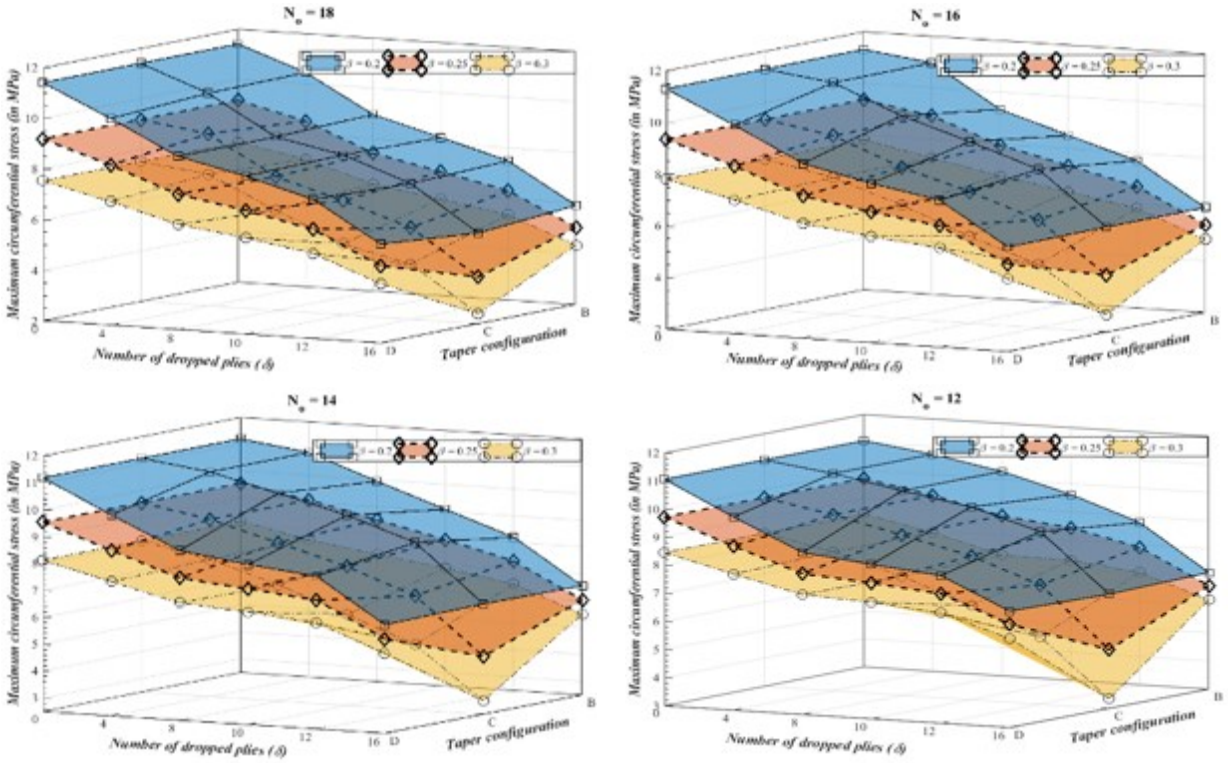

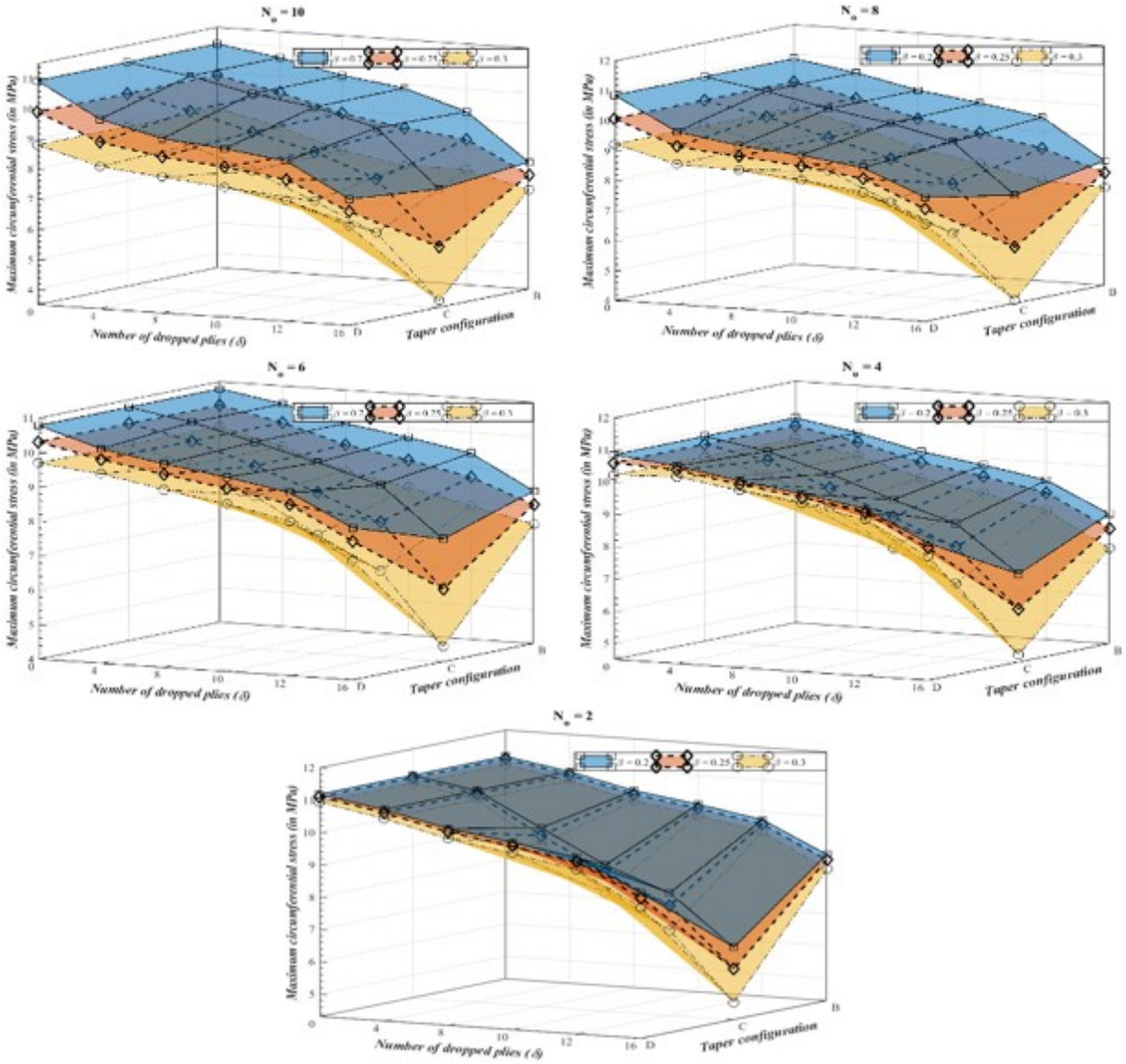

Figure 4.15 Variation of the maximum circumferential stress with the taper configuration and with the number of dropped plies in a rotating annular thickness-tapered cross-ply laminated disc with varying number of 0° plies and with the clamped-free boundary condition for different values of radius ratio

The following Tables 4.44 – 4.46 show the variation with the number of dropped plies and with the number of 0° plies of the maximum circumferential stress, in a rotating annular thickness-tapered cross-ply laminated disc with the clamped-free boundary condition for the beta values of 0.2, 0.25 and 0.3. The variation of the maximum circumferential stress has been shown for the different taper configurations of the laminated disc considered in the present study.

Maximum circumferential stress, σ_θ^{max} (in MPa) in a rotating annular thickness-tapered cross-ply laminated disc with taper configuration B and with the clamped-free boundary condition for different values of radius ratio							
Number of 0° plies (N_o)	Beta value of the disc	Number of dropped plies (δ)					
		0	4	8	10	12	16
18	$\beta = 0.2$	11.404	10.455	8.971	8.243	7.497	5.914
	$\beta = 0.25$	9.183	8.535	7.442	6.891	6.315	5.048
	$\beta = 0.3$	7.527	7.032	6.231	5.812	5.364	4.346
16	$\beta = 0.2$	11.302	10.958	9.329	8.5	7.697	6.059
	$\beta = 0.25$	9.355	8.898	7.949	7.328	6.704	5.397
	$\beta = 0.3$	7.813	7.276	6.762	6.322	5.852	4.829
14	$\beta = 0.2$	11.189	10.847	9.942	9.065	8.196	6.554
	$\beta = 0.25$	9.532	9.079	8.503	7.935	7.307	6.026
	$\beta = 0.3$	8.121	7.594	7.218	6.886	6.455	5.495
12	$\beta = 0.2$	11.06	10.734	10.281	9.619	8.777	7.157
	$\beta = 0.25$	9.713	9.266	8.692	8.429	7.894	6.688
	$\beta = 0.3$	8.451	7.942	7.3	7.276	7.002	6.184
10	$\beta = 0.2$	10.934	10.622	10.175	9.889	9.25	7.714
	$\beta = 0.25$	9.895	9.463	8.908	8.566	8.322	7.294
	$\beta = 0.3$	8.803	8.325	7.695	7.318	7.327	6.806
8	$\beta = 0.2$	10.858	10.524	10.08	9.798	9.461	8.151
	$\beta = 0.25$	10.077	9.675	9.139	8.808	8.42	7.763
	$\beta = 0.3$	9.224	8.751	8.14	7.77	7.345	7.267
6	$\beta = 0.2$	10.784	10.468	10.022	9.742	9.406	8.429
	$\beta = 0.25$	10.306	9.918	9.403	9.081	8.705	8.038
	$\beta = 0.3$	9.692	9.234	8.649	8.291	7.876	7.463
4	$\beta = 0.2$	10.853	10.52	10.068	9.782	9.444	8.532
	$\beta = 0.25$	10.602	10.232	9.737	9.426	9.059	8.081
	$\beta = 0.3$	10.217	9.806	9.258	8.917	8.517	7.463
2	$\beta = 0.2$	11.182	10.844	10.391	10.104	9.76	8.818
	$\beta = 0.25$	11.1	10.747	10.28	9.982	9.627	8.654
	$\beta = 0.3$	10.936	10.565	10.072	9.759	9.385	8.363

Table 4.44 Variation of the maximum circumferential stress (in *MPa*) with the number of 0° plies and with the number of dropped plies in a rotating annular thickness-tapered cross-ply laminated disc with taper configuration B and with the clamped-free boundary condition for different values of radius ratio

Maximum circumferential stress, σ_θ^{max} (in MPa) in a rotating annular thickness-tapered cross-ply laminated disc with taper configuration C and with the clamped-free boundary condition for different values of radius ratio							
Number of 0° plies (N_o)	Beta value of the disc	Number of dropped plies (δ)					
		0	4	8	10	12	16
18	$\beta = 0.2$	11.404	10.399	8.851	8.315	7.364	5.589
	$\beta = 0.25$	9.183	8.796	7.281	6.5	5.619	3.855
	$\beta = 0.3$	7.527	7.202	5.959	4.806	4.184	2.4
16	$\beta = 0.2$	11.302	10.958	9.85	9.028	8.132	6.074
	$\beta = 0.25$	9.355	8.898	7.847	7.078	6.165	4.206
	$\beta = 0.3$	7.813	7.275	6.39	5.354	4.447	2.683
14	$\beta = 0.2$	11.189	10.847	10.231	9.571	8.727	6.609
	$\beta = 0.25$	9.532	9.079	8.375	7.661	6.737	4.649
	$\beta = 0.3$	8.121	7.594	6.814	5.877	4.922	2.998
12	$\beta = 0.2$	11.06	10.733	10.281	9.864	9.142	7.077
	$\beta = 0.25$	9.713	9.266	8.696	8.112	7.241	5.097
	$\beta = 0.3$	8.451	7.941	7.237	6.353	5.394	3.345
10	$\beta = 0.2$	10.934	10.622	10.174	9.873	9.327	7.427
	$\beta = 0.25$	9.895	9.463	8.904	8.383	7.624	5.521
	$\beta = 0.3$	8.803	8.325	7.609	6.742	5.832	3.715
8	$\beta = 0.2$	10.858	10.524	10.079	9.729	9.254	7.609
	$\beta = 0.25$	10.077	9.675	9.114	8.545	7.842	5.878
	$\beta = 0.3$	9.224	8.751	8.013	7.087	6.199	4.094
6	$\beta = 0.2$	10.784	10.468	10.019	9.544	9.017	7.567
	$\beta = 0.25$	10.306	9.918	9.318	8.677	7.937	6.115
	$\beta = 0.3$	9.692	9.234	8.449	7.441	6.517	4.449
4	$\beta = 0.2$	10.853	10.52	9.95	9.278	8.674	7.235
	$\beta = 0.25$	10.602	10.231	9.497	8.735	7.937	6.149
	$\beta = 0.3$	10.217	9.805	8.903	7.77	6.802	4.727
2	$\beta = 0.2$	11.182	10.843	9.825	8.815	8.08	6.54
	$\beta = 0.25$	11.1	10.747	9.583	8.593	7.688	5.87
	$\beta = 0.3$	10.936	10.565	9.313	7.952	6.922	4.837

Table 4.45 Variation of the maximum circumferential stress (in *MPa*) with the number of 0° plies and with the number of dropped plies in a rotating annular thickness-tapered cross-ply laminated disc with taper configuration C and with the clamped-free boundary condition for different values of radius ratio

Maximum circumferential stress, σ_θ^{max} (in MPa) in a rotating annular thickness-tapered cross-ply laminated disc with taper configuration D and with the clamped-free boundary condition for different values of radius ratio							
Number of 0° plies (N_o)	Beta value of the disc	Number of dropped plies (δ)					
		0	4	8	10	12	16
18	$\beta = 0.2$	11.404	10.169	8.846	8.243	7.498	5.914
	$\beta = 0.25$	9.183	8.324	7.347	6.891	6.315	5.048
	$\beta = 0.3$	7.527	6.886	6.158	5.812	5.364	4.347
16	$\beta = 0.2$	11.302	10.07	8.765	8.174	7.697	6.059
	$\beta = 0.25$	9.355	8.483	7.507	7.06	6.704	5.397
	$\beta = 0.3$	7.813	7.173	6.448	6.113	5.852	4.828
14	$\beta = 0.2$	11.189	9.969	8.817	8.464	8.197	6.554
	$\beta = 0.25$	9.532	8.651	7.794	7.557	7.307	6.026
	$\beta = 0.3$	8.121	7.489	6.87	6.697	6.455	5.495
12	$\beta = 0.2$	11.06	9.875	8.77	8.504	8.268	7.157
	$\beta = 0.25$	9.713	8.831	8.013	7.841	7.616	6.688
	$\beta = 0.3$	8.451	7.838	7.269	7.151	6.935	6.184
10	$\beta = 0.2$	10.934	9.8	9.294	9.101	8.826	7.713
	$\beta = 0.25$	9.895	9.032	8.689	8.495	8.211	7.294
	$\beta = 0.3$	8.803	8.232	8.018	7.82	7.52	6.806
8	$\beta = 0.2$	10.858	9.78	9.46	9.276	8.999	8.151
	$\beta = 0.25$	10.077	9.279	9.091	8.913	8.634	7.763
	$\beta = 0.3$	9.224	8.693	8.632	8.46	8.174	7.267
6	$\beta = 0.2$	10.784	10.234	9.916	9.653	9.327	8.428
	$\beta = 0.25$	10.306	9.922	9.605	9.329	8.986	8.038
	$\beta = 0.3$	9.692	9.5	9.173	8.875	8.499	7.463
4	$\beta = 0.2$	10.853	10.631	10.309	10.037	9.702	8.767
	$\beta = 0.25$	10.602	10.505	10.197	9.923	9.582	8.627
	$\beta = 0.3$	10.217	10.302	10.009	9.727	9.371	8.363
2	$\beta = 0.2$	11.182	10.843	10.391	10.104	9.76	8.818
	$\beta = 0.25$	11.1	10.747	10.279	9.983	9.627	8.654
	$\beta = 0.3$	10.936	10.565	10.072	9.759	9.384	8.363

Table 4.46 Variation of the maximum circumferential stress (in *MPa*) with the number of 0° plies and with the number of dropped plies in a rotating annular thickness-tapered cross-ply laminated disc with taper configuration D and with the clamped-free boundary condition for different values of radius ratio

The following observations can be made from the variation of the maximum circumferential stress with the number of dropped plies and with the number of 0° plies, in a rotating annular thickness-tapered cross-ply laminated disc with the clamped-free boundary condition and with different taper configurations for the beta values of 0.2, 0.25 and 0.3, shown in the Figure 4.15 and Tables 4.44 – 4.46:

- Irrespective of the taper configuration, number of dropped plies and the number of $0°$ plies, the maximum circumferential stress always decreases with the increasing beta value of the rotating annular thickness-tapered cross-ply laminated disc with the clamped-free boundary condition. This variation of the maximum circumferential stress with the increasing beta value of the cross-ply disc is different from the variation of the maximum radial stress, wherein the latter, the radial stress first decreases with the increasing beta value of the disc with N_o = 18 up to N_o = 12 and then increases with the increasing beta value of the disc with N_o = 6 up to N_o = 2.
- Regardless of the taper configuration and the number of dropped plies, the percentage decrease in the maximum circumferential stress with the increasing beta value of the disc, decreases with the decreasing number of $0°$ plies in the thickness-tapered cross-ply laminated disc. In other words, the decrease in the amount of the circumferential stress with the increasing beta value becomes less significant as the number of $0°$ plies are reduced in the cross-ply laminated disc.

To study the relative effect of 0° plies on the percentage decrease in the maximum circumferential stress with the increasing beta value, a rotating annular thickness-tapered cross-ply laminated disc with δ = 4 and with taper configuration B and with the clamped-free boundary condition is chosen. The following Table 4.47 shows the variation with the number of 0° plies of the percentage decrease in the maximum circumferential stress with the increasing beta value of a thickness-tapered cross-ply laminated disc with taper configuration B and with the clamped-free boundary condition.

Since the rotating cross-ply laminated disc with a beta value of 0.2 is subjected to the maximum amount of circumferential stress, the value of the circumferential stress corresponding to β = 0.2 is considered as a benchmark while calculating the percentage decrease in the maximum

circumferential stress. Also, in the below Table, the percentage decrease in the maximum circumferential stress is calculated according to the following formula:

$$\text{Percentage decrease in the maximum circumferential stress}({}^{0.2}_{i}\eta) = \frac{(\text{Maximum stress value for } \beta = 0.2) - (\text{Maximum stress value for } \beta = i)}{\text{Maximum stress value for } \beta = 0.2} * 100 \quad (4.24)$$

where, i = 0.25 and 0.3.

Maximum circumferential stress and percentage decrease in the maximum circumferential stress in a rotating annular thickness-tapered cross-ply laminated disc with taper configuration B and with the clamped-free boundary condition					
$\delta = 4$					
Number of 0° plies (N_o)	Maximum circumferential stress (in MPa)			Percentage decrease in the maximum circumferential stress	
	$\beta = 0.2$	$\beta = 0.25$	$\beta = 0.3$	${}^{0.2}_{0.25}\eta$	${}^{0.2}_{0.3}\eta$
18	10.455	8.535	7.032	18.36	32.74
10	10.622	9.463	8.325	10.91	21.63
2	10.844	10.747	10.565	0.89	2.57

Table 4.47 Relative effect of 0° plies on the percentage decrease in the maximum circumferential stress with the increasing beta value of a thickness-tapered cross-ply laminated disc with taper configuration B and with the clamped-free boundary condition

It can be seen from the above Table 4.47 that the percentage decrease in the maximum circumferential stress with the increasing beta value, decreases with the decreasing number of 0° plies in a rotating annular thickness-tapered cross-ply laminated disc with the clamped-free boundary condition. In other words, irrespective of the number of dropped plies, the decrease in the amount of the maximum circumferential stress with the increasing beta value becomes less significant in a rotating annular thickness-tapered cross-ply laminated disc with lower number of 0° plies, as compared to the cross-ply disc with a relatively higher number of 0° plies. This observation is true for any taper configuration of the laminated disc considered in the present study.

To study the effect of taper configuration on the induced maximum circumferential stress in a rotating annular thickness-tapered cross-ply laminated disc with the clamped-free boundary condition, a disc with a beta value of 0.3 and with some random number of dropped plies and 0° plies is chosen.

The following Table 4.48 shows the comparison of the induced maximum circumferential stress corresponding to different taper configurations of a rotating annular thickness-tapered cross-ply laminated disc with the clamped-free boundary condition for beta value of 0.3.

Maximum circumferential stress, σ_{θ}^{max} (in MPa) in a rotating annular thickness-tapered cross-ply laminated disc with the clamped-free boundary condition for different taper configurations				
$\beta = 0.3$				
Number of 0° plies (N_o)	Taper configuration of the disc	Number of dropped plies (δ)		
		4	10	16
14	B	7.594	6.886	5.495
	C	7.594	5.877	2.998
	D	7.489	6.697	5.495
10	B	8.325	7.318	6.806
	C	8.325	6.742	3.715
	D	8.232	7.82	6.806
6	B	9.234	8.291	7.463
	C	9.234	7.441	4.449
	D	9.50	8.875	7.463

Table 4.48 Comparison of the maximum circumferential stress (in *MPa*) corresponding to different taper configurations of a rotating annular thickness-tapered cross-ply laminated disc with the clamped-free boundary condition for beta value of 0.3

It can be seen from the above Table 4.48 that irrespective of the number of 0° plies and the number of dropped plies, the rotating annular thickness-tapered cross-ply laminated disc with the taper configuration C and with the clamped-free boundary condition is subjected to the minimum amount of circumferential stress as compared to the other taper configurations. Furthermore, the difference between the amount of circumferential stress corresponding to different taper configurations is negligible for a lower number of dropped plies, i.e. $\delta = 4$, and the difference in

the maximum circumferential stress corresponding to different taper configurations, increases with the increasing number of dropped plies.

For instance, from the above Table 4.48 it can be seen that a rotating annular thickness-tapered cross-ply laminated disc with N_o = 10, δ = 16 and the taper configuration C will be subjected to 45.4 % less amount of the circumferential stress experienced by a cross-ply disc with the same number of 0° plies and the dropped plies, but with the taper configurations B and D.

The following Figure 4.16 shows the variation with the number of dropped plies and with the taper configuration of the maximum radial displacement, in a rotating annular thickness-tapered cross-ply laminated disc with varying number of 0° plies and with the clamped-free boundary condition for the beta values of 0.2, 0.25 and 0.3.

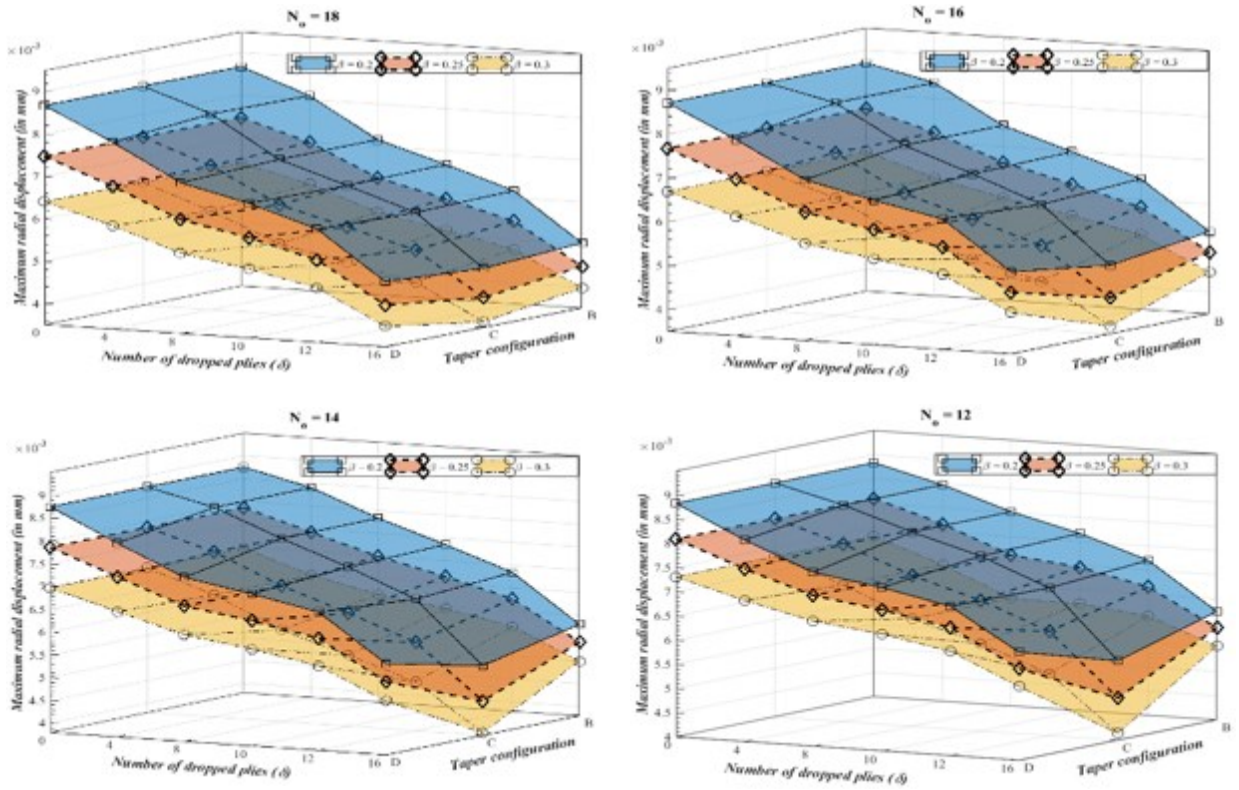

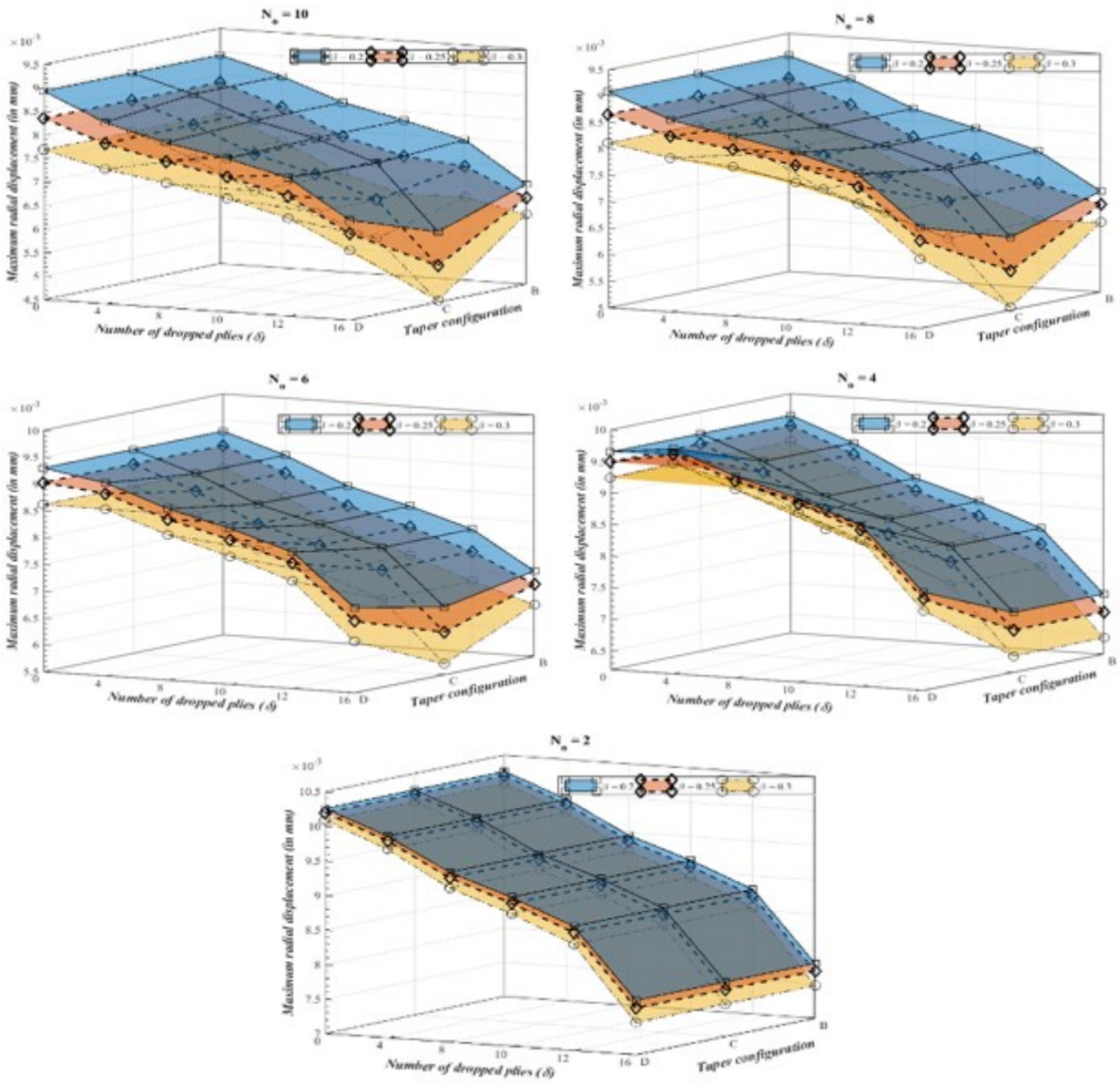

Figure 4.16 Variation of the maximum radial displacement with the taper configuration and with the number of dropped plies in a rotating annular thickness-tapered cross-ply laminated disc with varying number of 0° plies and with the clamped-free boundary condition for different values of radius ratio

The following Tables 4.49 – 4.51 show the variation with the number of dropped plies and with the number of 0° plies of the maximum radial displacement, in a rotating annular thickness-tapered cross-ply laminated disc with the clamped-free boundary condition for the beta values of 0.2, 0.25 and 0.3. The variation of the maximum radial displacement has been shown for the different taper configurations of the laminated disc considered in the present study.

Maximum radial displacement, u_r^{max} (in mm) in a rotating annular thickness-tapered cross-ply laminated disc with taper configuration B and with the clamped-free boundary condition for different values of radius ratio							
Number of 0° plies (N_o)	Beta value of the disc	Number of dropped plies (δ)					
		0	4	8	10	12	16
18	$\beta = 0.2$	0.00867	0.00809	0.00716	0.00668	0.00617	0.00504
	$\beta = 0.25$	0.00747	0.00699	0.00626	0.00587	0.00545	0.00449
	$\beta = 0.3$	0.0064	0.00601	0.00545	0.00513	0.00479	0.00398
16	$\beta = 0.2$	0.0087	0.00835	0.00748	0.00699	0.00648	0.00538
	$\beta = 0.25$	0.00766	0.00721	0.00664	0.00625	0.00583	0.00491
	$\beta = 0.3$	0.00668	0.00618	0.00584	0.00554	0.00521	0.00445
14	$\beta = 0.2$	0.00875	0.0084	0.00783	0.00735	0.00684	0.0058
	$\beta = 0.25$	0.00786	0.00742	0.00699	0.00665	0.00626	0.00541
	$\beta = 0.3$	0.00697	0.00648	0.00616	0.00595	0.00566	0.00499
12	$\beta = 0.2$	0.00883	0.00847	0.00801	0.00766	0.0072	0.00624
	$\beta = 0.25$	0.00809	0.00766	0.00711	0.00696	0.00665	0.0059
	$\beta = 0.3$	0.00731	0.00682	0.00622	0.00621	0.00605	0.00553
10	$\beta = 0.2$	0.00893	0.00857	0.0081	0.00781	0.00748	0.00663
	$\beta = 0.25$	0.00835	0.00792	0.00738	0.00705	0.00692	0.00634
	$\beta = 0.3$	0.00768	0.0072	0.0066	0.00624	0.00627	0.00599
8	$\beta = 0.2$	0.00908	0.00871	0.00823	0.00794	0.00759	0.00691
	$\beta = 0.25$	0.00865	0.00823	0.00769	0.00736	0.00698	0.00666
	$\beta = 0.3$	0.00811	0.00764	0.00705	0.00669	0.00628	0.00632
6	$\beta = 0.2$	0.0093	0.00893	0.00844	0.00814	0.00779	0.00709
	$\beta = 0.25$	0.00903	0.0086	0.00807	0.00775	0.00737	0.00684
	$\beta = 0.3$	0.00862	0.00816	0.00759	0.00723	0.00682	0.00646
4	$\beta = 0.2$	0.00965	0.00928	0.00879	0.00849	0.00813	0.00715
	$\beta = 0.25$	0.00949	0.0091	0.00859	0.00826	0.00788	0.00687
	$\beta = 0.3$	0.00924	0.00882	0.00827	0.00792	0.00752	0.00646
2	$\beta = 0.2$	0.01026	0.00992	0.00946	0.00916	0.0088	0.00779
	$\beta = 0.25$	0.0102	0.00985	0.00938	0.00907	0.00871	0.00768
	$\beta = 0.3$	0.01009	0.00973	0.00923	0.00892	0.00854	0.00747

Table 4.49 Variation of the maximum radial displacement (in *mm*) with the number of 0° plies and with the number of dropped plies in a rotating annular thickness-tapered cross-ply laminated disc with taper configuration B and with the clamped-free boundary condition for different values of radius ratio

Maximum radial displacement, u_r^{max} (in mm) in a rotating annular thickness-tapered cross-ply laminated disc with taper configuration C and with the clamped-free boundary condition for different values of radius ratio							
Number of 0° plies (N_o)	Beta value of the disc	Number of dropped plies (δ)					
		0	4	8	10	12	16
18	$\beta = 0.2$	0.00867	0.00812	0.00715	0.00664	0.00611	0.0049
	$\beta = 0.25$	0.00747	0.00689	0.00608	0.00566	0.00522	0.00421
	$\beta = 0.3$	0.0064	0.00583	0.00516	0.00483	0.00447	0.00364
16	$\beta = 0.2$	0.0087	0.00835	0.00749	0.00694	0.00635	0.00507
	$\beta = 0.25$	0.00766	0.00721	0.00639	0.00591	0.00541	0.00433
	$\beta = 0.3$	0.00668	0.00618	0.00542	0.00501	0.0046	0.00369
14	$\beta = 0.2$	0.00875	0.0084	0.00782	0.00729	0.00669	0.00533
	$\beta = 0.25$	0.00786	0.00742	0.00678	0.00628	0.00574	0.00455
	$\beta = 0.3$	0.00697	0.00648	0.00581	0.00536	0.00488	0.00386
12	$\beta = 0.2$	0.00883	0.00847	0.00801	0.00761	0.00705	0.00564
	$\beta = 0.25$	0.00809	0.00766	0.00711	0.00669	0.00615	0.00487
	$\beta = 0.3$	0.00731	0.00682	0.00622	0.0058	0.00528	0.00414
10	$\beta = 0.2$	0.00893	0.00857	0.0081	0.00781	0.00737	0.006
	$\beta = 0.25$	0.00835	0.00792	0.00738	0.00705	0.00659	0.00528
	$\beta = 0.3$	0.00768	0.0072	0.0066	0.00624	0.00577	0.00454
8	$\beta = 0.2$	0.00908	0.00871	0.00823	0.00794	0.00759	0.00638
	$\beta = 0.25$	0.00865	0.00823	0.00769	0.00736	0.00698	0.00575
	$\beta = 0.3$	0.00811	0.00764	0.00705	0.00669	0.00628	0.00506
6	$\beta = 0.2$	0.0093	0.00893	0.00844	0.00814	0.00779	0.00676
	$\beta = 0.25$	0.00903	0.0086	0.00807	0.00775	0.00737	0.00629
	$\beta = 0.3$	0.00862	0.00816	0.00759	0.00723	0.00682	0.0057
4	$\beta = 0.2$	0.00965	0.00928	0.00879	0.00849	0.00813	0.00715
	$\beta = 0.25$	0.00949	0.0091	0.00858	0.00826	0.00788	0.00687
	$\beta = 0.3$	0.00924	0.00882	0.00827	0.00792	0.00752	0.00646
2	$\beta = 0.2$	0.01026	0.00992	0.00946	0.00916	0.0088	0.00779
	$\beta = 0.25$	0.0102	0.00985	0.00938	0.00907	0.00871	0.00768
	$\beta = 0.3$	0.01009	0.00973	0.00923	0.00892	0.00854	0.00747

Table 4.50 Variation of the maximum radial displacement (in *mm*) with the number of 0° plies and with the number of dropped plies in a rotating annular thickness-tapered cross-ply laminated disc with taper configuration C and with the clamped-free boundary condition for different values of radius ratio

Maximum radial displacement, u_r^{max} (in mm) in a rotating annular thickness-tapered cross-ply laminated disc with taper configuration D and with the clamped-free boundary condition for different values of radius ratio							
Number of 0° plies (N_o)	Beta value of the disc	Number of dropped plies (δ)					
		0	4	8	10	12	16
18	$\beta = 0.2$	0.00867	0.00791	0.00706	0.00668	0.00618	0.00504
	$\beta = 0.25$	0.00747	0.00687	0.00619	0.00587	0.00545	0.00449
	$\beta = 0.3$	0.0064	0.00594	0.0054	0.00513	0.00479	0.00399
16	$\beta = 0.2$	0.0087	0.00797	0.00716	0.0068	0.00648	0.00538
	$\beta = 0.25$	0.00766	0.00707	0.00642	0.00612	0.00583	0.00491
	$\beta = 0.3$	0.00668	0.00622	0.00571	0.00547	0.00521	0.00445
14	$\beta = 0.2$	0.00875	0.00805	0.0074	0.00714	0.00684	0.00581
	$\beta = 0.25$	0.00786	0.00731	0.00677	0.00655	0.00626	0.00541
	$\beta = 0.3$	0.00697	0.00655	0.00614	0.00593	0.00566	0.00499
12	$\beta = 0.2$	0.00883	0.00817	0.0076	0.00738	0.00709	0.00624
	$\beta = 0.25$	0.00809	0.00757	0.00712	0.00692	0.00665	0.0059
	$\beta = 0.3$	0.00731	0.00692	0.00659	0.00642	0.00616	0.00553
10	$\beta = 0.2$	0.00893	0.00835	0.00801	0.00776	0.00744	0.00663
	$\beta = 0.25$	0.00835	0.0079	0.00761	0.00737	0.00705	0.00634
	$\beta = 0.3$	0.00768	0.00736	0.00715	0.00691	0.00658	0.00599
8	$\beta = 0.2$	0.00908	0.00863	0.0084	0.00817	0.00784	0.00691
	$\beta = 0.25$	0.00865	0.00831	0.00815	0.00792	0.0076	0.00666
	$\beta = 0.3$	0.00811	0.00791	0.00782	0.0076	0.00728	0.00632
6	$\beta = 0.2$	0.0093	0.0091	0.0087	0.00841	0.00805	0.00709
	$\beta = 0.25$	0.00903	0.0089	0.0085	0.0082	0.00784	0.00684
	$\beta = 0.3$	0.00862	0.00861	0.00821	0.00789	0.00751	0.00646
4	$\beta = 0.2$	0.00965	0.00977	0.0094	0.00911	0.00876	0.00776
	$\beta = 0.25$	0.00949	0.00968	0.00932	0.00903	0.00868	0.00766
	$\beta = 0.3$	0.00924	0.00954	0.00919	0.00889	0.00853	0.00747
2	$\beta = 0.2$	0.01026	0.00992	0.00946	0.00916	0.0088	0.00779
	$\beta = 0.25$	0.0102	0.00985	0.00938	0.00907	0.00871	0.00768
	$\beta = 0.3$	0.01009	0.00973	0.00923	0.00892	0.00854	0.00747

Table 4.51 Variation of the maximum radial displacement (in *mm*) with the number of 0° plies and with the number of dropped plies in a rotating annular thickness-tapered cross-ply laminated disc with taper configuration D and with the clamped-free boundary condition for different values of radius ratio

The following observations can be made from the variation of the maximum radial displacement with the number of dropped plies and with the number of 0° plies, in a rotating annular thickness-tapered cross-ply laminated disc with the clamped-free boundary condition and with different taper configurations for the beta values of 0.2, 0.25 and 0.3, shown in the Figure 4.16 and Tables 4.49 – 4.51:

- Irrespective of the taper configuration, number of dropped plies and the number of 0° plies, the maximum radial displacement decreases with the increasing beta value of the rotating annular thickness-tapered cross-ply laminated disc with the clamped-free boundary condition.
- Irrespective of the taper configuration and the number of dropped plies, the maximum radial displacement increases with the decreasing number of 0° plies in a rotating annular thickness-tapered cross-ply laminated disc with the clamped-free boundary condition.
- Irrespective of the taper configuration and the number of 0° plies, the maximum radial displacement decreases with the increasing number of dropped plies in a rotating annular thickness-tapered cross-ply laminated disc with the clamped-free boundary condition.
- Regardless of the taper configuration and the number of dropped plies, the percentage decrease in the maximum radial displacement with the increasing beta value, decreases with the decreasing number of 0° plies in the rotating annular thickness-tapered cross-ply laminated disc with the clamped-free boundary condition. In other words, the decrease in the amount of the maximum radial displacement with the increasing beta value becomes less significant as the number of 0° plies are reduced in the cross-ply laminated disc.

To study the relative effect of 0° plies on the percentage decrease in the maximum radial displacement with the increasing beta value, a rotating annular thickness-tapered cross-ply laminated disc with $\delta = 8$ and with taper configuration B and with the clamped-free boundary condition is chosen.

The following Table 4.52 shows the variation with the number of 0° plies of the percentage decrease in the maximum radial displacement with the increasing beta value of a rotating annular thickness-tapered cross-ply laminated disc with taper configurations B and with the clamped-free

boundary condition. Since the rotating annular cross-ply disc with a beta value of 0.2 is subjected to the maximum amount of radial displacement, the value of the displacement corresponding to β = 0.2 is considered as a benchmark while calculating the percentage decrease in the displacement. Also, in the below Table, the percentage decrease in the displacement is calculated according to the following formula:

$$\text{Percentage decrease in the maximum radial displacement}({}^{0.2}_{i}\eta) = \frac{(\text{Maximum displacement value for } \beta = 0.2) - (\text{Maximum displacement value for } \beta = i)}{\text{Maximum displacement value for } \beta = 0.2} * 100 \quad (4.25)$$

where, i = 0.25 and 0.3.

Maximum radial displacement and percentage decrease in the maximum radial displacement in a rotating annular thickness-tapered cross-ply laminated disc with taper configuration B and with the clamped-free boundary condition					
$\delta = 8$					
Number of 0° plies (N_o)	Maximum radial displacement (in mm)			Percentage decrease in the maximum radial displacement	
	$\beta = 0.2$	$\beta = 0.25$	$\beta = 0.3$	${}^{0.2}_{0.25}\eta$	${}^{0.2}_{0.3}\eta$
18	0.00716	0.00626	0.00545	12.57	23.88
14	0.00783	0.00699	0.00616	10.728	21.33
10	0.0081	0.00738	0.0066	8.89	18.52
6	0.00844	0.00807	0.00759	4.38	10.07
2	0.00946	0.00938	0.00923	0.84	2.43

Table 4.52 Relative effect of 0° plies on the percentage decrease in the maximum radial displacement with the increasing beta value of a thickness-tapered cross-ply laminated disc with taper configuration B and with the clamped-free boundary condition

It can be seen from the above Table 4.52 that the percentage decrease in the maximum radial displacement with the increasing beta value, decreases with the decreasing number of 0° plies in a rotating annular thickness-tapered cross-ply laminated disc with the clamped-free boundary condition. In other words, irrespective of the number of dropped plies, the decrease in

the amount of the maximum radial displacement with the increasing beta value becomes less significant in a rotating annular thickness-tapered cross-ply laminated disc with lower number of 0° plies, as compared to the cross-ply disc with a relatively higher number of 0° plies. This observation is true for any taper configuration of the laminated disc considered in the present study.

To study the effect of taper configuration on the induced maximum radial displacement in a rotating annular thickness-tapered cross-ply laminated disc with the clamped-free boundary condition, a disc with a beta value of 0.3 and with some random number of dropped plies and 0° plies is chosen. The following Table 4.53 shows the comparison of the induced maximum radial displacement corresponding to different taper configurations of a rotating annular thickness-tapered cross-ply laminated disc with the clamped-free boundary condition for beta value of 0.3.

Maximum radial displacement, u_r^{max} (in mm) in a rotating annular thickness-tapered cross-ply laminated disc with the clamped-free boundary condition for different taper configurations				
$\beta = 0.3$				
Number of 0° plies (N_o)	Taper configuration of the disc	Number of dropped plies (δ)		
		4	10	16
14	B	0.00648	0.00595	0.00499
	C	0.00648	0.00536	0.00386
	D	0.00655	0.00593	0.00499
10	B	0.0072	0.00624	0.00599
	C	0.0072	0.00624	0.00454
	D	0.00736	0.00691	0.00599
6	B	0.00816	0.00723	0.00646
	C	0.00816	0.00723	0.0057
	D	0.00861	0.00789	0.00646

Table 4.53 Comparison of the maximum radial displacement (in *mm*) corresponding to different taper configurations of a rotating annular thickness-tapered cross-ply laminated disc with the clamped-free boundary condition for beta value of 0.3

It can be seen from the above Table 4.53 that irrespective of the number of 0° plies and the number of dropped plies, the rotating annular thickness-tapered cross-ply laminated disc with the taper configuration C and with the clamped-free boundary condition is subjected to the minimum amount of radial displacement as compared to the other taper configurations. Furthermore, the

difference between the maximum radial displacement corresponding to different taper configurations is negligible for lower number of dropped plies, i.e. $\delta = 4$, and the difference in the maximum radial displacement corresponding to different taper configurations increases with the increasing number of dropped plies.

For instance, from the above Table 4.53, it can be noted that for a rotating annular thickness-tapered cross-ply laminated disc with N_o = 10 and δ = 16, the maximum radial displacement corresponding to the taper configurations B and D is the same and is equal to 0.00599 *mm,* while for the taper configuration C, the displacement amounts to 0.00454 *mm*, which is nearly 24.2 % less than the displacement experienced by a cross-ply disc with the same number of 0° plies and the dropped plies, but with the taper configurations B and D.

4.7.3 Symmetrically-balanced laminated discs

This sub-section presents the parametric study on the elastic response of rotating annular thickness-tapered discs made up of Graphite-Fiber Reinforced Plastic material and with the symmetrically-balanced configuration for the clamped-free boundary condition. The effects of different laminate configurations, radius ratio values, taper configurations and numbers of dropped plies on the radial stress and circumferential stress distributions, on the in-plane shear stress distribution, and on the radial displacement distribution in rotating annular thickness-tapered fiber-reinforced composite discs with the clamped-free boundary condition are studied. The various symmetrically-balanced configurations of the laminated disc have been mentioned earlier in the section 3.7.3. Graphical results for the stress and displacement distributions are presented and the percentage changes in the maximum stress and maximum displacement values with respect to the number of dropped plies in the symmetrically-balanced laminated disc are calculated.

4.7.3.1 Effect of dropped plies on the elastic response of symmetrically-balanced laminated discs

The effect of number of dropped plies on the radial and circumferential stress distributions, on the in-plane shear stress distribution and on the radial displacement distribution in a rotating annular thickness-tapered symmetrically-balanced laminated disc with the clamped-free boundary condition is studied for different taper configurations considered in the present thesis. To study the

effect of dropped plies on the elastic response of symmetrically-balanced laminated disc, a rotating disc with a beta value of 0.2 is chosen. Therefore, for this beta value, the disc has an inner radius of r_i = 24 *mm*, an outer radius of r_o = 120 *mm*, thickness at the hub, h_i = 2.4 *mm* with an individual ply thickness of t_k = 0.12 *mm,* and is rotating at a constant angular velocity of ω = 1000 *rad/s* i.e., 9554.14 *rpm*.

The following Figure 4.17 shows the variation with the number of dropped plies of the maximum radial stress in a rotating annular thickness-tapered symmetrically-balanced laminated disc with the clamped-free boundary condition. The variation of the maximum radial stress has been shown for different taper configurations of the laminated disc considered in the present study.

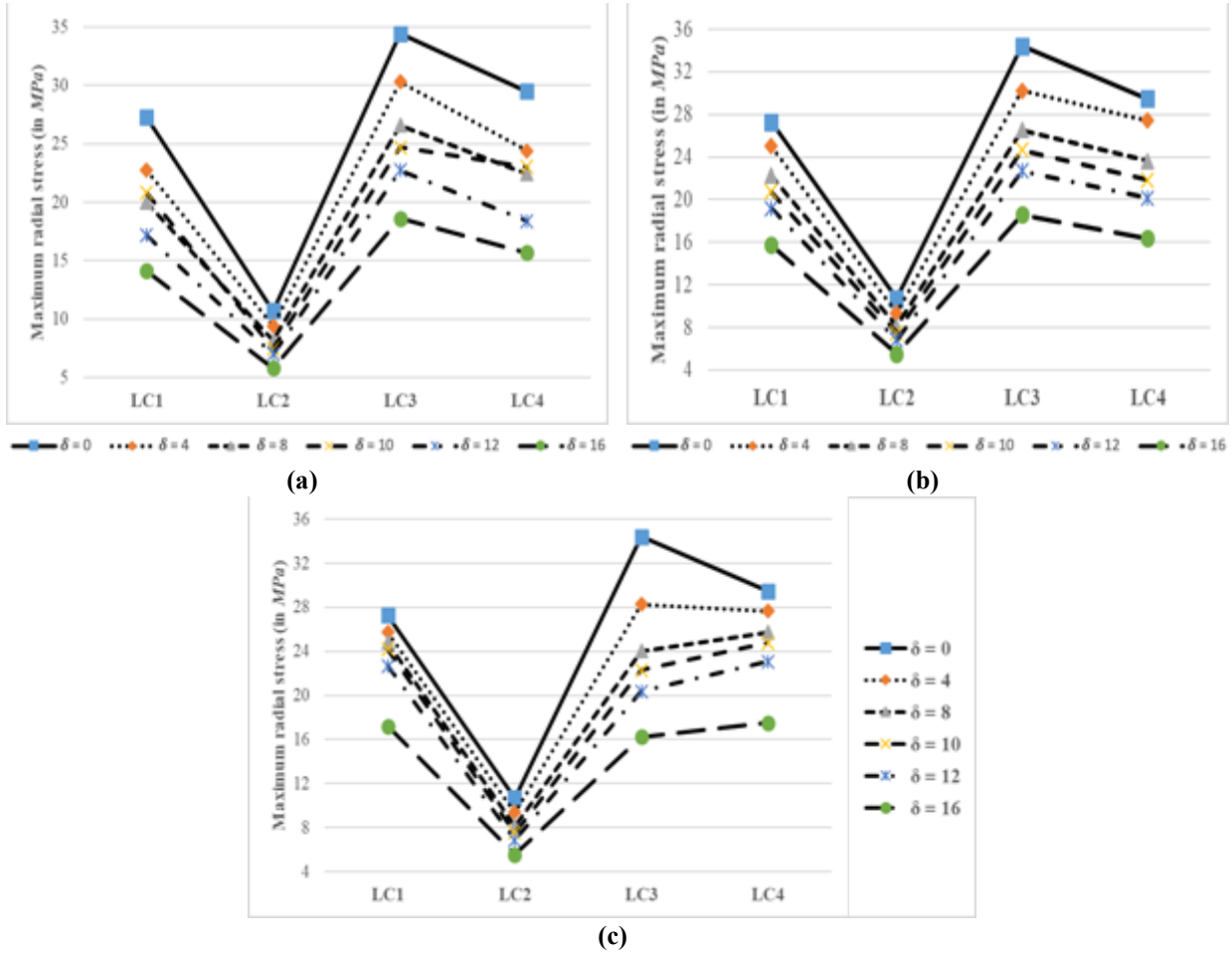

Figure 4.17 Variation of the maximum radial stress with the number of dropped plies in rotating annular thickness-tapered symmetrically-balanced laminated discs with the clamped-free boundary condition for **(a)** taper configuration B, **(b)** taper configuration C and **(c)** taper configuration D

The following Tables 4.54 and 4.55 show the variation of the maximum radial stress and the percentage decrease in the maximum radial stress with the number of dropped plies, in rotating annular thickness-tapered symmetrically-balanced laminated discs with taper configuration B and with the clamped-free boundary condition. Since the rotating disc with $\delta = 0$ is subjected to the maximum amount of radial stress, the value of the radial stress for $\delta = 0$ is considered as a benchmark while calculating the percentage decrease in the stress. Also, in the below Table 4.55, the percentage decrease in the maximum radial stress is calculated according to the formula given in the Equation (4.22).

Maximum radial stress, σ_r^{max} (in MPa) in rotating annular thickness-tapered symmetrically-balanced laminated discs with taper configuration B and with the clamped-free boundary condition						
$\beta = 0.2$						
Laminate configuration of the disc	Number of dropped plies (δ)					
	0	4	8	10	12	16
LC1	27.268	22.724	20.003	20.812	17.17	14.105
LC2	10.69	9.402	8.153	7.48	7.002	5.789
LC3	34.416	30.305	26.607	24.694	22.733	18.63
LC4	29.478	24.398	22.453	23.012	18.375	15.688

Table 4.54 Variation of the maximum radial stress (in MPa) with the number of dropped plies in rotating annular thickness-tapered symmetrically-balanced laminated discs with taper configuration B and with the clamped-free boundary condition

Percentage decrease in the maximum radial stress in rotating annular thickness-tapered symmetrically-balanced laminated discs with taper configuration B and with the clamped-free boundary condition					
$\beta = 0.2$					
Laminate configuration of the disc	Percentage decrease in the maximum radial stress				
	${}^{0}_{4}\eta_B$	${}^{0}_{8}\eta_B$	${}^{0}_{10}\eta_B$	${}^{0}_{12}\eta_B$	${}^{0}_{16}\eta_B$
LC1	16.66	26.64	23.68	37.03	48.27
LC2	12.05	23.73	30.03	34.5	45.85
LC3	11.95	22.69	28.25	33.95	45.87
LC4	17.23	23.83	21.94	37.67	46.78

Table 4.55 Variation of the percentage decrease in the maximum radial stress with the number of dropped plies in rotating annular thickness-tapered symmetrically-balanced laminated discs with taper configuration B and with the clamped-free boundary condition

The following Tables 4.56 and 4.57 show the variation of the maximum radial stress and the percentage decrease in the maximum radial stress with the number of dropped plies, in rotating annular thickness-tapered symmetrically-balanced laminated discs with taper configuration C and with the clamped-free boundary condition. Also, in the below Table 4.57, the percentage decrease in the maximum radial stress is calculated according to the formula given in the Equation (4.22).

Maximum radial stress, σ_r^{max} (in MPa) in rotating annular thickness-tapered symmetrically-balanced laminated discs with taper configuration C and with the clamped-free boundary condition						
$\beta = 0.2$						
Laminate configuration of the disc	Number of dropped plies (δ)					
	0	4	8	10	12	16
LC1	27.268	25.029	22.248	20.738	19.163	15.76
LC2	10.69	9.377	8.114	7.476	6.833	5.532
LC3	34.416	30.228	26.543	24.636	22.681	18.588
LC4	29.478	27.43	23.623	21.842	20.135	16.359

Table 4.56 Variation of the maximum radial stress (in *MPa*) with the number of dropped plies in rotating annular thickness-tapered symmetrically-balanced laminated discs with taper configuration C and with the clamped-free boundary condition

Percentage decrease in the maximum radial stress in rotating annular thickness-tapered symmetrically-balanced laminated discs with taper configuration C and with the clamped-free boundary condition					
$\beta = 0.2$					
Laminate configuration of the disc	Percentage decrease in the maximum radial stress				
	${}^{0}_{4}\eta_C$	${}^{0}_{8}\eta_C$	${}^{0}_{10}\eta_C$	${}^{0}_{12}\eta_C$	${}^{0}_{16}\eta_C$
LC1	8.21	18.41	23.95	29.72	42.2
LC2	12.28	24.1	30.07	36.08	48.25
LC3	12.17	22.88	28.42	34.1	45.99
LC4	6.95	19.86	25.9	31.69	44.5

Table 4.57 Variation of the percentage decrease in the maximum radial stress with the number of dropped plies in rotating annular thickness-tapered symmetrically-balanced laminated discs with taper configuration C and with the clamped-free boundary condition

The following Tables 4.58 and 4.59 show the variation of the maximum radial stress and the percentage decrease in the maximum radial stress with the number of dropped plies, in rotating annular thickness-tapered symmetrically-balanced laminated discs with taper configuration D and with the clamped-free boundary condition. Also, in the below Table 4.59, the percentage decrease in the maximum radial stress is calculated according to the formula given in the Equation (4.22).

Maximum radial stress, σ_r^{max} (in MPa) in rotating annular thickness-tapered symmetrically-balanced laminated discs with taper configuration D and with the clamped-free boundary condition						
$\beta = 0.2$						
Laminate configuration of the disc	Number of dropped plies (δ)					
	0	4	8	10	12	16
LC1	27.268	25.732	24.796	24.186	22.668	17.222
LC2	10.69	9.38	8.138	7.531	6.892	5.546
LC3	34.416	28.255	24.039	22.278	20.38	16.256
LC4	29.478	27.67	25.713	24.76	23.054	17.513

Table 4.58 Variation of the maximum radial stress (in MPa) with the number of dropped plies in rotating annular thickness-tapered symmetrically-balanced laminated discs with taper configuration D and with the clamped-free boundary condition

Percentage decrease in the maximum radial stress in rotating annular thickness-tapered symmetrically-balanced laminated discs with taper configuration D and with the clamped-free boundary condition					
$\beta = 0.2$					
Laminate configuration of the disc	Percentage decrease in the maximum radial stress				
	${}^{0}_{4}\eta_D$	${}^{0}_{8}\eta_D$	${}^{0}_{10}\eta_D$	${}^{0}_{12}\eta_D$	${}^{0}_{16}\eta_D$
LC1	5.63	9.07	11.3	16.87	36.84
LC2	12.25	23.87	29.55	35.53	48.12
LC3	17.9	30.15	35.27	40.78	52.77
LC4	6.13	12.77	16.01	21.79	40.59

Table 4.59 Variation of the percentage decrease in the maximum radial stress with the number of dropped plies in rotating annular thickness-tapered symmetrically-balanced laminated discs with taper configuration D and with the clamped-free boundary condition

The following observations can be made from the variation of the maximum radial stress and the percentage decrease in the maximum radial stress with the number of dropped plies, in rotating annular thickness-tapered symmetrically-balanced laminated discs with the clamped-free boundary condition for different taper configurations, shown in the Figure 4.17 and Tables 4.54 – 4.59:

- Irrespective of the laminate configuration and the taper configuration, the maximum radial stress decreases with the increasing number of dropped plies in rotating annular thickness-tapered symmetrically-balanced laminated discs with the clamped-free boundary condition.
- Irrespective of the taper configuration and the number of dropped plies, the rotating disc with LC3 configuration experiences the maximum amount of radial stress, whereas, the disc with LC2 configuration experiences the minimum amount of radial stress. For instance, a rotating annular thickness-tapered symmetrically-balanced laminated disc with δ = 12 and with the taper configuration C will experience a radial stress of 22.687 *MPa* for the LC3 configuration, whereas, a symmetrically-balanced disc with the same number of dropped plies and the same taper configuration will experience a radial stress of 6.833 *MPa* for the LC2 configuration.
- For the symmetrically-balanced laminated disc with LC1 and LC4 configurations, irrespective of the number of dropped plies, the rotating disc with the taper configuration B experiences the minimum amount of radial stress, whereas, the disc with the taper configuration D experiences the maximum amount of radial stress.
- For the symmetrically-balanced laminated disc with LC2 configuration, irrespective of the number of dropped plies, the rotating disc with taper configuration C experiences the minimum amount of radial stress, whereas, the disc with taper configuration B experiences the maximum amount of radial stress. Also, for the disc with LC3 configuration, the rotating disc with taper configuration D experiences the minimum amount of radial stress while the disc with taper configuration B experiences the maximum amount of radial stress.
- Irrespective of the laminate configuration, on comparing the maximum amount of percentage decrease in the radial stress corresponding to different taper

configurations, it can be seen that, for the disc with LC1 and LC4 laminate configurations, the percentage decrease in the maximum radial stress is maximum for the taper configuration B (48.27% and 46.78% respectively), whereas, for the disc with LC2 and LC3 configurations, the percentage decrease in the stress is maximum for the taper configurations C (48.25%) and D (52.77%) respectively.

The following Figure 4.18 shows the variation with the number of dropped plies of the maximum circumferential stress in a rotating annular thickness-tapered symmetrically-balanced laminated disc with the clamped-free boundary condition. The variation of the maximum circumferential stress has been shown for different taper configurations of the laminated disc considered in the present study.

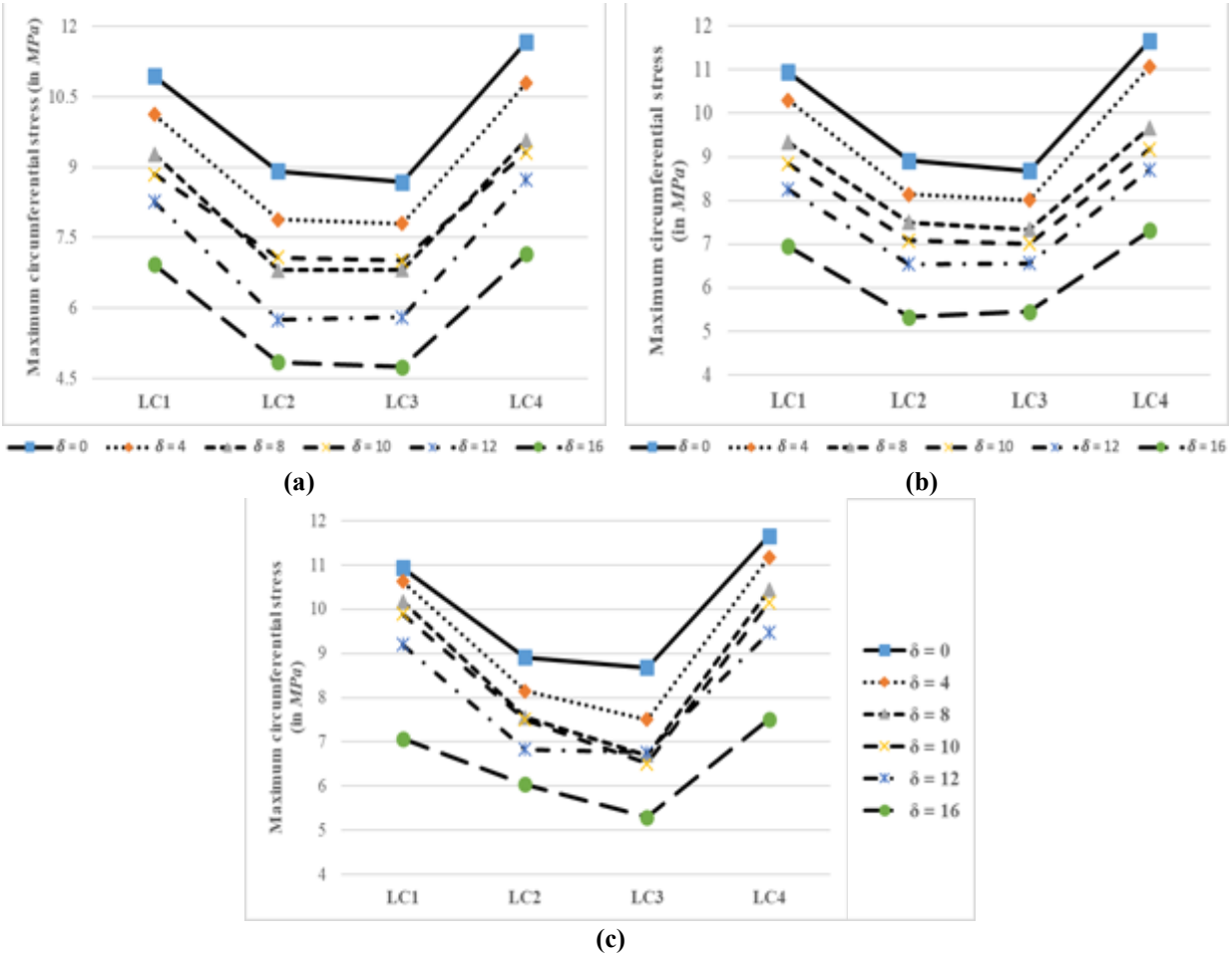

Figure 4.18 Variation of the maximum circumferential stress with the number of dropped plies in rotating annular thickness-tapered symmetrically-balanced laminated discs with the clamped-free boundary condition for **(a)** taper configuration B, **(b)** taper configuration C and **(c)** taper configuration D

The following Tables 4.60 and 4.61 show the variation of the maximum circumferential stress and the percentage decrease in the maximum circumferential stress with the number of dropped plies, in rotating annular thickness-tapered symmetrically-balanced laminated discs with taper configuration B and with the clamped-free boundary condition. Also, in the below Table 4.61, the percentage decrease in the maximum circumferential stress is calculated according to the formula given in the Equation (4.22).

Maximum circumferential stress, σ_θ^{max} (in MPa) in rotating annular thickness-tapered symmetrically-balanced laminated discs with taper configuration B and with the clamped-free boundary condition						
$\beta = 0.2$						
Laminate configuration of the disc	Number of dropped plies (δ)					
	0	4	8	10	12	16
LC1	10.934	10.123	9.28	8.847	8.266	6.926
LC2	8.913	7.88	6.806	7.074	5.754	4.853
LC3	8.683	7.803	6.821	7.015	5.806	4.745
LC4	11.659	10.79	9.572	9.309	8.734	7.149

Table 4.60 Variation of the maximum circumferential stress (in MPa) with the number of dropped plies in rotating annular thickness-tapered symmetrically-balanced laminated discs with taper configuration B and with the clamped-free boundary condition

Percentage decrease in the maximum circumferential stress in rotating annular thickness-tapered symmetrically-balanced laminated discs with taper configuration B and with the clamped-free boundary condition					
$\beta = 0.2$					
Laminate configuration of the disc	Percentage decrease in the maximum circumferential stress				
	${}^{0}_{4}\eta_B$	${}^{0}_{8}\eta_B$	${}^{0}_{10}\eta_B$	${}^{0}_{12}\eta_B$	${}^{0}_{16}\eta_B$
LC1	7.42	15.13	19.09	24.4	36.66
LC2	11.59	23.64	20.63	35.44	45.55
LC3	10.13	21.44	19.21	33.13	45.35
LC4	7.45	17.9	20.16	25.09	38.68

Table 4.61 Variation of the percentage decrease in the maximum circumferential stress with the number of dropped plies in rotating annular thickness-tapered symmetrically-balanced laminated discs with taper configuration B and with the clamped-free boundary condition

The following Tables 4.62 and 4.63 show the variation of the maximum circumferential stress and the percentage decrease in the maximum circumferential stress with the number of dropped plies, in rotating annular thickness-tapered symmetrically-balanced laminated discs with taper configuration C and with the clamped-free boundary condition. Also, in the below Table 4.63, the percentage decrease in the maximum circumferential stress is calculated according to the formula given in the Equation (4.22).

Maximum circumferential stress, σ_θ^{max} (in MPa) in rotating annular thickness-tapered symmetrically-balanced laminated discs with taper configuration C and with the clamped-free boundary condition						
$\beta = 0.2$						
Laminate configuration of the disc	Number of dropped plies (δ)					
	0	4	8	10	12	16
LC1	10.934	10.299	9.33	8.847	8.253	6.949
LC2	8.913	8.144	7.5	7.078	6.544	5.332
LC3	8.683	8.013	7.34	7.008	6.568	5.455
LC4	11.659	11.066	9.663	9.18	8.71	7.319

Table 4.62 Variation of the maximum circumferential stress (in MPa) with the number of dropped plies in rotating annular thickness-tapered symmetrically-balanced laminated discs with taper configuration C and with the clamped-free boundary condition

Percentage decrease in the maximum circumferential stress in rotating annular thickness-tapered symmetrically-balanced laminated discs with taper configuration C and with the clamped-free boundary condition					
$\beta = 0.2$					
Laminate configuration of the disc	Percentage decrease in the maximum circumferential stress				
	${}^{0}_{4}\eta_C$	${}^{0}_{8}\eta_C$	${}^{0}_{10}\eta_C$	${}^{0}_{12}\eta_C$	${}^{0}_{16}\eta_C$
LC1	5.81	14.67	19.09	24.52	36.45
LC2	8.63	15.85	20.59	26.58	40.18
LC3	7.72	15.47	19.29	24.36	37.18
LC4	5.09	17.12	21.26	25.29	37.22

Table 4.63 Variation of the percentage decrease in the maximum circumferential stress with the number of dropped plies in rotating annular thickness-tapered symmetrically-balanced laminated discs with taper configuration C and with the clamped-free boundary condition

The following Tables 4.64 and 4.65 show the variation of the maximum circumferential stress and the percentage decrease in the maximum circumferential stress with the number of dropped plies, in rotating annular thickness-tapered symmetrically-balanced laminated discs with taper configuration D and with the clamped-free boundary condition. Also, in the below Table 4.65, the percentage decrease in the maximum circumferential stress is calculated according to the formula given in the Equation (4.22).

Maximum circumferential stress, σ_θ^{max} (in MPa) in rotating annular thickness-tapered symmetrically-balanced laminated discs with taper configuration D and with the clamped-free boundary condition						
$\beta = 0.2$						
Laminate configuration of the disc	Number of dropped plies (δ)					
	0	4	8	10	12	16
LC1	10.934	10.622	10.174	9.89	9.198	7.069
LC2	8.913	8.147	7.548	7.503	6.831	6.044
LC3	8.683	7.502	6.695	6.508	6.761	5.299
LC4	11.659	11.174	10.43	10.152	9.468	7.516

Table 4.64 Variation of the maximum circumferential stress (in MPa) with the number of dropped plies in rotating annular thickness-tapered symmetrically-balanced laminated discs with taper configuration D and with the clamped-free boundary condition

Percentage decrease in the maximum circumferential stress in rotating annular thickness-tapered symmetrically-balanced laminated discs with taper configuration D and with the clamped-free boundary condition					
$\beta = 0.2$					
Laminate configuration of the disc	Percentage decrease in the maximum circumferential stress				
	${}^{0}_{4}\eta_D$	${}^{0}_{8}\eta_D$	${}^{0}_{10}\eta_D$	${}^{0}_{12}\eta_D$	${}^{0}_{16}\eta_D$
LC1	2.85	6.95	9.55	15.88	35.35
LC2	8.59	15.31	15.82	23.36	32.19
LC3	13.6	22.9	25.05	22.14	38.97
LC4	4.16	10.54	12.93	18.79	35.53

Table 4.65 Variation of the percentage decrease in the maximum circumferential stress with the number of dropped plies in rotating annular thickness-tapered symmetrically-balanced laminated discs with taper configuration D and with the clamped-free boundary condition

The following observations can be made from the variation of the maximum circumferential stress and the percentage decrease in the maximum circumferential stress with the number of dropped plies, in rotating annular thickness-tapered symmetrically-balanced laminated discs with the clamped-free boundary condition for different taper configurations, shown in the Figure 4.18 and Tables 4.60 – 4.65:

- Irrespective of the laminate configuration and the taper configuration, the circumferential stress decreases with the increasing number of dropped plies in rotating annular thickness-tapered symmetrically-balanced laminated discs with the clamped-free boundary condition.
- Irrespective of the taper configuration and the number of dropped plies, the rotating disc with LC4 configuration experiences the maximum amount of circumferential stress, whereas, the disc with LC3 configuration experiences the minimum amount of circumferential stress. For instance, a rotating annular thickness-tapered symmetrically-balanced laminated disc with $\delta = 12$ and with the taper configuration C will experience a circumferential stress of 8.71 *MPa* for the LC4 configuration, whereas, a symmetrically-balanced laminated disc with the same number of dropped plies and the same taper configuration will experience a circumferential stress of 6.568 *MPa* for the LC3 configuration.
- For the symmetrically-balanced disc with LC1, LC2 and LC4 configurations, irrespective of the number of dropped plies, the rotating disc with the taper configuration B experiences the minimum amount of circumferential stress, whereas, the disc with the taper configuration D experiences the maximum amount of circumferential stress. For instance, a rotating annular thickness-tapered symmetrically-balanced laminated disc with LC1, LC2 and LC4 configurations and with $\delta = 4$ will experience a radial stress of 10.123 *MPa*, 7.88 *MPa* and 10.79 *MPa* respectively, for the taper configuration B, whereas, a symmetrically-balanced laminated disc with the same number of dropped plies and the same laminate configurations will experience a radial stress of 10.622 *MPa,* 8.147 *MPa* and 11.174 *MPa* respectively, for the taper configuration D.

- For the symmetrically-balanced laminated disc with LC3 configuration, irrespective of the number of dropped plies, the rotating disc with the taper configuration C experiences the maximum amount of circumferential stress.
- Irrespective of the laminate configuration, on comparing the maximum amount of percentage decrease in the circumferential stress corresponding to different taper configurations, it can be seen that the percentage decrease in the maximum circumferential stress is maximum for the rotating annular thickness-tapered symmetrically-balanced laminated disc with taper configuration B.

The following Figure 4.19 shows the variation with the number of dropped plies of the maximum radial displacement in a rotating annular thickness-tapered symmetrically-balanced laminated disc with the clamped-free boundary condition. The variation of the maximum radial displacement has been shown for different taper configurations of the laminated disc considered in the present study.

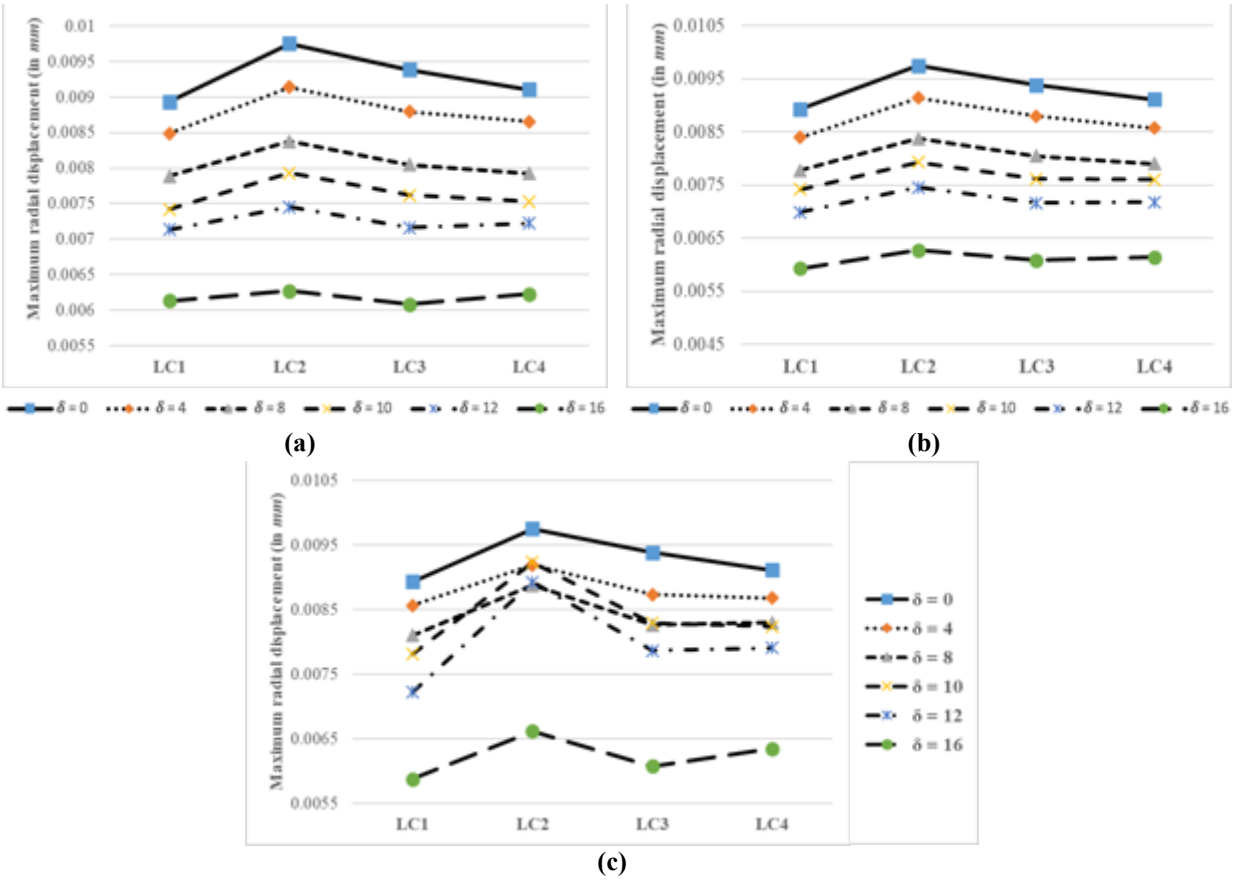

Figure 4.19 Variation of the maximum radial displacement with the number of dropped plies in rotating annular thickness-tapered symmetrically-balanced laminated discs with the clamped-free boundary condition for **(a)** taper configuration B, **(b)** taper configuration C and **(c)** taper configuration D

The following Tables 4.66 and 4.67 show the variation of the maximum radial displacement and the percentage decrease in the maximum radial displacement with the number of dropped plies, in rotating annular thickness-tapered symmetrically-balanced laminated discs with taper configuration B and with the clamped-free boundary condition. Since, the rotating disc with $\delta = 0$ is subjected to the maximum amount of radial displacement, the value of the displacement for $\delta = 0$ is considered as a benchmark while calculating the percentage decrease in the displacement. Also, in the below Table 4.67, the percentage decrease in the displacement is calculated according to the formula given in the Equation (4.23).

Maximum radial displacement, u_r^{max} (in mm) in rotating annular thickness-tapered symmetrically-balanced laminated discs with taper configuration B and with the clamped-free boundary condition						
$\beta = 0.2$						
Laminate configuration of the disc	Number of dropped plies (δ)					
	0	4	8	10	12	16
LC1	0.00893	0.00849	0.00789	0.00742	0.00713	0.00613
LC2	0.00975	0.00914	0.00837	0.00793	0.00745	0.00627
LC3	0.00938	0.00879	0.00805	0.00762	0.00716	0.00608
LC4	0.00911	0.00866	0.00793	0.00753	0.00722	0.00623

Table 4.66 Variation of the maximum radial displacement (in *mm*) with the number of dropped plies in rotating annular thickness-tapered symmetrically-balanced laminated discs with taper configuration B and with the clamped-free boundary condition

Percentage decrease in the maximum radial displacement in rotating annular thickness-tapered symmetrically-balanced laminated discs with taper configuration B and with the clamped-free boundary condition					
$\beta = 0.2$					
Laminate configuration of the disc	Percentage decrease in the maximum radial displacement				
	${}^{0}_{4}\eta_B$	${}^{0}_{8}\eta_B$	${}^{0}_{10}\eta_B$	${}^{0}_{12}\eta_B$	${}^{0}_{16}\eta_B$
LC1	4.93	11.65	16.91	20.16	31.35
LC2	6.26	14.15	18.67	23.59	35.69
LC3	6.29	14.18	18.76	23.67	35.18
LC4	4.94	12.95	17.34	20.75	31.61

Table 4.67 Variation of the percentage decrease in the maximum radial displacement with the number of dropped plies in rotating annular thickness-tapered symmetrically-balanced laminated discs with taper configuration B and with the clamped-free boundary condition

The following Tables 4.68 and 4.69 show the variation of the maximum radial displacement and the percentage decrease in the maximum radial displacement with the number of dropped plies, in rotating annular thickness-tapered symmetrically-balanced laminated discs with taper configuration C and with the clamped-free boundary condition. Also, in the below Table 4.69, the percentage decrease in the maximum radial displacement is calculated according to the formula given in the Equation (4.23).

Maximum radial displacement, u_r^{max} (in mm) in rotating annular thickness-tapered symmetrically-balanced laminated discs with taper configuration C and with the clamped-free boundary condition						
$\beta = 0.2$						
Laminate configuration of the disc	Number of dropped plies (δ)					
	0	4	8	10	12	16
LC1	0.00893	0.00839	0.00778	0.00742	0.00699	0.00593
LC2	0.00975	0.00914	0.00837	0.00793	0.00745	0.00627
LC3	0.00938	0.00879	0.00805	0.00762	0.00716	0.00608
LC4	0.00911	0.00857	0.0079	0.0076	0.00718	0.00614

Table 4.68 Variation of the maximum radial displacement (in *mm*) with the number of dropped plies in rotating annular thickness-tapered symmetrically-balanced laminated discs with taper configuration C and with the clamped-free boundary condition

Percentage decrease in the maximum radial displacement in rotating annular thickness-tapered symmetrically-balanced laminated discs with taper configuration C and with the clamped-free boundary condition					
$\beta = 0.2$					
Laminate configuration of the disc	Percentage decrease in the maximum radial displacement				
	${}^{0}_{4}\eta_C$	${}^{0}_{8}\eta_C$	${}^{0}_{10}\eta_C$	${}^{0}_{12}\eta_C$	${}^{0}_{16}\eta_C$
LC1	6.05	12.88	16.91	21.72	33.59
LC2	6.26	14.15	18.67	23.59	35.69
LC3	6.29	14.18	18.76	23.67	35.18
LC4	5.93	13.28	16.58	21.19	32.6

Table 4.69 Variation of the percentage decrease in the maximum radial displacement with the number of dropped plies in rotating annular thickness-tapered symmetrically-balanced laminated discs with taper configuration C and with the clamped-free boundary condition

The following Tables 4.70 and 4.71 show the variation of the maximum radial displacement and the percentage decrease in the maximum radial displacement with the number of dropped plies, in rotating annular thickness-tapered symmetrically-balanced laminated discs with taper configuration D and with the clamped-free boundary condition. Also, in the below Table 4.71, the percentage decrease in the maximum radial displacement is calculated according to the formula given in the Equation (4.23).

Maximum radial displacement, u_r^{max} (in mm) in rotating annular thickness-tapered symmetrically-balanced laminated discs with taper configuration D and with the clamped-free boundary condition						
$\beta = 0.2$						
Laminate configuration of the disc	Number of dropped plies (δ)					
	0	4	8	10	12	16
LC1	0.00893	0.00857	0.0081	0.00781	0.00722	0.00588
LC2	0.00975	0.00919	0.00888	0.00923	0.00893	0.00662
LC3	0.00938	0.00873	0.00826	0.00829	0.00787	0.00608
LC4	0.00911	0.00868	0.0083	0.00824	0.00791	0.00635

Table 4.70 Variation of the maximum radial displacement (in *mm*) with the number of dropped plies in rotating annular thickness-tapered symmetrically-balanced laminated discs with taper configuration D and with the clamped-free boundary condition

Percentage decrease in the maximum radial displacement in rotating annular thickness-tapered symmetrically-balanced laminated discs with taper configuration D and with the clamped-free boundary condition					
$\beta = 0.2$					
Laminate configuration of the disc	Percentage decrease in the maximum radial stress				
	${}^{0}_{4}\eta_D$	${}^{0}_{8}\eta_D$	${}^{0}_{10}\eta_D$	${}^{0}_{12}\eta_D$	${}^{0}_{16}\eta_D$
LC1	4.03	9.29	12.54	19.15	34.15
LC2	5.74	8.92	5.33	8.41	32.1
LC3	6.93	11.94	11.62	16.1	35.18
LC4	4.72	8.89	9.55	13.17	30.3

Table 4.71 Variation of the percentage decrease in the maximum radial displacement with the number of dropped plies in rotating annular thickness-tapered symmetrically-balanced laminated discs with taper configuration D and with the clamped-free boundary condition

The following observations can be made from the variation of the maximum radial displacement and the percentage decrease in the maximum radial displacement with the number of dropped plies, in rotating annular thickness-tapered symmetrically-balanced laminated discs with the clamped-free boundary condition for different taper configurations, shown in the Figure 4.19 and Tables 4.70 – 4.71:

- Irrespective of the laminate configuration and the taper configuration, the maximum radial displacement decreases with the increasing number of dropped plies in rotating annular thickness-tapered symmetrically-balanced laminated discs with the clamped-free boundary condition. This observation is only valid for the symmetrically-balanced laminated discs with taper configurations B and C. For the disc with taper configuration D, the variation of the maximum radial displacement with the increasing number of dropped plies can be elaborated as follows:
  I. For the symmetrically-balanced laminated disc with taper configuration D and with LC1 configuration, the maximum radial displacement decreases with the increasing number of dropped plies.
  II. For the disc with LC2 configuration, the maximum radial displacement first decreases with the increasing number of dropped plies till $\delta = 8$. The value of the radial displacement corresponding to $\delta = 10$ and $\delta = 12$ are approximately the same as the displacements corresponding to $\delta = 4$ and $\delta = 8$, respectively. Thereafter, the maximum radial displacement decreases with the increasing number of dropped plies and has a minimum value for $\delta = 16$.
  III. For the discs with LC3 and LC4 configurations, the maximum radial displacement first decreases with the increasing number of dropped plies till $\delta = 8$. The value of the radial displacement corresponding to $\delta = 10$ is approximately the same as the displacement corresponding to $\delta = 8$. Thereafter, the maximum radial displacement decreases with the increasing number of dropped plies and has a minimum value for $\delta = 16$.
- Irrespective of the taper configuration and the number of dropped plies, the rotating annular thickness-tapered symmetrically-balanced laminated disc with LC2 configuration experiences the maximum amount of radial displacement, whereas,

the disc with LC1 configuration experiences the minimum amount of radial displacement.

- Irrespective of the laminate configuration and the number of dropped plies, the rotating annular thickness-tapered symmetrically-balanced laminated disc with taper configuration C is subjected to the minimum amount of radial displacement, whereas, the disc with taper configuration D is subjected to the maximum amount of radial displacement.
- On comparing the maximum amount of percentage decrease in the radial displacement corresponding to different taper configurations, it can be seen that for the symmetrically-balanced laminated disc with LC1 configuration, the percentage decrease is maximum for taper configuration D, whereas, for the disc with LC2 and LC4 configurations, the percentage decrease is maximum for taper configuration C. For the disc with LC3 configuration, the maximum amount of percentage decrease in the radial displacement is the same among the different taper configurations considered in the present study.

The following Figure 4.20 shows the variation with the number of dropped plies of the maximum in-plane shear stress in a rotating annular thickness-tapered symmetrically-balanced laminated disc with the clamped-free boundary condition. The variation of the maximum in-plane shear stress has been shown for different taper configurations of the laminated disc considered in the present study.

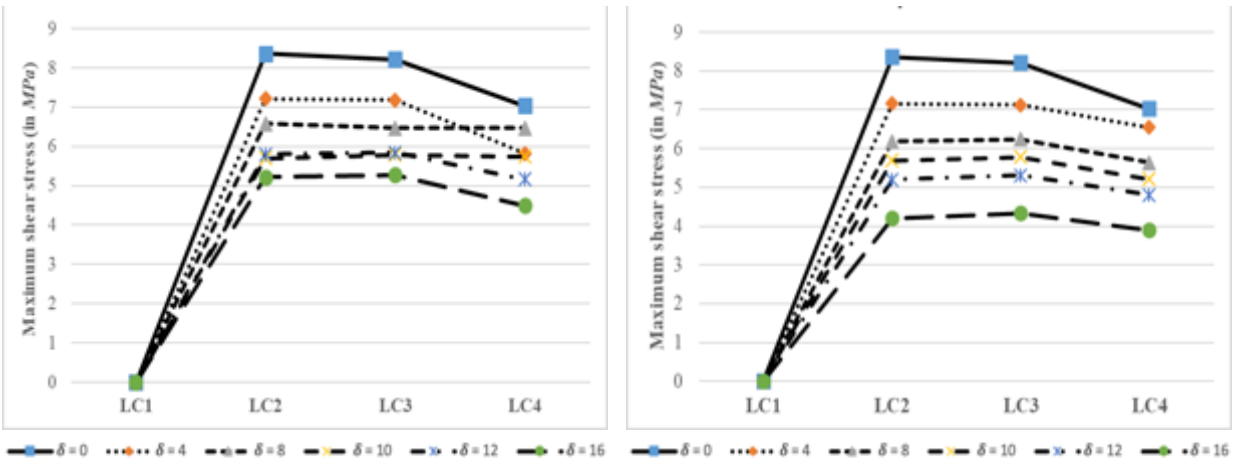

(a) **(b)**

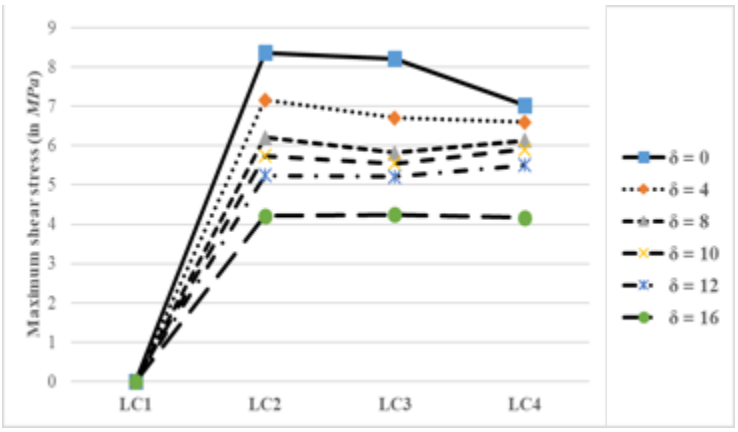

(c)

Figure 4.20 Variation of the maximum in-plane shear stress with the number of dropped plies in rotating annular thickness-tapered symmetrically-balanced laminated discs with the clamped-free boundary condition for **(a)** taper configuration B, **(b)** taper configuration C and **(c)** taper configuration D

The following Tables 4.72 and 4.73 show the variation of the maximum in-plane shear stress and the percentage decrease in the maximum shear stress with the number of dropped plies, in rotating annular thickness-tapered symmetrically-balanced laminated discs with taper configuration B and with the clamped-free boundary condition. Also, in the below Table 4.73, the percentage decrease in the maximum in-plane shear stress is calculated according to the formula given in the Equation (4.22).

Maximum in-plane shear stress, $\tau_{r\theta}^{max}$ (in MPa) in rotating annular thickness-tapered symmetrically-balanced laminated discs with taper configuration B and with the clamped-free boundary condition						
$\beta = 0.2$						
Laminate configuration of the disc	Number of dropped plies (δ)					
	0	4	8	10	12	16
LC1	0	0	0	0	0	0
LC2	8.361	7.209	6.574	5.703	5.798	5.185
LC3	8.21	7.184	6.462	5.783	5.846	5.274
LC4	7.032	5.824	6.464	5.745	5.159	4.574

Table 4.72 Variation of the maximum in-plane shear stress (in *MPa*) with the number of dropped plies in rotating annular thickness-tapered symmetrically-balanced laminated discs with taper configuration B and with the clamped-free boundary condition

Percentage decrease in the maximum in-plane shear stress in rotating annular thickness-tapered symmetrically-balanced laminated discs with taper configuration B and with the clamped-free boundary condition					
$\beta = 0.2$					
Laminate configuration of the disc	Percentage decrease in the maximum in-plane shear stress				
	${}^{0}_{4}\eta_B$	${}^{0}_{8}\eta_B$	${}^{0}_{10}\eta_B$	${}^{0}_{12}\eta_B$	${}^{0}_{16}\eta_B$
LC1	0	0	0	0	0
LC2	13.78	21.37	31.79	30.65	37.99
LC3	12.5	21.29	29.56	28.79	35.76
LC4	17.18	8.08	18.3	26.64	34.95

Table 4.73 Variation of the percentage decrease in the maximum in-plane shear stress with the number of dropped plies in rotating annular thickness-tapered symmetrically-balanced laminated discs with taper configuration B and with the clamped-free boundary condition

The following Tables 4.74 and 4.75 show the variation of the maximum in-plane shear stress and the percentage decrease in the maximum shear stress with the number of dropped plies, in rotating annular thickness-tapered symmetrically-balanced laminated discs with taper configuration C and with the clamped-free boundary condition. Also, in the below Table 4.75, the percentage decrease in the maximum in-plane shear stress is calculated according to the formula given in the Equation (4.22).

Maximum in-plane shear stress, $\tau_{r\theta}^{max}$ (in MPa) in rotating annular thickness-tapered symmetrically-balanced laminated discs with taper configuration C and with the clamped-free boundary condition						
$\beta = 0.2$						
Laminate configuration of the disc	Number of dropped plies (δ)					
	0	4	8	10	12	16
LC1	0	0	0	0	0	0
LC2	8.361	7.158	6.187	5.697	5.203	4.205
LC3	8.21	7.125	6.235	5.776	5.308	4.333
LC4	7.032	6.543	5.634	5.209	4.801	3.898

Table 4.74 Variation of the maximum in-plane shear stress (in *MPa*) with the number of dropped plies in rotating annular thickness-tapered symmetrically-balanced laminated discs with taper configuration C and with the clamped-free boundary condition

Percentage decrease in the maximum in-plane shear stress in rotating annular thickness-tapered symmetrically-balanced laminated discs with taper configuration C and with the clamped-free boundary condition					
$\beta = 0.2$					
Laminate configuration of the disc	Percentage decrease in the maximum in-plane shear stress				
	${}^{0}_{4}\eta_C$	${}^{0}_{8}\eta_C$	${}^{0}_{10}\eta_C$	${}^{0}_{12}\eta_C$	${}^{0}_{16}\eta_C$
LC1	0	0	0	0	0
LC2	14.39	26	31.86	37.77	49.71
LC3	13.22	24.06	29.65	35.35	47.22
LC4	6.95	19.88	25.92	31.73	44.57

Table 4.75 Variation of the percentage decrease in the maximum in-plane shear stress with the number of dropped plies in rotating annular thickness-tapered symmetrically-balanced laminated discs with taper configuration C and with the clamped-free boundary condition

The following Tables 4.76 and 4.77 show the variation of the maximum in-plane shear stress and the percentage decrease in the maximum shear stress with the number of dropped plies, in rotating annular thickness-tapered symmetrically-balanced laminated discs with taper configuration D and with the clamped-free boundary condition. Also, in the below Table 4.77, the percentage decrease in the maximum in-plane shear stress is calculated according to the formula given in the Equation (4.22).

Maximum in-plane shear stress, $\tau_{r\theta}^{max}$ (in MPa) in rotating annular thickness-tapered symmetrically-balanced laminated discs with taper configuration D and with the clamped-free boundary condition						
$\beta = 0.2$						
Laminate configuration of the disc	Number of dropped plies (δ)					
	0	4	8	10	12	16
LC1	0	0	0	0	0	0
LC2	8.361	7.16	6.206	5.739	5.248	4.216
LC3	8.21	6.705	5.815	5.552	5.209	4.249
LC4	7.032	6.6	6.134	5.907	5.499	4.175

Table 4.76 Variation of the maximum in-plane shear stress (in *MPa*) with the number of dropped plies in rotating annular thickness-tapered symmetrically-balanced laminated discs with taper configuration D and with the clamped-free boundary condition

Percentage decrease in the maximum in-plane shear stress in rotating annular thickness-tapered symmetrically-balanced laminated discs with taper configuration D and with the clamped-free boundary condition					
$\beta = 0.2$					
Laminate configuration of the disc	Percentage decrease in the maximum in-plane shear stress				
	${}^{0}_{4}\eta_D$	${}^{0}_{8}\eta_D$	${}^{0}_{10}\eta_D$	${}^{0}_{12}\eta_D$	${}^{0}_{16}\eta_D$
LC1	0	0	0	0	0
LC2	14.36	25.77	31.36	37.23	49.58
LC3	18.33	29.17	32.38	36.55	48.25
LC4	6.14	12.77	16	21.8	40.63

Table 4.77 Variation of the percentage decrease in the maximum in-plane shear stress with the number of dropped plies in rotating annular thickness-tapered symmetrically-balanced laminated discs with taper configuration D and with the clamped-free boundary condition

The following observations can be made from the variation of the maximum in-plane shear stress and the percentage decrease in the maximum shear stress with the number of dropped plies, in rotating annular thickness-tapered symmetrically-balanced laminated discs with the clamped-free boundary condition for different taper configurations, shown in the Figure 4.20 and Tables 4.72 – 4.77:

- Irrespective of the taper configuration and the laminate configuration, the maximum in-plane shear stress decreases with the increasing number of dropped plies in rotating annular thickness-tapered symmetrically-balanced laminated discs with the clamped-free boundary condition.
- Irrespective of the taper configuration and the number of dropped plies, the rotating annular thickness-tapered symmetrically-balanced laminated disc with LC2 configuration experiences the maximum amount of shear stress. This observation holds true for the taper configurations B and C. However, for the disc with taper configuration D, the variation of the maximum in-plane shear stress with the number of dropped plies can be elaborated as follows:
    I. For the thickness-tapered symmetrically-balanced laminated disc with $\delta = 4$, the in-plane shear stress is maximum for LC2 configuration. The stress decreases as the number of $45°$ plies are terminated from the laminate configuration, i.e., with the exception of LC1 configuration (which is a

cross-ply laminate configuration), the in-plane shear stress is minimum for LC4 configuration.

II. Unlike the variation of the maximum in-plane shear stress in a disc with $\delta = 4$, where the shear stress is maximum for LC2 configuration, the in-plane shear stress in a disc with $\delta = 8$, 10 and 12 is maximum for LC4 configuration. The maximum in-plane shear stress first reduces from LC2 to LC3 configuration and then increases to the maximum value for LC4 configuration.

III. For the rotating annular thickness-tapered symmetrically-balanced laminated disc with $\delta = 16$, the amount of in-plane shear stress is almost the same for LC2, LC3 and LC4 configurations (which is 4.216 *MPa*, 4.249 *MPa* and 4.175 *MPa* respectively).

- For the thickness-tapered symmetrically-balanced laminated discs with LC2 and LC3 configurations, irrespective of the number of dropped plies, the rotating disc with the taper configuration B experiences the maximum amount of the in-plane shear stress, whereas, for the disc with LC4 configuration, the shear stress is maximum for the disc with taper configuration D.
- Irrespective of the taper configuration, the percentage decrease in the maximum in-plane shear stress is maximum for a disc with LC2 configuration and the least for a disc with LC4 configuration. Furthermore, on comparing the percentage decrease in the in-plane shear stress corresponding to different taper configurations, it can be said that the percentage decrease in the in-plane shear stress is maximum for a disc with taper configuration C.

4.7.3.2 Effect of radius ratio on the elastic response of symmetrically-balanced laminated discs

The effect of radius ratio on the radial and circumferential stress distributions, on the in-plane shear stress distribution and on the radial displacement distribution in a rotating annular thickness-tapered symmetrically-balanced laminated disc is studied for different taper configurations considered in the present thesis. The variations of the maximum radial,

circumferential and the in-plane shear stresses and the maximum radial displacement with the taper configuration and with the number of dropped plies are studied for rotating annular thickness-tapered symmetrically-balanced laminated discs with the beta values of 0.2, 0.25 and 0.3.

The disc has a fixed outer radius of r_o = 120 *mm*, thickness at the hub of h_i = 2.4 *mm* with an individual ply thickness of t_k = 0.12 *mm,* and is rotating at a constant angular velocity of ω = 1000 *rad/s* i.e. 9554.14 *rpm*. The inner radius of the disc is dependent on the beta value taken into consideration which has been mentioned earlier in the Table 3.16.

The following Figure 4.21 shows the variation with the number of dropped plies and with the taper configuration, of the maximum radial stress in rotating annular thickness-tapered symmetrically-balanced laminated discs with different laminate configuration and with the clamped-free boundary condition for the above-considered beta values.

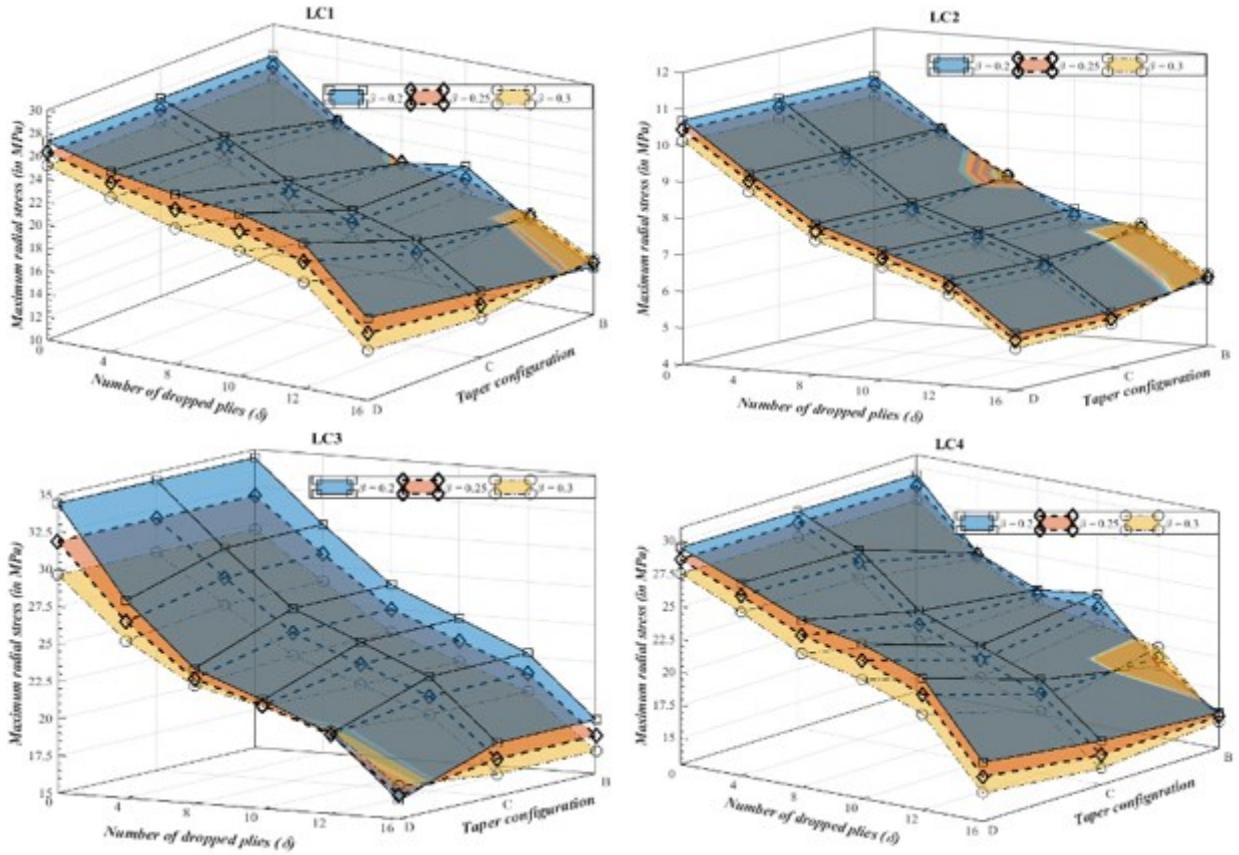

Figure 4.21 Variation of the maximum radial stress with the taper configuration and with the number of dropped plies in rotating annular thickness-tapered symmetrically-balanced laminated discs with the clamped-free boundary condition for different values of radius ratio

The following Tables 4.78 – 4.80 show the variation with the number of dropped plies of the maximum radial stress in rotating annular thickness-tapered symmetrically-balanced laminated discs with the clamped-free boundary condition for the beta values of 0.2, 0.25 and 0.3. The variation of the maximum radial stress has been shown for the different taper configurations of the laminated disc considered in the present study.

Maximum radial stress, σ_r^{max} (in *MPa*) in rotating annular thickness-tapered symmetrically-balanced laminated discs with taper configuration B and with the clamped-free boundary condition for different values of radius ratio							
Laminate configuration of the disc	Beta value of the disc	Number of dropped plies (δ)					
		0	4	8	10	12	16
LC1	$\beta = 0.2$	27.268	22.724	20.003	20.812	17.17	14.105
	$\beta = 0.25$	26.324	22.47	20.07	19.705	17.467	14.521
	$\beta = 0.3$	25.175	22.005	20.019	18.379	17.748	14.87
LC2	$\beta = 0.2$	10.69	9.402	8.153	7.48	7.002	5.789
	$\beta = 0.25$	10.442	9.34	8.233	7.287	7.098	5.887
	$\beta = 0.3$	10.126	9.216	8.267	7.044	7.222	5.983
LC3	$\beta = 0.2$	34.416	30.305	26.607	24.694	22.733	18.63
	$\beta = 0.25$	31.875	28.316	24.961	23.206	21.391	17.546
	$\beta = 0.3$	29.609	26.48	23.438	21.83	20.155	16.534
LC4	$\beta = 0.2$	29.478	24.398	22.453	23.012	18.375	15.688
	$\beta = 0.25$	28.601	24.269	22.101	21.941	19.039	15.438
	$\beta = 0.3$	27.513	23.967	21.534	20.659	19.849	15.051

Table 4.78 Variation of the maximum radial stress (in *MPa*) with the number of dropped plies in rotating annular thickness-tapered symmetrically-balanced laminated discs with taper configuration B and with the clamped-free boundary condition for different values of radius ratio

Maximum radial stress, σ_r^{max} (in *MPa*) in rotating annular thickness-tapered symmetrically-balanced laminated discs with taper configuration C and with the clamped-free boundary condition for different values of radius ratio							
Laminate configuration of the disc	Beta value of the disc	Number of dropped plies (δ)					
		0	4	8	10	12	16
LC1	$\beta = 0.2$	27.268	25.029	22.248	20.738	19.163	15.76
	$\beta = 0.25$	26.324	24.09	21.189	19.638	18.035	14.623
	$\beta = 0.3$	25.175	22.859	19.88	18.311	16.704	13.468
LC2	$\beta = 0.2$	10.69	9.377	8.114	7.476	6.833	5.532
	$\beta = 0.25$	10.442	9.155	7.911	7.281	6.644	5.35
	$\beta = 0.3$	10.126	8.872	7.656	7.036	6.409	5.209
LC3	$\beta = 0.2$	34.416	30.228	26.543	24.636	22.681	18.588
	$\beta = 0.25$	31.875	28.252	24.907	23.156	21.347	17.512
	$\beta = 0.3$	29.609	26.421	23.388	21.781	20.115	16.499
LC4	$\beta = 0.2$	29.478	27.43	23.623	21.842	20.135	16.359
	$\beta = 0.25$	28.601	26.465	22.566	20.762	19.04	15.29
	$\beta = 0.3$	27.513	25.216	21.274	19.467	17.756	14.249

Table 4.79 Variation of the maximum radial stress (in *MPa*) with the number of dropped plies in rotating annular thickness-tapered symmetrically-balanced laminated discs with taper configuration C and with the clamped-free boundary condition for different values of radius ratio

Maximum radial stress, σ_r^{max} (in *MPa*) in rotating annular thickness-tapered symmetrically-balanced laminated discs with taper configuration D and with the clamped-free boundary condition for different values of radius ratio							
Laminate configuration of the disc	Beta value of the disc	Number of dropped plies (δ)					
		0	4	8	10	12	16
LC1	$\beta = 0.2$	27.268	25.732	24.796	24.186	22.668	17.222
	$\beta = 0.25$	26.324	24.728	23.458	22.665	21.075	15.877
	$\beta = 0.3$	25.175	23.426	21.849	20.898	19.27	14.381
LC2	$\beta = 0.2$	10.69	9.380	8.138	7.531	6.892	5.546
	$\beta = 0.25$	10.442	9.157	7.936	7.336	6.703	5.364
	$\beta = 0.3$	10.126	8.874	7.679	7.091	6.467	5.142
LC3	$\beta = 0.2$	34.416	28.254	24.039	22.278	20.38	16.256
	$\beta = 0.25$	31.875	26.821	23.356	21.914	20.3	16.592
	$\beta = 0.3$	29.609	25.560	22.909	21.842	20.58	17.222
LC4	$\beta = 0.2$	29.478	27.668	25.713	24.76	23.054	17.513
	$\beta = 0.25$	28.601	26.701	24.559	23.512	21.785	16.394
	$\beta = 0.3$	27.513	25.448	23.151	22.029	20.305	15.167

Table 4.80 Variation of the maximum radial stress (in *MPa*) with the number of dropped plies in rotating annular thickness-tapered symmetrically-balanced laminated discs with taper configuration D and with the clamped-free boundary condition for different values of radius ratio

The following observations can be made from the variation of the maximum radial stress with the number of dropped plies in rotating annular thickness-tapered symmetrically-balanced laminated discs with the clamped-free boundary condition for the beta values of 0.2, 0.25 and 0.3, shown in the Figure 4.21 and Tables 4.78 – 4.80:

- Irrespective of the laminate configuration, the maximum radial stress decreases with the increasing beta value of the rotating annular uniform-thickness symmetrically-balanced laminated disc.
- For the thickness-tapered symmetrically-balanced laminated disc with LC1 configuration and with the taper configurations C and D, irrespective of the number of dropped plies, the maximum radial stress decreases with the increasing beta value of the disc. However, for the disc with taper configuration B and with $\delta = 4$ up to $\delta = 10$, the maximum radial stress first decreases with the increasing beta value of the disc. Thereafter, as the number of dropped plies is increased, the radial stress tends to increase with the increasing beta value of the disc.
- For the thickness-tapered symmetrically-balanced laminated disc with LC2 configuration and with the taper configurations C and D, irrespective of the number of dropped plies, the radial stress decreases with the increasing beta value of the disc. However, for the disc with taper configuration B and with $\delta = 4$, the radial stress first decreases with the increasing beta value of the disc. Thereafter, as the number of dropped plies is increased from $\delta = 4$ to $\delta = 16$, the radial stress then increases with the increasing beta value of the disc.
- For the thickness-tapered symmetrically-balanced laminated discs with LC3 and LC4 configurations, irrespective of the taper configuration, the maximum radial stress decreases with the increasing beta value of the disc. However, for the disc with LC3 configuration and with taper configuration D, the maximum radial stress increases with the increasing beta value of the disc for $\delta = 16$.

The following Figure 4.22 shows the variation with the number of dropped plies and with the taper configuration, of the maximum circumferential stress in rotating annular thickness-tapered symmetrically-balanced laminated discs with different laminate configuration and with the clamped-free boundary condition for the above-considered beta values.

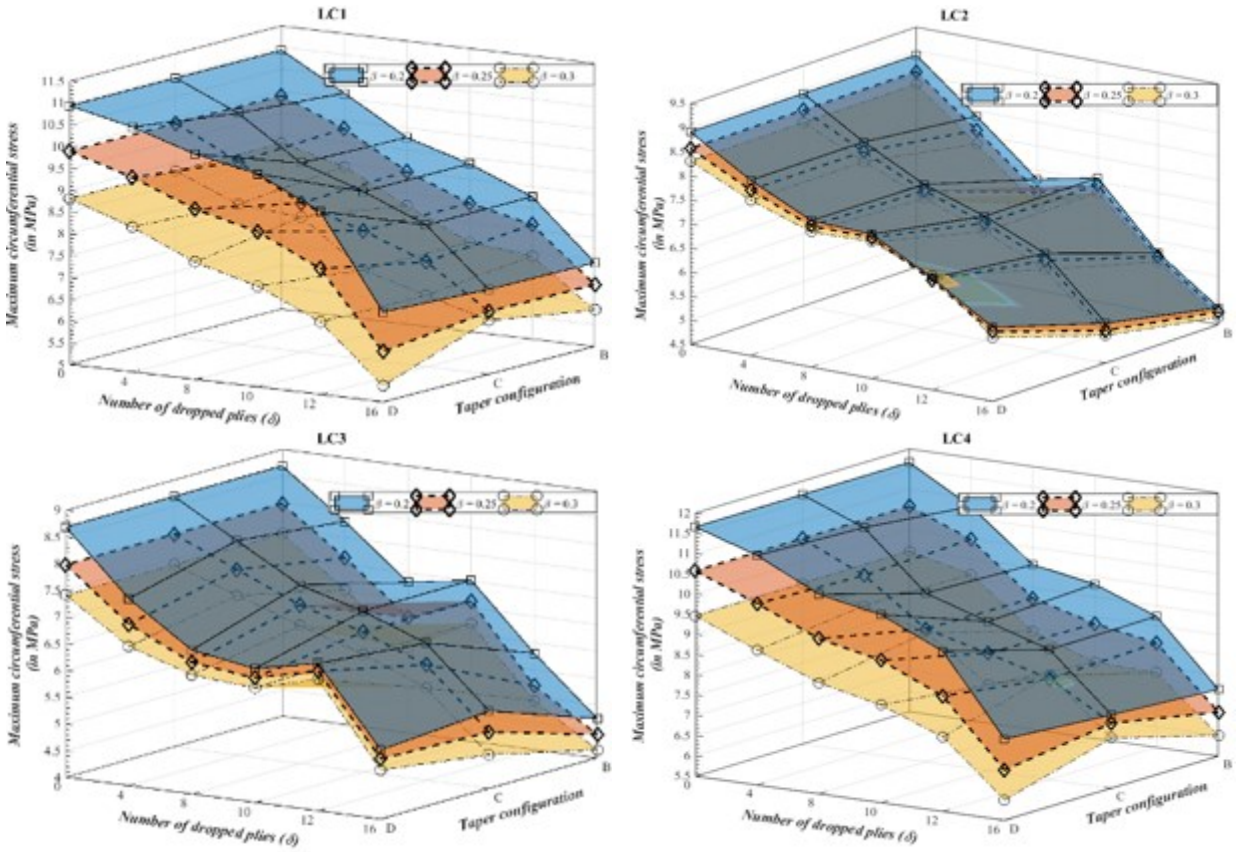

Figure 4.22 Variation of the maximum circumferential stress with the taper configuration and with the number of dropped plies in rotating annular thickness-tapered symmetrically-balanced laminated discs with the clamped-free boundary condition for different beta values

The following Tables 4.81 – 4.83 show the variation with the number of dropped plies of the maximum circumferential stress in rotating annular thickness-tapered symmetrically-balanced laminated discs with the clamped-free boundary condition for the beta values of 0.2, 0.25 and 0.3. The variation of the maximum circumferential stress has been shown for the different taper configurations of the laminated disc considered in the present study.

Maximum circumferential stress, σ_θ^{max} (in MPa) in rotating annular thickness-tapered symmetrically-balanced laminated discs with taper configuration B and with the clamped-free boundary condition for different values of radius ratio							
Laminate configuration of the disc	Beta value of the disc	Number of dropped plies (δ)					
		0	4	8	10	12	16
LC1	$\beta = 0.2$	10.934	10.123	9.28	8.847	8.266	6.926
	$\beta = 0.25$	9.895	9.307	8.503	7.943	7.624	6.421
	$\beta = 0.3$	8.806	8.443	7.712	7.053	6.91	5.839
LC2	$\beta = 0.2$	8.913	7.88	6.806	7.074	5.754	4.853
	$\beta = 0.25$	8.569	7.59	6.538	6.935	5.67	4.768
	$\beta = 0.3$	8.307	7.301	6.27	6.765	5.567	4.654
LC3	$\beta = 0.2$	8.683	7.803	6.821	7.015	5.806	4.745
	$\beta = 0.25$	7.976	7.115	6.167	6.628	5.197	4.446
	$\beta = 0.3$	7.409	6.521	5.594	6.208	4.917	4.161
LC4	$\beta = 0.2$	11.659	10.79	9.572	9.309	8.734	7.149
	$\beta = 0.25$	10.572	9.977	8.741	8.329	8.074	6.587
	$\beta = 0.3$	9.462	9.111	7.916	7.381	7.342	6.012

Table 4.81 Variation of the maximum circumferential stress (in *MPa*) with the number of dropped plies in rotating annular thickness-tapered symmetrically-balanced laminated discs with taper configuration B and with the clamped-free boundary condition for different values of radius ratio

Maximum circumferential stress, σ_θ^{max} (in MPa) in rotating annular thickness-tapered symmetrically-balanced laminated discs with taper configuration C and with the clamped-free boundary condition for different values of radius ratio							
Laminate configuration of the disc	Beta value of the disc	Number of dropped plies (δ)					
		0	4	8	10	12	16
LC1	$\beta = 0.2$	10.934	10.299	9.33	8.847	8.253	6.949
	$\beta = 0.25$	9.895	9.186	8.409	7.943	7.407	6.445
	$\beta = 0.3$	8.806	8.21	8.095	7.053	6.64	6.237
LC2	$\beta = 0.2$	8.913	8.144	7.5	7.078	6.544	5.332
	$\beta = 0.25$	8.569	7.941	7.367	6.933	6.397	5.179
	$\beta = 0.3$	8.307	7.733	7.21	6.758	6.212	5.077
LC3	$\beta = 0.2$	8.683	8.013	7.34	7.008	6.568	5.455
	$\beta = 0.25$	7.976	7.472	6.966	6.617	6.16	5.061
	$\beta = 0.3$	7.409	6.991	6.58	6.206	5.732	4.638
LC4	$\beta = 0.2$	11.659	11.066	9.663	9.18	8.71	7.319
	$\beta = 0.25$	10.572	9.88	8.779	8.394	7.983	7.113
	$\beta = 0.3$	9.462	9.132	8.698	7.62	8.081	6.742

Table 4.82 Variation of the maximum circumferential stress (in *MPa*) with the number of dropped plies in rotating annular thickness-tapered symmetrically-balanced laminated discs with taper configuration C and with the clamped-free boundary condition for different values of radius ratio

Maximum circumferential stress, σ_θ^{max} (in MPa) in rotating annular thickness-tapered symmetrically-balanced laminated discs with taper configuration D and with the clamped-free boundary condition for different values of radius ratio							
Laminate configuration of the disc	Beta value of the disc	Number of dropped plies (δ)					
		0	4	8	10	12	16
LC1	$\beta = 0.2$	10.934	10.622	10.174	9.89	9.198	7.069
	$\beta = 0.25$	9.895	9.463	8.907	8.566	7.887	6.16
	$\beta = 0.3$	8.806	8.325	7.695	7.318	6.668	5.373
LC2	$\beta = 0.2$	8.913	8.147	7.548	7.503	6.831	6.044
	$\beta = 0.25$	8.569	7.944	7.436	7.432	6.782	5.95
	$\beta = 0.3$	8.307	7.732	7.31	7.347	6.881	5.836
LC3	$\beta = 0.2$	8.683	7.502	6.695	6.508	6.761	5.299
	$\beta = 0.25$	7.976	7.022	6.463	6.333	6.619	5.133
	$\beta = 0.3$	7.409	6.608	6.232	6.146	6.461	4.925
LC4	$\beta = 0.2$	11.659	11.174	10.43	10.152	9.468	7.516
	$\beta = 0.25$	10.572	9.982	9.333	9.024	8.358	6.746
	$\beta = 0.3$	9.462	8.828	8.246	7.916	7.346	6.007

Table 4.83 Variation of the maximum circumferential stress (in MPa) with the number of dropped plies in rotating annular thickness-tapered symmetrically-balanced laminated discs with taper configuration D and with the clamped-free boundary condition for different values of radius ratio

The following observations can be made from the variation of the maximum circumferential stress with the number of dropped plies in rotating annular thickness-tapered symmetrically-balanced laminated discs with the clamped-free boundary condition for the beta values of 0.2, 0.25 and 0.3, shown in the Figure 4.22 and Tables 4.81 – 4.83:

- Irrespective of the laminate configuration, number of dropped plies and the taper configuration, the maximum circumferential stress in a rotating annular thickness-tapered symmetrically-balanced laminated disc decreases with the increasing beta value of the disc.
- Irrespective of the laminate configuration, taper configuration and the beta value, the maximum circumferential stress in a rotating annular thickness-tapered symmetrically-balanced laminated disc decreases with the increasing number of dropped plies.

The following Figure 4.23 shows the variation with the number of dropped plies and with the taper configuration, of the maximum radial displacement in rotating annular thickness-tapered

symmetrically-balanced laminated discs with different laminate configuration and with the clamped-free boundary condition for the above-considered beta values.

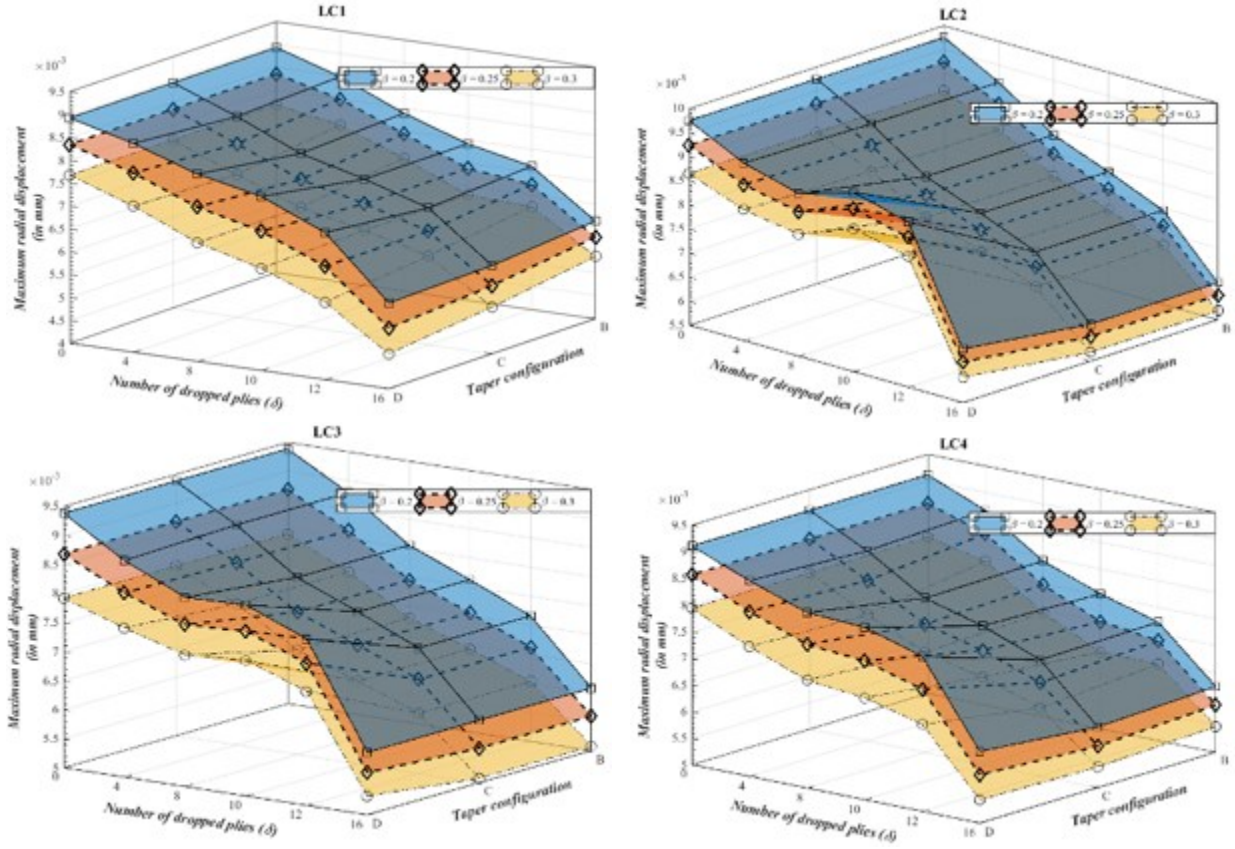

Figure 4.23 Variation of the maximum radial displacement with the taper configuration and with the number of dropped plies in rotating annular thickness-tapered symmetrically-balanced laminated discs with the clamped-free boundary condition for different beta values

The following Tables 4.84 – 4.86 show the variation with the number of dropped plies of the maximum radial displacement in rotating annular thickness-tapered symmetrically-balanced laminated discs with the clamped-free boundary condition for the beta values of 0.2, 0.25 and 0.3. The variation of the maximum radial displacement has been shown for the different taper configurations of the laminated disc considered in the present study.

Maximum radial displacement, u_r^{max} (in mm) in rotating annular thickness-tapered symmetrically-balanced laminated discs with taper configuration B and with the clamped-free boundary condition for different values of radius ratio							
Laminate configuration of the disc	Beta value of the disc	Number of dropped plies (δ)					
		0	4	8	10	12	16
LC1	$\beta = 0.2$	0.00893	0.00849	0.00789	0.00742	0.00713	0.00613
	$\beta = 0.25$	0.00835	0.008	0.00744	0.00688	0.00673	0.00578
	$\beta = 0.3$	0.00768	0.00743	0.00691	0.0063	0.00625	0.00536
LC2	$\beta = 0.2$	0.00975	0.00914	0.00837	0.00793	0.00745	0.00627
	$\beta = 0.25$	0.00924	0.00869	0.00799	0.00757	0.00713	0.00601
	$\beta = 0.3$	0.00865	0.00816	0.00752	0.00714	0.00673	0.00569
LC3	$\beta = 0.2$	0.00938	0.00879	0.00805	0.00762	0.00716	0.00608
	$\beta = 0.25$	0.00868	0.00814	0.00745	0.00705	0.00662	0.0056
	$\beta = 0.3$	0.00792	0.00743	0.0068	0.00643	0.00603	0.00508
LC4	$\beta = 0.2$	0.00911	0.00866	0.00793	0.00753	0.00722	0.00623
	$\beta = 0.25$	0.00857	0.00822	0.00748	0.00701	0.00687	0.00588
	$\beta = 0.3$	0.00794	0.00771	0.00696	0.00644	0.00643	0.00548

Table 4.84 Variation of the maximum radial displacement (in *mm*) with the number of dropped plies in rotating annular thickness-tapered symmetrically-balanced laminated discs with taper configuration B and with the clamped-free boundary condition for different values of radius ratio

Maximum radial displacement, u_r^{max} (in mm) in rotating annular thickness-tapered symmetrically-balanced laminated discs with taper configuration C and with the clamped-free boundary condition for different values of radius ratio							
Laminate configuration of the disc	Beta value of the disc	Number of dropped plies (δ)					
		0	4	8	10	12	16
LC1	$\beta = 0.2$	0.00893	0.00839	0.00778	0.00742	0.00699	0.00593
	$\beta = 0.25$	0.00835	0.00779	0.00721	0.00688	0.00648	0.00549
	$\beta = 0.3$	0.00768	0.00712	0.0066	0.0063	0.00594	0.00502
LC2	$\beta = 0.2$	0.00975	0.00914	0.00837	0.00793	0.00745	0.00627
	$\beta = 0.25$	0.00924	0.00869	0.00799	0.00757	0.00713	0.00601
	$\beta = 0.3$	0.00865	0.00816	0.00752	0.00714	0.00673	0.00569
LC3	$\beta = 0.2$	0.00938	0.00879	0.00805	0.00762	0.00716	0.00608
	$\beta = 0.25$	0.00868	0.00814	0.00745	0.00705	0.00662	0.0056
	$\beta = 0.3$	0.00792	0.00743	0.0068	0.00643	0.00604	0.00508
LC4	$\beta = 0.2$	0.00911	0.00857	0.0079	0.0076	0.00718	0.00614
	$\beta = 0.25$	0.00857	0.00801	0.00741	0.00714	0.00675	0.00578
	$\beta = 0.3$	0.00794	0.00737	0.00688	0.00664	0.00628	0.00539

Table 4.85 Variation of the maximum radial displacement (in *mm*) with the number of dropped plies in rotating annular thickness-tapered symmetrically-balanced laminated discs with taper configuration C and with the clamped-free boundary condition for different values of radius ratio

Maximum radial displacement, u_r^{max} (in mm) in rotating annular thickness-tapered symmetrically-balanced laminated discs with taper configuration D and with the clamped-free boundary condition for different values of radius ratio							
Laminate configuration of the disc	Beta value of the disc	Number of dropped plies (δ)					
		0	4	8	10	12	16
LC1	$\beta = 0.2$	0.00893	0.00857	0.0081	0.00781	0.00722	0.00588
	$\beta = 0.25$	0.00835	0.00792	0.00738	0.00705	0.00648	0.00533
	$\beta = 0.3$	0.00768	0.0072	0.0066	0.00624	0.0057	0.00477
LC2	$\beta = 0.2$	0.00975	0.00919	0.00888	0.00923	0.00893	0.00662
	$\beta = 0.25$	0.00924	0.00874	0.0085	0.00889	0.00861	0.00635
	$\beta = 0.3$	0.00865	0.00822	0.00804	0.00847	0.00822	0.00603
LC3	$\beta = 0.2$	0.00938	0.00873	0.00826	0.00829	0.00787	0.00608
	$\beta = 0.25$	0.00868	0.00817	0.00779	0.00784	0.00745	0.00573
	$\beta = 0.3$	0.00792	0.00757	0.00727	0.00734	0.00697	0.00533
LC4	$\beta = 0.2$	0.00911	0.00868	0.0083	0.00824	0.00791	0.00635
	$\beta = 0.25$	0.00857	0.0081	0.0077	0.00761	0.0073	0.00591
	$\beta = 0.3$	0.00794	0.00744	0.00703	0.00692	0.00664	0.00544

Table 4.86 Variation of the maximum radial displacement (in *mm*) with the number of dropped plies in rotating annular thickness-tapered symmetrically-balanced laminated discs with taper configuration D and with the clamped-free boundary condition for different values of radius ratio

The following observations can be made from the variation of the maximum radial displacement with the number of dropped plies in rotating annular thickness-tapered symmetrically-balanced laminated discs with the clamped-free boundary condition for the beta values of 0.2, 0.25 and 0.3, shown in the Figure 4.23 and Tables 4.84 – 4.86:

- Irrespective of the laminate configuration, number of dropped plies and the taper configuration, the maximum radial displacement in rotating annular thickness-tapered symmetrically-balanced laminated discs decreases with the increasing beta value of the disc.
- Irrespective of the laminate configuration, taper configuration and the beta value, the maximum radial displacement in a rotating annular thickness-tapered symmetrically-balanced laminated disc decreases with the increasing number of dropped plies. This observation is only valid for the symmetrically-balanced laminated discs with taper configurations B and C. The variation of the maximum radial displacement with the increasing number of dropped plies, in a rotating

annular thickness-tapered symmetrically-balanced laminated disc with taper configuration D has been explained earlier in this Chapter (see subsection 4.7.3.1).

The following Figure 4.24 shows the variation with the number of dropped plies and with the taper configuration of the maximum in-plane shear stress, in rotating annular thickness-tapered symmetrically-balanced laminated discs with different laminate configuration (except for LC1 configuration) and with the clamped-free boundary condition for the above-considered beta values.

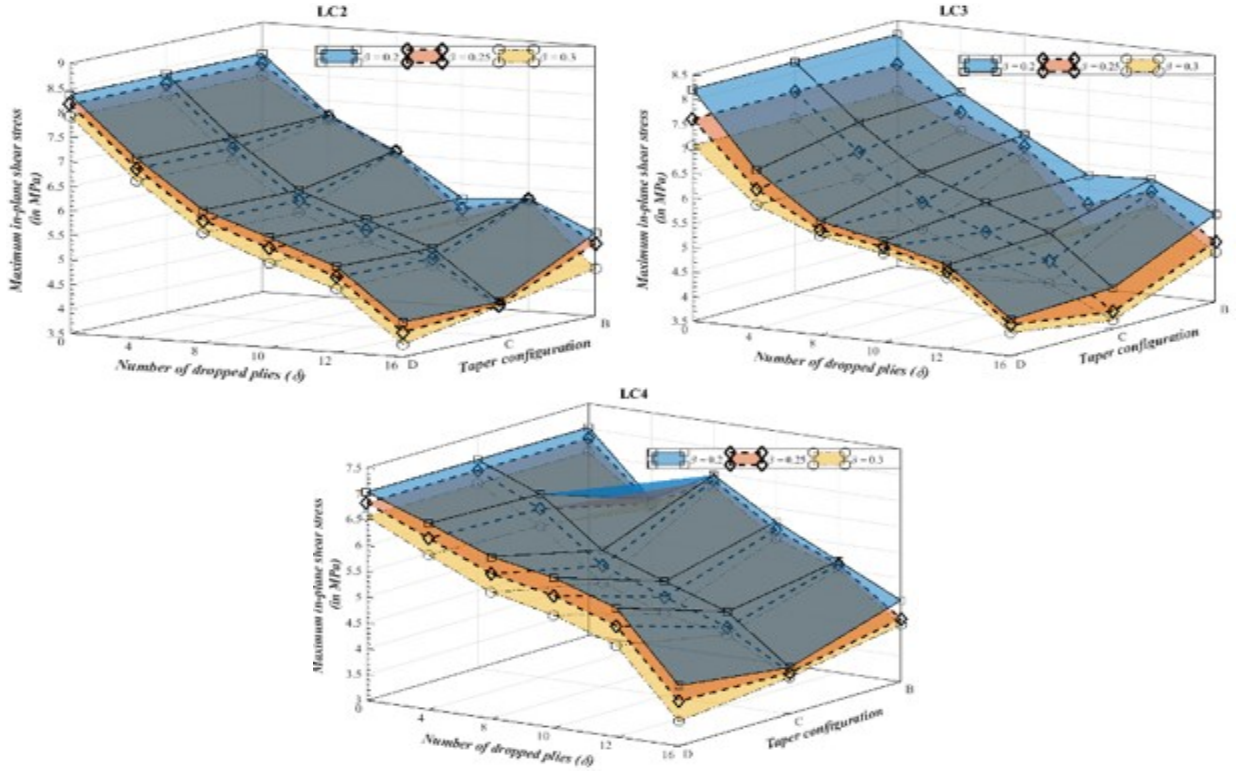

Figure 4.24 Variation of the maximum in-plane shear stress with the taper configuration and with the number of dropped plies in rotating annular thickness-tapered symmetrically-balanced laminated discs with the clamped-free boundary condition for different beta values

The following Tables 4.87 – 4.89 show the variation with the number of dropped plies of the maximum in-plane shear stress in rotating annular thickness-tapered symmetrically-balanced laminated discs with the clamped-free boundary condition for the beta values of 0.2, 0.25 and 0.3. The variation of the maximum in-plane shear stress has been shown for the different taper configurations of the laminated disc considered in the present study.

Maximum in-plane shear stress, $\tau_{r\theta}^{max}$ (in *MPa*) in rotating annular thickness-tapered symmetrically-balanced laminated discs with taper configuration B and with the clamped-free boundary condition for different values of radius ratio							
Laminate configuration of the disc	Beta value of the disc	Number of dropped plies (δ)					
		0	4	8	10	12	16
LC2	$\beta = 0.2$	8.361	7.209	6.574	5.703	5.798	5.185
	$\beta = 0.25$	8.167	7.171	6.552	5.489	5.781	4.976
	$\beta = 0.3$	7.919	7.093	6.526	5.245	5.75	4.465
LC3	$\beta = 0.2$	8.21	7.184	6.462	5.783	5.846	5.274
	$\beta = 0.25$	7.604	6.773	6.221	5.192	5.593	4.716
	$\beta = 0.3$	7.063	6.409	5.98	4.652	5.328	4.5
LC4	$\beta = 0.2$	7.032	5.824	6.464	5.745	5.159	4.574
	$\beta = 0.25$	6.823	5.734	6.366	5.58	5.095	4.216
	$\beta = 0.3$	6.563	5.634	6.235	5.415	4.994	4.1

Table 4.87 Variation of the maximum in-plane shear stress (in *MPa*) with the number of dropped plies in rotating annular thickness-tapered symmetrically-balanced laminated discs with taper configuration B and with the clamped-free boundary condition for different values of radius ratio

Maximum in-plane shear stress, $\tau_{r\theta}^{max}$ (in *MPa*) in rotating annular thickness-tapered symmetrically-balanced laminated discs with taper configuration C and with the clamped-free boundary condition for different values of radius ratio							
Laminate configuration of the disc	Beta value of the disc	Number of dropped plies (δ)					
		0	4	8	10	12	16
LC2	$\beta = 0.2$	8.361	7.158	6.187	5.697	5.203	4.205
	$\beta = 0.25$	8.167	6.947	5.972	5.482	4.99	4.137
	$\beta = 0.3$	7.919	6.702	5.729	5.236	4.846	4.112
LC3	$\beta = 0.2$	8.21	7.125	6.235	5.776	5.308	4.333
	$\beta = 0.25$	7.604	6.518	5.634	5.184	4.728	3.85
	$\beta = 0.3$	7.063	5.976	5.09	4.64	4.279	3.674
LC4	$\beta = 0.2$	7.032	6.543	5.634	5.209	4.801	3.898
	$\beta = 0.25$	6.823	6.255	5.332	4.906	4.498	3.797
	$\beta = 0.3$	6.563	5.931	5.002	4.576	4.358	3.71

Table 4.88 Variation of the maximum in-plane shear stress (in *MPa*) with the number of dropped plies in rotating annular thickness-tapered symmetrically-balanced laminated discs with taper configuration C and with the clamped-free boundary condition for different values of radius ratio

Maximum in-plane shear stress, $\tau_{r\theta}^{max}$ (in *MPa*) in rotating annular thickness-tapered symmetrically-balanced laminated discs with taper configuration D and with the clamped-free boundary condition for different values of radius ratio							
Laminate configuration of the disc	Beta value of the disc	Number of dropped plies (δ)					
		0	4	8	10	12	16
LC2	$\beta = 0.2$	8.361	7.16	6.206	5.739	5.248	4.216
	$\beta = 0.25$	8.167	6.95	5.99	5.524	5.034	4.007
	$\beta = 0.3$	7.919	6.703	5.745	5.227	4.787	3.761
LC3	$\beta = 0.2$	8.21	6.705	5.815	5.552	5.209	4.249
	$\beta = 0.25$	7.604	6.32	5.64	5.429	5.078	4.137
	$\beta = 0.3$	7.063	6	5.509	5.3	4.944	3.977
LC4	$\beta = 0.2$	7.032	6.6	6.134	5.907	5.499	4.175
	$\beta = 0.25$	6.823	6.311	5.805	5.558	5.149	3.871
	$\beta = 0.3$	6.563	5.985	5.445	5.181	4.774	3.484

Table 4.89 Variation of the maximum in-plane shear stress (in *MPa*) with the number of dropped plies in rotating annular thickness-tapered symmetrically-balanced laminated discs with taper configuration D and with the clamped-free boundary condition for different values of radius ratio

The following observations can be made from the variation of the maximum in-plane shear stress with the number of dropped plies in rotating annular thickness-tapered symmetrically-balanced laminated discs with the clamped-free boundary condition for the beta values of 0.2, 0.25 and 0.3, shown in the Figure 4.24 and Tables 4.87 – 4.89:

- Irrespective of the laminate configuration, number of dropped plies and the taper configuration, the maximum in-plane shear stress in rotating annular thickness-tapered symmetrically-balanced laminated discs decreases with the increasing value of the radius ratio.
- Irrespective of the laminate configuration, taper configuration and the beta value, the maximum in-plane shear stress in a rotating annular thickness-tapered symmetrically-balanced laminated disc decreases with the increasing number of dropped plies. This observation is only valid for the symmetrically-balanced laminated discs with LC2 and LC3 configurations. The variation of the maximum in-plane shear stress with the increasing number of dropped plies, in a rotating

annular thickness-tapered symmetrically-balanced laminated disc with LC4 configuration has been explained earlier in this Chapter (see subsection 4.7.3.1).

- For rotating annular thickness-tapered symmetrically-balanced laminated discs with LC2 and LC4 configurations and with taper configuration C, the decrease in the maximum in-plane shear stress with the increasing beta value of the disc is not that significant for $\delta = 16$, as compared to the decrease in the in-plane shear stress in discs with taper configurations B and D.
- For the rotating annular thickness-tapered symmetrically-balanced laminated disc with LC3 configuration and with taper configuration D, the decrease in the in-plane shear stress with the increasing beta value of the disc is not that significant for $\delta = 10$ up to $\delta = 16$, as compared to the decrease in the in-plane shear stress in discs with taper configurations B and C.

4.8 Conclusion

In this chapter, the elastic response of rotating annular thickness-tapered fiber-reinforced composite disc with the clamped-free boundary condition is presented. Different configurations of the internally-tapered discs have been considered and the cross-sectional view of the same are shown in section 4.2. In section 4.3, the total potential energy of the rotating annular thickness-tapered fiber-reinforced composite disc is derived by the addition of the strain energies and the work potentials of the fiber-reinforced plies and the isotropic resin pockets. In section 4.4, the Rayleigh-Ritz method based on the total potential energy is used to determine the elastic response of the rotating annular thickness-tapered composite disc. Finite element modeling of the different configurations of the internally-tapered discs with a ply drop-off value of 10 and with the clamped-free boundary condition has been carried out in ANSYS® R19.2 and is shown in section 4.5. In section 4.6, the results obtained for the elastic response of the rotating annular thickness-tapered fiber-reinforced composite disc using the Rayleigh-Ritz method are verified with the results obtained for the same using the finite element analysis software ANSYS® (using the SHELL181 element). A thorough parametric study is conducted in section 4.7 to demonstrate the effects of laminate configuration, fiber orientation, radius ratio, dropped plies and the taper configuration on the in-plane stress distributions and on the radial displacement distribution in a rotating annular

thickness-tapered disc made up of Graphite-Fiber Reinforced Plastic (NCT-301) material and with the clamped-free boundary condition. A summary of observations is as follows:

- The results obtained for the elastic response of the rotating annular thickness-tapered fiber-reinforced composite disc using the Rayleigh-Ritz method are in good agreement with the results obtained for the same using the finite element analysis software ANSYS® (using the SHELL181 element). Furthermore, the average percentage difference between the results obtained using the Rayleigh-Ritz method and that of the ANSYS® SHELL181 solution for a thickness-tapered disc with taper configuration B is relatively low as compared with the average percentage difference between the results obtained for the thickness-tapered disc with taper configuration D.
- Irrespective of the taper configuration, the induced maximum radial stress in the rotating annular thickness-tapered disc with uni-directional and symmetrically-balanced laminate configurations decreases with the increasing number of dropped plies. However, for the tapered disc with cross-ply laminate configurations, this variation of the radial stress with the dropped plies only holds true for the taper configurations B and C. The variation of the maximum radial stress with the dropped plies in a thickness-tapered cross-ply disc with taper configuration D is much more complex.
- Irrespective of the beta value and the number of dropped plies, the rotating annular thickness-tapered uni-directional laminated disc with taper configuration B experiences the maximum amount of radial stress, whereas, the thickness-tapered cross-ply laminated disc with taper configuration C experiences the maximum amount of radial stress, as compared to the other taper configurations considered in the present study. For the symmetrically-balanced laminated disc with LC1 and LC4 configurations, the radial stress is the highest for taper configuration D, whereas, for the discs with LC2 and LC3 configurations, the radial stress is the highest for taper configuration B.
- Irrespective of the taper configuration, laminate configuration of the symmetrically-balanced disc and the number of 0° plies in the cross-ply laminated disc, the induced maximum circumferential stress in the rotating annular thickness-tapered fiber-reinforced composite disc decreases with the increasing number of dropped plies. However, for the tapered disc with uni-directional laminate configuration, this variation

of the circumferential stress with the dropped plies only holds true for the taper configurations B and D. For the uni-directional disc with $[75]_{20}$ to $[90]_{20}$ laminate configuration and with the taper configuration C, the circumferential stress increases with the increasing number of dropped plies from $\delta = 10$ to $\delta = 12$.

- Irrespective of the beta value and the number of dropped plies, the rotating annular thickness-tapered uni-directional laminated disc with taper configuration B experiences the maximum amount of circumferential stress. However, for the tapered disc with uni-directional laminate configuration from $[0]_{20}$ to $[60]_{20}$, the induced circumferential stress is almost the same in each taper configuration. For the thickness-tapered disc with cross-ply configurations, irrespective of the number of 0° plies, the circumferential stress is always maximum for the taper configuration D and minimum for the taper configuration C. For the symmetrically-balanced laminated discs with LC1, LC2 and LC4 configurations, the circumferential stress is the highest for taper configuration D, whereas, for the discs with LC3 configuration, the stress is the highest for taper configuration C.
- Irrespective of the taper configuration, fiber orientation in the uni-directional laminated disc and the number of 0° plies in the cross-ply laminated disc, the radial displacement in the rotating annular thickness-tapered disc decreases with the increasing number of dropped plies. However, for the tapered disc with symmetrically-balanced laminate configuration, this variation of the radial displacement with the dropped plies only holds true for the taper configurations B and C. For the symmetrically-balanced laminated disc with taper configuration D, the variation of the radial displacement with the dropped plies is much more complex.
- Irrespective of the beta value, number of dropped plies, laminate configuration of the symmetrically-balanced laminated disc and the number of 0° plies in the cross-ply laminated disc, the radial displacement is maximum for the taper configuration D and minimum for the taper C. However, for the tapered disc with uni-directional laminate configurations, the arrangement of dropped plies within the tapered disc, or in other words, the taper configuration, has no effect on the amount of radial displacement induced in the thickness-tapered disc. That is, irrespective of the beta value and the

fiber orientation angle, the amount of radial displacement in the uni-directional laminated disc is the same for each taper configuration considered in the present study.

- Unlike the symmetrically-balanced laminated disc with LC2, LC3 and LC4 configurations, the rotating annular thickness-tapered discs with uni-directional and cross-ply laminate configurations does not experience any in-plane shear stress. The comparison of the results obtained for the in-plane shear stress in rotating annular symmetrically-balanced laminated discs using Rayleigh-Ritz method with the results obtained for the same using ANSYS SHELL181 element solution has been shown in the Table 3.37. Also, irrespective of the taper configuration, the shear stress in the symmetrically-balanced laminated disc decreases with the increasing number of dropped plies. Furthermore, irrespective of the beta value, on comparing the amount of in-plane shear stress among the different taper configurations, it is noted that for the disc with LC2 and LC3 configurations, the shear stress is maximum for taper configuration B, whereas, for the disc with LC4 configuration, the shear stress is maximum for taper configuration D.

Chapter 5

Conclusion

5.1 Major contributions

Thanks to the lightweight and design flexibility of the fiber-reinforced composite materials in comparison to isotropic materials, recent trends have shown the increasing use of composite materials in components such as fuselage, wings, turbofan blades and rotors in aerospace structures and in components such as disc brakes, frames and drive shaft in automobiles. It is needful to thoroughly examine the elastic behavior of such mechanical components that are composed of composite materials for their safe and reliable operation in the industry.

The present research work provides a basis for evaluating the elastic response of rotating annular uniform-thickness and thickness-tapered discs made of orthotropic and fiber-reinforced composite materials with various boundary conditions of engineering interest.

The prime contributions of the present thesis are as follows:

a. The Rayleigh-Ritz method based on the total potential energy with finite-element-like modification has been used to evaluate the elastic response of rotating annular thickness-tapered discs made of orthotropic materials with the free-free and the clamped-free boundary conditions. The method can also be used for uniform-thickness discs made of isotropic materials by making appropriate modifications. Also, the accuracy of the results obtained for the elastic response has been established based on the number of divisions of the thickness-tapered disc.
b. For the elastic analysis of thickness-tapered discs made of isotropic and orthotropic materials, two kinds of tapered discs have been considered: linearly-tapered disc and Stodola disc. Also, four different materials have been chosen for the elastic analysis of rotating annular linearly-tapered discs and Stodola discs, the material properties of which have been mentioned in the Table 2.3.
c. Effects of the degree of orthotropy of the material of the disc, taper profiles and values of the taper parameters have been studied on the in-plane stress distributions and on the radial displacement distribution in rotating annular thickness-tapered discs made of

isotropic and orthotropic materials with the free-free and the clamped-free boundary condition.

d. The Rayleigh-Ritz method based on the Classical Laminate Theory in cylindrical coordinate system has been used to evaluate the elastic response of rotating annular uniform-thickness and thickness-tapered discs made of fiber-reinforced composite materials with the clamped-free boundary condition. Also, for the elastic response, three different internal taper configurations of the thickness-tapered fiber reinforced composite disc have been considered, namely the taper configuration B (staircase arrangement of dropped plies), taper configuration C (overlapping continuous plies) and taper configuration D (continuous plies interspersed).
e. An extensive parametric study has been conducted to examine the influences of fiber orientation, radius ratio, rotational velocity, laminate configuration, number of dropped plies and the arrangement of dropped plies on the in-plane stress distributions and on the radial displacement distribution in rotating annular thickness-tapered fiber-reinforced composite discs with the clamped-free boundary condition.
f. Numerical and symbolic calculations to evaluate the elastic response of rotating annular thickness-tapered discs made of orthotropic materials and fiber-reinforced composite materials using the Rayleigh-Ritz method have been performed in the technical computing language MATLAB®.
g. The results obtained for the elastic response using the Rayleigh-Ritz method have been verified with the results obtained for the same using the closed-form analytical solutions wherever possible, as well as with the results obtained using the finite element analysis software ANSYS®. The finite element analysis has been performed using both SOLID185 and SHELL181 elements.

5.2 Conclusions

The principal conclusions of the present research work that provides an insight on the elastic behavior of rotating annular uniform-thickness and thickness-tapered discs made of orthotropic and fiber-reinforced composite materials are as follows:

a. Irrespective of the boundary condition, taper profile, value of the taper parameter and the degree of orthotropy of the material of the disc, the increase in the number of divisions of the thickness-tapered disc increases the accuracy of the results obtained for the elastic response of rotating annular thickness-tapered discs made of orthotropic materials using the Rayleigh-Ritz method with finite-element-like modification. In the present thesis, the results obtained for the elastic response using the Rayleigh-Ritz method with 8 terms in each of the assumed displacement functions along with 20 divisions of the thickness-tapered disc are in good agreement with the results obtained for the same using the closed-form analytical solutions available in the literature.
b. Irrespective of the boundary condition and the degree of orthotropy of the material of the disc, as the value of the linear taper parameter n and the Stodola taper parameter s increases, the radial and circumferential stresses and the radial displacement in a rotating annular thickness-tapered disc decrease.
c. Observations for different boundary conditions show that for the rotating annular thickness-tapered discs with the free-free boundary condition, irrespective of the thickness reduction ratio and the degree of orthotropy of the material of the disc, the linearly-tapered disc experiences relatively lower amount of radial stress as compared to the Stodola disc, whereas, for the rotating annular thickness-tapered discs with the clamped-free boundary condition, the Stodola disc experiences comparatively lower amounts of radial and circumferential stresses as compared to the linearly-tapered disc.
d. Irrespective of the boundary condition and the degree of orthotropy of the material of the disc, tapering has no effect on the loci of the points experiencing the maximum radial and circumferential stresses in a rotating annular linearly-tapered disc. Conversely, for the rotating annular Stodola disc with the clamped-free boundary condition, as the value of the Stodola taper parameter is increased, the loci of the points experiencing the maximum radial and circumferential stresses tend to shift from the hub of the disc to its geometric mean radius point and from the geometric mean radius point to the arithmetic mean radius point of the disc respectively.
e. Taking into account the effect of degree of orthotropy of the material of the disc on the elastic response of rotating annular thickness-tapered discs with the clamped-free boundary condition, it is observed that regardless of the taper profile and the values of

the taper parameters *n* and *s*, the lower the degree of orthotropy of the material of the disc is, the higher the radial stress induced in the disc will be and the lower the circumferential stress induced in the disc will be. Contrastingly, the radial displacement is always maximum in a rotating annular thickness-tapered disc made up of an isotropic material.

f. The results obtained for the elastic response of rotating annular uniform-thickness and thickness-tapered fiber-reinforced composite discs with the clamped-free boundary condition using the Rayleigh-Ritz in conjunction with the Classical Laminate Theory in cylindrical coordinate system are in good agreement with the results obtained for the same using ANSYS® SHELL181 element solution. In the present thesis, for the results obtained for the elastic response using the Rayleigh-Ritz method to converge with the results obtained for the same using the SHELL181 element solution, quadrilateral type face meshing is preferred over the triangular type face meshing, since the former is required for the proper orientation of the fibers in the composite plies.

g. As for the effect of uni-directional laminate configurations on the elastic response of rotating annular uniform-thickness fiber-reinforced composite discs with the clamped-free boundary condition, it is observed that irrespective of the beta value and the rotational velocity, the $[0]_{20}$ and the $[90]_{20}$ laminated discs experience the maximum amounts of radial and circumferential stresses respectively. Contrastingly, the radial displacement is maximum in the $[45]_{20}$ laminated disc.

h. Fiber orientation angle has a significant effect on the loci of the points experiencing the maximum radial and circumferential stresses in rotating annular uniform-thickness uni-directional laminated discs with the clamped-free boundary condition. It is observed that irrespective of the beta value of the disc, the locus of the point experiencing the maximum radial stress shifts from the hub of the disc to its arithmetic mean radius point, whereas the locus of the point experiencing the maximum circumferential stress shifts from the geometric mean radius point to the outer periphery of the disc.

i. The induced maximum radial stress in rotating annular uniform-thickness fiber-reinforced composite discs with the clamped-free boundary condition decreases with the increasing beta value of the disc for the uni-directional laminate configurations $[0]_{20}$ to $[50]_{20}$, whereas, for the discs with uni-directional laminate configurations

$[55]_{20}$ to $[90]_{20}$, the radial stress tends to relatively-slightly increase with the increasing beta value of the disc.

j. The study on the relative effect of 0° plies on the radial stress distribution in rotating annular uniform-thickness cross-ply laminated discs with the clamped-free boundary condition shows that for a cross-ply disc with a beta value of 0.2, the maximum radial stress decreases with the decreasing number of 0° plies. For the disc with a beta value of 0.25, the radial stress first increases with the decreasing value of N_0 (i.e., decreasing number of 0° plies) from $N_0 = 18$ up to $N_0 = 10$ and then decreases with decreasing value of N_0. Furthermore, for the disc with the beta value of 0.3, the radial stress first increases with the decreasing value of N_0 from $N_0 = 18$ up to $N_0 = 6$ and then decreases with decreasing value of N_0.

k. The study on the relative effect of 0° plies on the circumferential stress distribution in rotating annular uniform-thickness cross-ply laminated discs with the clamped-free boundary condition shows that for a cross-ply disc with a beta value of 0.2, the maximum circumferential stress first decreases with the decreasing value of N_0 from $N_0 = 18$ up to $N_0 = 6$ and then increases with decreasing value of N_0. However, for the discs with beta values of 0.25 and 0.3, the maximum circumferential stress always increases with the decreasing value of N_0. Additionally, irrespective of the beta value of the disc, the maximum radial displacement always increases with the decreasing number of 0° plies.

l. Considering the effect of radius ratio on the elastic response of rotating annular uniform-thickness cross-ply laminated discs with the clamped-free boundary condition, it is observed that, the maximum radial stress first decreases with the increasing beta value of the disc from N_0 = 18 up to N_0 = 8 and then increases with the increasing beta value of the disc on further dropping of 0° plies. Contrastingly, irrespective of the number of 0° plies, the maximum circumferential stress and the maximum radial displacement always decrease with the increasing beta value of the disc.

m. On comparing the elastic response of rotating annular uniform-thickness fiber-reinforced composite discs with various symmetrically-balanced configurations and with the clamped-free boundary condition, it is observed that irrespective of the beta value, the laminated discs with LC3 ($[0_2/(\pm 45)_4]_s$ and LC4 ($[(0/90/\pm 45)_2/(0/$

$90)]_s$) configurations experience the maximum amounts of radial and circumferential stress respectively. Contrastingly, the in-plane shear stress and the radial displacement are maximum in the laminated disc with LC2 ($[(\pm 45)_5]_s$) configuration.

n. Irrespective of the laminate configuration, the maximum radial and circumferential stresses, the in-plane shear stress and the maximum radial displacement in a rotating annular uniform-thickness symmetrically-balanced laminated disc with the clamped-free boundary condition decrease with the increasing beta value of the disc.

o. Irrespective of the taper configuration, the induced maximum radial stress in rotating annular thickness-tapered fiber-reinforced composite discs with uni-directional and symmetrically-balanced laminate configurations and with the clamped-free boundary condition decreases with the increasing number of dropped plies. However, for the thickness-tapered discs with cross-ply laminate configuration, this variation of the maximum radial stress with the number of dropped plies only holds true for the taper configurations B and C. For the thickness-tapered cross-ply discs with taper configuration D, the variation of radial stress with the number of dropped plies is much more complex.

p. Observations for different taper configurations show that irrespective of the beta value and number of dropped plies, the induced maximum radial stress in rotating annular thickness-tapered uni-directional laminated discs with the clamped-free boundary condition is maximum for taper configuration B, whereas, for the thickness-tapered cross-ply laminated discs, the radial stress is maximum for taper configuration C. Also, for the symmetrically-balanced laminated discs with LC1 and LC4 configurations, the radial stress is the highest for taper configuration D, whereas, for the discs with LC2 and LC3 configurations, the radial stress is the highest for taper configuration B.

q. Irrespective of the taper configuration, the induced maximum circumferential stress in rotating annular thickness-tapered fiber-reinforced composite discs with cross-ply and symmetrically-balanced laminate configurations and with the clamped-free boundary condition decreases with the increasing number of dropped plies. However, for the thickness-tapered discs with uni-directional laminate configurations, this variation of the maximum circumferential stress with the number of dropped plies only holds true for the taper configurations B and D. For the thickness-tapered uni-directional

laminated disc with taper configuration C, the variation of the maximum circumferential stress with the number of dropped plies is much more complex.

r. Observations for different taper configurations show that irrespective of the beta value and number of dropped plies, the induced maximum circumferential stress in rotating annular thickness-tapered uni-directional laminated discs with the clamped-free boundary condition is maximum for taper configuration B, whereas, for the thickness-tapered cross-ply laminated discs, the circumferential stress is maximum for taper configuration D. Also, for the symmetrically-balanced laminated discs with LC1, LC2 and LC4 configurations, the circumferential stress is the highest for taper configuration D, whereas, for the discs with LC3 configuration, the circumferential stress is the highest for taper configuration C.

s. Irrespective of the taper configuration, the induced maximum radial displacement in rotating annular thickness-tapered fiber-reinforced composite discs with uni-directional and cross-ply laminate configurations and with the clamped-free boundary condition decreases with the increasing number of dropped plies. However, for the thickness-tapered discs with symmetrically-balanced laminate configurations, this variation of the maximum radial displacement with the number of dropped plies only holds true for the taper configurations B and C. For the thickness-tapered symmetrically-balanced laminated discs with taper configuration D, the variation of the maximum radial displacement with the number of dropped plies is much more complex.

t. Observations for different taper configurations show that irrespective of the beta value and number of dropped plies, the induced maximum radial displacement in rotating annular thickness-tapered symmetrically-balanced and cross-ply laminated discs with the clamped-free boundary condition is maximum for taper configuration D. On the other hand, for the thickness-tapered uni-directional laminated discs, the arrangement of dropped plies within the tapered disc, i.e., the taper configuration has no effect on the induced maximum radial displacement in the rotating thickness-tapered disc. That is, irrespective of the beta value and the fiber orientation angle, the amount of radial displacement in the uni-directional laminated disc is the same for each taper configuration considered in the present study.

u. Irrespective of the taper configuration, the induced maximum in-plane shear stress in rotating annular thickness-tapered fiber-reinforced composite discs with symmetrically-balanced laminate configurations and with the clamped-free boundary condition decreases with the increasing number of dropped plies.
v. Observations for different taper configurations show that irrespective of the beta value and number of dropped plies, the induced maximum in-plane shear stress in rotating annular thickness-tapered symmetrically-balanced laminated discs with LC2 and LC3 configurations and with the clamped-free boundary condition is maximum for taper configuration B, whereas, for the disc with LC4 configuration, the in-plane shear stress is maximum for taper configuration D.

It can be seen from the above observations that the preferential use of fiber-reinforced composite materials over homogenous isotropic materials allows the designers to tailor the mechanical properties of the rotating discs. Some important design aspects are listed below:

a. The locus of the point experiencing the maximum amount of radial stress can be moved to locations far away from the hub of the clamped-free disc which may be subjected to internal pressure due to the shrink fit onto a mounting shaft. This can be achieved by changing the orientation of fibers along the radial direction of the uniform-thickness disc to its circumferential direction (see observation 5.2-h).
b. Applications which necessitate the requirement of ultralow clearance between the rotating disc and the guiding cylindrical surface require minimum radial displacement in the disc. This is observed in a circumferentially fiber-reinforced composite disc where the magnitude of the radial displacement is quite low as compared to the other configurations, but at an expense of maximum circumferential stress which decreases the burst speed of the disc. To increase the hoop burst speed, one could replace the circumferentially-reinforced plies with a certain number of radially-reinforced plies, so as to lower the average hoop stress in the disc.
c. In some applications it is required to lower the induced stresses and to increase the allowable speed while retaining some fixed geometric properties (such as fixed inner and outer radii and thickness at the hub). This can be achieved by tapering the orthotropic discs and/or dropping some plies at discrete locations within the uniform-thickness disc. Various taper configurations of the thickness-tapered disc can be

obtained depending on the arrangement of dropped plies, and by keeping in view the required beta value of the disc, one could select the desired taper configuration.

5.3 Recommendations for future work

The present research work is an attempt to evaluate the elastic response of rotating annular uniform-thickness and thickness-tapered discs made of orthotropic and fiber-reinforced composite materials with the free-free and the clamped-free boundary conditions, and to study the effects of various material and geometric parameters on the same. The present study of elastic response of rotating annular uniform-thickness and thickness-tapered discs can be continued in the future based on the following recommendations:

a. The present work based on the static linear analysis of rotating annular thickness-tapered discs can be extended to non-linear structural analysis involving geometric and structural non-linearities using von-Karman non-linear strains.
b. The in-plane stress and displacement analyses of rotating annular uniform-thickness and thickness-tapered discs performed using the Rayleigh-Ritz method presented in this thesis can be extended further by combining it with advanced finite element methods such as higher order and hierarchical finite element methods.
c. The possibility of viscoelastic stress relaxation and creep corresponding to the centrifugal loading of fiber-reinforced composite discs subjected to hygrothermal conditions can be taken into account. More reliable solutions for the static analysis of fiber-reinforced composite discs considering the change in material properties due to the temperature and moisture field can also be developed.
d. In industrial applications, the thickness of the rotating discs is much beyond the limits of Classical Laminate Theory. Therefore, in such cases, higher order shear deformation theories such as the Mindlin-Reissner theory and second order shear deformation theory can be considered to have better accuracy in predicting the elastic response of rotating annular uniform-thickness and thickness-tapered discs made of fiber-reinforced composite materials.

References

[1] A.M. Piramoon, *Composite Material Centrifuge Rotor*, U.S. Patent and Trademark Office, 1988.

[2] D.D. Tremelling, D. Wu, S.C. Englebretson et al., *Rotors for Rotating Machines with Hollow Fiber-Reinforced Composite Shaft*, U.S. Patent and Trademark Office, 2018.

[3] S.P. Timoshenko and J.N. Goodier, Theory of Elasticity, McGraw-Hill, New York, 1970.

[4] A.C. Ugural and S.K. Fenster, Advanced Mechanics of Materials and Applied Elasticity, 5th Edition, Boston: Pearson Education, Inc., 2011.

[5] S. Tang, "Elastic Stresses in Rotating Anisotropic Disks", *Int. J. Mech. Sci.*, Vol. 11, pp. 509-517, 1969.

[6] T.Y. Reddy and H. Srinath, "Elastic Stresses in a Rotating Anisotropic Annular Disk of Variable Thickness and Variable Density", *Int. J. Mech. Sci.*, Vol. 16, No. 1, pp. 85-89, 1974.

[7] C.I. Chang, "The Anisotropic Rotating Disks", *Int. J. Mech. Sci.*, Vol. 17, pp. 397-402, 1975.

[8] J. Kirkhope and G.J. Wilson, "Vibration and Stress Analysis of Thin Rotating Discs using Annular Finite Elements", *Journal of Sound and Vibration*, Vol. 44, No. 4, pp. 461-474, 1976.

[9] G. Genta, G. Belingardi and M. Gola, "A Study of the Stress Distribution in Rotating Orthotropic Discs", *Composites*, Vol. 10, No. 2, pp. 77-80, 1979.

[10] G. Genta and M. Gola, "The Stress Distribution in Orthotropic Rotating Disks", *Journal of Applied Mechanics*, Vol. 48, No. 3, pp. 559-562, 1981.

[11] B. De St. Venant, "Memoire sur la Distribution d'elasticite", *Journal des Math. Pures et Appl.*, Vol. 2, No. 8, 1863.

[12] K. Wolf, "Zeitschrift fur Angewaudte Mathematik und Mechanik", Vol. 15, pp. 249, 1935.

[13] G.L. Nigh and M.D. Olson, "Finite Element Analysis of Rotating Disks", *Journal of Sound and Vibration*, Vol. 77, No. 1, pp. 61 – 78, 1981.

[14] R.A. Cookson and S.K. Sathianathan, “Analysis of Steady Stresses in Rotating Anisotropic Discs”, *First A.M.E. Conference*, pp. 29 – 31, 1984.

[15] S. Amada, “Dynamic Shear Stress Analysis of Discs Subjected to Variable Rotations”, *Journal of Mechanical Engineering*, Vol. 28, No. 240, pp. 1029 – 1035, 1985.

[16] U. Guven, “Elastic-Plastic Stresses in a Rotating Annular Disk of Variable Thickness and Variable Density”, *Int. J. Mech. Sci.*, Vol. 34, No. 2, pp. 133-138, 1992.

[17] G.S. Ray and B.K. Sinha, “Profile Optimization of Variable Thickness Rotating Disc”, *Computers and Structures*, Vol. 42, No. 5, pp. 809 – 813, 1992.

[18] M.M. Megahed and M.S.A. Kader, “Elastoplastic Analysis of Rotating Shrink-Fitted Discs with Nonlinear Hardening Characteristics”, *Int. J. Solid Structures*, Vol. 30, No. 6, pp. 751 – 765, 1993.

[19] R. Jain, K. Ramachandra and K.R.Y. Simha, “Rotating Anisotropic Disc of Uniform Strength”, *International Journal of Mechanical Sciences*, Vol. 41, pp. 639 – 648, 1999.

[20] R. Jain, K. Ramachandra and K.R.Y. Simha, “Singularity in Rotating Orthotropic Discs and Shells”, *International Journal of Solids and Structures*, Vol. 37, pp. 2035 – 2058, 2000.

[21] N. Tutuncu, “Effect of Anisotropy on Inertio-Elastic Instability of Rotating Disks”, *International Journal of Solids and Structures*, Vol. 37, pp. 7609 – 7616, 2000.

[22] F. Zhou and A. Ogawa, “Elastic Solutions for a Solid Rotating Disk with Cubic Anisotropy”, *Journal of Applied Mechanics*, Vol. 69, pp. 81-83, 2002.

[23] A.N. Eraslan, “Elastic-Plastic Deformations of Rotating Variable Thickness Annular Disks with Free, Pressurized and Radially Constrained Boundary Conditions”, *International Journal of Mechanical Sciences*, Vol. 45, No. 3, pp. 643-667, 2003.

[24] Y. Kaya, “Analytical and Numerical Solutions to Rotating Orthotropic Disk Problems”, M.S. Thesis, Middle East Technical University, 2007.

[25] A.M. Zenkour and D.S. Mashat, “Stress Function of a Rotating Variable-Thickness Annular Disk using Exact and Numerical Methods”, *Engineering*, Vol. 3, No. 2, pp. 422-430, 2011.

[26] X.L. Peng and X.F. Li, “Elastic Analysis of Rotating Functionally Graded Polar Orthotropic Disks”, *International Journal of Mechanical Sciences*, Vol. 60, No. 4, pp. 84-91, 2012.

[27] L. Sondhi, S. Sanyal, K.N. Saha et al., "An Approximate Solution to the Stress and Deformation States of Functionally Graded Rotating Disks", *International Conference on Mechanical Engineering*, 2016.
(Source - http://dx.doi.org/10.1063/1.4958351)

[28] A.N. Eraslan, Y. Kaya and E. Varli, "Analytical Solutions to Orthotropic Variable Thickness Disk Problems", *Pamukkale University Journal of Engineering Sciences*, Vol. 22, No. 1, pp. 24-30, 2016.

[29] V. Yildirim, "Unified Exact Solutions to the Hyperbolically Tapered Pressurized/Rotating Disks Made of Nonhomogeneous Isotropic/Orthotropic Materials", *International Journal of Advanced Materials Research*, Vol. 4, No. 1, pp. 1-23, 2018.

[30] V. Yildirim, "The Complementary Functions Method (CFM) Solution to the Elastic Analysis of Polar Orthotropic Rotating Discs", *J. Appl. Comp. Mech.*, Vol. 4, No. 3, pp. 216-230, 2018.

[31] C.W. Bert, "Centrifugal Stresses in Arbitrarily Laminated, Rectangular-Anisotropic Circular Discs", *Journal of Strain Analysis*, Vol. 10, No. 2, pp. 84-92, 1975.

[32] S. Tsuda, E. Shiratori and K. Ikegami, "Rotating Strength of Laminated Composite Discs", *Journal of Mechanical Engineering*, Vol. 23, No. 180, pp. 822 – 830, 1980.

[33] E. Shiratori, K. Ikegami and T. Ishii, "Study on the High-Speed Rotating Disc Reinforced by Laminating and Hoop Winding Method", *Journal of Mechanical Engineering*, Vol. 24, No. 189, pp. 501 – 506, 1981.

[34] J.A. Gur and Y. Stavsky "On Rotating Polar Orthotropic Circular Disks", *Int. J. Solids Structures*, Vol. 17, pp. 57 – 67, 1981.

[35] G. Genta, M. Gola and A. Gugliotta, "Axisymmetric Computation of the Stress Distribution in Orthotropic Rotating Discs", *Int. J. Mech. Sci.*, Vol. 24, No. 1, pp. 21 – 26, 1982.

[36] M.R. Sitzer, "Stress Distribution in Rotating Aeolotropic Laminated Heterogenous Disc under Action of a Time-Dependent Loading", *Journal of Applied Mathematics and Physics*, Vol. 36, pp. 134-145, 1985.

[37] H.V. Lakshminarayana, "Finite Element Analysis of Rotating Laminated Composite Annular Discs", *Composites*, Vol. 17, No. 1, pp. 42-48, 1986.

[38] M. Carpino, "Analysis of a Laminate Disk Rotating near a Flat Plate", *Journal of Tribology*, Vol. 115, pp. 578 – 583, 1993.

[39] N. Tutuncu, "Effect of Anisotropy on Stresses in Rotating Discs", *Int. J. Mech. Sci.*, Vol. 37, No. 8, pp. 873-881, 1995.

[40] F. Hild and F.A. Leckie, "Fiber Distribution in Reinforced Ceramic Rotating Discs", *International Gas Turbine and Aeroengine Congress and Exposition*, 1995.

[41] N. Tutuncu and A. Durdu, "Determination of Buckling Speed for Rotating Orthotropic Disk Restrained at Outer Edge", *AIAA Journal*, Vol. 36, No. 1, pp. 89 – 93, 1998.

[42] J.F. Durodola and O. Attia, "Property Gradation for Modification of Response of Rotating MMC Discs", *Material Science and Technology*, Vol. 16, pp. 919 – 924, 2000.

[43] S.M. Arnold, A.F. Saleeb and N.R. Al-Zoubi, "Deformation and Life Analysis of Composite Flywheel Disk Systems", *Composites*, Vol. 33, pp. 433 – 459, 2002.

[44] M. Tahani, A. Nosier and S.M. Zebarjad, "Deformation and Stress Analysis of Circumferentially Fiber-Reinforced Composite Disks", *International Journal of Solids and Structures*, Vol. 42, pp. 2741 – 2754, 2005.

[45] K.N. Koo, "In-plane Stress Analysis of Rotating Composite Disks", *Journal of the Korean Society of Composite Materials*, Vol. 18, No. 4, pp. 8 – 13, 2005.

[46] A.M. Zenkour and M.N.M Allam, "On the Rotating Fiber-Reinforced Viscoelastic Composite Solid and Annular Disks of Variable Thickness", *International Journal for Computational Methods in Engineering Science and Mechanics*, Vol. 7, No. 1, pp. 21-31, 2006.

[47] H. Callioglu, M. Topcu and A.R. Tarakcilar, "Elastic-Plastic Stress Analysis of an Orthotropic Rotating Disc", *International Journal of Mechanical Sciences*, Vol. 48, pp. 985-990, 2006.

[48] B. C. Fabien, "The Influence of Failure Criteria on the Design Optimization of Stacked-Ply Composite Flywheels", *Struct Multidisc Optim*, Vol. 33, pp. 507-517, 2007.

[49] K.N. Koo, "Elastic Stresses and Failure of Rotating Cross-Ply Laminated Disks", *Journal of Mechanical Science and Technology*, Vol. 23, pp. 1508-1514, 2009.

[50] K.N. Koo and G.A. Lesieutre, "Vibration and Critical Speeds of Composite-Ring Disks for Data Storage", *Journal of Sound and Vibration*, Vol. 329, pp. 833-847, 2010.

[51] A. Almasi, “Application and Stress Analysis of Laminated Composites for High-Speed Impellers of Process Centrifugal Compressors”, *J. Process Mechanical Engineering*, Vol. 226, No. 5, pp. 256-260, 2011.

[52] F. Zhou, A. Ogawa and R. Hashimoto, “Strain and Stress Distribution in a Rotating Disk made by 2D C/C Laminated Composites”, *Proceedings of the 2001 International Conference on Composite Materials*, Beijing, 2001

[53] V. Yildirim, “The Complementary Functions Method Solution to the Functionally Graded Polar Orthotropic Rotating Hyperbolic Disks with Both Radially and Circumferentially Aligned Fibers”, *International Journal of Engineering & Applied Sciences*, Vol. 10, No. 4, pp. 276-290, 2018.

[54] C. Delvadiya, “Dynamic Analysis of Tapered Circular Discs made of Isotropic and Orthotropic Materials using Rayleigh-Ritz Method and ANSYS”, M.A.Sc. Thesis, Concordia University, 2016.

[55] N. Baddour, “A Modelling and Vibration Analysis of Spinning Disks”, Ph.D. Thesis, University of Toronto, 2001.

[56] P.J.G. Schreurs, “Linear Plate Bending and Laminate Theory”, M020, Eindhoven University of Technology, Eindhoven, NB, 2008.

[57] J.M. Berthelot, Composite Materials: Mechanical Behavior and Structural Analysis, New York: Springer, 1999.

[58] A. Zabihollah, “Vibration and Buckling Analysis of Tapered Composite Beams using Conventional and Advanced Finite Element Formulations”, M.A.Sc. Thesis, Concordia University, 2003.

[59] S. Akhlaque, “Buckling Analysis of Tapered Composite Plates using Ritz Method based on Classical and Higher Order Theories”, M.A.Sc. Thesis, Concordia University, 2005.

[60] K.W. Gan, G. Allegri and S.R. Hallett, “A Simplified Layered Beam Approach for Predicting Ply Drop Delamination in Thick Composite Laminates”, *Materials & Design*, Vol. 108, pp. 570 – 580, 2016.

[61] ANSYS Inc., “ANSYS Mechanical APDL Element Reference”, 2013.

Appendix A

The following Figures A.1 (a) and A.1 (b) show the geometry, node locations and the element coordinate system for the SOLID185 and SHELL181 elements respectively.

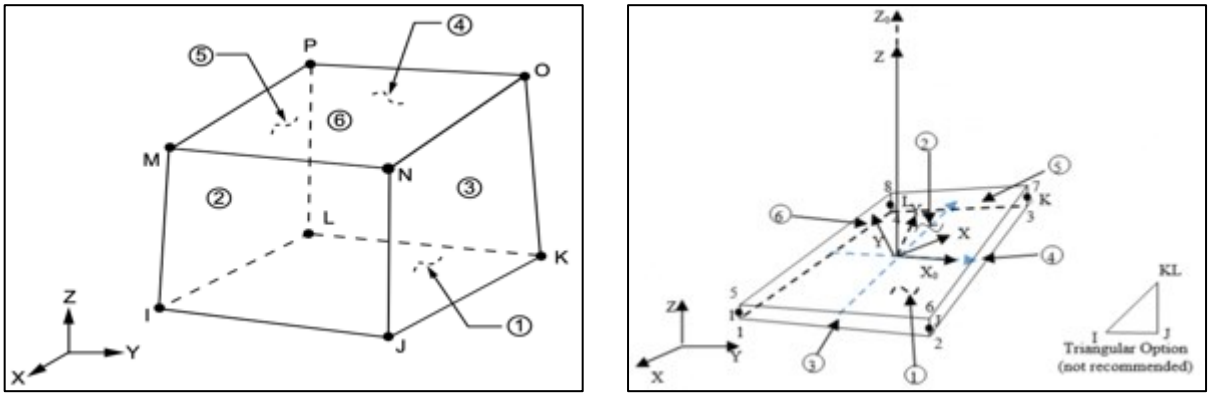

(a) SOLID185 element **(b)** SHELL181 element

Figure A.1 Geometry, node locations and element coordinate system for **(a)** SOLID185 [61] and **(b)** SHELL181 element [61]

The SOLID185 is a 3-Dimensional, 8-node solid element that exhibits quadratic displacement behavior. The element is defined by 8 nodes and has 3 translational degrees of freedom at each node, i.e., translations in the nodal x, y and z directions (UX, UY and UZ). The element supports plasticity, creep, hyper-elasticity, stress-stiffening, large deflection and large strain capabilities [61].

The SHELL181 element is suitable for analyzing thin to moderately-thick shell structures. It is a 4-node element with 6 degrees of freedom at each node i.e., 3 translational degrees of freedom in the nodal x, y and z directions (UX, UY and UZ) and 3 rotational degrees of freedom about the x, y and z-axes (ROTX, ROTY and ROTZ). The element is best suited for linear, large rotation and/or large strain non-linear applications [61].